



MONASH University

**(Improved) micro-climate modelling assessment of the
influence of water sensitive urban design on human thermal
comfort**

Kerry Nice

M.E.S, Monash University
B.A, University of Colorado

A thesis submitted for the degree of Doctor of Philosophy at
Monash University in 2016
School of Earth, Atmosphere and Environment

Copyright notice

©The author (2016). Except as provided in the Copyright Act 1968, this thesis may not be reproduced in any form without the written permission of the author.

I certify that I have made all reasonable efforts to secure copyright permissions for third-party content included in this thesis and have not knowingly added copyright content to my work without the owner's permission.

Abstract

With urban areas facing future longer duration heat-waves and temperature extremes from climate change and growing urban development, adaptation strategies are needed. Examining the role that increased tree cover and water availability can have on human thermal comfort (HTC) in urban areas as part of these strategies has been done using observations, but further work requires a modelling tool suited for this task. Sufficient model resolution is needed to resolve variables used to calculate HTC, as well as the ability to model the physiological processes of vegetation and their interaction with water and with the rest of the urban environment. The lack of such a model has been identified as a research gap in the urban climate area and has impaired the ability to fully examine the use of urban greenery and water for improved human thermal comfort.

A new model, VTUF-3D (Vegetated Temperatures Of Urban Facets), addresses this gap by embedding the functionality of the MAESPA tree process model (Duursma & Medlyn 2012), that can model individual trees, vegetation, and soil components, within the TUF-3D (Krayenhoff & Voogt 2007) urban micro-climate model. An innovative tiling approach, allows the new model to account for important vegetative physiological processes and shading effects using configurable templates to allow representation of any type of vegetation or water sensitive design feature. The high resolution of VTUF-3D is sufficient to examine the processes that drive human thermal comfort (HTC). This allows detailed calculations of surface temperatures, mean radiant temperature (T_{mrt}), and a HTC index, the universal thermal climate index ($UTCI$), across an urban canyon.

An extensive validation process, using three different observation data sets to validate a number of different and key aspects of the VTUF-3D model, has shown it performs well and is suitable for use to examine critical questions relating to the role of vegetation and water in the urban environment.

A demonstration of the model using modelling scenarios of varying canopy cover shows that average peak daytime HTC improvements of 1°C UTCI (and 2.3°C UTCI) are possible in doubling (and quadrupling) existing street cover canopies, with localised effects under canopy cover approaching 5°C UTCI. These scenarios also show the value of the existing canopy cover, as reductions and elimination of existing cover can create reductions in HTC of 2°C UTCI. In addition, reductions in average air temperature (T_a) across urban canyons can differ by 1°C between streets with differing canopy cover.

After the development, validation, and demonstration of this new model, it is now possible to conduct further analysis to quantify the impact each individual tree can have on temperatures in urban canyons. Further, the model can help inform the optimal arrangement and quantity of trees to maximise temperature moderation effects and be used to generate best practices guidelines for urban greening.

Declaration

This thesis contains no material which has been accepted for the award of any other degree or diploma at any university or equivalent institution and that, to the best of my knowledge and belief, this thesis contains no material previously published or written by another person, except where due reference is made in the text of the thesis.

Signature:

Print Name:

Date:

Acknowledgements

Although it feels like I alone spent vast amounts of time sitting in my office developing this model and writing the thesis, the following people were also there, supporting and helping me finish this project:

- This couldn't have happened without Andrew Coutts, who was full of ideas and enthusiasm, found problems and solutions, and read and reread this thesis numerous times.
- Nigel Tapper who got this project on its feet, cleared the way for it, and gave much valuable advice and input along the way.
- Jason Beringer, who offered many valuable suggestions and advice early on in the project.
- Financial support from the City of Melbourne and the CRC for Water Sensitive Cities.
- Scott Krayenhoff for supplying his TUF-3D model to this project as well as advice on how to tear it apart and put it back together again.
- Remko Duursma, Belinda Medlyn, and numerous other researchers who created the MAESPA model (and MAESTRA and SPA and many other models which grew into MAESPA).
- Peter Isaac, who got me into this mess in the first place.
- To everybody in the climate group at Monash University, for support, encouragement, and shared pain.
- To my friends, who finally stopped asking, so have you finished your PhD. yet?
- And of course to Ché, for massive support and endless patience during the whole mad adventure.

Contents

Copyright notice	ii
Abstract	iii
Declaration	iv
Acknowledgements	v
1 Introduction	1
1.1 Project overview	1
1.2 Urban growth	1
1.2.1 Growing urbanism	2
1.3 Climate change	2
1.3.1 Temperatures	2
1.3.2 Extremes	3
1.4 Urban water management	5
1.5 Increased urbanisation and urban warmth	6
1.5.1 The challenge of changing urban areas	6
1.6 Thermal comfort	7
1.6.1 Strategies to promote thermal comfort	8
1.6.2 Conventional strategies through mechanical cooling	8
1.6.3 Urban morphology strategies	8
1.7 Cooling through urban greening	9
1.7.1 Water sensitive urban design (WSUD) as mitigation and adaptation	10
1.8 Research aim	11
1.9 Research objectives	12
1.10 Research questions	13

2 Literature review	14
2.1 Literature review overview	14
2.2 Urban climates	14
2.2.1 Contributors to urban warmth	14
2.2.2 Urban energy and water budgets	17
2.2.3 Soil/water, plant and atmosphere interactions	19
2.3 Interactions of humans, climate, and urban areas	21
2.3.1 Human Thermal Comfort (HTC)	21
2.3.2 HTC in outdoor areas	23
2.3.3 Mean radiant and air temperatures	24
2.3.4 Calculating HTC of urban areas	24
2.4 Modelling scales and modelled properties	24
2.4.1 Global scale	24
2.4.2 Meso and Local scale	25
2.4.3 Micro-scale	26
2.4.4 Characteristics to classify models	26
2.5 Inclusion of vegetation in urban models	27
2.5.1 Non-integrated vegetation	27
2.5.2 Transpiration modelling techniques	28
2.5.2.1 Big Leaf	28
2.5.2.2 Ball-Berry stomatal conductance	28
2.5.2.3 Penman-Monteith equation	29
2.5.3 Inclusion of vegetation in urban canopy models	30
2.5.3.1 Single layer UCM	30
2.5.3.2 Multi-layer UCM	31
2.5.3.3 Shading effects in UCMs	31
2.5.3.4 UCM modelling and HTC	32
2.5.4 Urban vegetation modelling at local scales	32
2.5.4.1 Tree and canyon radiation modelling at local scale	32
2.5.4.2 Transpiration modelling at local scale	32
2.5.4.3 Urban vegetation modelling at local scales and HTC	32
2.5.5 Urban vegetation modelling at micro-scales	32
2.5.5.1 Simple radiation integration	33

2.5.5.2	Direct vegetation modelling through ray tracing techniques	33
2.5.5.3	Direct modelling using CFD techniques	33
2.5.5.4	ENVI-met	34
2.5.5.5	CFD frameworks	35
2.5.6	Transpiration at micro-scales	35
2.5.7	Micro-scaled vegetation modelling	35
2.6	Possible tools to model urban vegetation at a micro-scale	36
2.6.1	TUF-3D	36
2.6.2	MAESPA	37
2.6.2.1	Canopy components	38
2.6.2.2	Water balance components	39
2.6.2.3	Heat soil balance components	40
2.6.2.4	Application of MAESPA for urban modelling	41
2.6.3	Tool creation for modelling urban vegetation	41
2.7	Cooling through urban greening	41
2.8	Research gaps in modelling urban micro-climates	42
3	Methodology	44
3.1	Project objectives	44
3.1.1	Research aim and questions	45
3.2	Research stages	45
3.2.1	Objective 1 detail - creation of the VTUF-3D modelling tool	46
3.2.1.1	VTUF-3D/MAESPA vegetation/radiation interactions	46
3.2.1.2	VTUF-3D energy balance modelling with MAESPA tiles	46
3.2.2	Objective 2 - validation of VTUF-3D modelling tool	47
3.2.2.1	Comparison to Preston data	47
3.2.2.2	Comparison to City of Melbourne Gipps/George St. street tree study	47
3.2.2.3	Comparison to Smith St. single tree study	47
3.2.3	Objective 3 detail - demonstration of new VTUF-3D model with canopy cover scenarios	48
3.3	Summary of research steps	48
4	Creation of the VTUF-3D urban micro-climate model to support assessments of WSUD influences on HTC at a micro-scale in urban canyons	49

4.1	Overview of changes	49
4.2	Model description	52
4.2.1	Radiative processes	52
4.2.1.1	Radiative transfer	52
4.2.1.2	Stomatal conductance	54
4.2.1.3	Calculation of leaf temperature and leaf water potential	54
4.2.1.4	Total canopy transpiration	55
4.2.1.5	Conduction and surface temperatures	55
4.2.1.6	Soil surface temperature	56
4.2.1.7	Energy balance partitioning during simulation timesteps	56
4.2.2	Convection	57
4.2.2.1	Wind speed profile	57
4.2.2.2	Temperature profile and canopy energy budget	58
4.2.2.3	Surface convection	58
4.2.3	Water balance	59
4.2.3.1	Infiltration	59
4.2.3.2	Root water uptake	59
4.2.3.3	Soil evaporation	60
4.2.3.4	Canopy interception	61
4.2.3.5	Drainage	61
4.2.3.6	Hydraulics of the soil-to-leaf pathway	61
4.2.4	T_{mrt} and UTCI	61
4.2.4.1	Globe temperature calculation	62
4.2.4.2	T_{mrt} calculation	63
4.2.4.3	UTCI calculation	63
4.3	VTUF-3D model integration	64
4.3.1	TUF-3D shading logic	64
4.3.2	Integrating vegetation shading and modified ray tracing logic in VTUF-3D	65
4.3.3	MAESPA vegetation transmission and energy balance functionality overview	69
4.3.4	VTUF-3D use of MAESPA differential shading values	70
4.3.5	MAESPA configurations creation	70
4.3.6	MAESPA tree parameterisations	71
4.3.6.1	MAESPA olive tree (<i>Olea europaea</i>) parameterisation	71

4.3.6.2 MAESPA brushbox tree (<i>Lophostemon Confertus</i>) parameterisation	73
4.3.6.3 MAESPA grass parameterisation	74
4.4 Running VTUF-3D	75
4.4.1 Overview of changes in TUF-3D	75
4.4.2 MAESPA energy flux conversions	75
4.4.3 Loading MAESPA data	75
4.4.4 Radiation transmission in Maespa	76
4.4.5 VTUF-3D use of MAESPA shading values	76
4.4.6 Implementation and batch utility	77
4.5 Design conclusions	77
5 Validation and assessment of improved performance of the VTUF-3D model to model urban areas	79
5.1 Overview of VTUF-3D validation process	79
5.1.1 Validation objectives	79
5.2 Model validation using Preston flux observations	80
5.2.1 Preston validation overview	80
5.2.2 Preston validation results and discussion	85
5.2.2.1 Observation validation scenario	85
5.2.2.2 No vegetation baseline scenario	89
5.2.3 Preston validation intercomparison results and discussion	89
5.2.4 Preston validation conclusions	92
5.3 Model testing and validation using City of Melbourne, George and Gipps St. dataset	92
5.3.1 George St. and Gipps St. overview	92
5.3.2 George/Gipps St. validation results	96
5.3.3 George St. and Gipps St. validation conclusion	102
5.4 Model testing and validation using Smith St dataset	103
5.4.1 Smith St validation overview	103
5.4.2 Smith St validation results	106
5.4.3 Smith St validation conclusion	109
5.5 VTUF-3D validation conclusion	109
6 A demonstration of the VTUF-3D model: an assessment of the impact of urban canopy cover on HTC using canopy cover scenarios	111

6.1	VTUF-3D canopy cover scenarios	111
6.2	VTUF-3D Preston canopy cover scenarios	112
6.2.1	Preston scenarios methods	112
6.2.2	Preston scenario results	112
6.3	City of Melbourne, Gipps St. scenarios	114
6.3.1	Gipps St. scenarios methods	114
6.3.2	Gipps St. scenarios results	117
6.4	VTUF-3D urban canopy cover scenarios conclusions	119
7	Conclusion	122
7.1	Key/Major findings	122
7.2	Research implications	123
7.3	Contribution to the research field	124
7.4	Future research	125
Appendices		126
A	TUF-3D configuration files	128
A.1	parameters.dat	128
A.2	forcing.dat	130
B	New VTUF-3D configuration process	132
B.1	VTUF-3D and MAESPA configuration changes	132
B.2	Configuration generation	132
B.2.1	Overview	132
B.2.2	Create streets and buildings	133
B.3	treemap.dat	133
C	VTUF-3D configuration creation	135
C.1	Domain creation	135
C.2	Create post-processing scripts	135
C.3	VTUF-3D Post-processing	135
C.4	Scripts	136
	References	137

List of Figures

1.1 Time series of areally averaged extremes indices (Frich et al. 2002) between 1870 and 2099 using grid boxes in Australia with the observed data.	3
1.2 CMIP5 multi-model mean geographical changes (relative to a 1981-2000 reference period in common with CMIP3) under RCP8.5 and 20-year smoothed time series for RCP2.6, RCP4.5 and RCP8.5 in the (a) annual maximum of daily maximum temperature and (b) tropical nights (number of days above 20°C) (Sillmann et al. 2013, p. 1067).	4
1.3 Melbourne heat index thresholds (Nicholls et al. 2008, p. 378).	5
1.4 Water flowing into Melbourne's main water supply reservoirs (annual totals) (Melbourne Water 2016b).	6
1.5 Spatial variability of the Melbourne urban heat island at 0100, 23 March 2006.. .	7
1.6 WSUD techniques and urban micro-climate (Coutts et al. 2012, p. 6).	10
1.7 WSUD techniques and urban micro-climate (Coutts et al. 2013).	11
2.1 Characteristic time and space scales associated with atmospheric phenomena (Sturman et al. 1999, p. 612).	15
2.2 Effects of urbanisation on processes affecting climate at local- and regional-scales (Cleugh & Grimmond 2012, p. 50).	16
2.3 Urban surface radiation budget (Oke 1988b, p. 473).	17
2.4 Urban surface energy budget (Oke 1988b, p. 473).	18
2.5 Urban surface water budget (Oke 1988b, p. 473).	18
2.6 Boundary layer structures over a city (Oke 1988b, p. 473).	19
2.7 The water balance and internal flows of water in a soil-plant-atmosphere system	20
2.8 PMV and thermal sensation (Hamdi et al. 1999, p. 168).	22
2.9 Elements of the operational procedure and concept of UTCI as categorised equivalent temperature derived from the dynamic response of a thermo-physiological model coupled with a behavioural clothing model (Bröde et al. 2013, p. 17). .	23
2.10 Various scales related to wind climate (Murakami et al. 1999, p. 58).	25
2.11 Characteristics used to classify models (Grimmond et al. 2010, p. 1270). . . .	26

2.12 Basic cubic cell and surface patch structure of TUF-3D (Krayenhoff & Voogt 2007, p. 437).	36
2.13 An example TUF-3D domain with a bounding wall and the sub-domain S_d (chosen to coincide with the central urban unit) in lighter shades (Krayenhoff & Voogt 2007, p. 437).	37
2.14 MAESPA process flowchart (Duursma & Medlyn 2012).	38
2.15 MAESPA water balance flowchart (Duursma & Medlyn 2012).	40
2.16 MAESPA stand (Duursma & Medlyn 2012).	41
4.1 VTUF-3D energy balance modelling with vegetation MAESPA tiles.	50
4.2 Integration of MAESPA tree model into VTUF-3D radiation fluxes routines, in which tiled instances of MAESPA vegetation (in green) are used to calculate radiation transmission for VTUF-3D placeholder vegetation structures (in grey).	50
4.3 VTUF-3D model process flow	51
4.4 Basic cubic cell and surface patch structure of TUF-3D (Krayenhoff & Voogt 2007, p. 437).	52
4.5 Calculation of radiation penetration in MAEPSPA using gridded tree structures (Duursma 2008).	54
4.6 Building height arrays, input through the bldht array, used to calculate z_H and create the surf_shade array.	64
4.7 Initial view angles ray tracing, run during model initialisation to determine which surfaces are visible to each other.	65
4.8 TUF-3D unmodified shading logic in which each surface performs four ray traces (from each surface quarter) towards the sun and determines sunlit percentage based on how many rays leave the domain without meeting an obstruction. Trees do not exist in this version (they will be added in Figure 4.10) but are shown to illustrate how their impact is missing from the unmodified logic.	66
4.9 Vegetation height arrays, input through the veght array, used to create the vegshade array.	66
4.10 VTUF-3D modified shading, timestep ray tracing, using the same process as the unmodified logic but setting a flag for any ray that encounters vegetation.	67
4.11 VTUF-3D modified shading, reverse ray tracing. For any rays that encounter vegetation in forward ray tracing, reverse ray traces are performed to allocate radiation to intervening encountered surfaces.	68
4.12 VTUF-3D/MAESPA vegetation/radiation interactions	69
5.1 Preston suburb and modelled area. Adapted from Google Maps (2015).	80
5.2 Digitisation of modelled Preston suburban street	82
5.3 Preston validation domain configured building heights (0, 5, 10m) and locations.	82
5.4 Preston validation domain configured vegetation heights (0, 5, 10m) and locations.	83

5.5 Preston observations during the validation period of 9 February - 10 March 2004.	84
5.6 Pr04Val scenario modelled vs. observations for Q_H , Q_E , Q^* , and Q_G fluxes for the period 10 February-10 March 2004.	86
5.7 Pr04Val run 30 day hourly average VTUF-3D flux comparisons to Preston flux observations for the period 10 February-10 March 2004, with error bars at observations standard deviations.	86
5.8 Pr04Val run 30 day hourly average VTUF-3D flux comparisons to Preston flux observations for the period 10 February-10 March 2004, with error bars at standard deviations.	87
5.9 Pr04Val modelled Q_E vs. Preston Q_E observations including observation of daily high/low temperatures and hourly rain totals for the period 10 February-10 March 2004.	88
5.10 Pr04NoVeg scenario modelled vs. observations for Q_H , Q_E , Q^* , and Q_G fluxes for the period 10 February-10 March 2004.	90
5.11 Pr04NoVeg run 30 day hourly average VTUF-3D flux comparisons to Preston flux observations for the period 10 February-10 March 2004, with error bars at observations standard deviations.	90
5.12 Median of the mean modelled flux, MBE, and RMSE for the surface fluxes determined for two month periods, for the models classified by their representation of vegetation. Note the scales are different for each flux (Best & Grimmond 2012).	91
5.13 RMSE VTUF-3D vs. Intercomparison results comparison for Preston validations scenarios for 10 February-10 March 2004.	91
5.14 Location and photos of each street: Gipps St. (OPN), and George St. (TRD). Aerial view of the streets highlighting individual station locations and tree canopy coverage in Gipps St. (OPN), and George St. (TRD) (Coutts et al. 2015a, p.58).	93
5.15 George St/Gipps St - Modelled domains with 4 and 3 observation stations located on street	95
5.16 Building heights (top) / Vegetation cover (bottom) - George St (left), Gipps St. (right)	96
5.17 Daily maximum, minimum, and mean temperatures of Gipps/George St. observations during the validation period of 31 January - 1 March 2012.	97
5.18 George St. GeorgeValidation scenario point comparison of T_{mrt} of 4 observation stations to modelled points.	98
5.19 George St. GeorgeValidation scenario point comparison of $UTCI$ of 4 observation stations to modelled points.	98
5.20 Gipps St. GippValidation scenario point comparison of T_{mrt} of 3 observation stations to modelled points.	99
5.21 Gipps St. GippValidation scenario point comparison of $UTCI$ of 3 observation stations to modelled points.	99

5.22 George St. GeorgeValidation scenario four observation stations (TRD_2, TRD_3, TRD_4, and TRD_5) values of T_{mrt} aggregated into hourly averages over 30 days compared to modelled points, with error bars at observation standard deviations.	100
5.23 Gipps St. GippValidation scenario three observation stations (OPN_3, OPN_4, and OPN_5) values of T_{mrt} aggregated into hourly averages over 30 days compared to modelled points, with error bars at observation standard deviations.	101
5.24 Gipps St. GippValidation scenario three observation stations (OPN_3, OPN_4, and OPN_5) values of $UTCI$ aggregated into hourly averages over 30 days compared to modelled points, with error bars at observation standard deviations.	101
5.25 George/Gipps St. modelled T_{can} from scenarios GeorgeValidation and GippValidation compared to observed T_a of George St. 4 treed canopy stations and Gipps St. 3 open canopy stations, aggregated into hourly averages over February 2012 modelled period.	103
5.26 Effects of urban canyon shadowing on east and west sides of the street on vegetation physiological response (Gebert et al. 2012).	104
5.27 View of Smith St., Melbourne site and locations on street of observed eucalyptus and olive trees. Red outline showing modelled area. Adapted from Gebert et al. (2012).	104
5.28 Extraction of modelled Q_E values for olive trees (highlighted with yellow boxes) on the east and west sides of Smith St. from validation simulation SmithStVal.	106
5.29 VTUF-3D SmithStVal validation showing modelled transpiration along each west and east tree location (of Figure 5.28) for 23 February 2012. Also shown, observed transpiration values for the same tree location.	107
5.30 VTUF-3D SmithStVal validation showing 18 day hourly average of fluxes along each east and west tree location.	107
5.31 Smith St. scenario SmithStVal forcing shortwave radiation for February 23, 2012.108	
 6.1 Preston tree canopy configuration for four scenarios, PrestonScenarios1- NoTree, PrestonScenarios2-HalfTree, PrestonScenarios3-Trees, and PrestonScenarios4-DoubleTrees, representing zero trees, 50% reduction of trees, existing Preston canopy cover, and doubled canopy cover.	113
6.2 UTCI ($^{\circ}\text{C}$) of surfaces at 0m height for four scenarios, PrestonScenarios1-NoTree, PrestonScenarios2-HalfTree, PrestonScenarios3-Trees, and PrestonScenarios4-DoubleTrees, for modelled timestep 14 February 2004 at 2pm.	114
6.3 Modelled UTCI ($^{\circ}\text{C}$) average of all surfaces at 0m height for four scenarios, PrestonScenarios1- NoTree, PrestonScenarios2-HalfTree, PrestonScenarios3-Trees, and PrestonScenarios4-DoubleTrees over 13-14 February 2004 / Differences in UTCI ($^{\circ}\text{C}$) average of all surfaces at 0m height between baseline PrestonScenarios3-Trees scenario and other three scenarios over 13-14 February 2004.	115

6.4 Modelled canyon air temperature (T_{can}) of four scenarios, PrestonScenarios1-NoTree, PrestonScenarios2-HalfTree, PrestonScenarios3-Trees, and PrestonScenarios4-DoubleTrees over 13-14 February 2004 / Differences of T_{can} between baseline PrestonScenarios3-Trees scenario and other three scenarios over 13-14 February 2004.	115
6.5 Differences in UTCI ($^{\circ}\text{C}$) of all surfaces at 0m height between baseline PrestonScenarios4-DoubleTrees scenario and PrestonScenarios3-Trees at modelled timestep 14 February 2004 2pm. Locations of trees (and extending canopy) shown of baseline PrestonScenarios3-Trees scenario (in red) and added trees (and canopy) in PrestonScenarios4-DoubleTrees scenario (in green).	116
6.6 Gipps St. tree canopy configuration for five scenarios, CoMGippScenarios1-NoTree, CoMGippScenarios2-HalfTree, CoMGippScenarios3-Trees, CoMGippScenarios4- DoubleTrees, CoMGippScenarios5-4xTrees, representing 0 trees, 50% reduction in trees, existing canopy cover, doubled canopy cover, and quadruple canopy cover.	117
6.7 UTCI ($^{\circ}\text{C}$) of surfaces at 0m height for five scenarios, CoMGippScenarios1-NoTree, CoMGippScenarios2-HalfTree, CoMGippScenarios3-Trees, CoMGippScenarios4- DoubleTrees, CoMGippScenarios5-4xTrees, for modelled timestep 24 February 2012 3pm.	118
6.8 Differences in UTCI ($^{\circ}\text{C}$) of all surfaces at 0m height between baseline CoMGippScenarios3-Trees scenario and CoMGippScenarios5-4xTrees at modelled timestep 24 February 2012 3pm. Locations of trees (and extending canopy) shown of baseline CoMGippScenarios3-Trees scenario (in red) and added trees (and canopy) in CoMGippScenarios5-4xTrees scenario (in green).	119
6.9 Modelled UTCI ($^{\circ}\text{C}$) average of all surfaces at 0m height for five scenarios, CoMGippScenarios1-NoTree, CoMGippScenarios2-HalfTree, CoMGippScenarios3-Trees, CoMGippScenarios4-DoubleTrees, CoMGippScenarios5-4xTrees over 23-24 February 2012 / Differences in UTCI ($^{\circ}\text{C}$) average of all surfaces at 0m height between baseline CoMGippScenarios3-Trees scenario and other four scenarios over 23-24 February 2012.	120
6.10 Modelled canopy air temperature (T_{can}) of five scenarios, CoMGippScenarios1-NoTree, CoMGippScenarios2-HalfTree, CoMGippScenarios3-Trees, CoMGippScenarios4 -DoubleTrees and, CoMGippScenarios5-4xTrees over 23-24 February 2012 / Differences of T_{can} between baseline CoMGippScenarios3-Trees scenario and other four scenarios over 23-24 February 2012.	121

List of Tables

1.1	Australian projected population and demographic changes	2
1.2	Projected changes to statewide annual average rainfall, best-estimate outcome in a no-mitigation case (percent change relative to 1990) (Garnaut 2008, p.116).	5
1.3	Design aspects to decrease exposure to high temperatures (PWC 2011, p. 40). . .	9
2.1	Summary of origin of the various components of the MAESPA model (Duursma & Medlyn 2012).	38
2.2	Summary of approaches of the canopy components of the MAESPA model. . . .	39
2.3	Summary of approaches of the water balance components of the MAESPA model.	40
2.4	Summertime E (from Aquacycle simulations) converted to diurnal heating rates and the consequent effect on peak afternoon air temperatures for each of the seven scenarios relative to a ‘desert’ (Mitchell et al. 2008, p. 2898).	42
4.1	VTUF-3D modified shading, timestep ray tracing results for Figure 4.10	68
4.2	MAESPA tree parameterisations common attributes.	72
4.3	MAESPA olive tree (<i>Olea europaea</i>) parameterisation, tree dimensions for an example 5x5m grid (to be rescaled for taller/shorter modelled trees).	72
4.4	MAESPA olive tree (<i>Olea europaea</i>) parameterisation, with parameter values taken from cited literature sources.	72
4.5	MAESPA brushbox tree (<i>Lophostemon Confertus</i>) parameterisation, tree dimensions for an example 5x5m grid (to be rescaled for taller/shorter modelled trees).	73
4.6	MAESPA brushbox tree (<i>Lophostemon Confertus</i>) parameterisation, with parameter values taken from cited literature sources.	73
4.7	MAESPA grass, tall fescue (<i>Festuca arundinacea</i>), layer as a box tree on the ground covering the plot area.	74
4.8	MAESPA grass, tall fescue (<i>Festuca arundinacea</i>), layer as a box tree on the ground covering the plot area, with parameter values taken from cited literature sources.	74
4.9	MAESPA variables loaded.	76
5.1	VTUF-3D validation matrix.	80

5.2 Preston land cover breakdowns: using expert and manual classification methods and average of both methods in 500m radius from observation tower (Coutts et al. 2007), Darebin Council land cover fractions (Nury 2015), modelled Preston 5m resolution validation domain land cover fractions (all in percentages).	81
5.3 Preston validation site properties (Coutts et al. 2007).	83
5.4 Preston validation scenario model parameters.	84
5.5 Preston simulations and Intercomparison project compared.	85
5.6 Gipps/George St. validation site characteristics (Coutts et al. 2015a).	94
5.7 George St./Gipps St. observation station sky view factors (Coutts et al. 2015a).	95
5.8 George/Gipps St. validation scenario model parameters.	95
5.9 George St. GeorgeValidation and Gipps St. GippsValidation scenarios T_{mrt} and $UTCI$ predicted vs. observations statistical performance.	97
5.10 Smith St. validation site properties (Gebert et al. 2012).	105
5.11 Smith St. SmithStVal validation scenario model parameters.	105
6.1 Preston canopy cover scenarios.	112
6.2 Gipps St. canopy cover scenarios.	116

List of Symbols

- $(q_w, T_d - q)$ specific humidity deficit (kg kg^{-1})
- A_{canopy} canopy area (m^2)
- A_{mm} 2-dimensional tree area (mm^2)
- A_{leaf} total leaf area (m^2)
- A_n leaf net assimilation rate ($\mu\text{mol m}^{-2}\text{s}^{-1}$)
- A surface area of a sphere of diameter D, of value 0.15m, ($=\pi 0.15^2 \text{m}^2$)
- A ground area (m^2)
- A available energy given by $A = RN - G$ (W m^{-2})
- B_i parameters in the leaf area density distributions within the tree crown or canopy (i=1, 2, and 3 for vertical distribution and 4, 5, and 6 for horizontal distribution)
- C_b volumetric heat capacity of layer b ($\text{J m}^{-2}\text{K}^{-1}$)
- C_s CO_2 concentration at the leaf surface ($\mu\text{mol mol}^{-2}$)
- C heat loss through convection from the surface of a clothed body (W m^{-2})
- D_0 an empirically determined coefficient
- D_{eff} effective diffusivity of the soil pore space ($\text{m}^2 \text{s}^{-1}$)
- D_i drainage out of layer i (mm)
- D_w diffusivity of water vapour (function of soil temperature) ($\text{m}^2 \text{s}^{-1}$)
- D diameter of sphere (m)
- D leaf-to-air vapour pressure deficit (Pa)
- ET evapotranspiration (mm, $\text{kg m}^{-2}\text{s}^{-1}$)
- E_d heat loss through water evaporation from the skin (W m^{-2})
- E_{re} heat loss through respiration (W m^{-2})
- E_{sw} heat loss through sweating (W m^{-2})
- E_E equivalent evaporation ($=2.45 \times 10^6 \text{ J m}^{-2}\text{h}^{-1}$)
- E_L leaf level transpiration rate ($\mu\text{mol m}^{-2}\text{s}^{-1}$)

E_a actual evapotranspiration ($\text{kg m}^{-2}\text{s}^{-1}$)

E_i root water uptake (canopy transpiration) out of layer i (mm)

E_o surface vapour pressure (Pa)

$E_{s,i}$ soil evaporation out of layer i (mm)

E_s rate of evaporation (mm)

E_w wet evaporation rate (mm t^{-1})

E evapotranspiration (mm, $\text{kg m}^{-2}\text{s}^{-1}$)

F_1 total-area fraction of irradiated leafs on a branch

F_R cumulative fraction of fine roots to depth z (m)

F_{p-N} angle factor between a person and surface N

F moisture release by combustion (mm, $\text{kg m}^{-2}\text{s}^{-1}$)

$G_{b,b+1}^m$ conductive heat flux between layers b and b + 1 at timestep m (W m^{-2})

$G_{a,m}$ boundary layer conductance to heat transfer ($\text{mol m}^{-2}\text{s}^{-1}$)

$G_{s,t}$ total conductance from the soil air space to the air above the boundary layer (m s^{-1})

G_{ws} conductance of water vapour through the soil pore space (m s^{-1})

H_{blt} building height (m)

H_{crown} crown height (m)

H_{trunk} trunk height (m)

H_{can} summed canopy patch convective sensible heat fluxes per canopy plan area (W m^{-2})

H_{top} convective sensible heat flux density between canopy air and boundary layer (W m^{-2})

H convective sensible heat flux density (W m^{-2})

H tree height (m)

H internal body heat production (W m^{-2})

I_i infiltration into layer i (mm)

I piped water supply per unit horizontal area (mm, $\text{kg m}^{-2}\text{s}^{-1}$)

$K \downarrow_{dif,i}$ initial incident diffuse shortwave (W m^{-2})

$K \downarrow_{dif}$ domain-level incoming diffuse shortwave (W m^{-2})

$K \downarrow_{dir,i}$ initial incident direct shortwave (W m^{-2})

$K \downarrow_{dir}$ domain-level incoming direct shortwave (W m^{-2})

$K \downarrow$ downward shortwave radiative flux density (W m^{-2})

$K \uparrow$ upward shortwave radiative flux density (W m^{-2})

K_{th} soil thermal conductivity ($\text{W m}^{-1}\text{K}^{-1}$)

LAI leaf area index ($\text{m}^2 \text{ m}^{-2}$)

$L \downarrow_{i,sky}$ initial incident sky-derived longwave (W m^{-2})

$L \downarrow_{sky}$ domain-level incoming longwave (W m^{-2})

$L \downarrow$ downward longwave radiative flux density (W m^{-2})

$L \uparrow$ upward longwave radiative flux density (W m^{-2})

$L_{A,i}$ area of the ith leaf over ground area (m^2)

L_T total canopy leaf area index ($\text{m}^2 \text{ m}^{-2}$)

L_d relative leaf area density within the tree crown (m^{-1})

L_d thickness of the dry layer at the soil surface (m)

$L_{v,i}$ fine root density (mm^{-3}) in layer i

L dry respiration heat loss (W m^{-2})

Nu Nusselt number (-)

PMV predicted mean vote (PMV)

P_a partial vapour pressure (Pa)

P_o vapour pressure of water at infinite temperature ($=7.5152 \times 10^8$ mb)

P_u surface water for infiltration (snow melt + throughfall) (mm)

Pr Prandtl number (-)

P precipitation (mm)

Q_C soil heat transport (to deeper soil layers) (W m^{-2})

$Q_{E,canopy}$ latent heat flux calculated from *canopystore* (W m^{-2})

$Q_{E,et}$ latent heat flux calculated from *et* (W m^{-2})

$Q_{E,evap}$ latent heat flux calculated from *evapstore* (W m^{-2})

$Q_{E,soil}$ latent heat flux calculated from *soilstore* (W m^{-2})

$Q_{E,veg}$ calculation of vegetation latent heat flux (W m^{-2})

Q_E latent heat flux (W m^{-2})

Q_F anthropogenic heat (W m^{-2})

$Q_{G,street}$ calculation of street ground heat storage (W m^{-2})

$Q_{G,veg}$ calculation of vegetation ground heat storage (W m^{-2})

Q_{GI} global radiation (solar + downward thermal) (W m^{-2})

Q_G ground heat storage (W m^{-2})

$Q_{H,veg}$ calculation of vegetation sensible heat flux (W m^{-2})

Q_H sensible heat flux (W m^{-2})

Q_L longwave radiation (W m^{-2})

Q_{veg}^* calculation of vegetation net radiation flux density (W m^{-2})

Q^* net radiation flux density (W m^{-2})

R_A aerodynamic resistance (s m^{-1})

R_s surface resistance (s m^{-1})

$R'(h)$ crown radius at the relative crown height h (m)

R_i^{q+1} radiation reflected by patch i at reflection $q + 1$

R_j^q radiation reflected by patch j at reflection q

$R_{lg,i}$ longitudinal resistance to water flow ($\text{MPa s m}^2 \text{ mol}^{-1}$)

$R_{rad,i}$ radial resistance to water uptake (across the root epidermis to the xylem) ($\text{MPa s m}^2 \text{ mol}^{-1}$)

$R_{sr,i}$ soil-to root surface hydraulic resistance ($\text{MPa s m}^2 \text{ mol}^{-1}$)

$R_{sr,t}$ total hydraulic resistance for all soil layers combined ($\text{MPa s m}^2 \text{ mol}^{-1}$)

Re Reynolds number (-)

R ideal gas constant ($=8.314 \text{ J mol}^{-1}\text{K}^{-1}$)

R heat loss by radiation from the surface of a clothed body (W m^{-2})

S^* $S^* = S/S_{max}$

S_0 solar constant ($=1367 \text{ W m}^{-2}$)

S_i soil water storage in layer i (mm)

S_{max} maximum solar irradiance that would be received in the absence of the atmosphere (W m^{-2})

S horizontal solar irradiance (W m^{-2})

$T(z)$ air temperature at height z (K)

T_a dry bulb air temperature (K)

T_{cl} clothing surface temperature

T_{mrt} mean radiant temperature ($^{\circ}\text{C}$)

$T_{s,1}$ soil surface temperature (K)

$T_{s,2}$ soil temperature at layer 2 (K)

$T_{sfc,i}$ surface temperature of patch i (K)

T_{sfc} surface temperature (K)

T_1 temperature of the shallowest layer (K)

T_N surface temperature of surface N (K)

T_{air} air temperature (K)

T_a air temperature at z_{ref} (K)

T_b temperature of layer b (K)

T_{can} canopy air temperature ($z < z_H$) (K)

T_{conv} converging canyon temperature (K)

T_g globe temperature (K)

$T_{log}(z)$ air temperature profile above z_H (K)

T_m temperature of the deepest layer (K)

T_o temperature (K)

$T_{sfc,veg}$ vegetation surface temperature (K)

T_s soil surface temperature (K)

Time time (seconds)

T temperature (K)

$U(z)$ wind speed at height z (m s^{-1})

$UTCI$ universal thermal climate index

U_a wind speed at z_{ref} (m s^{-1})

$U_{eff}(z)$ effective wind speed at height z (m s^{-1})

V_w partial molal volume of water ($\text{m}_3 \text{ mol}^{-1}$)

W_{can} water storage of the canopy (mm)

W_i water storage of the layer i (mm)

Z total soil depth (m)

ΔA net moisture advection (kg; $\text{kg m}^{-3}\text{s}^{-1}$)

ΔH_{vap} enthalpy of evaporation ($=42809 \text{ J mol}^{-1}$)

ΔQ_A net advective (horizontal air movement) heat flux (W m^{-2})

ΔQ_S storage heat flux density (volume) (W m^{-2})

ΔS net moisture storage (kg; $\text{kg m}^{-3}\text{s}^{-1}$)

Δ_s slope of the specific humidity/ temperature curve between the air temperature T_D and the surface temperature of the vegetation T_s ($\text{kg kg}^{-1} \text{ }^\circ\text{C}$)

Δr net run-off (mm, $\text{kg m}^{-2}\text{s}^{-1}$)

Δt timestep size (s)

Δx_b depth of layer b (m)

$\Delta z_{1,2}$ depth difference between the second and first layer (m)

Ψ_L leaf water potential (MPa)

$\Psi_{R,i}$ root xylem water potential in layer i (MPa)

$\Psi_{S,i}$ soil water potential in layer i (MPa)

Ψ_f reference water potential (MPa)

$\Psi_{i,external}$ view factor from patch i to external surfaces

$\Psi_{i,j}$ view factor from patch i to patch j

$\Psi_{i,sky}$ sky view factor of surface patch i

$\Psi_{j,i}$ view factor from patch j to patch i

$\Psi_{s,1}$ soil water potential in the surface layer (MPa)

α_g globe albedo (=0.05)

α_i shortwave albedo of patch i

α_{sfc} surface albedo (=0.15)

α_{veg} shortwave albedo of vegetation

α shortwave albedo

β parameter which specifies the shape of the distribution

χ_i angle between patch i's normal vector and the vector pointing in the direction of the sun (degrees)

δA change in rate of assimilation ($\text{mol m}^{-2}\text{s}^{-1}$)

δE change in the rate of transpiration per unit area of leaf ($\text{mol m}^{-2}\text{s}^{-1}$)

ϵ_a longwave emissivity of the atmosphere

ϵ_g globe emissivity (=0.95)

ϵ_i longwave emissivity of patch i

ϵ_{sfc} surface longwave emissivity

ϵ_{veg} longwave emissivity of vegetation

ϵ longwave emissivity

γ degree of implicitness (conduction) (i.e. $\gamma = 0$ is explicit, $\gamma = 1$ is implicit)

γ latent heat of water ($=2.47 \times 10^6 \text{ J kg}^{-1}$)

λ_f frontal-area-to-plan area ratio

λ_p building-to-plan area ratio

ω_s tortuosity of the soil air space (-)

\overline{T}_r mean radiant temperature (K)

$\overline{\Psi_R}$ mean root water potential (MPa)

ϕ infiltration parameter (0-1)

ϕ solar zenith angle (degrees)

ρ density of air ($=1.2 \text{ kg m}^{-3}$)

σ Stefan-Boltzmann constant ($=5.67 \times 10^{-8} \text{ W m}^{-2}\text{K}^{-4}$)

θ_1 soil volumetric water content of layer 1 ($\text{m}^3 \text{ m}^{-3}$)

θ_i soil volumetric water content of the dry layer at the soil surface ($\text{m}^3 \text{ m}^{-3}$)

θ solar zenith angle

c_ρ specific heat of air at constant pressure ($=1.01 \times 10^3 \text{ J kg}^{-1} \text{ K}^{-1}$)

$c_{air,H}$ average heat capacity per unit plan area of air below z_H ($\text{J m}^{-2}\text{K}^{-1}$)

$c_{w,kj}$ conversion to watts ($=1\text{W}/1000\text{KJ/sec}$)

c conversion to molar units

$diam_{stem}$ stem diameter (m)

d earth-sun distance ($=1 \text{ A.U.}$)

d index of agreement ($0 \leq d \leq 1$)

e_a partial water vapour pressure of the air (kPa)

e_a water vapour pressure at z_{ref} (hPa)

e_{sat} saturated vapour pressure (kPa)

e_s partial water vapour pressure of the soil pore space (kPa)

et evapotranspiration (mm)

$f(D)$ function of the leaf-to-air vapour pressure deficit (D)

f_{dir} fraction of the total horizontal solar irradiance, S , due to the direct beam of the sun

g_0 conductance when A_n is zero ($\text{mol m}^{-2}\text{s}^{-1}$)

g_1 conductance empirical parameter

g_B boundary layer conductance ($\text{mol m}^{-2}\text{s}^{-1}$)

g_C canopy conductance ($\text{mol m}^{-2}\text{s}^{-1}$)

g_V total conductance to water vapour ($\text{mol m}^{-2}\text{s}^{-1}$)

g_s leaf-level stomatal conductance to CO_2 ($\text{mol m}^{-2}\text{s}^{-1}$)

g_s leaf-level stomatal conductance to H₂O (mol m⁻²s⁻¹)

h_i heat transfer coefficient (W m⁻²K⁻¹)

h_{top} convective heat transfer coefficient between canopy air and boundary layer (W m⁻²K⁻¹)

h relative height within the tree crown or the canopy

h convective heat transfer coefficient (W m⁻²K⁻¹)

k_1 thermal conductivity of the surface (W m⁻¹K⁻¹)

k_L total leaf-specific hydraulic conductance (mmol m⁻²s⁻¹MPa⁻¹)

k_p plant component of the leaf-specific hydraulic conductance (mmol m⁻²s⁻¹MPa⁻¹)

k_V von Karman's constant

k thermal conductivity of the fluid (i.e. air) (W m⁻¹ K⁻¹)

l_p length of a patch side (m)

$m_{mol,w}$ molar mass of water (=18.0152g mol⁻¹)

m timestep index

n_{hts} number of building heights

n_{roofs} number of roofs

n total number of patches

q_o surface humidity (kg kg⁻¹)

q_w, T_d saturated specific humidity at dry-bulk temperature, T_D (kg kg⁻¹)

r_{xcrown} crown radius in x direction (m)

r_{ycrown} crown radius in y direction (m)

r_1 free throughfall fraction (0-1)

r_2 canopy drainage parameter (mm)

r_3 canopy drainage parameter (-)

r_a aerodynamic resistance to the transport of water vapour from the surface to the reference level z (s m⁻¹)

r_c (Monteith) canopy resistance to the transport of water from some region within or below the evaporating surface to the surface itself, and is expected to be a function of the stomatal resistance of individual leaves. Under wet-canopy conditions $r_c = 0$ (s m⁻¹)

r_{sti} effective surface resistance of the leaves of ith area (s m⁻¹)

r_{st} effective surface resistance of the leaves (s m⁻¹)

$r_{w,i}$ wall roughness coefficient of patch i

rh relative humidity (%)

r horizontal distance from the centre of the tree trunk (m)

s_f steepness of the response of $f\Psi_L$ to Ψ_L

tr transpiration ($\text{mmol H}_2\text{O m}^{-2}\text{s}^{-1}$)

u_z wind speed measured at a height of z_H (m s^{-1})

ws_{cm} wind speed (cm s^{-1})

ws wind speed (m s^{-1})

$z_{0,Ht}$ roughness length (m)

z_{0town} roughness length for momentum (domain) (m)

z_0 roughness length (m)

z_D displacement height (m)

z_{Ht} measurement height of wind speed (m)

z_H mean building height (m)

z_H measurement height of wind speed (m)

z_{PD} zero-plane displacement height (m)

$z_{horz,i}$ height of patch forcing $U(z)$ and $T(z)$ above street level of patch i (m)

z_i depth to the bottom of layer i (m)

z_{ref} reference height for forcing data (m)

z height in the model domain (m)

CSUD climate sensitive urban design

HTC human thermal comfort

PBM process based model

RMSE root mean square error

SEB surface energy balance model

UBL urban boundary layer

UHI urban heat island

WSUD water sensitive urban design

Chapter 1

Introduction

1.1 Project overview

Urban areas are facing a growing number of problems. Populations of urban areas are becoming denser and demographics are shifting towards increased older and elderly citizens. There are rapid conversions of green spaces into urban areas. Climate trends are towards increased average temperatures and increasing temperature extremes. At the same time, there is an increasing understanding of impacts to human health of extreme temperatures. These factors leave those in urban areas in an increasingly dangerous position. In coming years, strategies are needed to adapt to and deal with these challenges.

From an examination of a range of different studies exploring cooling effects of urban greenery, it is clear that increased vegetation and water does have an impact, from city-wide scale down to a micro-climate street level scale (Coutts et al. 2012). Shading and evapotranspiration are cited (Bowler et al. 2010) as the main drivers of these cooling effects. Also cited are factors of vegetation density, orientation, and amounts of irrigation used.

Incorporating water sensitive urban design (WSUD) and urban greening principles into urban areas can be an effective way to deal with many of these problems. WSUD is premised on the use of stormwater as an additional urban water source. It uses engineered and natural features (trees and vegetation) to capture, filter, and store water, while restoring a more natural water balance distorted by impervious surfaces and other modifications to previously natural landscapes (Wong & Brown 2009).

However, guidance on how to most effectively use WSUD is lacking, as well as solid quantitative assessments of how well WSUD can perform in urban areas in terms of heat mitigation. In addition, no suitable tool exists to make these assessments. Therefore, this project aims to create a tool suited to this purpose, undertake an extensive and robust validation, and demonstrate how the tool can be applied to quantify the effectiveness of WSUD on human thermal comfort. This tool will allow users to conduct assessments of the most effective arrangements of WSUD features to help inform WSUD best practice. With this tool and the guidance gained from it, WSUD can be used in the most effective ways to help solve many of these pressing problems.

1.2 Urban growth

Urban areas are quickly changing, presenting challenges on how best to manage them for those growing populations. Urban areas are now the most common environment for human

habitation, with 54% of the world's population living in urban areas in 2014 (UNDESA 2015). Projections are for even larger and more crowded cities in the future (WHO 2016). As the home to the majority of the world's population, understanding the climate in urban areas is critical to protecting human health in the face of rapid changes overtaking these areas.

1.2.1 Growing urbanism

Currently, the majority of the world's population is living in cities, 54% in 2014, growing by approximately 1.8% yearly (WHO 2016). Australia, as with all developed nations, is even more intensely urbanised (PDDESA 2007) with 66% of the population already living in a capital city in 2012 and numbers projected to increase to 74% by 2061 (ABS 2013). In addition, Australia is growing rapidly. ABS (2013) projects that population will grow from 22.7 million in 2012 to 36.8-48.3 million in 2061 and 42.4-70.1 million in 2101.

Australia is also ageing rapidly. The median age in years will increase from 37.4 in 2012 to 41.0-44.5 in 2061. This will include a shift of 22% of the population in 2061 over 65 years old (and 25% in 2101) compared to 14% in 2012 and a growth in those over 85 years from 2% in 2012 to 5% and 6% in 2061 and 2101 (ABS 2013) (summarised in Table 1.1).

Table 1.1: Australian projected population and demographic changes (ABS 2013).

	2012	2061	2101
Population (millions)	22.7	36.8-48.3	42.4-70.1
In capital cities (%)	66	74	
Median age (years)	37.3	41.0-44.5	
Over 65 (%)	14	22	25
Over 85 (%)	2	5	6

1.3 Climate change

Uncertainty exists over what the exact impacts will be of a changing climate around the globe and in urban areas. The next section will examine a number of aspects of climate change and their possible impacts on human thermal comfort in urban areas. An understanding of these impacts is a first step in formulating urban responses to these changes to protect human health.

1.3.1 Temperatures

While there are international efforts under way to limit future emissions and reduce the intensity of temperature increases, in the near term, these efforts will likely fall short. An analysis of the pledges from the 2009 Copenhagen Accord concludes the promised reductions are inconsistent with meeting the lower bounds of a 1.5°C increase (UNEP 2011), while an analysis of Paris COP21 pledges (without increasing emission reduction ambitions by 2030) predicts only a 8% likelihood of limiting warming to 2°C (Fawcett et al. 2015). Furthermore, Ranger et al. (2012) finds that it is already too late to limit average global mean temperature increases to less than 1.5°C . If inaction continues into the future, these increases could be significantly greater than 1.5°C (Sanderson et al. 2011).

Climate change projections by Collins et al. (2013) predict global mean surface temperature increases for 2081-2100 relative to 1986-2005 of 0.3-1.7°C , 1.1-2.6°C , 1.4-3.1°C , and 2.6-4.8°C under scenarios RCP2.6, RCP4.5, RCP6.0, and RCP8.5. The four scenarios represent

the amount of total radiative forcing in year 2100 relative to 1750 (2.6 W m⁻², for example). And the scenarios represent, respectively, different human responses to climate change (from mitigation through stabilisation to high emissions) and ending CO₂ concentrations of 421 ppm, 538 ppm, 670 ppm, and 936 ppm.

These are global average projections. The distribution of increases across Australia are predicted by CSIRO (2008) to see larger rises in inland areas than in coastal regions (which contain the main population centres), so the major urban areas of Australia might not see these full temperature rises (rises of 1.0-1.2°C inland compared to 0.7-0.9°C) (Garnaut 2008).

While the exact magnitude of increases are unknown, it is quite likely that urban areas in Australia will have to adapt to at least a 1°C or greater average local temperature increase in the near future and even greater increases in the long term. These future temperature increases are a first large challenge for urban areas, a challenge which adaptation strategies using WSUD could address.

1.3.2 Extremes

While increases in global average temperatures (and associated local temperature increases) could have significant impacts on urban areas and human health, an even more significant challenge is the trend of increasing temperature extremes. Increasing extremes will be manifested through more frequent extreme events, for example, increasing frequency of heat waves. They can also bring increases in intensity, in the case of heat waves, longer heat wave durations and hotter days within heat waves. Globally, projected trends in extreme temperatures are towards increasing numbers of warm extremes (both higher temperature days and number of these days) and decreasing numbers of cold extremes which will be further driven by increasing mean temperatures (Nicholls & Alexander 2007).

In Australia, projections of future trends are for increasing warmer nights and while seeing decreasing frost days (Alexander & Arblaster 2009) (Figure 1.1b), with the changes accelerating sharp rises of these predicted in the future under Intergovernmental Panel on Climate Change (IPCC) B1, A1B, and A2 scenarios. More worrisome are predictions concerning increasing extremes, such as longer duration (Figure 1.1a) and more intense heat waves (Figure 1.1b) (Alexander & Arblaster 2009) detailed in the IPCC Fourth Assessment Report (IPCC 2007) and shown in predictions of warmer days and warmer nights (Figure 1.2) contained in the IPCC Fifth Assessment Report (IPCC 2013a).

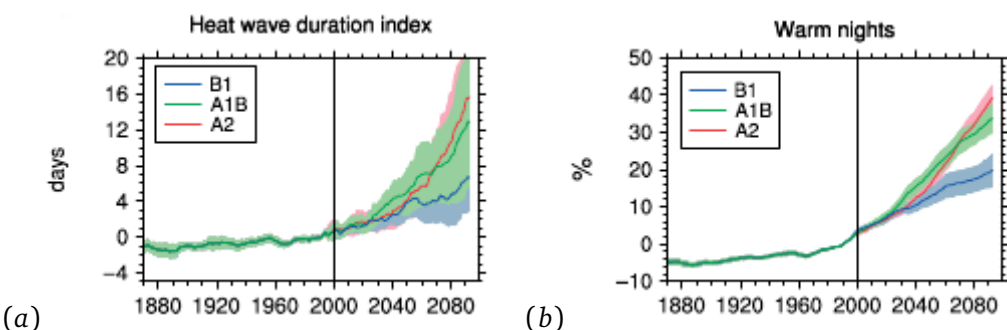


Figure 1.1: (a,b) Time series of areally averaged extremes indices (Frich et al. 2002) between 1870 and 2099 using grid boxes in Australia with the observed data (Alexander & Arblaster 2009, p. 430).

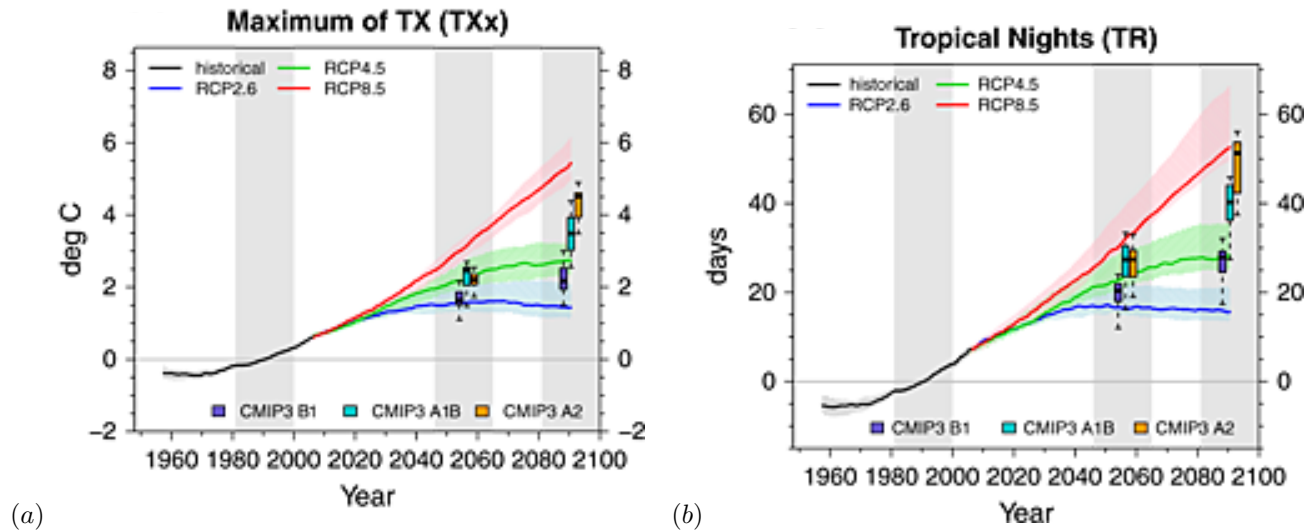


Figure 1.2: CMIP5 multi-model mean geographical changes (relative to a 1981-2000 reference period in common with CMIP3) under RCP8.5 and 20-year smoothed time series for RCP2.6, RCP4.5 and RCP8.5 in the (a) annual maximum of daily maximum temperature and (b) tropical nights (number of days above 20°C) (Sillmann et al. 2013, p. 1067).

Extreme events are found to be of great significance in contributing to human mortality, reaching their highest values during heat episodes (Laszewski & Jendritzky 2002). Research has identified that when particular thresholds are exceeded, namely heat wave duration or day and night average temperature, mortality rates tend to increase (Katsouyanni et al. 1993; Nicholls et al. 2008), with areas with intense but irregular heat waves showing the greatest sensitivity (Kalkstein & Smoyer 1993).

The European heat wave of 2003 caused 15,000 excess deaths in France (Poumadère et al. 2005) as well as increases in excess mortality of 66%, 100%, 128%, and 146% in age groups 60-70, 70-80, 80-90, and over 90 years old in Germany (Heudorf & Meyer 2005). Allen et al. (2016) attributed anthropogenic climate change for a 70% and 20% increase in heat-related mortality in Paris and London during the 2003 heat wave, with 506 deaths (of 735) and 64 deaths (of 315) attributable to climate change in the two cities.

Work examining heat thresholds (Figure 1.3) shows that moderating mean temperatures by just a few degrees could potentially have significant impact in reducing excess mortality, especially in older more vulnerable portions of the population (Loughnan et al. 2010b). Moderating night-time temperatures (as a component of daily averages) might be just as important as daytime maximums, as a respite and time for recovery (Bi et al. 2011).

Given these concerns over human health, as well as other aspects essential for supporting human habitation, possible mitigation and adaptation in urban areas to these trends need to be examined.

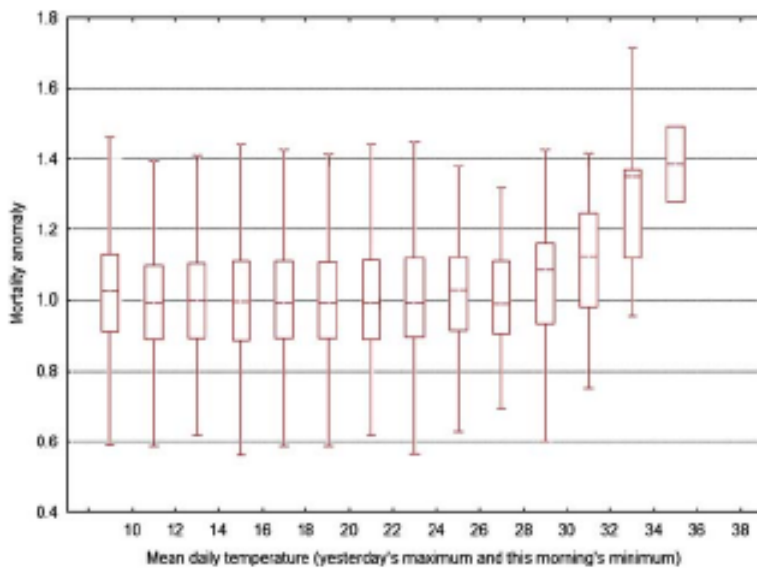


Figure 1.3: Melbourne heat index thresholds (Nicholls et al. 2008, p. 378).

1.4 Urban water management

A major challenge facing urban areas is securing urban water supplies. In Australia, a significant component of climate change is a projected decrease in rainfall. All Australian states are projected to see a significant rainfall decrease over the next century (Table 1.2). This is a trend already influencing, along with other factors, run-off flowing into Melbourne's reservoirs (Figure 1.4), dropping from an average of 615 GL/year in 1913-1996 to 377 GL/year in 1997-2008 (Melbourne Water 2016b). These flows have rebounded, at the end of the Millennium drought, to an average over the period 2010-2015 of 503 GL/year (Melbourne Water 2016b), however these rates are still below historic levels, as well as having occurred during a strong La Niña (Bureau of Meteorology 2012b).

In hydrological modelling of Australian catchments, Jones et al. (2006) found that a 1% decrease in rainfall can lead to a corresponding 2-3x decrease in run-off. Growing populations combined with decreasing rainfall and decreased run-off will mean decreasing water availability for urban areas in the future under existing water management strategies. Interventions will be needed in some combination of; modifying water collection and storage infrastructure, influencing usage behaviour, and locating alternative water supply sources.

Table 1.2: Projected changes to statewide annual average rainfall, best-estimate outcome in a no-mitigation case (percent change relative to 1990) (Garnaut 2008, p.116).

	NSW	Vic.	Qld.	SA	WA	Tas.	NT	ACT
2030	-2.5	-3.5	-2.4	-4.2	-4.1	-1.4	-2.5	-2.8
2070	-9.3	-12.9	-9.6	-15.5	-14.9	-5.1	-9.0	-10.3
2100	-13.7	-19.0	-12.7	-22.9	-21.9	-7.8	-13.3	-15.2

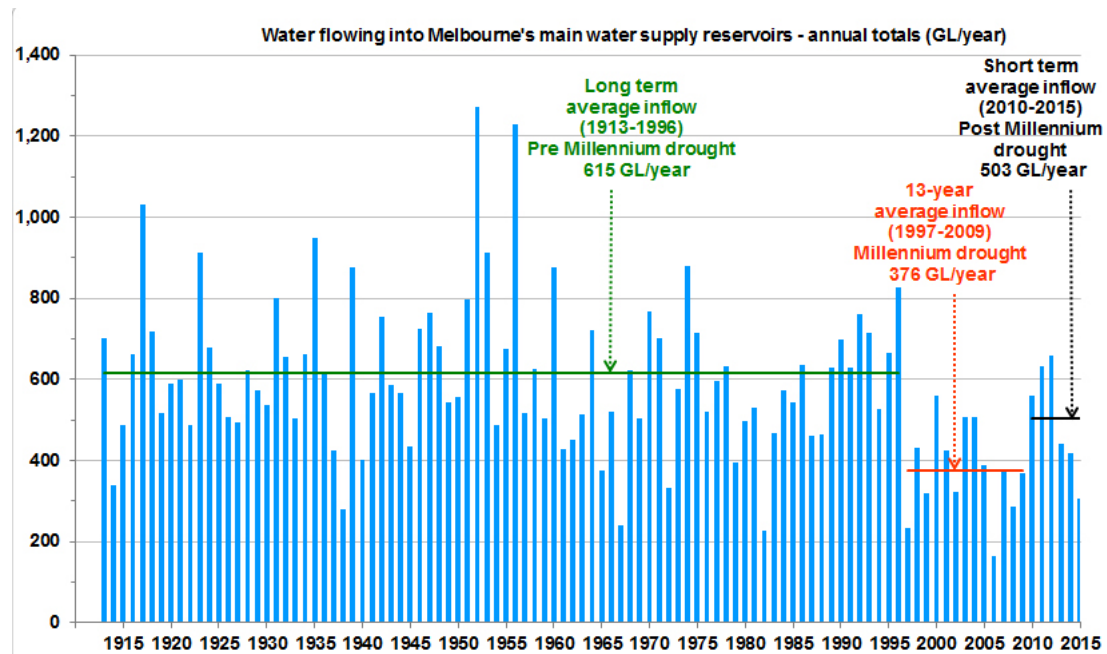


Figure 1.4: Water flowing into Melbourne's main water supply reservoirs (annual totals) (Melbourne Water 2016b).

1.5 Increased urbanisation and urban warmth

Much attention has been devoted to studying the climate and changes at a global level and possible impacts of these changes (IPCC 2007), but much less at a micro-climate level. Micro-climates are the scale at which people live and experience climate and weather. One implication of increased urbanisation is the urban heat island (UHI) effect (Figure 1.5), that is increased warmth in urban areas due to a range of factors including increased daytime heat storage, decreased night-time heat release, and decreased evapotranspiration (Arnfield 2003; Coutts et al. 2007; Chow et al. 2012).

As seen in the discussion of extremes (Section 1.3.2), exceeding thresholds of average daytime and night time temperatures can contribute to significant increases in mortality and morbidity, which are exacerbated by urban surfaces that do not cool off as rapidly at night. Further, the projections of increasing heat extremes from climate change do not include the additional warming influences of urban areas.

1.5.1 The challenge of changing urban areas

As cities such as Melbourne are becoming more populous and must accommodate those increased housing needs, changing morphologies present a challenge to the health of the population. Housing trends in cities like Melbourne have been towards newly built detached dwellings in the outer suburbs as well as an increase of medium density housing in the inner and middle suburbs (Peter McNabb & Associates Pty Ltd & University of Melbourne Research Team 2001). Market demand is also emphasising increasing the supply of low to medium density housing (DSE 2002).

The latest planning strategy from the Victorian Government proposes to focus on several areas to fulfil these shortfalls. City centres will be densified (as well as growth encouraged in regional

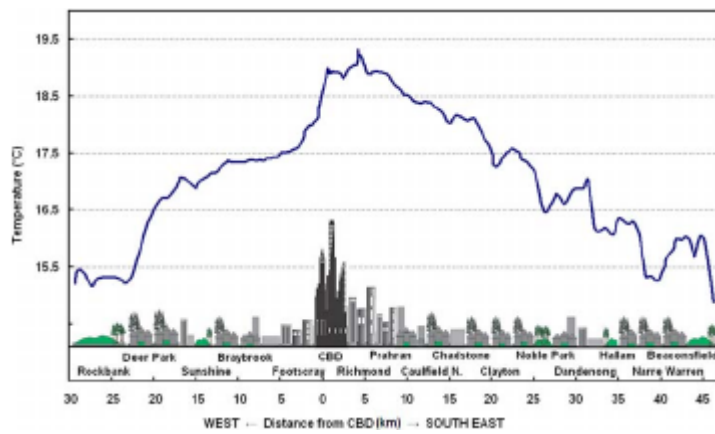


Figure 1.5: Spatial variability of the Melbourne urban heat island at 0100, 23 March 2006. Maximum urban heat island intensity of around 4°C with peak warming in the CBD and high density commercial and residential development to the east of the CBD. Recorded weather at the Melbourne Regional Office at midnight was 19.4°C with a westerly wind of 3 knots. The previous day's maximum temperature was 27.0°C (Coutts et al. 2010, p. 30).

satellite cities) while ensuring a fixed urban growth boundary is maintained to limit urban sprawl (State of Victoria 2014).

Political resistance to increased growth (and increased density infill and redevelopment) in some areas might have the effect of locking those areas off from change (Derkley 2014; Masanauskas 2013). This necessitates other areas will need to be redeveloped as much higher density to accommodate the needed growth. The physical results will likely modify the urban morphologies substantially into a tighter weave of high density and low density housing.

If these changes bring reduced green spaces and increased impervious surfaces, these changes will cause impacts to urban climates (Section 1.7). Coutts et al. (2007) suggests that unless heat mitigation interventions are considered, these changes will lead to worsening thermal comfort and increased heat storage with increased seasonal and diurnal exposure to these worsening conditions. Therefore, it will be important to understand the impacts of these changes on urban climates and whether WSUD will have utility in mitigating those changes.

1.6 Thermal comfort

Mitigation strategies to urban heat cannot be evaluated unless their effectiveness can be quantified. A brief discussion is needed here to find a method to link the influences of climate and built environments on the subjective experiences of humans and of their comfort and well-being (including situations which are stressful or even dangerous).

Research into thermal comfort has created techniques to make these links and determine thermal comfort levels from measurable properties of the surrounding environment. Many of the topics discussed previously, such as UHI or global mean temperature rises, have very large scale influences, but in order to examine the impacts on humans, the environment a few metres around a person at the human scale (or micro-scale), will need to be examined.

This topic will be covered in greater detail in the literature review (Section 2.3.1), but as seen there, a key parameter (in addition to air temperature, wind speed, and humidity levels) in

determining human thermal comfort (HTC) levels is mean radiant temperature (T_{mrt}). As these are derived from the temperatures of surrounding surfaces, the impacts that WSUD can have on modifying these surface temperatures and the subsequent impact on HTC levels flowing from those will require small scale observations (or model predictions) to capture these interactions.

1.6.1 Strategies to promote thermal comfort

HTC has now been established in this project as a method to capture climate and urban morphology interactions, as well as a method to rank the success of strategies to mitigate the challenges facing urban areas. In light of the goal of promoting HTC, some basic strategies can now be examined for their abilities to promote thermal comfort.

Best case mitigation strategies include plans to reduce CO₂ emissions through increased public transport and greater energy efficiency (ClimateWorks 2010) as well as projects to increase CO₂ storage in vegetation and trees (City of Melbourne 2011). However, as with the expected action (or inaction) on global emission reductions up to now being too little and too late to mitigate some level of warming (Section 1.3), mitigation in urban areas also will not be enough. Changes to urban climates in the future will require adaptation to the expected increases in mean temperatures and extremes.

1.6.2 Conventional strategies through mechanical cooling

Air conditioning will likely be an important adaptation response. Refrigerated air cooling usage has increased massively in Australia in recent years, increasing nationally from 25% of homes to 60% between 1999 and 2005 (ESS 2006). Achieving comfortable conditions of 23-24°C , the range ASHRAE (2008) recommends that humans are comfortable at and free of temperature stress, is only possible with air conditioning on hot and extremely hot days, and these expectations have lead to widespread usage (Strengers 2008).

For adaptation to heat wave emergencies, government adaptation strategies depend heavily on cooling through air conditioning, both in private homes and public centres (such as shopping malls, leisure centres, theatres) (Victoria Department of Health 2010). The Australian national framework (PWC 2011) outlines a planning and response strategy including a predictive warning system, ensuring the electricity grid is able to handle peak loads, and improving access to artificial cooling, especially for more vulnerable portions of the population.

Air conditioning accounts for more than 50% peak load on the electricity grid on hot days (Watt et al. 2003) causing increased carbon emissions and increased anthropogenic heat load, both at the electricity generation point and in urban areas. While these strategies make it possible for humans to cope with the conditions, these emissions and added heat load will further exacerbate mitigation responses and require larger adaptation strategies in the future.

Further, an over-reliance on air conditioning creates vulnerabilities based on the reliability of electricity supplies during heat waves and a de-acclimatisation to heat, increasing the risks of heat waves (Loughnan et al. 2012). It also restricts adaptation to indoor areas and does not account for transit or other necessities to be outdoors. Complimentary and alternative strategies will be needed to reduce outdoor temperatures and heat exposure in those areas.

1.6.3 Urban morphology strategies

Reforming urban areas can be a way to create urban areas more adapted to heat. Some of these techniques (detailed in Table 1.3) include using building materials with higher albedos/lower

thermal mass, insulating buildings against heat gain, and using vegetation for shading and evaporative cooling. These approaches redesign buildings so that they take advantage of shading, ventilation, reflections, and insulation for improved thermal comfort inside the buildings.

Table 1.3: Design aspects to decrease exposure to high temperatures (PWC 2011, p. 40).

Design aspect	Description	Environmental benefit	Individual benefit
Green roofs	Roof of a building that is partially or completely covered with vegetation	Carbon sequestration, water retention, energy conservation, reduced greenhouse gas emissions, UHI mitigation	Reduce heat-related illnesses, increase thermal comfort
Use materials with low thermal mass / increase albedo	The reflecting power of a surface. Increasing reflectivity over absorption in building materials	Reduce energy use and greenhouse gas emission, UHI mitigation	Reduce heat-related illnesses, increase thermal comfort
Use building compliance standards that promote environmental design	Six Star building ratings (accepted in all states except Tasmania and the NT), LEED (Leadership in Energy and Environmental Design) compliance standards	Increase building energy efficiency, reduce energy use and greenhouse gas emissions	Reduce heat-related and respiratory illnesses, positive aspects of increased natural light in workplace
Building insulation	Any object used to insulate buildings. Insulation can reduce heat gain	Increase energy efficiency of buildings, reduce energy use and greenhouse gas emissions	Increase thermal comfort, reduce heat-related illnesses and respiratory illnesses

Passive design, using building materials suited to reflecting solar radiation, as well as redesigning arrangements of buildings in urban morphologies so that they benefit from cooling effects through their orientation to wind flow and solar shading, can decrease the need for internal artificial cooling in buildings (Taylor & Guthrie 2008). These techniques can be taken further to help moderate temperatures in the surrounding areas. Modifications of building heights (Yamaoka et al. 2008) and street orientations and building materials (Ali-Toudert & Mayer 2006a) can lead to improved thermal comfort for those in urban canyons. Through these design changes, urban areas begin to generate their own resilience to heat rather than continuing a dependence on mechanical (and energy intensive) cooling methods.

1.7 Cooling through urban greening

While urban buildings and their arrangements can be designed to promote cooling effects, the rest of the urban canyon can also be designed to this end as well. Urban greenery can contribute to cooling effects in two different ways, through shading and increased evapotranspiration. A meta-analysis by Bowler et al. (2010) of a wide range of urban greening studies showed that a park was on average 0.94°C cooler than surrounding urban areas. A number of studies have found cooling effects of 0.5 °C to close to 3°C as well as larger localised shading effects of up to 12°C in physiologically equivalent temperatures (PET) (Tsiros 2010; Shashua-Bar & Hoffman 2000; Shashua-Bar et al. 2010; Spangenberg & Shinzato 2008) through urban greenery.

This issue will be considered in more detail in the literature review, and indeed, providing the tools to fill the gaps found in the understanding and quantification of cooling effects of urban greening will be the major focus of this project.

1.7.1 Water sensitive urban design (WSUD) as mitigation and adaptation

In examining the possible mitigation and adaptation strategies available to provide improved HTC in urban areas in light of all the challenges facing these areas, the use of WSUD can be considered an extension of both the cases of urban morphology changes and urban greening. Through increased incorporation of water sensitive principles into an urban landscape (Wong & Brown 2009), trees and other vegetation are added to fulfil a number of ecosystem services such as nutrient/pollution filtration. Stormwater is captured and stored and reused instead of being expelled from the system as waste water, allowing maintenance of the vegetation and increased use of water without having to draw more heavily on external sources.

Coutts et al. (2012) proposes an extension to WSUD, Climate Sensitive Urban Design (CSUD), which also includes the use of WSUD and WSUD features (especially the vegetated components shown in Figure 1.6) for urban climate benefits. The three mechanisms they cite to provide these benefits are oasis effects (cooling through evapotranspiration), the use of WSUD augmented water supplies to promote healthy vegetation, which provides shading and transpiration cooling effects, and finally the reduction of surface temperatures (Figure 1.7). However, with only a small body of work in this area, Coutts et al. (2012) cites the need for additional research to fully explore these possibilities. Indeed, the need for further research in this area will drive much of the research in this project.

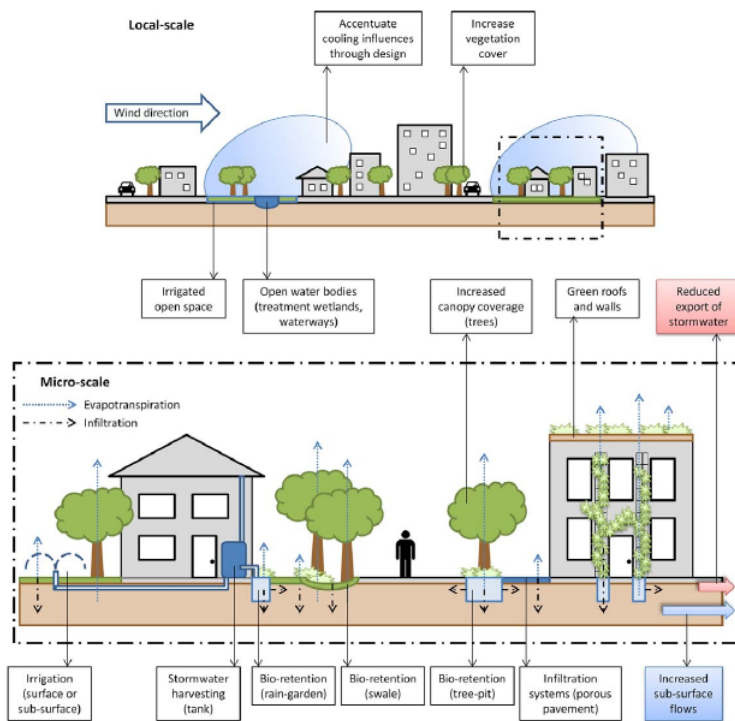


Figure 1.6: WSUD techniques and urban micro-climate (Coutts et al. 2012, p. 6).

Many of the changes that WSUD and CSUD provide reverse the drivers that Oke (1982) cites as contributors to UHI (Section 1.5). These include conversion of impervious surfaces to pervious to promote water infiltration to the soil, reduction of sensible heat fluxes by shifting the surface energy balance towards greater latent energy fluxes, and by using natural cooling to reduce the amount of artificial cooling needed (as well as their associated anthropogenic heat emissions).

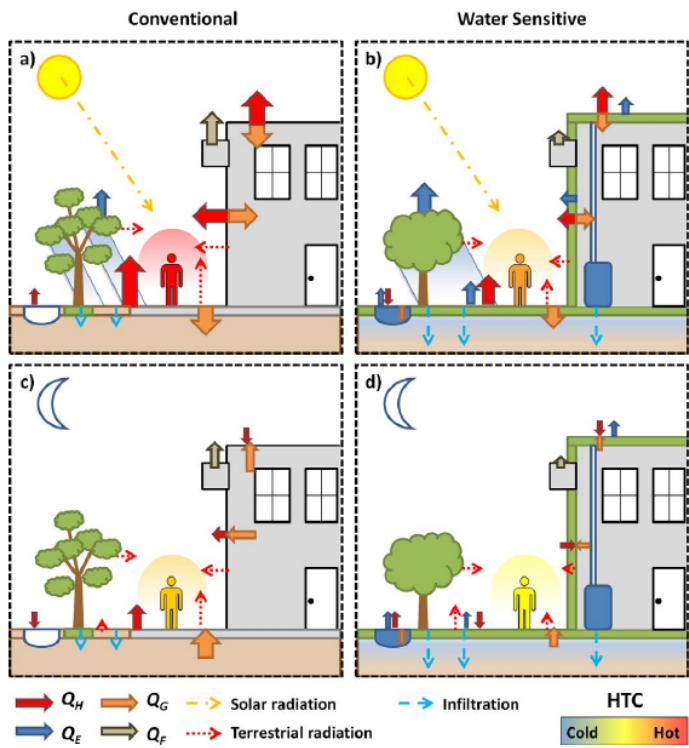


Figure 1.7: WSUD techniques and urban micro-climate (Coutts et al. 2013).

While there is a body of research, highlighted by Bowler et al. (2010), showing that parks act as cooler parts of urban areas, there has been less work done examining the effect of integrating park elements into urban areas and how that can bring those cooling benefits to the urban area at large. New urban development or re-development designed to encourage evapotranspiration and energy dispersal through latent energy fluxes can reduce the need for artificial air conditioning (saving the amount of anthropogenic heat released as well as a savings in CO₂ emissions) (Coutts et al. 2010).

WSUD features can facilitate these adaptations through features such as rainwater tanks, rain-gardens, wetlands, swales, infiltration systems, tree-pits, and porous pavements which increase soil moisture and increase the vegetation and availability of water in urban areas. In addition to these engineered features, trees and other types of vegetation are also considered to be WSUD features in their own right. The use of these features can promote changes at a local/neighbourhood scale, such as larger scale shading and cooling plumes from irrigated open space and water bodies. Improvements of HTC can also be felt at the micro-scale through increased shading, reduced sensible heat fluxes and ground heat storage.

1.8 Research aim

What is fundamentally needed is a tool to help inform urban planning and urban greening at the micro-scale to assess multiple development scenarios and determine the most effective way to achieve thermally comfortable urban spaces. That is the main aim of this research project, to develop, evaluate, and demonstrate this tool.

The lack of a suitable and accessible assessment tool (as will be shown in the Literature Review, Section 2.6) is a research gap. Furthermore, the lack of this assessment tool is a barrier to

bringing urban climate knowledge into urban planning. Urban planners are not able to use evidence based planning, evaluating differing design scenarios and their thermal comfort performance. This leaves urban areas increasingly vulnerable to urban heat and climate change progression as uninformed urban development continues.

1.9 Research objectives

In order to achieve the research aim, a number of objectives will need to be achieved. The key research objectives proposed for this project are:

- 1. Development of a modelling tool suitable to model specialised requirements of WSUD features to determine HTC at a micro-scale level.**

This new model, VTUF-3D (Vegetated Temperatures Of Urban Facets), needs to:

- Predict climate parameters in complex 3-D urban environments.
- Make accurate predictions of mean radiant temperatures in complex urban geometry.
- Capture the processes driving energy and water budgets of urban climates (Section 2.2.2) and interactions of the three layers of soil, plants, and atmosphere (Section 2.2.3) and their interactions with buildings and urban surfaces.
- Predict at a sufficient resolution (micro-scaled) to resolve human interactions with their surroundings and supply necessary parameters to calculate human thermal comfort index values (such as $UTCi$).
- Contain functionality to directly model or parameterise a variety of vegetation and WSUD features.

The creation of this model will require a unique and novel approach to modelling urban climates at a micro-scale, starting with careful design decisions to balance complexity and accuracy with usability, accessibility, and performance.

- 2. A validation of the new model**, particularly in critical areas of the model's operation and outputs, to determine the accuracy and limitations of the model. Determine the model's suitability to accurately capture important dynamics of WSUD and assess HTC improvements.

The validation steps will include:

- An evaluation of the surface energy balance of the model, which is a critical element of model performance in terms of surface energy partitioning. This will be achieved by comparing model output to flux tower observations and performing energy flux comparisons and error analysis as a measurement of accuracy.
- An evaluation of the model's accuracy in both temporal and spatial terms, using comparisons of modelled output to observations, examining parameters such as $UTCi$ and T_{mrt} . This will ensure that the model can resolve the detail across an urban canyon, and do so properly across a diurnal cycle.
- Validate VTUF-3D's ability to resolve the urban environment's influence, the geometry and make up of an urban canyon. These include validations that VTUF-3D can accurately reproduce:
 - * The periods of illumination and shading of the vegetation due to buildings and other elements of vegetation.

- * The predicted results of vegetation shading and transpiration in any location in an urban area.

3. Demonstration of the VTUF-3D model's ability to assess HTC impacts of WSUD.

Finally, a demonstration of the model's ability to fulfil the aim of this research project will be done. The bulk of future tasks VTUF-3D will be called on to perform will be comparisons of scenarios of future possible urban plans and assessments of how different arrangements and urban components influence thermal comfort. This demonstration will examine tree canopy cover variation scenarios and show the predicted outcome on HTC from a range of possible streetscape variations. The completion of this objective, examining one aspect of WSUD's influence on HTC, will show the utility of VTUF-3D in assessing and maximising the urban climate benefits of WSUD.

1.10 Research questions

This project is undertaken in this context. Urban areas are facing increasing challenges from growing and ageing populations. Climate change, urban warmth, and reduced rainfall are increasing the health risks of already vulnerable populations.

Thermal comfort analysis can be a method to assess these risks and compare different mitigation strategies. Studies on urban greening show they can have a cooling effect in urban areas. WSUD techniques will integrate vegetation into urban areas as well as provide water necessary to maintain it.

The lack of a model needed to understand the role vegetation, and other WSUD features, can play in influencing urban climates leads to the following research questions for this project:

- Can a model be devised for HTC assessments of WSUD?
- Can this new model be shown to be accurate and suitable for these assessments?
- Finally, can this new model be demonstrated as able to start answering questions and inform planning decisions with urban climate knowledge about how to best utilise urban greening to maximise the thermal comfort impacts?

Chapter 2

Literature review

2.1 Literature review overview

In this next section, a number of topics need to be introduced and examined to understand the background of this research, place it within the literature, and identify the research gap it will address. The first is urban climates, how they work and what drives them. The second is to examine how studies into human thermal comfort (HTC) allow this subjective experience to be quantified and how urban climates can impact HTC. Next, a review will determine the current state of the art in modelling of urban areas, especially in accounting for the impacts of vegetation. Finally, the building blocks needed to fulfil the overall aim of this project, potential modelling tools uncovered during this literature review, will be described.

2.2 Urban climates

The impact of urban landscapes upon its climate is the result of varying terrain and complex interactions of the atmosphere with the land features and artificial structures. These areas can act quite differently from natural terrains, causing urban areas to be significantly warmer than rural areas under the same climatic conditions, creating an urban heat island (UHI). Understanding these phenomena, their causes, and possible solutions requires examination starting at the most basic components and drivers, including the budgets of energy and water available to drive temporal and spatial variations in these areas.

Urban areas are impacted by meteorology and climate phenomena at a number of different scales (the range of spatial and temporal scales shown in Figure 2.1). Impacts will largely be seen at the scales which can resolve these areas, the local and micro-scales. Local scale encompasses the range of somewhat less than 1 to 10s of kilometres, while micro-scale resolution is under 1km. The micro-scale will predominate this project, as this is the scale which resolves humans and the environment that most directly impacts them.

2.2.1 Contributors to urban warmth

The emergence of UHI effects can be attributed to a number of factors unique in urban areas. Oke (1982) outlines a number of contributions to the effect which alter the surface energy balances in urban areas leading to increased sensible heat and storage fluxes and decreased latent energy fluxes. These include, at the canopy layer:

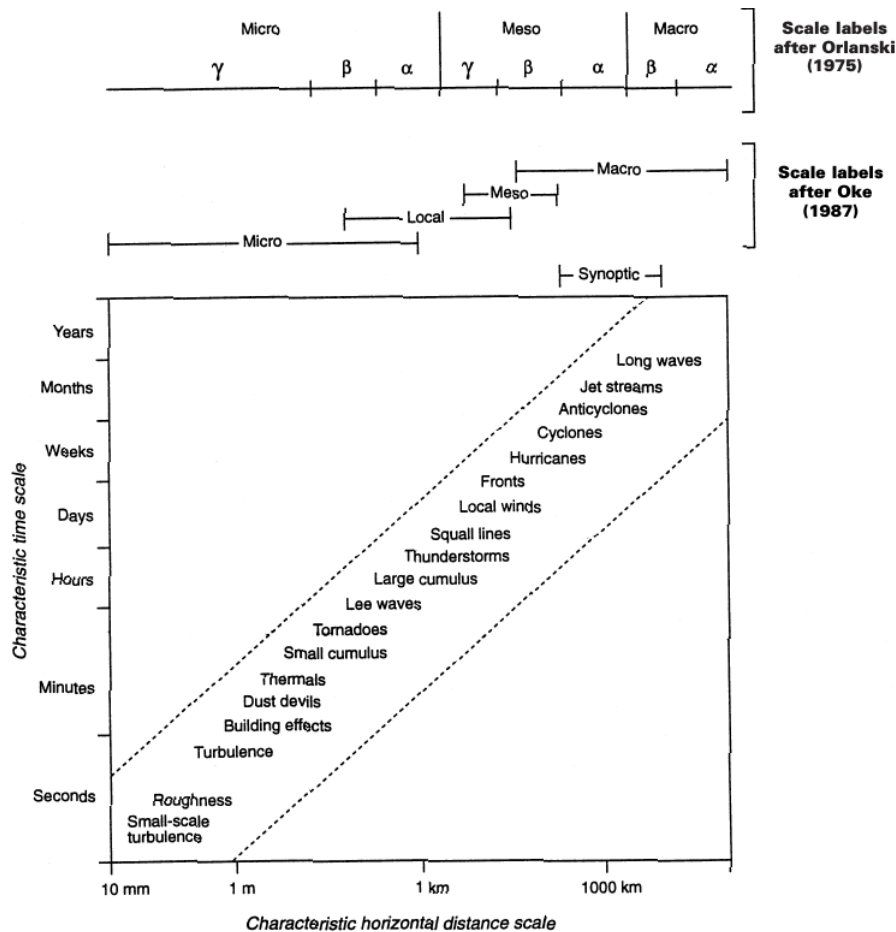


Figure 2.1: Characteristic time and space scales associated with atmospheric phenomena (Sturman et al. 1999, p. 612).

- 1) Absorption of short-wave radiation by urban canyons due to increased surface areas and multiple reflections of the energy.
- 2) Air pollution absorption and re-emission of downward long-wave radiation.
- 3) Long-wave radiation trapping in urban canyons due to a decreased sky view.
- 4) Human activity (buildings and transportation) creating additional anthropogenic heat emissions.
- 5) Emission of sensible heat increases due to the increased thermal admittance of urban materials.
- 6) Impervious surfaces leading to decreased latent energy fluxes.
- 7) Physical barriers to wind flow decreasing turbulent heat transport.

Especially important items to consider are items 5 and 6, surfaces and materials which reduce water infiltration into the soil, with reduced potentials for cooling through evapotranspiration, and increased sensible heat fluxes. As seen earlier in the Introduction (Section 1.7), conversion of these impervious surfaces to pervious in urban areas have cooling potential at a city-wide scale and more importantly for human thermal comfort (HTC), at a micro-scale.

At the boundary layer, Oke (1982), adds additional considerations which further alter the surface energy balance of urban areas, leading to the development of a boundary layer UHI including:

- 1) Air pollution at this level increasingly absorbing short-wave radiation.
- 2) Human emissions emitting anthropogenic heat at higher levels through chimneys and stacks.
- 3) A canopy heat island effect increasing sensible heat fluxes from roofs below the boundary layer.
- 4) Increased sensible fluxes from items 2 and 3 along with increased urban turbulence resulting in a greater downward heat flux from the urban boundary layer (UBL) capping inversion above.

In addition, other impacts due to urbanisation, particularly flowing from land use changes can have a wide ranging effect on the climate at a number of scales (as shown in Figure 2.2) and modify many of the physical parameters and processes and further shift energy balances in these areas. For example, modifications of surface types and landscape morphologies can lead to changes in surface roughness levels and soil moisture storage and infiltration capabilities leading to changes in sensible and latent heat fluxes and soil moistures (Cleugh & Grimmond 2012). As energy balance and water balance parameters change, these modify the way these landscapes react to and influence urban climate conditions.

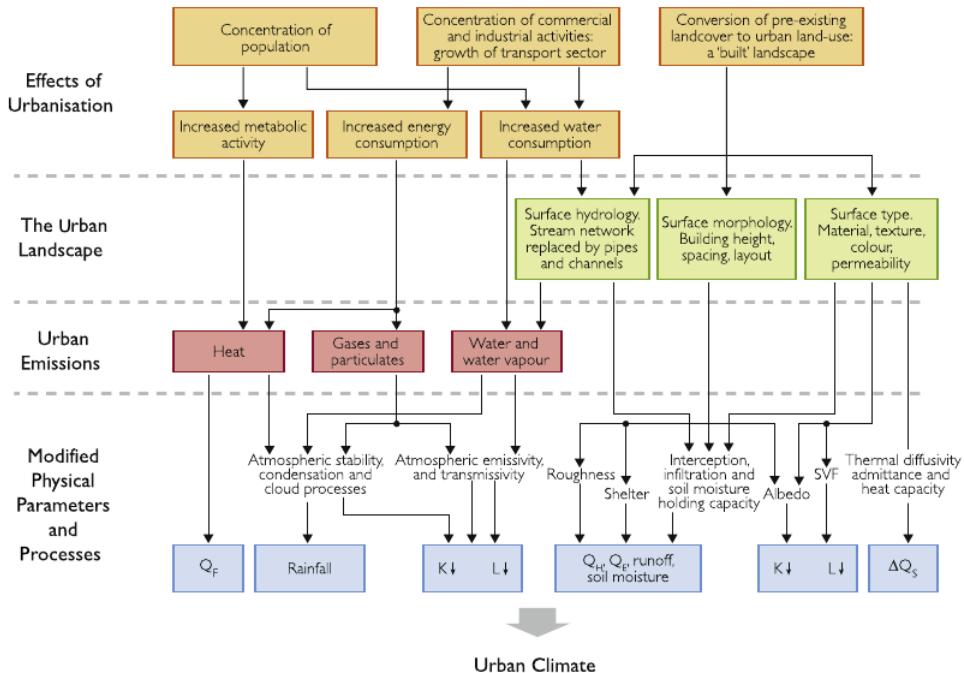


Figure 2.2: Effects of urbanisation on processes affecting climate at local- and regional-scales
(Cleugh & Grimmond 2012, p. 50).

2.2.2 Urban energy and water budgets

In order to understand the impacts due to modified energy balance parameters, a review of what these parameters are and how they work is needed. Incoming solar radiation (short-wave radiation from the sun) is the main driver of the energy budget of a urban micro-climate. The surface radiation budget of an urban area is defined by Oke (1988b) in Figure 2.3 and in Equation (2.2.1):

$$Q^* = K \downarrow - K \uparrow + L \downarrow - L \uparrow \quad (2.2.1)$$

with Q^* being net radiation, balanced by terms for incoming (\downarrow) and outgoing (\uparrow) K (short-wave solar radiation) and L (long-wave thermal radiation).

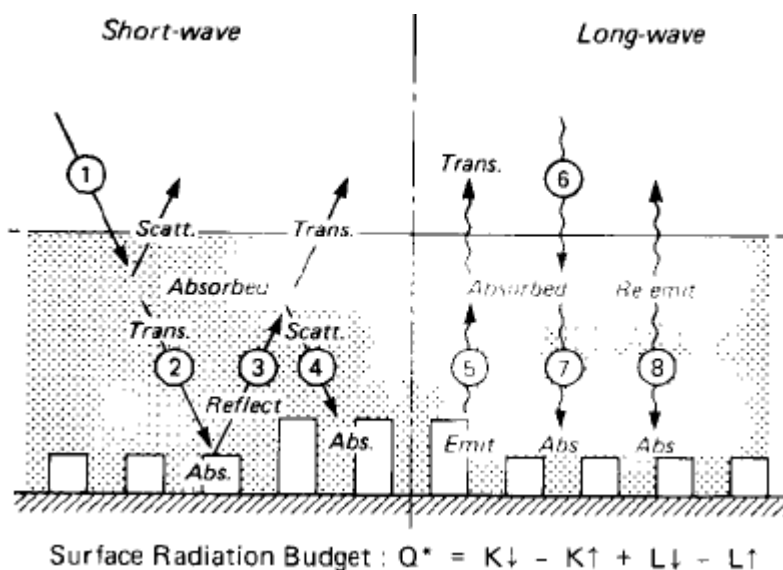


Figure 2.3: Urban surface radiation budget (Oke 1988b, p. 473).

Incoming short-wave solar radiation can be scattered in the atmosphere, transmitted through and either absorbed by the surface or reflected back out. Reflected short-wave will be re-scattered or transmitted outward as well as absorbed and stored. Absorbed short-wave radiation accordingly will be re-radiated as long-wave radiation, following possible paths of transmission outward or reabsorbed by the surface.

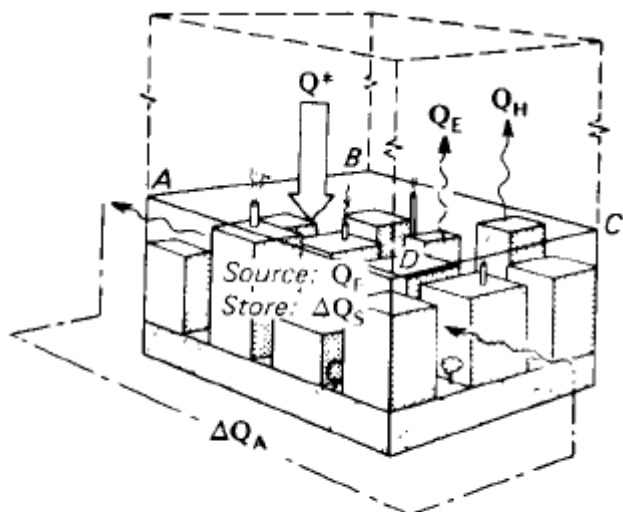
The surface energy budget, in more detail, within an urban environment is described by Oke (1988b) in Figure 2.4 and in Equation (2.2.2):

$$Q^* + Q_F = Q_H + Q_E + \Delta Q_S + \Delta Q_A \quad (2.2.2)$$

with Q^* being net radiation, Q_F anthropogenic heat, Q_H sensible heat flux (heated air), Q_E latent heat flux (through evapotranspiration), ΔQ_S heat storage (within the environment), and ΔQ_A net advective (horizontal air movement) heat flux.

The role water plays in an urban micro-climate can be described by the surface water budget, given by Oke (1988b) in Figure 2.5 in Equation (2.2.3):

$$P + F + I = E + \Delta r + \Delta S + \Delta A \quad (2.2.3)$$

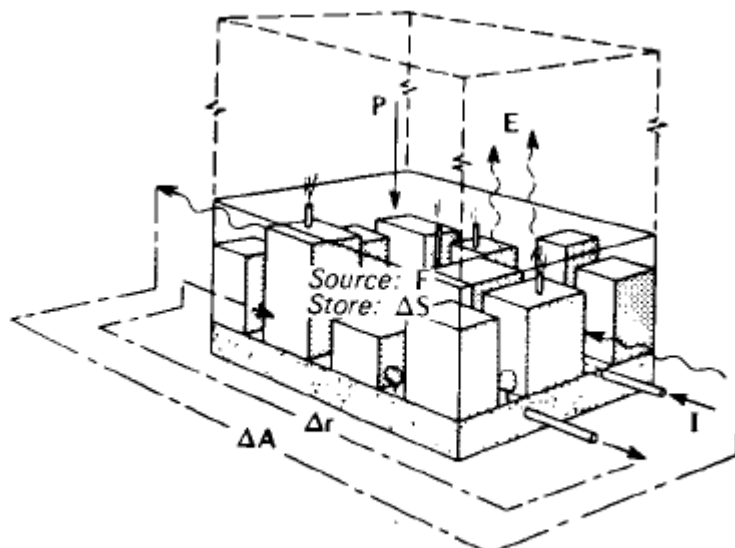


$$\text{Surface Energy Budget :}$$

$$Q^* + Q_F = Q_H + Q_E + \Delta Q_S + \Delta Q_A$$

Figure 2.4: *Urban surface energy budget (Oke 1988b, p. 473).*

where P is precipitation, F is moisture release by combustion, I is the piped water supply, E is evapotranspiration, Δr is net run-off, ΔS is net moisture storage, and ΔA is net moisture advection. The evapotranspiration term (E) links together the energy and water budgets as evapotranspiration (latent energy) is an important cooling element in an environment.



$$\text{Surface Water Budget :}$$

$$P + F + I = E + \Delta r + \Delta S + \Delta A$$

Figure 2.5: *Urban surface water budget (Oke 1988b, p. 473).*

A final consideration in the drivers of an urban micro-climate is the role wind plays in temperature variations across an environment. Oke (1988b) presents idealised representations of atmospheric boundary layers (Figure 2.6-a) and the downwind effects created by features on the surface (Figure 2.6-b). The urban canopy layer (UCL) extends from ground level to the top

of urban buildings where these features create roughness with wind flow patterns and layer mixing. These effects extend upward through the urban boundary layer (UBL), finally leading to the planetary boundary layer (PBL), where effects are not seen. At a micro-climate level, wind provides mechanical mixing of atmospheric layers. Reduced wind speeds may have the effect of allowing warmer temperatures to build during a warm afternoon.

On the other hand, a calm night will tend to support reduced temperatures more than one where wind mixes warmer air aloft with colder ground air (Ahrens 2004). However, in urban areas, a lack of mixing might also contribute to a warmer canopy layer, reducing the amount of heat mixed away on calm nights, and contributing to retention of heat (creating an urban heat island) (Oke 1988a). Features within an urban micro-climate which either encourage or discourage wind and the mechanical mixing of warmer and cooler air layers will do much to create temperature variations across this area.

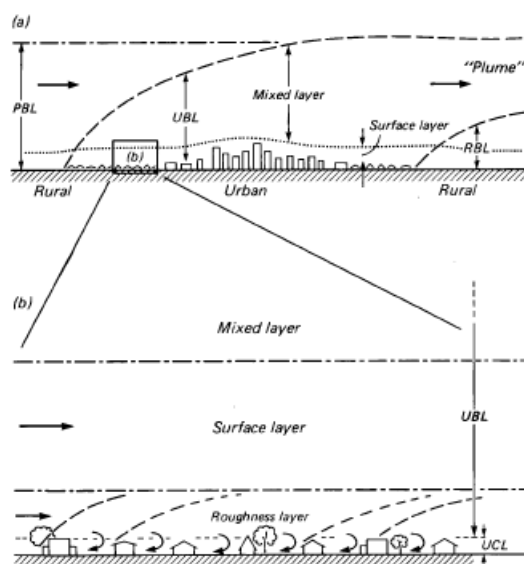


Figure 2.6: Boundary layer structures over a city (Oke 1988b, p. 473).

2.2.3 Soil/water, plant and atmosphere interactions

In examining an urban environment, the interactions of water through soil and plants with the atmosphere have important implications on urban micro-climates. The water cycle, starting from the soil through plants to the atmosphere and back to the soil is a complex process. Philip (1966) describes it as the ‘soil-plant-atmosphere-continuum’.

Water flow between the three layers (Figure 2.7) can be examined individually through different scientific disciplines. However, a complete understanding, as well as accounting for the mechanisms facilitating these transfers, requires that all the interactions must be considered as a whole. Furthermore, examining the impact WSUD features (consisting of vegetation and water) can have on urban climates through modelling, accurate representation of these interactions is especially critical. It is also important to understand the impact urban areas can have on vegetation.

The water cycle within soil, plants, and atmosphere is ultimately driven by solar energy, providing water through evaporation from soil surfaces and bodies of water, leading to precipitation (Bonan 2002). Input to the urban vegetation water cycle is through this precipitation, which either lands on the vegetation or the ground (Oke 1987). In urban climates, an important

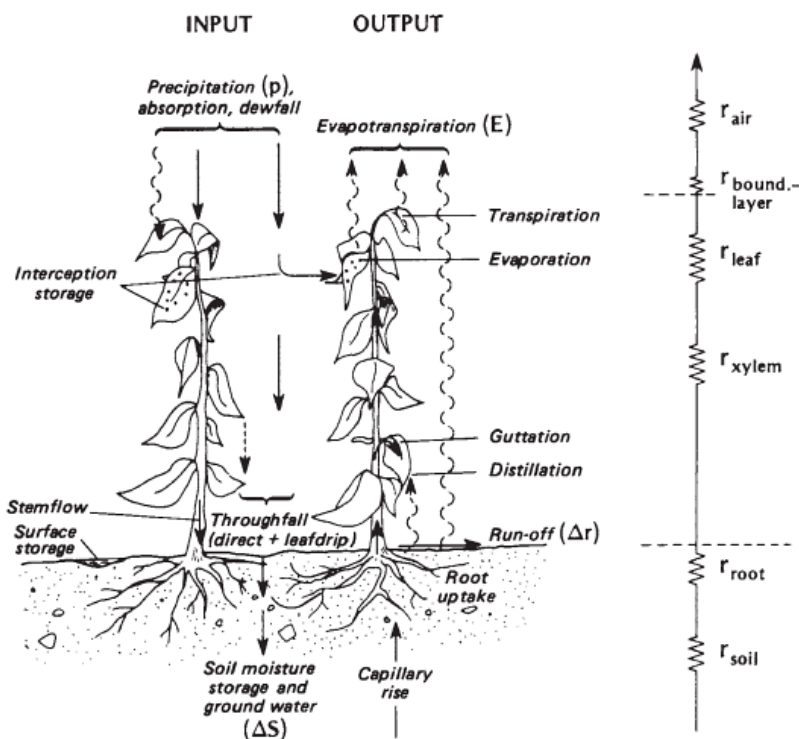


Figure 2.7: The water balance and internal flows of water in a soil-plant-atmosphere system. At the right is the electrical analogue of the flow of water from the soil moisture to the atmospheric sink via the plant system (Oke 1987, p. 125).

extra input, in addition to the natural precipitation inputs, is irrigation and other anthropogenic sources of water. This source can often and substantially exceed precipitation amounts (Grimmond et al. 1986; Mitchell et al. 2001; 2003).

Of the small amount of precipitation intercepted and stored on the canopy surface (inception), most of this water quickly evaporates back to the atmosphere (Bonan 2002). Water which falls on the ground surface has a number of different possible paths. Water is temporarily stored on the ground surface by ponding, with amounts which exceed the rate with which it can be absorbed by the soil, or if the soil has reached its saturation point, it will be lost through surface runoff (Bonan 2002). It can also be lost from the soil surface through evaporation, with the rate determined by the evaporative demand of the atmosphere (driven by solar radiation, temperature, wind speed, and relative humidity levels) (Cambell & Norman 1998).

These same evaporative demands will also drive the process of removal of moisture from the soil. This can potentially lead to the wilting point, where soil moisture is too low (or remaining soil moisture is too tightly held by the soil to be accessible), leaving plant roots unable to extract any more and the plant wilts and can not recover (Kirkham 2014; Briggs & Shantz 1912).

Ponded water on the soil surface can also follow the path of soil infiltration. Infiltration rates will be determined by the amount of water in the soil, which determines the hydraulic conductivity of the soil (Oke 1987) as well as the composition and texture of the soil (Green & Ampt 1911). Water will continue to move downward, driven by gravitational and matric (surface tension) forces slowly over weeks towards ground water storage (Cambell & Norman 1998; Bonan 2002).

Water storage also occurs in the vegetation itself. Indeed, plants are mostly composed of water, with green portions of plants up to 80-90% water, while woody parts are around 45-60% water by weight (Ali 2010). The output paths of the water cycle from the soil upward are shown in Figure 2.7. Root uptake extracts water from the soil, at rates determined by the extent of root development, the individual plant's vascular system efficiency, and ease of internal sap flow (Oke 1987).

Water loss through evaporation (unsaturated air uptake of water on wet surfaces) and transpiration (evaporation from leaves of water moving from the soil and through the plant), or together known as evapotranspiration, determine the water needs of a plant (Bonan 2002). Rates of evapotranspiration are determined by a number of different factors.

A resistance network (such as in an electrical circuit) is a useful way to consider the flow of water through the plant system (Cambell & Norman 1998) (Figure 2.7). Solar radiation will be the primary driver of water usage, with higher net energy providing more potential to evaporate water (Bonan 2002). This is followed by the air's capacity to remove moisture. Less humid air provides a greater evaporative demand than humid air (Bonan 2002). Finally, calm conditions allow humidity levels to increase (creating lower vapour deficits) while windy days replace humid air with drier air, allowing higher rates of evaporation to continue (Bonan 2002).

In response, plants can resist or regulate water loss through its resistance network (Figure 2.7), with its primary tool stomatal closure (Cambell & Norman 1998). This is the use of the stomata, an opening in the leaf to take in CO₂, necessary for photosynthesis, but at the cost of water vapour loss. Plants will close their stomata under conditions of low light, dry soil, and high CO₂ concentrations (Bonan 2002), but also under conditions of high vapour pressure deficits (a high difference between air's humidity and its potential humidity levels) (Cambell & Norman 1998). Strategies of stomatal regulation can vary widely between plant species (Tuzet et al. 2003; Bush et al. 2008; Litvak et al. 2012).

This section highlights the importance of the interconnections between water, soil, plants, and climatic conditions of urban areas. Maintenance of healthy trees and other urban greenery must account for these factors, especially if the vegetation is to be used for thermal comfort benefits in urban areas. Many conditions common in urban areas, identified by Coutts et al. (2012) and Coutts (2014), such as impervious surfaces (which alter soil infiltration potentials), dry areas with high vapour deficits, reduced shading (leading to higher radiation exposure and higher surface temperatures) are just a few conditions which can lead to highly stressed vegetation and reduced human thermal comfort.

2.3 Interactions of humans, climate, and urban areas

Adding humans to these large numbers of interactions between climate and urban areas adds another level of complexity. Human thermal comfort (HTC) is a subjective experience for each individual based on a number of factors making measuring HTC a difficult proposition. In order to understand human interactions with the built environment and climate and quantify HTC, it is necessary to draw on research in this area.

2.3.1 Human Thermal Comfort (HTC)

Research has established methods to measure and quantify HTC. Determining factors include temperatures (air and radiant) and humidity levels, but also include wind velocity, clothing, and activity levels (Olesen 1982). Physiological factors such as age, gender, height, and weight

also influence HTC. Variations in HTC are seen when external forces such as temperature and humidity changes combined with heat loss due to wind, insulation through clothing, and heat gains through external radiation levels impact a person's ability to maintain a body core temperature.

Thermal comfort is an subjective experience and can vary due to individual characteristics such as gender, age, weight, and height and activity level (ASHRAE 2009). Metabolic rates are used to account for these differences. A unit of 1 met (equivalent to 58.15 W m^{-2}) represents an average male adult at rest, with variations calculated from different activity levels (ASHRAE 2009) as well as different results for other body types and demographics, such as children (Haddad et al. 2013).

Thermal balances for the body are expressed in Equation (2.3.1)

$$H - E_d - E_{sw} - E_{re} - L = R + C \quad (2.3.1)$$

where H is internal body heat production (W m^{-2}), E_d is heat loss through water evaporation from the skin (W m^{-2}), E_{sw} is heat loss through sweating (W m^{-2}), E_{re} is heat loss through respiration (W m^{-2}), L is dry respiration heat loss (W m^{-2}), R is heat loss by radiation from the surface of a clothed body (W m^{-2}), and C is heat loss through convection from the surface of a clothed body (W m^{-2}).

A reorganisation of these factors and making some factors constants, leaves the term L . Inserting values for the insulating value of clothing, ambient dry-bulb temperature, and relative humidity, wind speed and metabolic rate allows you to solve the equation for L following Jones (2001) in Equation (2.3.2)

$$L = F(P_a, T_a, T_{mrt}, T_{cl}) \quad (2.3.2)$$

where P_a is partial vapour pressure (Pa), T_a is dry bulb air temperature, T_{mrt} is mean radiant temperature, and T_{cl} is clothing surface temperature.

Simple inputs of temperature and humidity combined with clothing levels, wind speed, and activity levels can be scaled on a seven point scale from hot to neutral to cold (Figure 2.8) to calculate predicted mean vote (PMV). This index describes levels of satisfaction with a thermal environment. Further calculations of PPD (predicted percentage dissatisfied) can add in a value of weight for overall dissatisfaction (0-100%) of comfort (Olesen 1982).

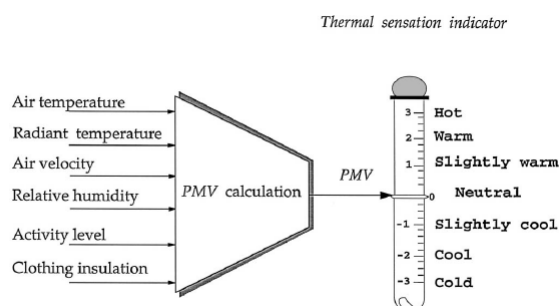


Figure 2.8: PMV and thermal sensation (Hamdi et al. 1999, p. 168).

2.3.2 HTC in outdoor areas

HTC in complex areas remains a topic of some controversy. de Dear (2004) concludes that the PMV-PPD model of Fanger (1972) is an ingenious way to model and manage requirements for building heating, ventilation, and air conditioning (HVAC), but finds it a little too “one size fits all” and less suitable for more complex situations, such as naturally ventilated buildings that are not static and centrally controlled through HVAC.

Spagnolo & de Dear (2003) particularly identified outdoor areas as an area of research that had not been covered adequately yet and were especially complex due to a larger number of factors that need to be quantified such as radiation loading and wind velocity. They also found that psychological expectations led to widening or skewing of comfort zones. These could vary due to acclimatisation to a particular location/climate zone. This is in line with work done by Loughnan et al. (2010a) which established varying extreme temperature thresholds for different urban areas in Australia.

As there are varying versions of PMV scales, research has been undertaken to find a universal scale which fits all situations, especially in complex environments such as outdoor areas. Other measures of thermal sensation have been developed, such as Gagge's ET* (Gagge et al. 1971) and SET* (de Dear et al. 1997).

The Universal Thermal Climate Index (*UTCI*) has been found to be a good indicator of thermal comfort with a high sensitivity to meteorological conditions (Spagnolo & de Dear 2003; Blazejczyk et al. 2012). Like PMV and other HTC indexes, it uses a combination of meteorological input, physiological input, clothing, and activity levels (Figure 2.9) to generate an equivalent ‘feels like’ temperature (in °C *UTCI*). This project will use *UTCI* as the index to indicate HTC.

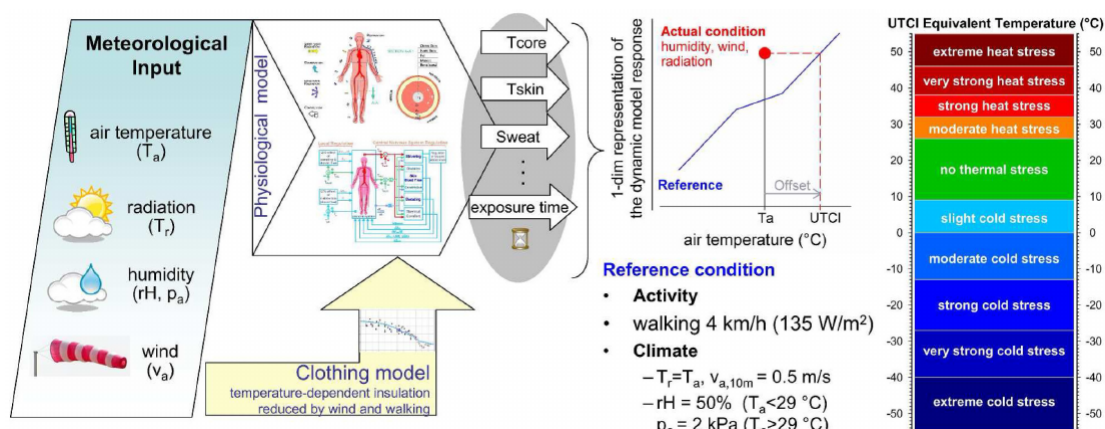


Figure 2.9: Elements of the operational procedure and concept of UTCI as categorised equivalent temperature derived from the dynamic response of a thermo-physiological model coupled with a behavioural clothing model (Bröde et al. 2013, p. 17).

The implications uncovered here in quantifying the HTC benefits of WSUD are that a number of variables are needed to make these calculations. Any modelling predictions will need to provide values of air temperature, radiant temperature, wind speed, and relative humidity, with radiant temperature being especially important.

In this study, as the overall focus is to understand how our built environments support human health and well being, HTC will be a key indicator used in examining urban micro-climates and the effectiveness of WSUD. This will drive a strong focus on surface temperatures, in

particular, as well as other parameters necessary to quantify HTC. The requirements for these parameters, as will be shown later in this literature review, will play a major part in determining the suitability (and later design) of a modelling tool.

2.3.3 Mean radiant and air temperatures

Mean radiant temperature (T_{mrt}) is a key variable in calculating human thermal comfort, indeed the most important under hot conditions (Matzarakis et al. 2010; Winslow et al. 1936). ASHRAE (2009) defines T_{mrt} as “*the uniform temperature of an imaginary enclosure in which radiant heat transfer from the human body equals the radiant heat transfer in the actual non-uniform enclosure.*” The mean radiant temperature (K), \bar{T}_r , can be calculated from the temperatures of surrounding surfaces in Equation (2.3.3)

$$\bar{T}_r^4 = T_1^4 F_{p-1} + T_2^4 F_{p-2} + \cdots + T_N^4 F_{p-N} \quad (2.3.3)$$

where T_N is the surface temperature of surface N (K) and F_{p-N} is the angle factor between a person and surface N.

2.3.4 Calculating HTC of urban areas

With these four measurable parameters (air temperature, humidity, wind speed, and mean radiant temperature), it is possible to make measurements of different urban areas (or model them) and make a connection to the human thermal comfort of these areas. In addition, changes to urban morphologies can be quantified in how much they improve (or worsen) the thermal comfort of these new areas compared to other arrangements. Calculations of T_{mrt} and other HTC calculations will be examined in greater depth in Section 4.2.4.

2.4 Modelling scales and modelled properties

Modelling has long been used as a tool to examine the climate. Observations can be used to study urban areas but measurements can only be taken of existing layouts. In order to look at varying scenarios, different layouts, and different morphologies, modelling needs to be the tool to examine these new and different areas.

To work efficiently and accurately, models are designed using a variety of strategies and techniques to fit best with the intended use and scale. According to Oke (2009), it is important that urban climate models include all processes that are appropriate to scale and that models are validated with data measured at the correct scale. To understand the difficulties in and specialised requirements of modelling urban climates, especially when they contain vegetation, an introduction to some of the issues with scale and techniques in climate modelling in general must first be made.

2.4.1 Global scale

The most commonly known climate models are global scaled, used extensively in the IPCC assessments examining global climate change (IPCC 2013b) as well as by meteorological organisations for weather predictions. Global scale covers scales from 2000 km to the entire globe. These models are commonly atmospheric general circulation models (GCM) modelling radiation, heat, water vapour and momentum fluxes across the land-surface atmosphere

interface. A component of these models, land surface schemes (LSS), are designed to calculate the temporal evolution of these fluxes, differentiating between bare ground and vegetation fluxes. Urban areas are unlikely to be represented in any significant way in these models as the resolution is not sufficient to resolve these relatively small areas.

2.4.2 Meso and Local scale

To look at urban climates, higher resolution scales are needed. Meso-scale covers the range from 2000 km to 2 km, further subdivided into meso- α (200-2000 km), meso- β (20-200 km), and meso- γ (2-20 km) (Pielke 1984). Regional scaled modelling resolves at the meso- α range. Local scaled modelling, resolving at a city-wide level, sits within the meso- β and - γ scales.

These models allow examination of rural and urban areas and how interactions with an urban canopy (buildings and other structures as well as urban trees) impacts climate conditions at these more local scales. These models are commonly scaled down global models, relying heavily on land surface schemes (LSS) and urban components to calculate the interactions of these urban canopies.

However, individual features of urban areas are unlikely to be modelled directly at this scale as the model resolution is still too coarse to resolve them. Panels 3 and 4 of Figure 2.10 shows the greatest detail which can be resolved at this scale. In addition, urban LSS schemes such as SURFEX (Masson et al. 2013) and LUMPS (Grimmond & Oke 2002) are designed to use percentages of urban cover types (roads, buildings, soil, water, etc.), using tiles to represent these fractions, then aggregate those results up to the desired scale. Detailed resolution of HTC impacts are not possible using these techniques as they do not resolve the scale at which people experience thermal comfort and cannot capture the diversity of HTC conditions within the urban canopy layer.

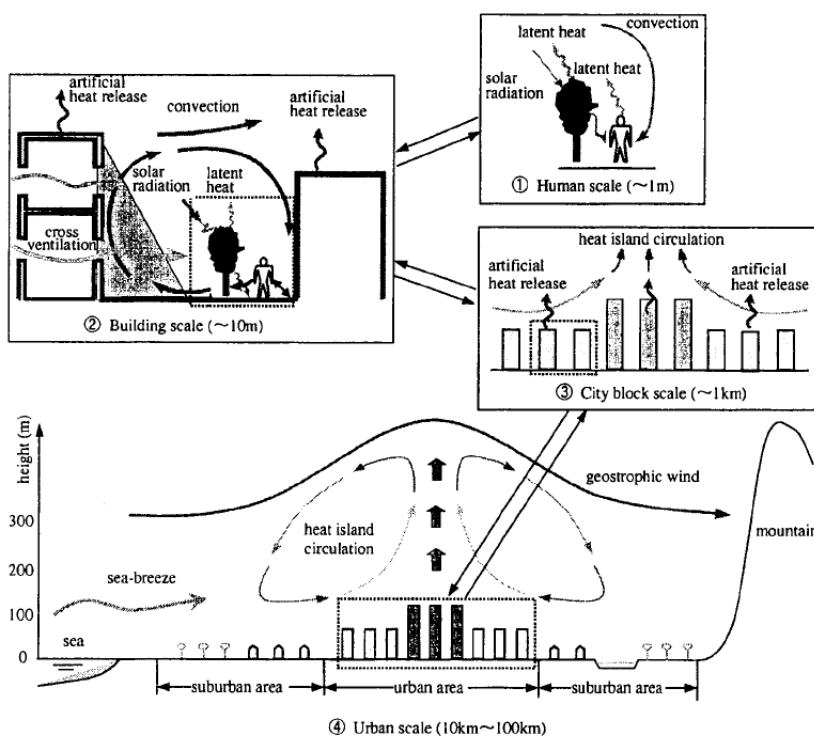


Figure 2.10: Various scales related to wind climate (Murakami et al. 1999, p. 58).

2.4.3 Micro-scale

Micro-scaled modelling brings resolutions down to within a city block (and finer) scale, with the most detailed models resolving down to a few metres. At this scale, human scale HTC issues can be resolved. The scale depicted in Panels 1 and 2 of Figure 2.10 finally start to explicitly resolve the detail needed to resolve the interactions that drive HTC.

For this study, the examination of HTC requires modelling at a sufficient scale to resolve the parameters necessary to calculate HTC (air temperature, humidity, wind speed, and mean radiant temperature). In addition, vegetation needs to be accounted for in the modelling in order to determine the impact of urban greening through both shading and transpiration. Thus, in order to best quantify the thermal comfort benefits of HTC, modelling will need to be done at the micro-scale.

2.4.4 Characteristics to classify models

A variety of approaches and means of parameterising various urban features are used to model urban areas, falling into twelve categories. These categories, used in Grimmond et al. (2010) to evaluate a wide variety of meso and local scaled urban models, are illustrated by Figure 2.11. This framework can be used to describe critical components of urban models at various scales.

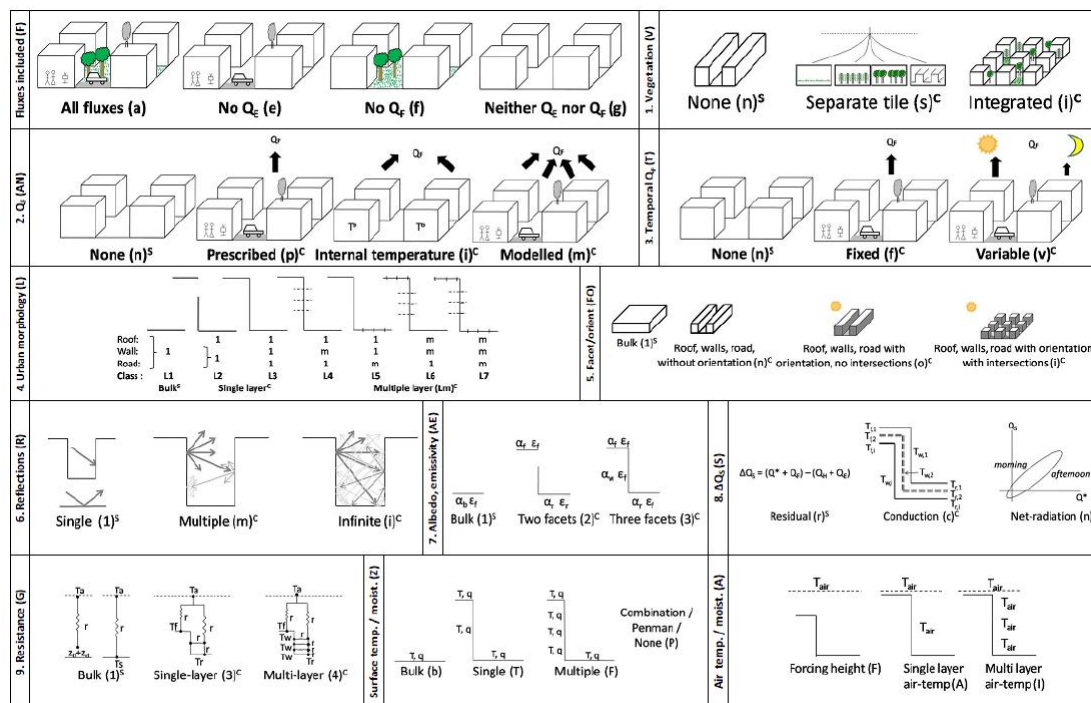


Figure 2.11: Characteristics used to classify models (Grimmond et al. 2010, p. 1270).

Modelling requires decisions about and trade-offs between complexity, accuracy, and efficiency to perform best for the intended purpose. This project will need to examine many different design decisions to find an appropriate way to assess HTC at a micro-scale. This review of many of these techniques can be instructive and helps set the context for the later review of state of the art in modelling urban vegetation and the ultimate goal to assess the HTC impacts of this vegetation. However, many of these methods will not be appropriate or provide the level of resolution needed.

The geometry of the urban canyons can be addressed in a number of different approaches, with increasing levels of complexity and detail. Urban areas can be treated as a simple slab or with walls, roads, and intersections (Figure 2.11 Panels 4 and 5). These features can interact with fluxes (reflections, albedos, and heat storage) in single or multiple levels of interaction (Figure 2.11 Panel 6). For this project, detail of building and road facets from even the most complex technique in Figure 2.11 Panel 5 (roofs, walls, roads, and intersections) will be insufficient to resolve the detail needed to model specific scenarios and placements of vegetation in urban canyons.

However, other design decisions might be appropriate and applicable to micro-scaled modelling of vegetation. A modeller can choose whether all fluxes are considered or not. If Q_F (anthropogenic heat) is considered, it can be calculated or set to a reasonable constant (Figure 2.11 Panel 2).

Vegetation can be considered and modelled as an integrated module or a separate tile (Figure 2.11 Panel 1). Vegetation modelling can be simplified into something that is merely an obstacle to sunlight and wind, or include all its processes of photosynthesis and water storage and transfer. As the Grimmond et al. (2010) and Grimmond et al. (2011) model inter-comparison study concluded, the implication of not including vegetation is that there will be no accounting for latent energy fluxes except in periods immediately following rainfall events. These two papers found that models that did not include vegetation modelling performed less well than those that did.

While the main goal of WSUD treatments is increased water security and water filtration, quantifying the possible human thermal comfort benefits due to increased evapotranspiration through increased water and vegetation in urban canyons is desirable. This can then aid in WSUD design decisions to deliver multiple benefits. Modelling the increased amounts of latent energy fluxes, increased shading from trees, and differences attributable to conversion of impervious surfaces to pervious can quantify the possible benefits to HTC of these changes. Understanding the changes in warming and cooling patterns across daytime and night-time can help combat effects of UHI. Understanding if increased numbers of trees and other obstacles will lead to changed wind flow and lead to reduced cooling through mechanical mixing is also important.

2.5 Inclusion of vegetation in urban models

For this project, finding a suitable method to include vegetation will be a major decision. Before making this decision, an examination of how vegetation has been included in other urban models is needed. Generally, these techniques differ in terms of the scale being modelled and the aspect of the vegetation under consideration (transpiration vs. radiation effects), the level of integration of vegetation within the model, and whether the vegetation effects are being considered as an average impact across an entire domain (or sub-domain) or whether each vegetation item will have an individual impact.

2.5.1 Non-integrated vegetation

A simple way to look at vegetation is in isolation from the rest of the urban area being modelled, an approach in which the vegetation is not integrated into the domain. An example of this is seen in attempting to quantify the impacts of vegetation through its influence on T_{mrt} , which is an important factor in human thermal comfort. In Tan et al. (2015), the approach taken was to observe and measure rates of plant evapotranspiration of a rooftop garden, as well as

its albedo, then use regression analysis to predict T_{mrt} . While a relation was found between the two parameters and T_{mrt} , other important influences of vegetation might have not been considered in this modelling. It is also not possible to quantify the impacts of the urban area on the vegetation. While these non-integrated techniques are useful to help estimate some of the effects of vegetation, more sophisticated and integrated methods will need to be used.

2.5.2 Transpiration modelling techniques

Transpiration of vegetation is an important component of the overall effect vegetation can have in urban areas, so techniques must be identified to calculate this and integrate them into modelling tools. There are a number of commonly used techniques used across a number of different modelling scales. This examination will begin by discussing the details about how many of these techniques work.

Big Leaf

A scheme commonly known as the ‘big leaf’ model uses stomatal resistance, that is the resistance of the flow of CO_2 and water vapour through the stomata in leaves (Bailey & Davies 1981). Calculations of r_{st} , effective surface resistance of the leaves (s m^{-1}) are performed in Equation (2.5.1)

$$r_{st} = \rho(Q^*(T_o) - q_o)/E_o \quad (2.5.1)$$

where ρ , the air density (kg m^{-3}), the Q^* , the net radiation flux density (W m^{-2}), T_o , the temperature (K), q_o , the surface humidity (kg kg^{-1}), and E_o , the surface vapour pressure (Pa) (Kowalczyk et al. 1991).

Then r_{st} is calculated over an area in Equation (2.5.2)

$$1/r_{st} = A^{-1} \sum_i L_{A,i}/r_{sti} \quad (2.5.2)$$

where $L_{A,i}$ is the area of the i th leaf over ground area A where the leaf area index (LAI) is the total leaf area per unit of ground area (Kowalczyk et al. 1991). A variation of the ‘big leaf’ model is the two leaf model, where the canopy is represented as two areas of sunlit and shaded leaves (Wang & Leuning 1998).

These parameterisations require few parameters and can be efficiently computed and are commonly used in land surface climate modelling (Dai et al. 2004). A limitation is that the surface must be wholly and uniformly vegetated and is an upscaling from a single leaf (Jarvis & McNaughton 1986).

Ball-Berry stomatal conductance

Another variation of the stomatal conductance model is the widely used Ball-Berry type approach (Ball et al. 1987; Duursma & Medlyn 2012). The calculation of g_s , the leaf-level stomatal conductance to CO_2 ($\text{mol m}^{-2}\text{s}^{-1}$), is formulated as Equation (2.5.3)

$$g_s = g_0 + g_1 \frac{A_n}{C_s} \times f(D) \quad (2.5.3)$$

where g_0 the conductance when A_n is zero ($\text{mol m}^{-2}\text{s}^{-1}$), g_1 a conductance empirical parameter, A_n is the leaf net assimilation rate ($\mu\text{mol m}^{-2}\text{s}^{-1}$), $f(D)$ a function of the leaf-to-air vapour pressure deficit (D), and C_s , the CO_2 concentration at the leaf surface ($\mu\text{mol mol}^{-2}$).

Variations of this model, using different options for the $f(D)$ function, are:

- 1) The Ball-Berry model (Ball et al. 1987) in Equation (2.5.4)

$$f(D) = 1/rh \quad (2.5.4)$$

where rh is relative humidity (%). This variation is considered satisfactory for well watered vegetation (Tuzet et al. 2003).

- 2) The Ball-Berry-Leuning model (Leuning 1995) in Equation (2.5.5)

$$f(D) = 1/(1 + D/D_0) \quad (2.5.5)$$

where D is leaf-to-air vapour pressure deficit (Pa) and D_0 is an empirically determined coefficient. This variation was formulated to account for slow changes in soil water content in plants that might experience some water stress (Wang & Leuning 1998; Tuzet et al. 2003).

- 3) The Ball-Berry-Opti model (Medlyn et al. 2011) in Equation (2.5.6)

$$f(D) = 1/\sqrt{D} \quad (2.5.6)$$

where D is leaf-to-air vapour pressure deficit (Pa). This is a variation based on findings of vegetation variations of g_s to maintain a constant $\delta E/\delta A$, the limiting magnitude of the transpiration ratio (of energy and rate of assimilation) (Cowan & Farquhar 1977).

- 4) The Tuzet model (Tuzet et al. 2003) uses Equation (2.5.7)

$$f(D) = \frac{1 + \exp[s_f \Psi_f]}{1 + \exp[s_f (\Psi_f - \Psi_L)]} \quad (2.5.7)$$

where Ψ_L is leaf water potential (MPa), Ψ_f is reference water potential (MPa), and s_f is steepness of the response of $f\Psi_L$ to Ψ_L . This is a further variation of Leuning (1995) to better account for diurnal responses of stomata of water limited vegetation (Tuzet et al. 2003).

The use of this stomatal conductance approach requires more detailed parameters than ‘big leaf’, but this detail allows modelling of specific species as well as variations of canopy size and vegetation health and drilling down to specific items of vegetation (Duursma & Medlyn 2012) as opposed to a canopy-wide average.

Penman-Monteith equation

The Penman-Monteith equation is used to calculate net evapotranspiration (ET) from an open area of vegetation using commonly available weather records of radiation levels, temperature, humidity, and wind speed. Different types of vegetation surfaces will have different values for aerodynamic resistance (R_A) and surface resistance (R_S), yielding evapotranspiration values appropriate for those surfaces (Penman 1948).

A formulation of this equation (Penman 1948; Monteith 1965) calculates E_a , the actual evapotranspiration ($\text{kg m}^{-2}\text{s}^{-1}$), in Equation (2.5.8)

$$E_a = \frac{\Delta_S A + \rho c_p (q_w, T_d - q) / r_a}{\gamma [\Delta_S + (c_p / \gamma) (1 + r_c / r_a)]} \quad (2.5.8)$$

where:

Δ_S is slope of the specific humidity/ temperature curve between the air temperature T_D and the surface temperature of the vegetation T_s ($\text{kg kg}^{-1} \text{ }^\circ\text{C}$),

A is available energy given by $A = RN - G$ (W m^{-2}),

ρ is density of air ($= 1.2 \text{ kg m}^{-3}$),

c_p is specific heat of air at constant pressure ($= 1.01 \times 10^3 \text{ J kg}^{-1} \text{ K}^{-1}$),

q_w, T_d is saturated specific humidity at dry-bulk temperature, T_D (kg kg^{-1}),

$(q_w, T_d - q)$ is specific humidity deficit (kg kg^{-1}),

r_a is aerodynamic resistance to the transport of water vapour from the surface to the reference level z (s m^{-1}),

γ is latent heat of water ($= 2.47 \times 10^6 \text{ J kg}^{-1}$),

r_c is (Monteith) canopy resistance to the transport of water from some region within or below the evaporating surface to the surface itself, and is expected to be a function of the stomatal resistance of individual leaves. Under wet-canopy conditions $r_c = 0$ (s m^{-1}).

This equation is a widely used technique to estimate ET in models, such as in the Soil and Water Assessment Tool (SWAT) (Neitsch et al. 2011). However, the approach can be a modelling challenge. The input parameters (aerodynamic and canopy resistance) are highly sensitive, requiring great care in accurate estimations (Beven 1979) and these parameters can be quite site specific (Sumner & Jacobs 2005).

This is the case when land surfaces are treated as one homogeneous surface without differentiating between soil evaporation and transpiration (Overgaard 2005). Applying these techniques to a complex urban environment with a diversity of trees will prove even more challenging. However, depending on the intended modelling purpose and decisions about trade-offs, this technique (or some of the others), might prove to be suitable for that purpose. Further examination on a case by case basis is needed.

2.5.3 Inclusion of vegetation in urban canopy models

A first way to examine these different cases is through intended modelling scale. Starting at a meso-scale, meso-scaled atmospheric models do not have sufficient resolution to resolve individual urban features (such as streets, buildings, and vegetation), but their coupling with urban canopy models (UCMs) has allowed their influence to be incorporated.

As the scale of these models are city-wide or neighbourhood-scaled at best, they can capture temporal patterns, but are insufficient in spatial resolution to capture the effects of individual elements of vegetation or even small groupings of vegetation. However, these models can still be useful tools to look at such questions as cooling impacts of modifying a city's canopy cover and those impacts of heat related mortality (Chen et al. 2014a).

Single layer UCM

UCM models can generally be classified as either single-layer or multi-layer, where single-layer represent the entire urban canopy atmospheric layer as a single entity and multi-layer models represent it as a number of differing (vertical) layers. For single layer UCMs, these parameterisations include the Town Energy Balance (TEB) model (Masson 2000), a single slab UCM (Kusaka et al. 2001), simple urban energy balance model for meso-scale simulations

(SUMM) (Kanda et al. 2005), an energy balance UCM (Harman & Belcher 2006), and the community land model (CLM3) (Oleson et al. 2008). Some of these, Masson (2000), have included basic urban hydrology (evaporation from streets and roofs) and the latent heat fluxes resulting from that, but have not integrated vegetation.

Of interest to this study is a modification of TEB, TEB-Veg (Lemonsu et al. 2012) that has included vegetation. TEB divides the urban energy budget across three surfaces (roofs, walls, and road) of an idealised urban canyon (Masson 2000). TEB-Veg (Lemonsu et al. 2012) has added vegetation to the urban canyons using the Soil Biosphere and Atmosphere (ISBA) module (Noilhan & Planton 1989), running it twice in grid squares which contain tiles of vegetation and of urban vegetation. Using the results from these calculation steps, the fluxes are aggregated in proper proportions to roofs, walls, roads, and gardens. The SURFEX model (Masson et al. 2013) also incorporates the TEB-Veg and ISBA modules to allow tiled modelling of four types of surfaces, nature, towns, inland water, and oceans.

Also of interest is the vegetated urban canopy model (VCUM), using ‘Big Leaf’ modelling (Section 2.5.2.1) as the basis for its urban canopy modelling (Lee & Park 2008; Lee 2011). The model contains a nearly complete scheme for modelling vegetation. Of interest to accounting for physical processes important to modelling WSUD impacts, it accounts for a number of physical processes such as heat and hydraulic conduction in soil layers, basic hydrological processes, energy balances of vegetated surfaces, and photosynthesis effects of urban vegetation. Shadow and radiation absorption by vegetation are calculated by using the leaf area density profile function based on Yamada (1982) and Lalic & Mihailovic (2004) which might be suitable for finding average temperatures but not detailed temperature gradients in an urban canyon.

Multi-layer UCM

Multi-layer UCMs include parameterisation from Martilli et al. (2002), Kondo et al. (2005), Vu et al. (2002), Otte & Lacser (2004), and Dupont et al. (2004). Of these, only Dupont et al. (2004) considers some number of vegetation tile types in the urban environment by applying a drag-force approach (DA) to modify the turbulent length scale parameterisation inside the canopy (Martilli et al. 2002; Lacser & Otte 2002), while heat fluxes and surface temperatures are determined by the coupled soil model SM2-U (Dupont et al. 2002). While these multi-layer parameterisations have the potential for more accurate representations, the lack of certainty about urban drag coefficient values requires a number of assumptions to be made (Lee & Park 2008).

Shading effects in UCMs

At meso-scales, shading effects of trees haven’t been explicitly integrated into meso-scaled UCM models until Wang et al. (2016) integrated shade trees into the Weather Research and Forecasting urban canopy model (WRF-UCM) (Chen et al. 2011). WRF’s UCM uses a ‘big canyon’ representation of urban geometry, which means a simplified 2D canyon, using a resistance network of energy transport (Wang et al. 2011). The Princeton UCM (PUCM) (Wang et al. 2013) is also a variation, adding basic hydrological processes.

Capturing the radiative shading effects of vegetation in Wang et al. (2016), modifying Martilli et al. (2002), was accomplished by calculating the view factors and shading effects through stochastic ray-tracing using Monte Carlo techniques (Krayenhoff et al. 2014; Wang 2014). Additions have also included spatial averaged mean air flows within buildings and urban canopies (Krayenhoff et al. 2015).

UCM modelling and HTC

Modifications to UCM parameterisations to include vegetation have added significant abilities to assess the impacts of urban vegetation. However, as their resolutions are generally meso-scaled (local scaled at best), they still lack sufficient resolution to detail HTC impacts of vegetation and must therefore scale up and generalise the HTC experiences.

2.5.4 Urban vegetation modelling at local scales

Progressing towards a higher resolution scale, local scale modelling techniques often use surface energy balance (SEB) based schemes as the framework to resolve the radiation movement within the modelling domain. SEB schemes use the surface radiation budget equations (detailed in Section 2.2.2) to calculate missing terms, generally sensible heat flux (Q_H) and latent energy fluxes (Q_E). Given meteorological values for net radiation, temperature, humidity, wind speed as well as surface and land cover breakdowns, partitioning of the remaining fluxes is calculated using a variety of strategies (Grimmond et al. 2010).

Tree and canyon radiation modelling at local scale

The Surface Urban Energy and Water Balance Scheme (SUEWS) (Järvi et al. 2011) model is the major example of a local scaled SEB model that can include vegetation and its effects. Fluxes Q_H and Q_E are partitioned from the available energy, using a version of the Holtslag & Van Ulden (1983) combination type model with coefficients determined for urban areas (Loridan et al. 2011). Vegetation is not directly modelled but accounted for in the repartitioning of the available energy based on the percentage breakdown of land cover.

Transpiration modelling at local scale

Vegetation (and associated soil) transpiration modelling techniques at local scales can also be demonstrated with SUEWS. Urban water scenarios, based on Grimmond et al. (1986), account for soil moisture and drainage, surface and soil run-off, irrigation, precipitation, and evapotranspiration and calculate overall transpiration using the Penman-Monteith equation (Grimmond & Oke 1991). Validations showed that the model performed well reproducing varying scenarios in Vancouver and Los Angeles of urban fractions and vegetation cover (Järvi et al. 2011) as well as in Helsinki (Järvi et al. 2014).

Urban vegetation modelling at local scales and HTC

Modelling vegetation at local scales would be suitable for most urban modelling and looking at vegetation effects at a city-wide or neighbourhood scale. However, as with meso-scaled models coupled with UCMs, the results will lack the micro-climate detail needed to make HTC assessments of individual elements of vegetation.

2.5.5 Urban vegetation modelling at micro-scales

At a micro-scaled level, a number of different paths towards modelling vegetation effects on HTC emerge. However, at this scale, existing models generally only integrate the tree and canyon radiation effects through different methods of resolving energy movement through the urban canyon with varying levels of complexity.

Simple radiation integration

At the simplest level of complexity, stand models such as SOLWEIG (SOLWEIG 2011) and RayMan (Matzarakis et al. 2007; 2010), are used to predict T_{mrt} values. With both, vegetation is accounted for through sky view factors and the shading effect of vegetation using small numbers of input parameters (average albedo and emissivities of buildings and the ground) as well as meteorological forcing data (temperature, humidity, and incoming short-wave radiation). Neither consider the other possible cooling effects of increased latent energy fluxes and the repartitioning of the energy balances.

While SOLWEIG only models long-wave and short-wave radiation fluxes, validations of the model indicate that this simple approach captures T_{mrt} fluctuations (an important variable in calculating HTC) reasonably accurately (Lindberg & Grimmond 2011; Lindberg et al. 2008).

In a comparison of SOLWEIG and RayMan to observed values of T_{mrt} , Chen et al. (2014b) found RayMan was able to calculate T_{mrt} accurately at a fine temporal resolution but is limited as a stationary model (to a single point and single timestep). They further found that SOLWEIG performed well at fine spatial resolutions but less well at fine temporal resolution. SOLWEIG is also limited by its inability to calculate surface temperatures (T_{sfc}) (Chen et al. 2014b), which is assumed to be the same as the air temperature.

Both these models appear to be useful tools to assess the influence of vegetation T_{mrt} (and its influence on HTC) but there remain limitations on their overall uses in assessing vegetation influences because they do not account for the important ‘soil-plant-atmosphere continuum’ that drives transpiration, and latent heat fluxes, shown to be a critical component of the urban energy balance.

Direct vegetation modelling through ray tracing techniques

Only recent computer hardware advances have made direct modelling techniques possible for most modelling questions, as these are computationally intense tasks. Modelling complex interactions of a tree canopy, such as radiation transfer, evapotranspiration, and energy flux partitioning, have involved two main strategies, deterministic and stochastic methods. Recent innovations using computer graphics techniques and graphics processing units (GPUs) have started to undertake these tasks (Bailey et al. 2014; 2016). Even these require compromises in balancing complexity and processing demands.

Historically, deterministic methods (Jeans 1917; Hottel & Cohen 1958), have attempted solving radiative transfer modelling using simplified geometries but have been unable to scale to more complex interactions and geometries. More recently, ray tracing using Monte Carlo techniques (Farmer & Howell 1998) have been able to better handle realistic geometries but quickly require compromises in complexity (Bailey et al. 2014). While promising, these techniques are still beyond widespread usage.

Direct modelling using CFD techniques

Direct simulations using CFD techniques have also been progressing rapidly. Models of this category largely evolved modelling micro-scale wind flow to look at pollution dispersion in urban areas, such as MIMO (Kunz et al. 2000) and MITRAS (Mikroskaliges Chemie, Transport und Strömungsmodell) (Schlünzen et al. 2011). Both can be coupled with meso-scale models (MEMO and METRAS respectively) to set initial states and boundary conditions but do not use feedback (Ehrhard et al. 2000). Both are based on computational fluid dynamics (CFD) using Reynolds-averaged Navier-Stokes (RANS) equations (Schlünzen et al. 2003). MITRAS has been used to model local-scale temperature gradients and their effects on circulation in

an urban canyon (Bohnenstengel et al. 2004) and the thermodynamic pieces of the model (shading/incoming radiation and evaporation from different types of greenery) are currently being improved. Neither model is available outside of a research context and both models are very difficult to configure and operate which limits their wide spread suitability modelling WSUD features.

At micro-scales, techniques of computational fluid dynamics (CFD) can be used to model flows around an urban landscape, including features such as buildings and trees. This is a ground-up approach (as opposed to GCM), starting with the smallest interactions at a detailed level and building those up to a larger picture. Mathematical models used in this technique are based on the Navier-Stokes equation, which describes the motion of fluids. This equation is solved in three different ways, Direct Numerical Simulation (DNS), Large Eddy Simulation (LES), or Reynolds Averaged Navier-Stokes (RANS). DNS attempts to solve all the spatial scales within the flows and as a consequence is generally far too computationally intense for all but the smallest simulation. LES reduces the computational intensity through low-pass filtering, that is, filtering out the smaller scale pieces of the solution and concentrating on the larger scaled pieces. RANS uses mathematical techniques to simplify solutions of Navier-Stokes by separating fluctuating and averaging pieces (Yamada & Koike 2011).

ENVI-met

ENVI-met (Bruse 1999) is another CFD-based model, which has been increasingly used for study of vegetation impacts at a micro-scale (Wang et al. 2015; Lehmann et al. 2014; Konarska et al. 2014; Declet-Barreto et al. 2012; Shahidan et al. 2012), requiring an in depth examination of uses and limitations in modelling HTC impacts of vegetation. Validation of ENVI-met, in a number of published studies, has encountered difficulties. Ali-Toudert & Mayer (2006b) found that the values predicted by the model were probably overstated due to higher than expected radiation fluxes predicted by the model. Krüger et al. (2011) focused on wind speeds as a validation for ENVI-met's accuracy and found initial wind speeds of greater than 2 m s^{-1} to be unreliable and a limitation. As ENVI-met cannot be run through forcing data, these difficulties will be difficult to work around.

Acero & Herranz-Pascual (2015) found that wind speeds do not correctly represent observed values and did not find a good relationship between observed and modelled T_{mrt} . Spangenberg & Shinzato (2008) showed average air temperatures and diurnal amplitude were lower than expected when compared with observed results and had to adjust the simulation's starting temperature and wind speed to bring the results into agreement in the morning and evening hours.

In validations in research projects at Monash University, reproducing spatial temperature gradients, as well as temporal variations, seen in observational data with ENVI-met was challenging. As ENVI-met is unable to use external forcing data, the relatively static weather conditions (wind and humidity) predicted by ENVI-met might have had an impact on the modelled results, being unable to drive variability seen in observational data. The model is slow to warm up during the day and slow to cool down at night, under-predicting daytime maximums and over-predicting night time minimums. Modelled temperatures varied from 2°C to 6° C from observed values (Nice 2011).

Simplified vegetation modelling, modelled as a one dimensional column, using the leaf area density to describe amount and placement of leaves, as well as a one dimensional column of soil (Bruse 2004) might contribute to the difficulty in validating latent energy values predicted by ENVI-met. For calculation of all the fluxes, ENVI-met lacks rigorous radiation schemes that calculate multiple reflections and accurate view factors (Bruse & Fleer 1998; Krayenhoff 2005).

Diagnosing exact causes for divergences is difficult without model source code (which is not available from this closed source model). As latent energy flux modelling is critical for evaluating the benefits of WSUD features, ENVI-met's utility in modelling WSUD will be limited until further investigation can find reasons for the inaccuracies. Difficulties arise when trying to examine the results in detail and in ways other than the developers have provided. The output files are proprietary binary files which require reverse engineering to access the data directly. More importantly without available model source code (or active developer support), troubleshooting modelling results is difficult.

CFD frameworks

A final approach to micro-climate modelling, taken particularly by a number of researchers in Japan, is hand-coding simulations using CFD frameworks such as OpenFOAM (OpenFOAM 2011) or STAR-CD (CD-adapco 2011). These frameworks provide C++ libraries to solve a wide variety of CFD related problems such as incompressible/compressible flows, particle tracking flows, and heat transfers as well as methods to create customised solvers. Meshes of various types are provided to be configured into any shape with any number of faces and edges in order to represent features in the simulations.

Computational wind engineering (CWE) techniques were designed to accurately model processes such as wind load on buildings, particle dispersion, and heat and moisture movement, all in small domains (under 1 km) (Mochida et al. 2011). Published reports of micro-climate modelling through these techniques report detailed and accurate results.

Emphasis in these studies is generally centred around wind and particle dispersion (Janhall 2015), but fluxes which influence these flows are sometimes also added, along with features such as vegetation and the impacts they have on these flows. Nesting them within meso-scaled climate models to provide boundary conditions can add further accuracy to the simulations (Yamada & Koike 2011). Only a handful of studies have attempted modelling human thermal comfort impacts of vegetation (Gromke et al. 2015) or other important WSUD features such as water bodies (Tominaga et al. 2015) using CFD techniques (excluding ENVI-met studies discussed in Section 2.5.4).

2.5.6 Transpiration at micro-scales

Simpler models, used to assess HTC impacts of vegetation at a micro-scale, do not consider the effects of vegetation transpiration. This applies to models such as SOLWEIG and RayMan that only consider the impacts of shading effects on T_{mrt} .

However, CFD based models use many of the same approaches used by the local and meso-scaled models. For example, ENVI-met uses a stomatal conductance approach based on Deardorff (1978) to calculate transpiration from available soil moisture, while Gromke et al. (2015) uses a calculation of vegetated transpirational cooling through a function of (specified values of) leaf area density and a 'volumetric cooling power'.

2.5.7 Micro-scaled vegetation modelling

In the micro-scaled modelling of urban vegetation, two contrasting approaches are seen. The first, a highly simplified approach in which only radiation is considered, but in which vegetation transpiration is not addressed. This category includes models such as SOLWEIG and RayMan. While these approaches have been shown to be effective in modelling some aspects of urban vegetation HTC impacts, they cannot capture all the impacts. The other approach is extremely

detailed and complex, based on CFD modelling. Movement of radiation can be resolved in great detail and transpiration of vegetation can also be added to these domains using a variety of techniques.

However, what is missing is a more accessible approach, which can balance detail, complexity, and accuracy with efficiency and usability. As such a model does not exist, some consideration will need to be given to how a model like this can be designed and built. This discussion will follow in the next section.

2.6 Possible tools to model urban vegetation at a micro-scale

2.6.1 TUF-3D

The micro-scale TUF-3D model fits into the surface energy balance class of models, but is first introduced here instead because of the possibilities it presents in creating a tool which can model urban vegetation at a micro-scale. The Temperatures of Urban Facets in 3D (TUF-3D) model (Krayenhoff & Voogt 2007) simulates energy balances through a 3D raster model (Figures 2.12 and 2.13). TUF-3D uses separate modules to model radiation, conduction, and convection in order to predict fluxes of sensible heat, conduction, and radiation. Multiple reflections of solar radiation are included. Shading is calculated.

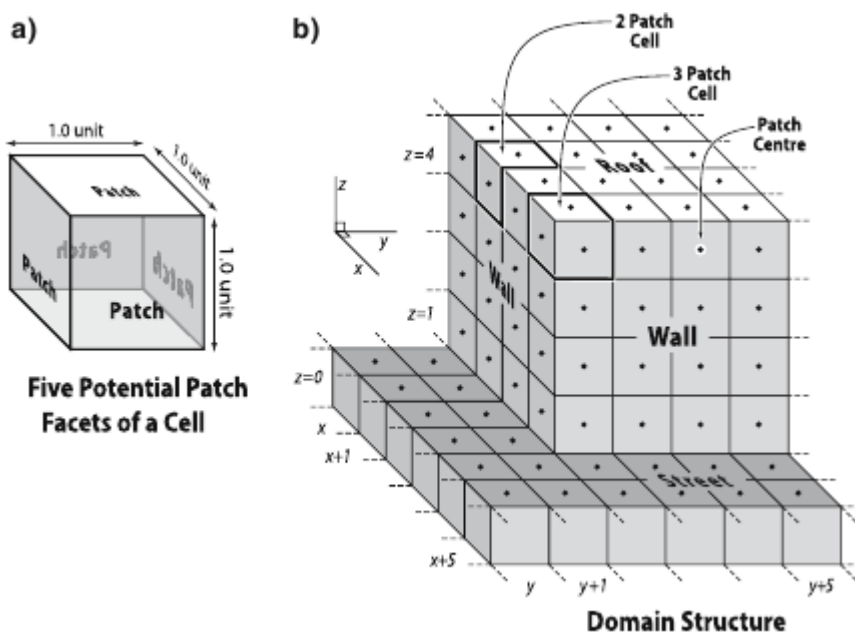


Figure 2.12: Basic cubic cell and surface patch structure of TUF-3D (Krayenhoff & Voogt 2007, p. 437).

Convection has been simplified into a 1D equation instead of more computationally intense methods such as large eddy simulations (LES) or Reynolds-averaged Navier-Stokes (RANS). The model is 3D in radiative exchanges only. Latent energy flux modelling has been added to TUF-3D by other researchers to compare urban surfaces (concrete, grass and AstroTurf) (Yaghoobian et al. 2010). However, other types of vegetation, especially trees, are not currently modelled in TUF-3D. The model does not currently account for water in urban canyons in any stage of the water cycle.

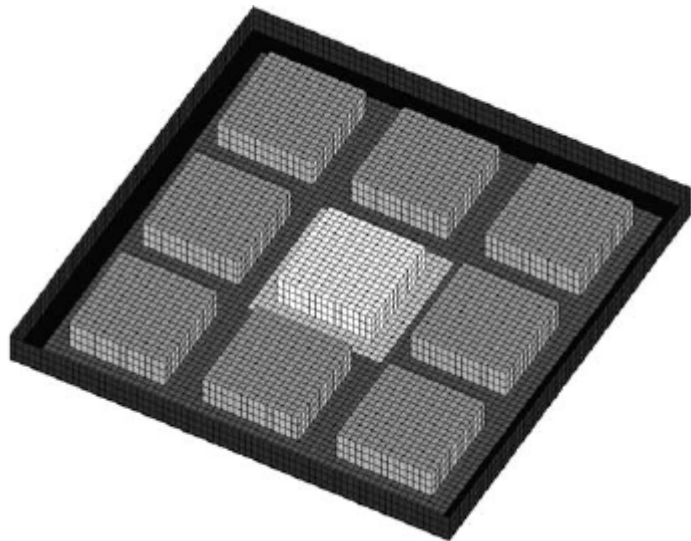


Figure 2.13: An example TUF-3D domain with a bounding wall and the sub-domain S_d (chosen to coincide with the central urban unit) in lighter shades (Krayenhoff & Voogt 2007, p. 437).

These features will be added to the model as a objective (Section 3.2.1) of this project creating a model which can be used to examine WSUD scenarios in detail at a micro-scale. TUF-3D was built from radiative flux movements from the ground up and that's where its strength lies, as surface temperatures and mean radiant temperatures are critical for determining HTC. The simplifications in the convection scheme are anticipated to strike a suitable balance between complexity and computational intensity and accuracy and resolution.

2.6.2 MAESPA

In order to supply the modelling capability to include vegetation in the TUF-3D domains, a model capable of simulating effects of trees and vegetation is needed. For this task, MAESPA (Duursma & Medlyn 2012) has been chosen.

MAESPA is a soil-plant-atmosphere model and provides forest canopy radiation absorption and photosynthesis functionality, in addition to water balances. It is a process-based model (PBM), modelling the interactions among environmental drivers, plant and canopy structure, leaf physiology and soil water availability and their combined effects on water use and carbon uptake (Figure 2.14).

MAESPA is derived from two previous models, MAESTRO (later rewritten and renamed as MAESTRA) (Wang & Jarvis 1990; Medlyn 2004) and SPA (Williams et al. 2001b). The MAESTRA model is a tree array model that uses detailed radiative transfer calculations and leaf physiology to calculate radiation absorption, photosynthesis and transpiration of individual trees, growing singly or in a population (Medlyn 2004; Wang & Jarvis 1990). SPA is a process-based model, with a focus on the impacts of water availability on forest canopies. The sources and origins of the various components in MAESPA are shown in Table 2.1.

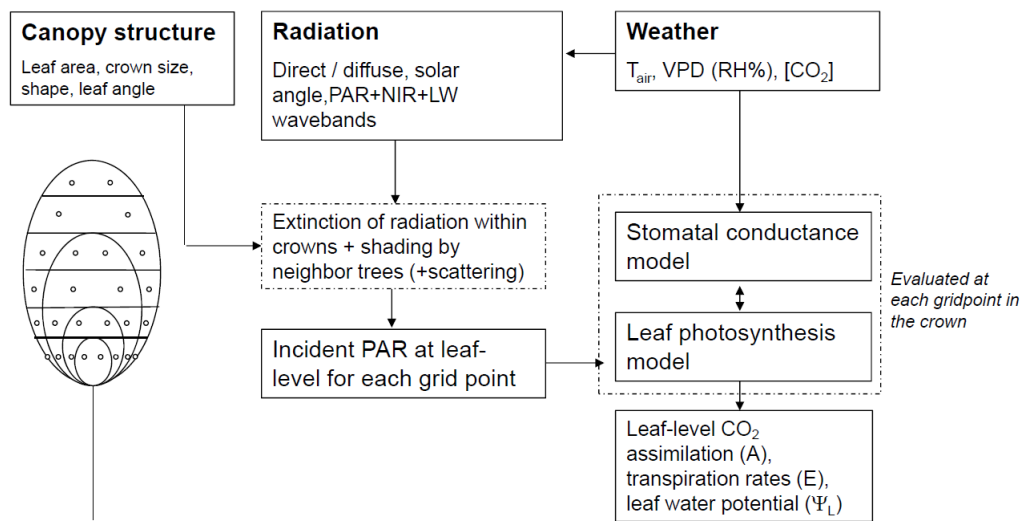


Figure 2.14: MAESPA process flowchart (Duursma & Medlyn 2012).

Table 2.1: Summary of origin of the various components of the MAESPA model (Duursma & Medlyn 2012).

Model component	Source
Radiative transfer	MAESTRA
Leaf energy balance	MAESTRA
Leaf photosynthesis	MAESTRA
Stomatal conductance (g_s), leaf and canopy transpiration	MAESTRA
Additional models for g_s	Tuzet et al. (2003); Medlyn et al. (2011)
Canopy interception	SPA
Soil drainage	SPA
Soil evaporation	SPA
Soil surface energy balance	SPA
Soil temperature profile	SPA
Soil water balance	SPA
Infiltration	BROOK90; Federer et al. (2003)
Root water uptake	Modified from SPA; Taylor & Keppler (1975)
Soil water retention and hydraulic conductivity	Campbell (1974)

Canopy components

For MAESPA, the functionality of the canopy components was largely described by Wang & Jarvis (1990) with its origins in the MAESTRO model. The canopy of individual trees is built based on several possible shapes (cones, cylinders, ellipsoids, etc.) and using parameters of length, height, and width. These canopies are broken down into a number of grid points. Radiation transfer (of direct and diffuse radiation) and interactions (shading effects and sun movement) from three different wavelengths (photosynthetically active radiation (PAR), near infra-red (NIR), and long-wave) are modelled in the crown grid points using the approaches detailed in Table 2.2.

Calculations differ based on whether the canopy section is sunlit or shaded. Calculations of stomatal conductance, photosynthesis, and transpiration follow for each grid point. Photosynthesis uses the Farquhar et al. (1980) model.

Stomatal conductance (discussed in Section 2.5.2.2) uses the Ball-Berry approach (Ball et al. 1987), with options to use a number of variations, the Ball-Berry model (Ball et al. 1987) in Equation (2.5.4), the Ball-Berry-Leuning model (Leuning 1995) in Equation (2.5.5), the Ball-Berry-Opti model (Medlyn et al. 2011) in Equation (2.5.6), and the Tuzet model (Tuzet et al. 2003) in Equation (2.5.7). As previously discussed, the first variation is suitable for well watered vegetation, while the other variations perform better under water limited cases.

As a basis for an urban vegetation modelling tool, this combination of canopy components in MAESPA has many advantages. The model requires a large number of physical and physiological parameters to be set for each item of vegetation, either through observations of modelled species or using values from the literature. While this will add to the complexity of model configuration, it does allow for precise scenario creation using any type and species of vegetation.

The model is complex and detailed, with a good level of three dimensional detail in the canopy structure, allowing for detailed examinations of interactions between the structure of the canopy and the canopy processes (Medlyn 2004). This is a strength in urban modelling. Urban ecosystems are highly heterogeneous, with large spatial variations of surfaces, vegetation, built and non-built structures (Cadenasso et al. 2007). The combination of the MAESTRA and SPA models into MAESPA can account for non-homogeneous stand structure (Duursma & Medlyn 2012), built on a base of modelling a single tree of arbitrary size and shape, either scaling up to an entire stand or modelling an array of unique trees (Figure 2.16), allowing a wide variety of variations to be explored.

Table 2.2: Summary of approaches of the canopy components of the MAESPA model.

Canopy component	Source
Radiative transfer	Wang & Jarvis (1990)
Scattering of radiation	Norman (1979)
Leaf area within crowns is assumed to be distributed randomly, or to follow a beta-distribution in horizontal and/or vertical directions	Wang et al. (1990)
Separate leaf area into sunlit and shaded leaf area	Norman (1993)
Photosynthesis	Farquhar et al. (1980)
Stomatal conductance	Ball et al. (1987)
Calculation of leaf temperature and leaf water potential	Penman-Monteith; Penman (1948)

Water balance components

The water balance components in MAESPA (Table 2.3 and Figure 2.15) largely have their origins in SPA. Soil moisture is stored in a (user defined) number of layers and infiltration, root water uptake, and soil evaporation are modelled through these layers. Infiltration is based on the BROOK90 model (Federer et al. 2003). Root uptake is based on Jackson et al. (1996) using a parallel soil-to-root resistance approach and root resistance (radial resistance) to uptake. Soil evaporation takes place through a thin dry top layer based on the water vapour pressure differences between air spaces in the soil and the air above. This was developed by Choudhury & Monteith (1988) and modified by Williams et al. (2001a).

Modelled rainfall, based on (Rutter et al. 1975), can either collect in the canopy until the canopy pool is filled or fall straight through. Evapotranspiration of rainfall collected in the canopy is calculated by the Penman-Monteith equation (Section 2.5.2.3). Drainage is calculated

from the soil hydraulic conductivity based on the SPA model (Williams et al. 2001b). Finally, the hydraulics of the soil-to-leaf pathway use a number of equations based on an approach of Campbell (1974).

MAESPA provides a robust base of functionality to bring the water cycle into micro-scaled urban vegetation modelling. MAESPA is the first PBM to connect plant physiological functions and vegetation canopy structures while also including detailed water balance and soil-plant hydraulics (Duursma & Medlyn 2012). MAESPA also includes suitable techniques to correctly capture water limited functioning (Duursma & Medlyn 2012). This is especially useful in modelling urban areas, which often expose urban vegetation to harsh conditions and challenges of water availability (Coutts 2014; Coutts et al. 2012).

Table 2.3: Summary of approaches of the water balance components of the MAESPA model.

Water balance component	Source
Infiltration	BROOK90; Federer et al. (2003)
Root water uptake	Jackson et al. (1996)
Soil evaporation	Choudhury & Monteith (1988), modified by Williams et al. (2001a)
Canopy interception	Rutter et al. (1975)
Drainage	
Hydraulics of the soil-to-leaf pathway	Campbell (1974)

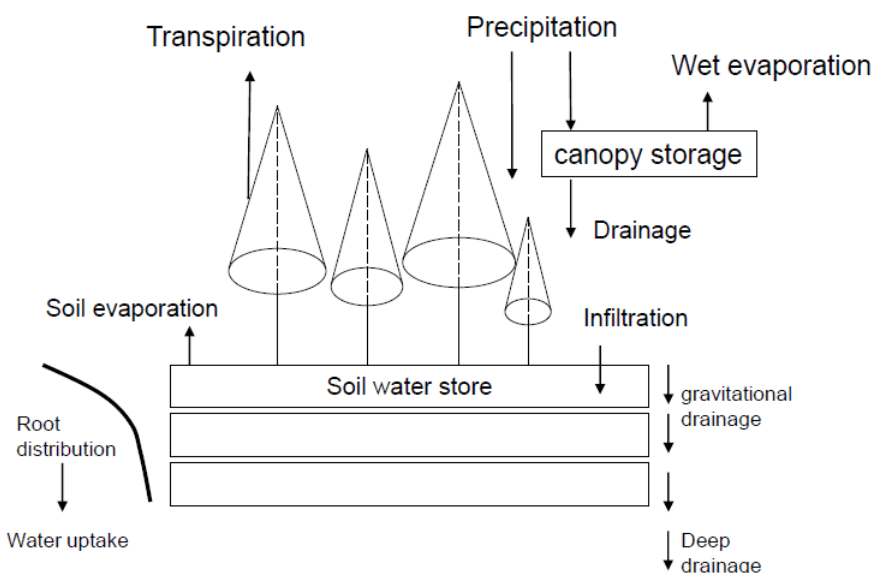


Figure 2.15: MAESPA water balance flowchart (Duursma & Medlyn 2012).

Heat soil balance components

The final set of components in MAESPA make up the heat soil balance functionality. These consist of soil surface temperatures and the soil temperature profiles. Soil surface temperatures are calculated from the energy balances of net radiation, sensible and latent energy fluxes, and ground storage. Heat transfer in the soil is based on the SPA model and Williams et al.

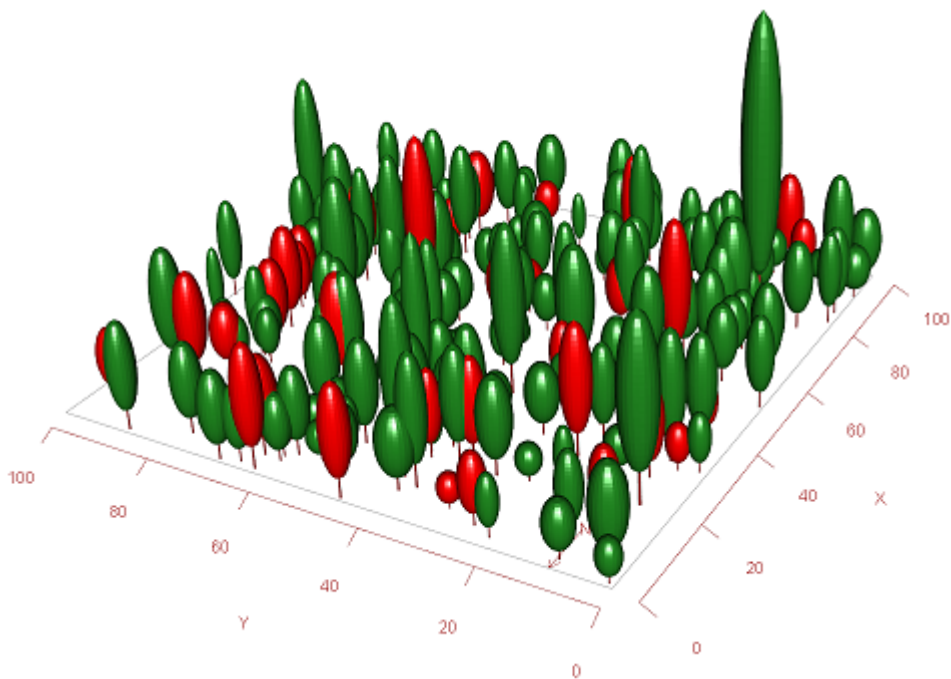


Figure 2.16: MAESPA stand (Duursma & Medlyn 2012).

(2001b). In this, Crank-Nichols (Press et al. 1990) solves the Fourier heat transport equation and generates a soil temperature profile and solves the heat flux movement between layers.

Application of MAESPA for urban modelling

While MAESPA was designed for a completely different modelling purpose than HTC assessments in urban areas, the model does provide a complete set of functionality to model a single tree (or scale up to model a stand of trees) (Figure 2.16). The processes modelled as described above and shown in flowchart form (Figures 2.14 and 2.15) could be leveraged to provide missing modules to model vegetation physiology and water balances.

2.6.3 Tool creation for modelling urban vegetation

It is anticipated that the marriage of the TUF-3D model with the MAESPA model will create a tool suitable for modelling urban vegetation at a micro-scale. The creation and validation of this model will be the major objective of this project. Afterwards, the model will be used to demonstrate its ability to quantify the cooling effects of urban greening. The theoretical basis of, as well as the current state of observational and modelling work with urban greening, will be covered in the next section.

2.7 Cooling through urban greening

While urban buildings and their arrangements can be designed to promote cooling effects, the rest of the urban canyon can also be designed to this end. Studies on urban vegetation have shown that they can also provide cooling benefits. Rosenfeld et al. (1998) found that street trees in Los Angeles accounted for \$58 million in savings from cooler urban surfaces from shading effects. At a citywide scale (local scale) using all aspects of vegetation cooling, Rosenzweig et al. (2009), in a modelling study, examined different scenarios of heat mitigation in New York

City and found that widespread greenery could reduce city-wide average air temperatures by 0.4°C to 0.7°C during hot afternoons.

Urban greenery can contribute to cooling effects in two different ways, through shading and increased transpiration. Observational studies of street tree shading have found temperature reductions could be obtained of 0.4°C to 2.2°C on streets in Athens during the afternoon (Tsiros 2010). Shashua-Bar & Hoffman (2000) observed average shade effects of 2.8°C with an effective range of cooling of 20-60m. These two studies (both at a scale approaching micro-scale) highlight some highly localised cooling effects, as opposed to the average widespread effects of the New York City scenario.

In addition to shading effects, a modelling analysis (at a micro-scale using ENVI-met) considered increased canopy cover, albedo modification, and orientation effects in relation to shade trees and found a cooling effect to be 3-4°C (Shashua-Bar et al. 2010). Other observational and modelling studies (at a micro-scale) found shade trees only contributed about 1.1°C cooling in air temperatures but in terms of thermal comfort, physiologically equivalent temperatures (PET) were reduced by 12°C (Spangenberg & Shinzato 2008).

At the local scale, Mitchell et al. (2008) used modelling to examine temperature reductions using a variety of scenarios, including WSUD treatments (such as swales, rain gardens, and wetlands) and found a 0.5°C decrease in temperature over conventional urban layouts (Table 2.4).

Table 2.4: Summertime E (from Aquacycle simulations) converted to diurnal heating rates and the consequent effect on peak afternoon air temperatures for each of the seven scenarios relative to a ‘desert’ (Mitchell et al. 2008, p. 2898).

Scenario	Summer E(mm day ⁻¹)	Average heating rate (°C h ⁻¹)	δT_{amax} (°C)
Conventional urban layout	1.58	1.64	-4.6
Wetland added to conventional urban layout	1.61	1.63	-4.7
Grass swales added to conventional urban layout	1.60	1.64	-4.6
Vegetated roof conversion	1.73	1.59	-5.0
Full vegetated WSUD treatment train	1.76	1.58	-5.1
Full vegetated WSUD treatment train with 50% reduction in garden watering	1.60	1.63	-4.6
Full vegetated WSUD treatment train with 100% reduction in garden watering	1.44	1.69	-4.2
Desert	0.00	2.15	0.00

2.8 Research gaps in modelling urban micro-climates

Modelling tools are needed to resolve full temperature gradients (as well as wind speed and humidity in order to calculate HTC) across a modelled urban canyon. In addition, proper modelling of latent energy fluxes and vegetation is critical to WSUD studies, as a desired side effect of WSUD is localised cooling effects due to increased water and vegetation within the urban canyon.

A large number of models were found that include vegetation that model at a local scale. However, the coarseness of their predictions do not allow resolution of critical parameters needed to calculate HTC. Their necessary simplification and parameterisation of urban canopy processes mean they are not detailed enough to capture spatial and temporal variations in HTC within the urban canopy. The detailed interactions between vegetation and the built form are averaged in local scale LSS, when in fact, HTC is highly variable at the micro-scale due to variable shading patterns.

Only one model at this scale was found to resolve shading effects themselves. However, as with all the other UCMs, these results were averaged upward, thus the detail is ultimately lost. These detailed interactions also influence vegetation transpiration behaviour across the diurnal cycle. This important aspect of HTC impacts of vegetation can not be captured without these interactions.

At a micro-climate scale, there are a number of models surveyed in the literature review, none of them are suitable to model WSUD. This was primarily due to either difficulties with these requirements or exclusion of these features by design. Many of them only integrated shading and radiation effects of the vegetation but did not include vegetation physiological process and urban water cycles. While this allows some analysis of the impact of vegetation on urban T_{mrt} , as with the local scaled models, the transpiration impacts of vegetation can not be captured. This leaves the ability to assess WSUD features incomplete.

The rest of the micro-scaled models surveyed were CFD based. They can provide very detailed resolution of wind, particle, and radiation movement. Many of them have added vegetation processes processes through many of them same techniques used in the local and meso-scaled models. While many of these techniques can capture some of the impacts of vegetation, they do not lend themselves to the flexibility and wide variety of vegetation modelling that can be found in a model like MAESPA. As a result of these factors, this category of models remains extremely complex and computationally intense, and inaccessible to less expert users, while also lacking the ability to model highly detailed mixes of vegetation.

What is needed is an approach that fits in between these two levels of complexity, a new innovative method to balance detail, accuracy, and complexity with efficiency and usability, while also being able to consider a wide variety of vegetation types and arrangements. This approach needs to capture the detailed movement of radiation through complex urban areas integrated with a widely configurable amount of vegetation. It also needs to balance this complexity against usability to create a model that can be widely used to consider a large variety of questions about HTC impacts of urban vegetation in support of urban planning decisions and guidelines.

The TUF-3D model has been identified as a starting point for a new model which will address these problems, however the lack of vegetation and water modelling leaves it incomplete. Coupling TUF-3D with the MAESPA model, to plug in any type of vegetation and include those processes and influences, can create the model needed for assessing WSUD features in support of HTC in urban areas and fill these gaps is this research area.

Once this model, the VTUF-3D model (Vegetated Temperatures Of Urban Facets), is complete, it can be used to start assessing the impacts of WSUD. This is a very large gap which needs to be filled to use WSUD in the most effective way to protect human health in light of all the concerning trends progressing in urban areas.

Chapter 3

Methodology

3.1 Project objectives

In order to facilitate the integration of urban greening into the landscape and inform planning decisions with urban climate knowledge about how to best utilise urban greening to maximise the thermal comfort impacts and meet the challenges of urban heat, a suitable model is needed. This model, devised for HTC assessments of WSUD, will need to be at the right scale, to test the impacts of different urban configurations on HTC. The introduction and literature review have shown that this model does not currently exist. Therefore, the first objective of this project will be to create this modelling tool.

The context for this model was examined in the literature review. In it, urban climates and its main drivers were examined. Human thermal comfort was introduced as a method to quantify climate conditions in urban areas and their effects on human health and well being. In both of these, lie important implications for modelling tools that will be able to accurately model these physical processes and assess the resulting impacts on HTC. As an added complication, modelling the impacts of WSUD in these areas, using techniques from Section 1.7.1, adds additional specialised requirements and requires special attention to the changes WSUD can cause in some of the driving processes in urban areas, particularly radiation effects and transpiration (soil-plant-atmosphere continuum).

There are a number of models available and techniques suitable to model urban areas, and to a lesser extent, to include vegetation as part of this assessment. The literature review highlighted a wide variety of techniques currently used to assess urban vegetation impacts at a range of scales. Influences of vegetation are generally integrated into models in two different ways, using the radiation and shading effects of the vegetation and including the influence of vegetation transpiration. At local and meso-scales, transpiration effects are added by schemes such as 'Big Leaf', where a single leaf is scaled up to an entire urban canopy. Likewise, while only one model has explicitly modelled shading effects of vegetation, these effects are also scaled upwards. At this scale, it is not possible to examine the HTC impacts of vegetation because this scaling up of results only allows an averaged view of the urban area.

At micro-scales, models are also split into two different categories. In the first, simpler models only consider the radiation and shading effects while not considering the transpiration. These can be useful tools but cannot show the entire picture without considering the transpiration effects. The other category contains CFD based models that can resolve air flow in great detail but at a high computational cost. Vegetation transpiration calculations can be added as well using many of the same techniques used in the local and meso-scaled models. However, CFD

micro-scaled methods have remained somewhat inaccessible and complex while validations of their ability to capture vegetated effects have not always proved successful.

3.1.1 Research aim and questions

Consideration of all models available confirms there are currently no models existing to handle the specialisation required to also assess WSUD features and their impacts on HTC in urban areas. This leads to the research aim for this project:

To develop an urban micro-climate modelling tool to support the implementation of urban greening and the development of thermally comfortable urban environments.

The research questions this project proposes to answer are:

- **Can a micro-scale climate model be devised for HTC assessments of WSUD?**
- **Can this new micro-climate model be shown to be accurate and suitable for these assessments?**
- **Finally, can this new micro-climate model be demonstrated as able to answer questions and inform planning decisions about how to best utilise urban greening to maximise the thermal comfort impacts of WSUD?**

3.2 Research stages

In the literature review, two models, TUF-3D (Section 2.6.1) and MAESPA (Section 2.6.2), were found to potentially contain all the functionality and techniques needed. However, as individual models, neither can be used for the desired purpose and their functionality must be combined to complete the finished modelling tool. As a new model created from these two models, the model will be able to model all the associated processes (vegetation processes, water cycle, and latent energy fluxes) at a scale suitable to resolve the required parameters necessary to calculate HTC.

In pursuit of the research aim and answering the research questions, this project will have a number of key objectives. The design, engineering, and analysis objectives (described at a high level) include the following:

- Two models, TUF-3D and MAESPA will be synthesised into a new model, VTUF-3D (Vegetated Temperatures Of Urban Facets), using the base surface energy balance framework of TUF-3D and the functionality from MAESPA to account for vegetation structural and physiological processes.
- A validation process will determine the level of improvement over the existing models and accuracy of this new VTUF-3D model in resolving the impacts of urban greenery. Three different datasets will be used to validate the model. Flux tower data (Coutts et al. 2007) will allow validation of surface energy balance partitioning. Spatial observations of $UTCI$ and T_{mrt} (White et al. 2012; Coutts et al. 2015a) will measure the model's spatial and temporal accuracy in capturing these two parameters. Finally, Gebert et al. (2012) observations will test the model's ability to resolve the urban environment's influence (through the urban canyon's geometry and composition creating differing conditions in the canyon) on the urban vegetation.

- A demonstration of the newly created VTUF-3D model's shows the ability to assess the impact of WSUD treatments on HTC at a micro-scale in urban areas. In this project, this demonstration will assess varying levels of canopy cover and quantify improvements in HTC using both temperature scales (air and radiant temperatures) as well as HTC indexes (using UTCI).

3.2.1 Objective 1 detail - creation of the VTUF-3D modelling tool

Modifications will be done to the TUF-3D model to enable modelling of urban vegetation and WSUD features. This will also require adding latent energy fluxes, an external (outdoor) water cycle, and vegetation processes to the TUF-3D model to support modelling of these features. This model already models at a micro-scale using a simplified 3D scheme, however latent energy fluxes are not currently modelled. In addition, vegetation is not accounted for in this model along with the shading effects and the latent energy fluxes associated with vegetation.

Two major additions need to be made to the TUF-3D model. These are the VTUF-3D/MAESPA vegetation/radiation interactions and VTUF-3D energy balance modelling with MAESPA tiles. The full details of these improvements are detailed in the VTUF-3D design chapter (Chapter 4) but the overall approach will be described briefly below.

VTUF-3D/MAESPA vegetation/radiation interactions

TUF-3D uses cubes (and their surfaces) as the basic building block for the modelling domain. This works well for buildings and roads but presents challenges for adding vegetation, due to their varieties of shapes. This will be overcome by using placeholder shapes in VTUF-3D that approximate their structure but use MAESPA's underlying functionality to model the vegetation using its library of vegetation shapes. VTUF-3D will expand TUF-3D's configuration system by adding in configuration files to map the placeholder vegetation representations to MAESPA vegetation representations.

The second step in adding the vegetation/radiation interactions is modifying TUF-3D's shading routines. At each timestep during the simulation, the transmission of short-wave and long-wave radiation is traced through the domain and applied to the surfaces receiving them. If vegetation is encountered during these transmissions, MAESPA functionality is used to determine the transmission, absorption, or reflection, and modifies the eventual amount that is applied to receiving surfaces. These modified amounts will account for the shading effects of the vegetation and drive changes in the surfaces' surface temperatures and energy balances, which in turn will drive modifications to overall canyon temperatures.

VTUF-3D energy balance modelling with MAESPA tiles

In addition to the radiation interactions between the vegetation and the other surfaces and structures in the domain, the physiological processes of the vegetation must be represented, and the evapotranspiration and water storage of the soils must also be calculated. This will be achieved by tiling MAESPA instances across the ground surfaces in VTUF-3D. Normally, TUF-3D ends each timestep by calculating the energy balances of each surface using the received and lost energy during that timestep.

In VTUF-3D, each ground surface can now contain a MAESPA tile to handle the vegetation and soil processes, such as water uptake, transpiration, photosynthesis, soil water movement and surface evaporation. The MAESPA tile will contain layers of soil, a vegetated or unvegetated surface, and any number of trees (or other types of vegetation). Before VTUF-3D calculates the energy balances of each surface, calculations of fluxes and an energy balance for the vegetation

is loaded from the MAESPA tile. These results are used to adjust the partitioning of fluxes in the energy balance step and the ending states are stored in the VTUF-3D surface as the starting conditions for the next timestep.

3.2.2 Objective 2 - validation of VTUF-3D modelling tool

After the integration of these two models into VTUF-3D, the model will be able to model a wide variety of WSUD features (features which includes trees and other urban vegetation in addition to engineered features) and assess their impacts to HTC. However, validations need to be run to ensure the model is accurate and functioning properly. A number of different observational data sets will be used to validate a number of different aspects of the new model.

Comparison to Preston data

A first set of observations, a data set collected in Preston (in Melbourne, Australia) by Coutts et al. (2007), contains a year's worth of flux tower observations. Comparisons of VTUF-3D modelled output to observations of energy fluxes (Q^* , Q_H , Q_G , and Q_E) allows verification of the basic drivers of urban climates. These validations will be based around error analysis of d index of agreement and RMSE values between the two.

This data set was also used in the recent International Urban Energy Balance Models Comparison Project (Grimmond et al. 2010; 2011). As this validation will use the same forcing data as in the Comparison project, this will allow the performance of the model to be directly compared to the other urban models in this comparison project.

Comparison to City of Melbourne Gipps/George St. street tree study

A second set of observations will be used to evaluate VTUF-3D's ability to reproduce mean radiant temperature (T_{mrt}) and HTC indexes ($UTCi$). These observations, from George St. and Gipps St. in the City of Melbourne (White et al. 2012; Coutts et al. 2015a), were recorded at a number of different locations on each street. A comparison, based around error analysis of d index of agreement and RMSE values, will validate VTUF-3D's ability to predict accurate results of T_{mrt} and $UTCi$ at these specific points in the streetscape over a diurnal cycle.

Comparison to Smith St. single tree study

A final set of validations will be based on a tree study campaign recorded at Smith St. in Melbourne (Gebert et al. 2012; Coutts 2014). This data set includes weather data recorded at a number of locations along this street, but also contains physiological data (transpiration) collected from Lorikeet Summer Scentsation (*Eucalyptus olivacea*) and Tolley's Upright (*Olea europaea*) based tree pits.

Accurate reproduction of the Smith St scenario will be an important validation of VTUF-3D's ability to model WSUD features, as tree pits are a WSUD feature of high interest. These scenarios also validate VTUF-3D's modelling of canopies and their interactions with the urban environment. This also includes verification of the urban environment's impact of vegetation (variable illumination due to the street and building geometry) and differing responses of the vegetation at different locations in the streetscape.

3.2.3 Objective 3 detail - demonstration of new VTUF-3D model with canopy cover scenarios

The final stage of the project will demonstrate that the aim of this project has been fulfilled, that a suitable model has been developed to support the implementation of urban greening and development of thermally comfortable urban environments. This demonstration will use this new model to examine some of the impacts of WSUD on HTC in urban areas at a micro-scale. A set of scenarios will concentrate on varying levels of canopy cover and this canopy cover's impact on HTC in the streetscape. This demonstration sets the stage for the use of VTUF-3D to conduct future detailed studies of a wide variety of factors to maximise the benefits of WSUD infrastructure and urban greening on HTC in urban areas.

3.3 Summary of research steps

A clear sequential procedure has been detailed here in the Methodology that will directly address the research objectives and answer the research questions. Development in FORTRAN will complete the improvements required in the design chapter, Chapter 4. Next a validation of the modelled output from scenarios built from the three sets of observational data in Chapter 5 and will be conducted using analysis tools in R and Python. Finally, the final objective, a demonstration of the new model's ability to model WSUD scenarios, will be completed in Chapter 6, building on the validation scenarios and using many of the analysis tools from the validation chapter.

Chapter 4

Creation of VTUF-3D urban micro-climate model to support assessments of WSUD influences on HTC at a micro-scale in urban canyons

4.1 Overview of changes

To model the impacts of increased water and vegetation on human thermal comfort in urban areas requires modifications to TUF-3D (Krayenhoff & Voogt 2007). TUF-3D in its unmodified form lacks functionality for the physical representation of vegetation along with their physiological processes. Also missing are latent energy fluxes and the water cycle associated with soil, vegetation, evaporation, and precipitation.

Two major changes must be made to the TUF-3D model to add this missing functionality. The first is representation of vegetation's physical form and radiative interactions within an urban canyon. This is done using placeholder vegetation structures which load data calculated by MAESPA (Duursma & Medlyn 2012) for vegetation absorption, transmission, and reflection of each individually modelled vegetation element (Figure 4.1).

VTUF-3D (Vegetated Temperatures Of Urban Facets) uses cube shaped structures (as TUF-3D uses to represent buildings) to represent vegetation. These cubes store the surface properties and states and interact with the rest of the VTUF-3D domain. The vegetation's true shape is represented in MAESPA and accessed through the simulation by loading that calculated data. This allows quantifying shading effects and the cooling benefits that can bring.

The second major change required is including the physiological processes of vegetation and soil in the model. Using a novel approach, MAESPA tiles replace VTUF-3D ground surfaces with vegetated MAESPA surfaces and use results of MAESPA's photosynthesis and water cycle routines to modify VTUF-3D's energy balance calculations. Each embedded MAESPA surface calculates a full 3 dimensional tree (along with associated soil and movement of water) and feeds results back to VTUF-3D ground surface energy balances (Figure 4.1).

At the conclusion of each timestep, VUF-3D calculates the energy balance of each surface. Incoming radiation energy and existing stored energy are partitioned into new values of storage

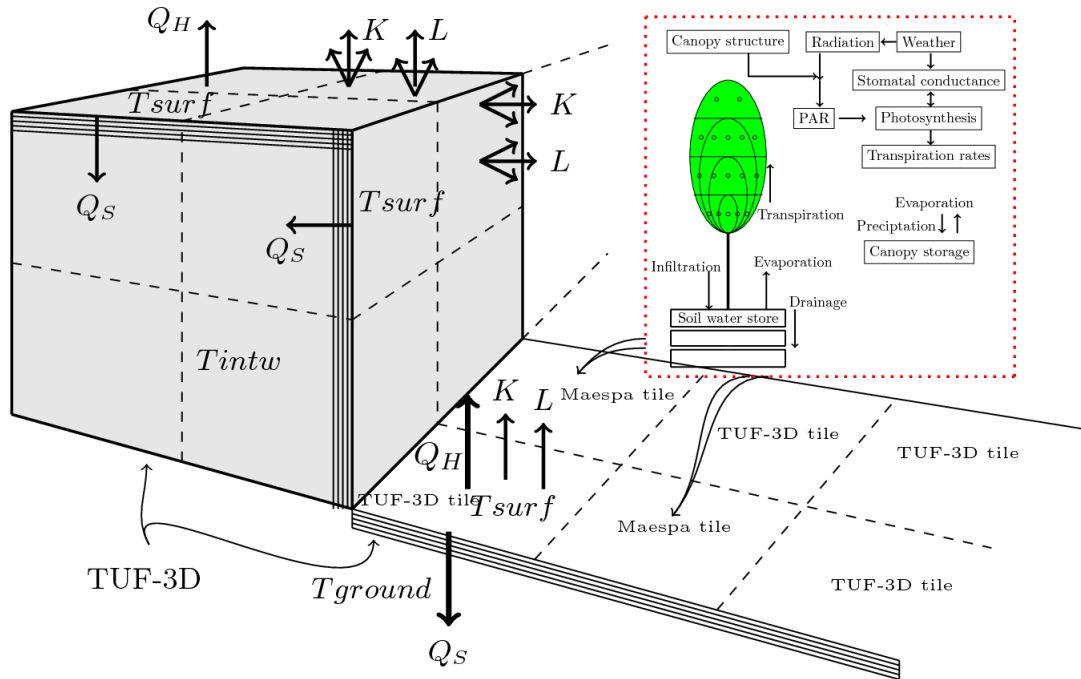


Figure 4.1: VTUF-3D energy balance modelling with vegetation MAESPA tiles.

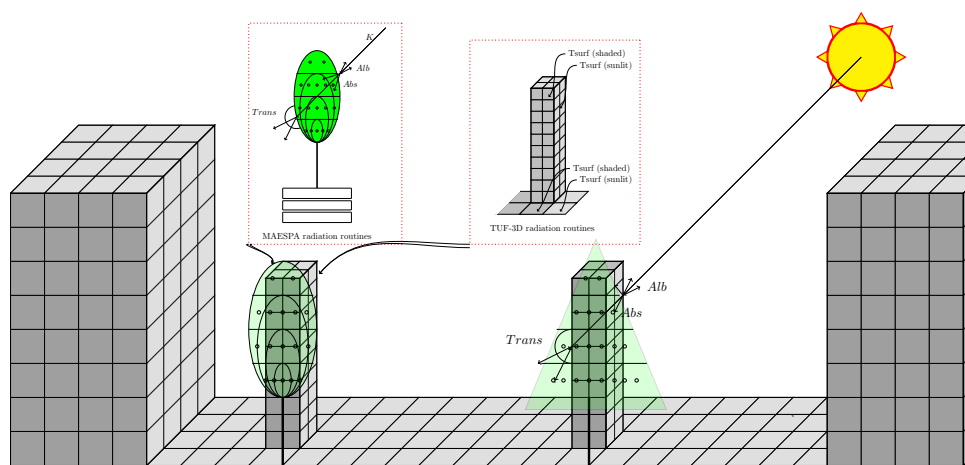


Figure 4.2: Integration of MAESPA tree model into VTUF-3D radiation fluxes routines, in which tiled instances of MAESPA vegetation (in green) are used to calculate radiation transmission for VTUF-3D placeholder vegetation structures (in grey).

and radiated heat. In order to account for the addition of vegetation, these energy balances have been modified to account for latent energy fluxes and the physiological processes of vegetation.

In VTUF-3D, a variable for latent energy is added and energy allocated to it from the pool of available energy. The vegetation is treated as a flat two dimensional ground surface tile. This is done by tiling multiple instances of MAESPA (each individual tree with its unique configuration) into surfaces that have vegetation (Figure 4.1). These instances have calculated, in three dimensions using the canopy structure, radiation transmission, energy fluxes, and soil water storage for each individual tree.

If a surface does not contain vegetation, VTUF-3D runs its normal energy balance calculations. If a surface does contain vegetation, VTUF-3D loads the pre-calculated fluxes (in Section 4.3.3). The tiling is structured by the *treemap.dat* configuration file (Section 4.4.3). This file maps an X,Y grid location to its unique tree configurations, properties, and characteristics.

Being able to model the soil/water, plant and atmosphere interactions allows the role of water to be quantified in urban areas. The entire cycle of soil moisture to vegetation transpiration and evaporation can be examined for its micro-climatic benefits.

In this chapter, the three distinct models will be differentiated in the following way. TUF-3D will refer to the unmodified TUF-3D model. MAESPA is the unmodified MAESPA model. VTUF-3D refers to the modified TUF-3D model, including the embedded functionality from MAESPA, which will be the end product of this chapter.

The overall process flow of this new VTUF-3D model is shown in Figure 4.3.

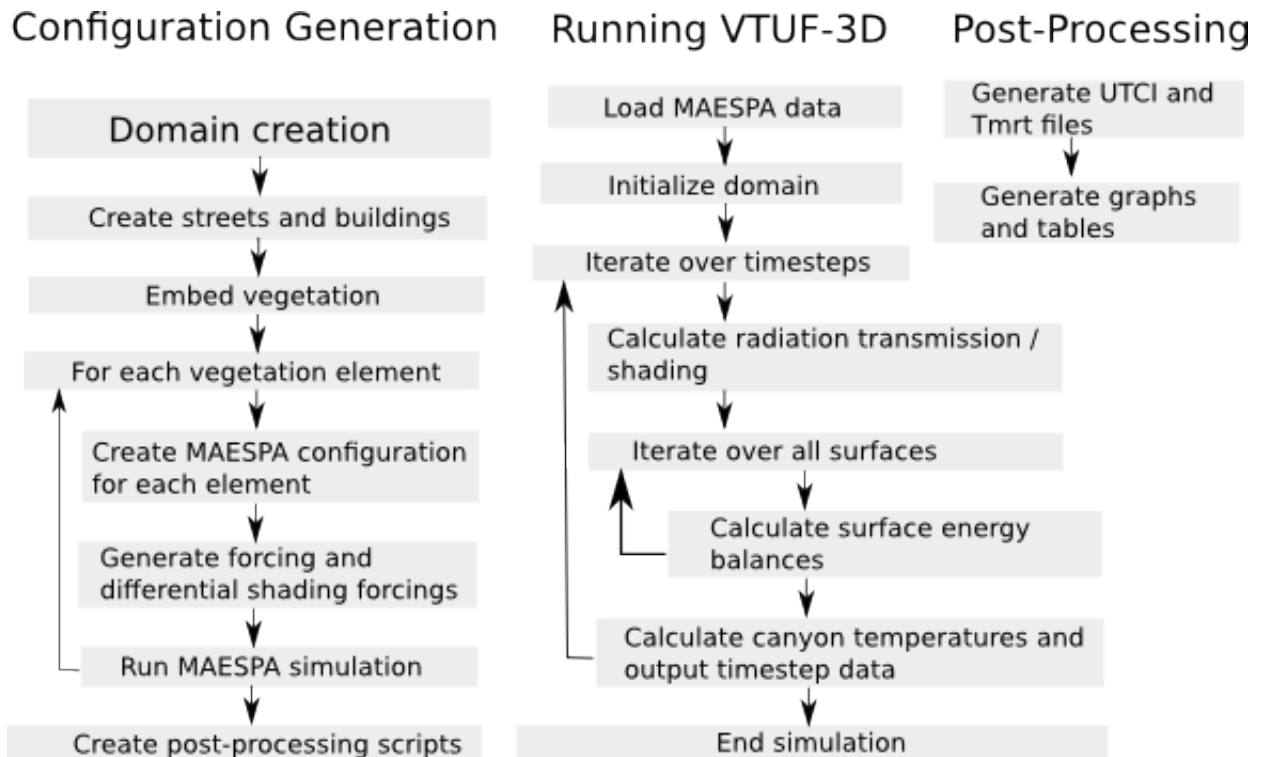


Figure 4.3: VTUF-3D model process flow.

4.2 Model description

In the following section, the VTUF-3D model is detailed. This model is constructed largely using the TUF-3D model, as described in Krayenhoff & Voogt (2007) and previously detailed in Section 2.6.1, leaving all its components largely unchanged except for the two interactions as described in the overview of changes. The vegetation functionality is added through the MAESPA model (Duursma & Medlyn 2012) (previously detailed in Section 2.6.2), with some of its components running in parallel and replacing some of the TUF-3D components in some parts of a modelled domain. The linkage components will be described later in this chapter in Section 4.3.

4.2.1 Radiative processes

Radiative transfer

In order to track the movement and allocation of radiation, VTUF-3D's modelling domain is built up in 3-D using cubes and their surfaces (Figure 4.4). Ray tracing is used to determine visibility of each surface to each other, matched using plane parallel analytical equations of Siegel & Howell (2001) and Hottel & Sarofim (1967). Surface patch sky view factors are calculated in Equation (4.2.1)

$$\Psi_{i,sky} = 1 - \sum_{j=1}^n \Psi_{i,j} - \Psi_{i,external} \quad (4.2.1)$$

where $\Psi_{i,sky}$ is the sky view factor of surface patch i, $\Psi_{i,j}$ is the view factor from patch i to patch j, $\Psi_{i,external}$ is the view factor from patch i to external surfaces, and n is the total number of patches (Krayenhoff & Voogt 2007).

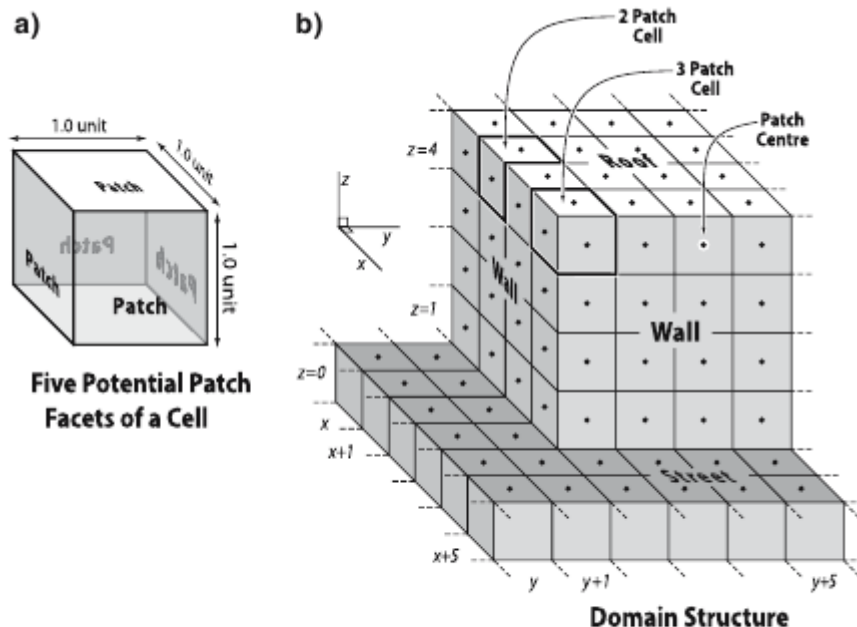


Figure 4.4: Basic cubic cell and surface patch structure of TUF-3D (Krayenhoff & Voogt 2007, p. 437).

Ray tracing is done of direct shortwave radiation to determine sunlit and shaded patterns on the 3-D urban surface using a modified version of the Soux et al. (2004) algorithm. In this, surface patches are divided into quarters, each tested through ray tracing to determine a percentage of illumination of each surface patch.

The initial incident direct shortwave (W m^{-2}), $K \downarrow_{dir,i}$, is calculated for each patch i based on sun angle and patch orientation in Equation (4.2.2)

$$K \downarrow_{dir,i} = \frac{\cos(\chi_i) K \downarrow_{dir}}{\cos(\phi)} \quad (4.2.2)$$

where ϕ is the solar zenith angle (degrees), χ_i is the angle between patch i 's normal vector and the vector pointing in the direction of the sun (degrees), and $K \downarrow_{dir}$ is the domain-level incoming direct shortwave (W m^{-2}).

The initial incident diffuse shortwave (W m^{-2}), $K \downarrow_{dif,i}$, is calculated in Equation (4.2.3)

$$K \downarrow_{dif,i} = \Psi_{i,sky} K \downarrow_{dif} \quad (4.2.3)$$

where $K \downarrow_{dif}$ is the domain-level incoming diffuse shortwave (W m^{-2}).

The initial incident sky-derived longwave (W m^{-2}), $L \downarrow_{i,sky}$, is calculated from sky-derived levels in Equation (4.2.4)

$$L \downarrow_{i,sky} = \Psi_{i,sky} L \downarrow_{sky} \quad (4.2.4)$$

where $L \downarrow_{sky}$ is the domain-level incoming longwave (W m^{-2}).

Reflections and absorption of longwave and shortwave are modelled using a radiosity approach (radiative reflection and emission treated as perfectly diffuse). Reflections are calculated iteratively until a user-defined threshold is reached. Reflections (R_i^{q+1} , the radiation reflected by patch i at reflection $q + 1$) are calculated for shortwave in Equation (4.2.5) and longwave in Equation (4.2.6)

$$R_i^{q+1} = \alpha_i \sum_{j=1}^n \Psi_{j,i} R_j^q \quad (4.2.5)$$

where α_i is shortwave albedo of patch i and $\Psi_{j,i}$ is the view factor from patch j to patch i , and

$$R_i^{q+1} = (1 - \epsilon_i) \sum_{j=1}^n \Psi_{j,i} R_j^q \quad (4.2.6)$$

where ϵ_i is longwave emissivity of patch i . Patch absorptions are calculated similarly.

For vegetated parts of the domain, radiative transfer is calculated by components from MAESPA (Duursma & Medlyn 2012). Incoming radiation, both photosynthetic radiation (PAR) and near infrared (NIR) is partitioned into direct and diffuse using Weiss & Norman (1985). Canopy structure is calculated based on Wang & Jarvis (1990), using a grid structure of 60 grid points. In this grid (Figure 4.5, also Figure 2.1), mean leaf area density is calculated as well as fractions of leaf inclinations at each point.

Calculation of L_d , the relative leaf area density within the tree crown (m^{-1}), is shown in Equation (4.2.7) (Wang et al. 1990)

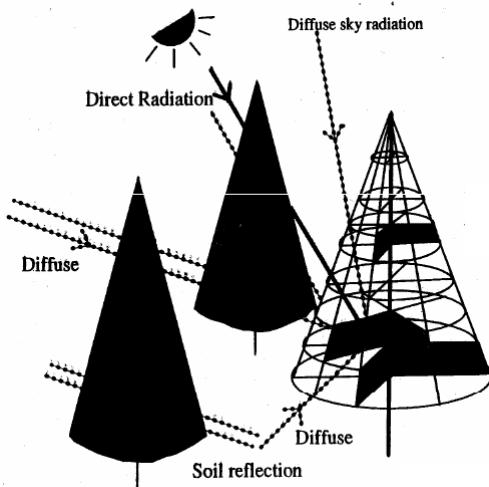


Figure 4.5: Calculation of radiation penetration in MAEPSA using gridded tree structures (Duursma 2008).

$$L_d = (F_1 / HR'^2(h)) B_1 h^{B_2} (1-h)^{B_3} B_4 r^{B_5} (1-r)^{B_6} \quad (4.2.7)$$

where F_1 is the total-area fraction of irradiated leafs on a branch, H is the tree height (m), h is the relative height within the tree crown or the canopy, B_i is the parameters in the leaf area density distributions within the tree crown or canopy ($i=1, 2$, and 3 for vertical distribution and $4, 5$, and 6 for horizontal distribution), r is the horizontal distance from the centre of the tree trunk (m), and $R'(h)$ is the crown radius at the relative crown height h (m).

A variety of crown shapes are supported through variations of $R'(h)$, including crown shapes:

Of conical tree, $R'(h) = R(1-h)$

Of half-ellipsoidal, $R'(h) = R\sqrt{[(1+h)(1-h)]}$

Of paraboloidal, $R'(h) = R\sqrt{(1-h)}$

Absorption and scattering of radiation (PAR, NIR, and thermal radiation) by the canopy is calculated using Norman (1979) given inputs of incident flux densities, beam fractions of PAR and NIR and the structural properties of the tree (calculated above).

Stomatal conductance

Stomatal conductance within the vegetation uses MAESPA components based on the Ball-Berry type approach (Ball et al. 1987; Duursma & Medlyn 2012). This is fully detailed in the Literature Review (Section 2.5.2.2) in Equation (2.5.3).

Calculation of leaf temperature and leaf water potential

Solving Equation (2.5.7), the Tuzet variation of the Ball-Berry stomatal conductance, using E_L , leaf level transpiration rate ($\mu\text{mol m}^{-2}\text{s}^{-1}$), to find Ψ_L , the leaf water potential (MPa), then can be used to estimate leaf temperature throughout the canopy. For each grid point, E_L is calculated with the Penman-Monteith equation, using the boundary layer conductance and total conductance (all detailed in the next section, Section 4.2.1.4). Leaf temperature is found by iteratively closing the energy balance of the leaf, based on Wang & Leuning (1998).

Total canopy transpiration

Canopy transpiration is calculated using the Penman-Monteith equation (fully described in the Literature review in Section 2.5.2.3). It is calculated by summing the application of the equation to each grid point using the calculated amounts of absorbed radiation (PAR, NIR, and thermal) for each tree.

g_B , boundary layer conductance ($\text{mol m}^{-2}\text{s}^{-1}$), is calculated following Jones (1992) in Equation (4.2.8)

$$g_B = \frac{c \times k_V^2 \times u_z}{[\log((z_H - z_D)/z_0)]^2} \quad (4.2.8)$$

where k_V is the von Karman's constant, u_z is the wind speed measured at a height of z_H (m s^{-1}), c is the conversion to molar units, z_0 is the roughness length (m), z_D is the displacement height (m), and z_H is the measurement height of wind speed (m).

g_V , the total conductance to water vapour ($\text{mol m}^{-2}\text{s}^{-1}$) is calculated using Jones (1992) in Equation (4.2.9)

$$g_V = 1/\left(\frac{1}{g_C} + \frac{1}{g_B}\right) \quad (4.2.9)$$

where g_C is the canopy conductance ($\text{mol m}^{-2}\text{s}^{-1}$), and g_V is the boundary layer conductance ($\text{mol m}^{-2}\text{s}^{-1}$).

The output of the canopy transpiration is used in Section 4.2.1.3 for leaf temperature calculations.

Conduction and surface temperatures

Heat conduction between the layers in each surface in VTUF-3D (based on TUF-3D) is calculated in a 1-D equation (based on Masson (2000)) in Equation (4.2.10)

$$T_b^{m+1} - T_b^m = \frac{\Delta t}{C_b \Delta x_b} (\gamma(G_{b-1,b}^{m+1} - G_{b,b+1}^{m+1}) + (1-\gamma)(G_{b-1,b}^m - G_{b,b+1}^m)) \quad (4.2.10)$$

where T_b is the temperature of layer b (K), C_b is the volumetric heat capacity of layer b ($\text{J m}^{-2}\text{K}^{-1}$), Δx_b is the depth of layer b (m), Δt is the timestep size (s), m is the timestep index, γ is the degree of implicitness (conduction) (i.e. $\gamma = 0$ is explicit, $\gamma = 1$ is implicit, and $G_{b,b+1}^m$ is the conductive heat flux between layers b and $b + 1$ at timestep m (W m^{-2})).

In order to calculate the surface temperature (the boundary condition for the surface), using the energy balance of the surface (based on a version of Arnfield (1990)), Equation (4.2.11) is solved for T_{sfc} at the next timestep T_{sfc}^{m+1} for each surface.

$$\begin{aligned} & (1-\alpha)K \downarrow^{m+1} + \epsilon(L \downarrow^{m+1} - \sigma(T_{\text{sfc}}^{m+1})^4) \\ & - h^{m+1}(T_{\text{sfc}}^{m+1} - T^{m+1}(z)) - \frac{k_1(T_{\text{sfc}}^{m+1} - T_1^m)}{\frac{1}{2}\Delta x_1} = 0 \end{aligned} \quad (4.2.11)$$

Soil surface temperature

For soil surface temperatures, for vegetated surfaces, this functionality is taken from the MAESPA components. Given the soil energy balance equation, Equation (4.2.12)

$$Q^* + Q_E + Q_C + Q_H = 0 \quad (4.2.12)$$

where Q^* is the net radiation flux density (W m^{-2}), Q_E is the latent heat flux (W m^{-2}), Q_C is the soil heat transport (to deeper soil layers) (W m^{-2}), and Q_H is the sensible heat flux (W m^{-2}), $T_{s,1}$, the soil surface temperature (K), is found by finding the values that provide closure to the energy balance in the following equations.

The first parameter to find the energy balance closure is calculated in the net radiation equation, Equation (4.2.13)

$$Q_L = Q_{GI} - Q^* = \epsilon \sigma T_s^4 \quad (4.2.13)$$

where Q_L is the longwave radiation (W m^{-2}), Q_{GI} is global radiation (solar + downward thermal (W m^{-2})), ϵ is the longwave emissivity, σ is the Stefan-Boltzmann constant ($=5.67 \times 10^{-8} \text{ W m}^{-2}\text{K}^{-4}$), and T_s is the soil surface temperature (K).

The second parameter, soil latent energy flux (Q_E) is calculated in the "soil evaporation" section, (Section 4.2.3.3).

The third parameter, soil heat transport (Q_C) is calculated in Equation (4.2.14)

$$Q_C = K_{th}(T_{s,2} - T_{s,1})/\Delta z_{1,2} \quad (4.2.14)$$

where $T_{s,1}$ is the soil surface temperature (K), $T_{s,2}$ is the soil temperature at layer 2 (K), $\Delta z_{1,2}$ is the depth difference between the second and first layer (m), and K_{th} is the soil thermal conductivity ($\text{W m}^{-1}\text{K}^{-1}$).

Finally, the fourth parameter needed to find the energy balance closure used to find soil surface temperature is the sensible heat flux (Q_H), calculated in Equation (4.2.15)

$$Q_H = c_p \rho G_{a,m}(T_{s,1} - T_{air}) \quad (4.2.15)$$

where c_p is the specific heat of air at constant pressure ($=1.01 \times 10^3 \text{ J kg}^{-1} \text{ K}^{-1}$), ρ is the density of air ($=1.2 \text{ kg m}^{-3}$), $G_{a,m}$ is the boundary layer conductance to heat transfer ($\text{mol m}^{-2}\text{s}^{-1}$), and T_{air} is the air temperature (K).

Energy balance partitioning during simulation timesteps

As the simulation proceeds through each time step, an energy balance is performed on each surface. For each surface with vegetation, the surface temperature (T_{sfc}) is set to the value calculated by MAESPA for that tree. The following describe the differences from the normal calculations the unmodified TUF-3D uses to calculate the energy balances needed by VTUF-3D to partition the energy fluxes of a vegetated surface.

Net radiation, is calculated in Equation (4.2.16) (Q_{veg}^* for vegetated grid squares, otherwise Q^*),

$$\begin{aligned} Q_{veg}^* &= K \downarrow - (\alpha_{veg} K \downarrow) + \epsilon_{veg} L \downarrow - \epsilon_{veg} \sigma (T_{sfc,veg})^4 \\ Q^* &= K \downarrow - (\alpha K \downarrow) + \epsilon L \downarrow - \epsilon \sigma (T_{sfc})^4 \end{aligned} \quad (4.2.16)$$

where α_{veg} of vegetation is set to 0.20 and ϵ_{veg} of vegetation set to 0.97 (Oke 1987, p. 12), otherwise α and ϵ are set to user configured values (model default values are 0.10 and 0.92 (Krayenhoff & Voogt 2007)), and σ is the Stefan-Boltzmann constant ($=5.67 \times 10^{-8} \text{ W m}^{-2}\text{K}^{-4}$), and $T_{sfc,veg}$ is the vegetation surface temperature, or T_{sfc} for non-vegetated surfaces.

For sensible heat fluxes (Q_H), vegetation is accounted for differently by using the T_{sfc} of the vegetation instead of the TUF-3D T_{sfc} value in Equation (4.2.17) and will yield a different result using the MAESPA vegetation T_{sfc} than if the TUF-3D surface temperature had been used

$$Q_{H,veg} = h_i(T_{sfc,veg} - T_{conv}) \quad (4.2.17)$$

where h_i is the previously calculated heat transfer coefficient ($\text{W m}^{-2}\text{K}^{-1}$), $T_{sfc,veg}$ is the vegetation surface temperature (K) and T_{conv} is the converging canyon temperature (K).

For latent energy fluxes (Q_E), $Q_{E,veg}$ is the value for the grid square calculated in the MAESPA tree calculations, loaded from the MAESPA data, and using the conversion in Equation (4.4.2).

Finally, ground storage fluxes (Q_G) are calculated as a residual of $Q^* - Q_H - Q_E$. Calculation of Q_G uses Equation (4.2.18) for grid squares containing vegetation, while non-vegetated grid squares use Equation (4.2.19) to calculate the street ground storage fluxes

$$Q_{G,veg} = Q_{veg}^* - Q_{H,veg} - Q_{E,veg} \quad (4.2.18)$$

$$Q_{G,street} = k_1(T_{sfc} - T_1) \frac{2}{T_m} \quad (4.2.19)$$

where k_1 is the thermal conductivity of the surface ($\text{W m}^{-1}\text{K}^{-1}$), T_1 is the temperature of the shallowest layer (K), and T_m is the temperature of the deepest layer (K).

4.2.2 Convection

Convection is implemented as an adaptation of the facet-averaged approach of Masson (2000). Horizontal advective exchanges are not considered, which is considered to be a reasonable approach given the well-mixed nature of canopy layer air (Krayenhoff & Voogt 2007). A more accurate but computationally intensive approach could be undertaken using a computational fluid dynamics (CFD) method. However, forcing by the convection between facets is likely less important than the forcing of surface temperatures through the shaded and unshaded radiation distribution and its interactions of surface material properties (Krayenhoff & Voogt 2007). The following sub-modules are completely contained in TUF-3D (Krayenhoff & Voogt 2007).

Wind speed profile

The wind speed profile within the roughness sub-layer (RSL), a log profile based on Masson (2000), Kusaka et al. (2001), and Harman et al. (2004), $U(z)$, the wind speed at height z (m s^{-1}), is calculated in Equation (4.2.20)

$$U(z) = U_a \ln\left(\frac{z - z_D}{z_{0town}}\right) / \ln\left(\frac{z_{ref} - z_D}{z_{0town}}\right), (z \geq z_H) \quad (4.2.20)$$

where z_D is the displacement height (m), z is the height in the model domain (m), z_H is the mean building height (m), z_{0town} is the roughness length for momentum (domain) (m), z_{ref} is the reference height for forcing data (m), and U_a is the wind speed at z_{ref} (m s^{-1}).

An exponential profile is used for the urban canopy, based on Masson (2000) and Rotach (1995), calculating $U(z)$, the wind speed at height z (m s^{-1}), in Equation (4.2.21)

$$U\left(\frac{z_H}{2}\right) = U(z_H) \exp\left(\frac{-\lambda_f}{2(1-\lambda_p)}\right) \quad (4.2.21)$$

where z_H is the mean building height (m), λ_f is the frontal-area-to-plan area ratio, either user defined or based on Raupach (1992), and λ_p is the building-to-plan area ratio.

Temperature profile and canopy energy budget

The temperature profile treats canyon temperature (T_{can}) as constant for $z < z_H$, allowing a single canopy-air energy budget.

Calculation of T_{can} , the canopy air temperature ($z < z_H$) (K), uses the energy budget of the air volume below $z = z_H$ in Equation (4.2.22)

$$T_{can}^{m+1} = T_{can}^m + \left[\frac{\Delta t(H_{can}^{m+1} - H_{top}^{m+1})}{c_{air,H}^{m+1}} \right] \quad (4.2.22)$$

where m is the timestep index, H_{can} is the summed canopy patch convective sensible heat fluxes per canopy plan area (W m^{-2}), H_{top} is the convective sensible heat flux density between canopy air and boundary layer (W m^{-2}), $c_{air,H}$ is the average heat capacity per unit plan area of air below z_H ($\text{J m}^{-2}\text{K}^{-1}$), and Δt is the timestep size (s).

Calculation of H_{top} , in which 'top' is an imaginary surface at $z = z_H$, is performed in Equation (4.2.23)

$$H_{top}^{m+1} = h_{top}^{m+1}(T_{can}^m - T_a^{m+1}) \quad (4.2.23)$$

where m is the timestep index, h_{top} is the convective heat transfer coefficient between canopy air and boundary layer ($\text{W m}^{-2}\text{K}^{-1}$), using Mascart et al. (1995) and z_{0town} , T_{can} is the canopy air temperature ($z < z_H$) (K), and T_a is the air temperature at z_{ref} (K).

Overall, the vertical air temperature profile is given in Equation (4.2.24)

$$T(z) = \begin{cases} T_{log}(z), & (z \geq z_H); \\ T_{can}, & (z < z_H) \end{cases} \quad (4.2.24)$$

where $T(z)$ is the air temperature at height z (K), T_{can} is the canopy air temperature ($z < z_H$) (K), and $T_{log}(z)$ is the air temperature profile above z_H (K).

Surface convection

The convective sensible heat flux density (W m^{-2}), H , from a horizontal patch i is calculated in Equation (4.2.25)

$$H_i = h_i(T_{sfc,i} - T(z_{horz,i})) \quad (4.2.25)$$

where $T_{sfc,i}$ is the surface temperature of patch i (K), h is the convective heat transfer coefficient ($\text{W m}^{-2}\text{K}^{-1}$), $T(z)$ is the air temperature at height z (K), and $z_{horz,i}$ is the height of the patch centre.

Convection from walls is also calculated using Equation (4.2.25) where h_i is calculated in Equation (4.2.26)

$$h_i = r_{w,i}(11.8 + 4.2U_{eff}(z_i)) - 4.0 \quad (4.2.26)$$

where $r_{w,i}$ is the wall roughness coefficient of patch i, z_i is the depth to the bottom of layer i (m), and $U_{eff}(z)$ is the effective wind speed at height z (m s^{-1}).

4.2.3 Water balance

Water cycle functionality is supplied by MAESPA modules. Each item of vegetation will be individually modelled using a single instance of MAESPA, supported by the built in water balance routines. Soil layers are configurable (set to 10 by default). Overall water storage is calculated in these layers as S_i , soil water storage in layer i (mm), using Equation (4.2.27)

$$\begin{aligned} \frac{dS_i}{dt} &= I_i - E_i - D_i \text{ for } i > 1, \text{ and} \\ \frac{dS_i}{dt} &= I_i - E_i - D_i - E_{s,i} \text{ for layer 1} \end{aligned} \quad (4.2.27)$$

where I_i is the infiltration into layer i (mm), E_i is the root water uptake (canopy transpiration) out of layer i (mm), D_i is the drainage out of layer i (mm), and $E_{s,i}$ is the soil evaporation out of layer i (mm).

Infiltration

Infiltration is based on a function from the BROOK90 model (Federer et al. 2003). Rain falling on the soil surface infiltrates through Equation (4.2.28) calculating I_i , infiltration into layer i (mm)

$$\begin{aligned} \text{For } i=1, \quad I_i &= P_u \times (z_i/Z)^\phi \\ \text{For } i>1, \quad I_i &= P_u \times \left(\left(\sum_1^i z_i \right) / Z \right)^\phi - \left(\left(\sum_1^{i-1} z_i \right) / Z \right)^\phi \end{aligned} \quad (4.2.28)$$

where z_i is the depth to the bottom of layer i (m), Z is the total soil depth (m), ϕ is an infiltration parameter (0-1), and P_u is the surface water for infiltration (snow melt + throughfall) (mm).

Root water uptake

Root water uptake is calculated in Equation (4.2.29) calculating F_R , the cumulative fraction of fine roots to depth z (m)

$$F_R = (1 - \beta^{100-z_i}) / (1 - \beta^{100-Z}) \quad (4.2.29)$$

where β is the parameter which specifies the shape of the distribution (adapted from Jackson et al. (1996)) z_i is the depth to the bottom of layer i (m), and Z is the total soil depth (m).

Next, treating the root system as a number of resistances in parallel, Equation (4.2.30) calculates E_i , the root water uptake (canopy transpiration) out of layer i (mm)

$$E_i = (\Psi_{S,i} - \Psi_{R,i}) / (R_{sr,i} + R_{rad,i} + R_{lg,i}) \quad (4.2.30)$$

where $\Psi_{S,i}$ is the soil water potential in layer i (MPa), $\Psi_{R,i}$ is the root xylem water potential in layer i (MPa), R_{sr} is the soil-to root surface hydraulic resistance ($\text{MPa s m}^2 \text{ mol}^{-1}$), R_{rad} is the radial resistance to water uptake (across the root epidermis to the xylem) ($\text{MPa s m}^2 \text{ mol}^{-1}$), and R_{lg} is the longitudinal resistance to water flow ($\text{MPa s m}^2 \text{ mol}^{-1}$).

In order to solve Equation (4.2.30) simultaneously across multiple soil layers, calculation of E_i are simplified in Equation (4.2.31) (using assumptions of Taylor & Keppler (1975))

$$E_i \propto L_{v,i}(\Psi_{S,i} - \bar{\Psi}_R) \quad (4.2.31)$$

where $\bar{\Psi}_R$ is the mean root water potential (MPa), and $L_{v,i}$ is the fine root density (mm^{-3}) in layer i.

Soil evaporation

Soil evaporation is only drawn through the top later, assumed to travel through a thin dry layer at the soil surface, and is based on models developed by Choudhury & Monteith (1988) and Williams et al. (2001a). Calculation of E_s , the rate of evaporation (mm), is based on the difference between vapour pressure differences in soil pore space and the air above, in Equation (4.2.32)

$$E_s = G_{s,t} k_1 (e_s - e_a) \quad (4.2.32)$$

where k_1 is the thermal conductivity of the surface ($\text{W m}^{-1}\text{K}^{-1}$), $G_{s,t}$ is the total conductance from the soil air space to the air above the boundary layer (m s^{-1}), e_a is the partial water vapour pressure of the air (KPa), and e_s is the partial water vapour pressure of the soil pore space (KPa).

Calculation of G_{ws} , the conductance of water vapour through the soil pore space (m s^{-1}), is calculated in Equation (4.2.33) (as the thickness of the layer of dry soil at the surface increases, more resistance to air evaporation is created),

$$G_{ws} = D_{eff} (\theta_1 / L_d) \quad (4.2.33)$$

where D_{eff} is the effective diffusivity of the soil pore space ($\text{m}^2 \text{ s}^{-1}$), θ_1 is the soil volumetric water content of layer 1 ($\text{m}^3 \text{ m}^{-3}$), and L_d is the thickness of the dry layer at the soil surface (m).

Calculation of D_{eff} , the effective diffusivity of the soil pore space ($\text{m}^2 \text{ s}^{-1}$), is calculated in Equation (4.2.34), accounting for changes in diffusivity with changing soil temperatures,

$$D_{eff} = \omega_s \theta_1 D_w \quad (4.2.34)$$

where ω_s is the tortuosity of the soil air space (-), and D_w is the diffusivity of water vapour (function of soil temperature) ($\text{m}^2 \text{ s}^{-1}$).

Finally, e_s , the partial water vapour pressure of the soil pore space (KPa), is calculated in Equation (4.2.35)

$$e_s = e_{sat} \times \exp\{\Psi_{s,1} V_w / RT_s\} \quad (4.2.35)$$

where e_{sat} is the saturated vapour pressure (KPa) (calculated from temperature based on Jones (1992)), $\Psi_{s,1}$ is the soil water potential in the surface layer (MPa), V_w is the partial molal volume of water ($\text{m}_3 \text{ mol}^{-1}$), R is the ideal gas constant ($=8.314 \text{ J mol}^{-1}\text{K}^{-1}$), and T_s is the soil surface temperature (K).

Canopy interception

In order to account for canopy interception of precipitation, the Rutter et al. (1975) rainfall interception model is used. In this, rain can either fall through the canopy to the ground or be intercepted by the canopy in a slowly draining canopy pool. For the second option, the canopy pool is filled until reaching a maximum volume, after which any additional rainfall immediately follows the first pathway to the ground. Some amount of water is also evaporated from the canopy. The equation describing the change of W_{can} , the water storage of the canopy (mm), in Equation (4.2.36)

$$\frac{dW_{can}}{dt} = (1 - r_1)P - E_w - e^{r_2 + r_3 W_{can}} \quad (4.2.36)$$

where r_1 is the free throughfall fraction (0-1), r_2 is a canopy drainage parameter (mm), r_3 is a canopy drainage parameter (-), E_w is the wet evaporation rate (mm t^{-1}), and P is precipitation (mm).

Drainage

Drainage of soil water is solved downward, layer by layer, in which the change of W_i , the water storage of the layer i (mm), is calculated in Equation (4.2.37), based on the soil hydraulic conductivity (m/s) in each layer,

$$\frac{dW_i}{dt} = D_i - 1(\theta_i - 1) - D_i(\theta_i) \quad (4.2.37)$$

where D_i is the drainage out of layer i (mm) and θ_i is the soil volumetric water content of the dry layer at the soil surface ($\text{m}^3 \text{ m}^{-3}$).

Hydraulics of the soil-to-leaf pathway

Hydraulics of the soil-to-leaf pathway, k_L , the total leaf-specific hydraulic conductance ($\text{mmol m}^{-2}\text{s}^{-1}\text{MPa}^{-1}$), is calculated in Equation (4.2.38)

$$k_L = 1 / (\frac{1}{k_p} + R_{sr,t} \times L_T) \quad (4.2.38)$$

where k_p is the plant component of the leaf-specific hydraulic conductance ($\text{mmol m}^{-2}\text{s}^{-1}\text{MPa}^{-1}$), L_T is the total canopy leaf area index ($\text{m}^2 \text{ m}^{-2}$), and $R_{sr,t}$ is the total hydraulic resistance for all soil layers combined ($\text{MPa s m}^2 \text{ mol}^{-1}$) (estimated using the single root model of Gardner (1960)).

4.2.4 Tmrt and UTCI

VTUF-3D provides output of downward and upward shortwave and longwave and T_{sfc} for each surface at each time step. Air temperature for the canyon, T_{can} , calculated in Equation (4.2.22)

is also provided for each timestep. Using these and values of vapour pressure from the forcing data and wind speed at street level (calculated in Equation (4.2.20)), the values for T_{mrt} and $UTCI$ are calculated for each surface. Options in the model are available to either calculate $L \downarrow$ or use forcing values. Based on this, different options can be used to calculate the following equations.

Globe temperature calculation

Calculations of mean radiant temperature T_{mrt} uses a two step procedure. Globe temperature (T_g) is solved, using an iterative relaxation solution, using a formulation of Liljegren et al. (2008) in Equation (4.2.39)

$$\begin{aligned} A\epsilon_g\sigma T_g^4 &= \frac{A}{2}\epsilon_g\sigma(\epsilon_a T_a^4 + \epsilon_{sfc} T_{sfc}^4) \\ &+ \frac{A}{2}(1 - \alpha_g)(1 - f_{dir})S \\ &+ \frac{A}{4}(1 - \alpha_g)f_{dir}S/\cos(\theta) \\ &+ \frac{A}{2}(1 - \alpha_g)\alpha_{sfc}S \\ &- Ah(T_g - T_a) \end{aligned} \quad (4.2.39)$$

where A , is the surface area of a sphere of diameter D , of value 0.15m, ($=\pi 0.15^2 \text{m}^2$), ϵ_a , the longwave emissivity of the atmosphere (see Equation (4.2.41)), ϵ_g , the globe emissivity ($=0.95$), h , the convective heat transfer coefficient ($\text{W m}^{-2}\text{K}^{-1}$) (see Equation (4.2.40)), σ , the Stefan-Boltzmann constant ($=5.67 \times 10^{-8} \text{ W m}^{-2}\text{K}^{-4}$), T_a , the dry bulb air temperature (K) (using T_{can}), T_{sfc} , the surface temperature (K), S , the horizontal solar irradiance (W m^{-2}) calculated from the total of absorbed and reflected shortwave resulting from Equation (4.2.5), θ , the solar zenith angle, α_{sfc} , the surface albedo ($=0.15$), α_g , the globe albedo ($=0.05$), and f_{dir} , the fraction of the total horizontal solar irradiance, S , due to the direct beam of the sun (see Equation (4.2.44)).

The convective heat transfer coefficient, h , is calculated using Equation (4.2.40)

$$Nu = 2.0 + 0.6Re^{1/2}Pr^{1/3}; \quad h = k/DNu \quad (4.2.40)$$

where Nu is the Nusselt number (-), Re , the Reynolds number (-), Pr , the Prandtl number (-), and k , the thermal conductivity of the fluid (i.e. air) ($\text{W m}^{-1} \text{ K}^{-1}$) (Liljegren et al. 2008).

Depending on user defined scenario model configuration settings, a number of terms in Equation (4.2.39) can use internally calculated values. $\sigma(\epsilon_a T_a^4 + \epsilon_{sfc} T_{sfc}^4)$ will be replaced with $L \downarrow + L \uparrow$, the result of reflections of $L \downarrow_{i,sky}$ calculated in Equation (4.2.6). $(1 - f_{dir})S$ will be replaced with $K \downarrow_{dir}$ and $f_{dir}S/\cos(\theta)$ with $K \downarrow_{dir}$, both the result of calculations of shortwave reflections in Equation (4.2.5).

Also, for vegetated grid squares, the terms for $L \downarrow$ and $L \uparrow$ will be replaced with calculations of $L \downarrow$ and $L \uparrow$ from $\epsilon\sigma T^4$ where $T_{s,1}$, soil surface temperature (K), is used as the temperature term for the $L \uparrow$ calculation while leaf temperature (from Section 4.2.1.3) is used for $L \downarrow$. Otherwise, the following sequence of equations are used to calculate the terms for Equation (4.2.39).

ϵ_a is calculated using Oke (1987) in Equation (4.2.41)

$$\epsilon_a = 0.575 * (rh * e_a)^{0.143} \quad (4.2.41)$$

where e_a is calculated using Equation 3 of Buck (1981) in Equation (4.2.42).

$$e_a = 6.1121 \exp\left(17.502 \frac{T_a - 273.15}{T_a - 32.18}\right) \quad (4.2.42)$$

The calculation of relative humidity is completed using a form of the Clausius-Clapeyron Equation in Equation (4.2.43)

$$rh = \frac{100e_a}{P_o e^{-\Delta H_{vap}/RT}} \quad (4.2.43)$$

where e_a is the vapour pressure (mb) (read from the forcing data), P_o the vapour pressure of water at infinite temperature ($=7.5152 \times 10^8$ mb), ΔH_{vap} is the enthalpy of evaporation ($=42809$ J mol $^{-1}$), R is the ideal gas constant ($=8.314$ J mol $^{-1}$ K $^{-1}$), and T is the temperature (K).

Values of f_{dir} are calculated using Liljegren et al. (2008) in Equation (4.2.44)

$$f_{dir} = \begin{cases} \exp(3 - 1.34S^* - 1.65/S^*) & \theta \leq 89.5^\circ; \\ 0, & \theta > 89.5^\circ, \end{cases} \quad (4.2.44)$$

where $S^* = S/S_{max}$ and S , the horizontal solar irradiance (W m $^{-2}$).

S_{max} is calculated in Equation (4.2.45)

$$S_{max} = S_0 \cos(\theta)/d^2, \theta \geq 89.5^\circ; \quad (4.2.45)$$

where S_0 is the solar constant ($=1367$ W m $^{-2}$) and d , the earth-sun distance ($=1$ A.U.).

T_{mrt} calculation

Using T_g , calculated in Equation (4.2.39), the second step in calculating T_{mrt} proceeds in Equation (4.2.46) of Kántor & Unger (2011)

$$T_{mrt} = \left((T_g + 273.15)^4 + \frac{1.1 \times 10^8 ws_{cm}^{0.6}}{\epsilon_g D^{0.4}} \times (T_g - T_a) \right)^{0.25} - 273.15 \quad (4.2.46)$$

where ws_{cm} is the wind speed (cm s $^{-1}$).

$UTCI$ calculation

Finally, the $UTCI$ for each surface is calculated, using the Bröde (2009) $UTCI$ formula, in Equation (4.2.47)

$$UTCI = f(T_a, ws, rh, T_{mrt}) \quad (4.2.47)$$

generating a *UTCI* value for each surface, using input of T_a , air temperature (using T_{can}), ws , wind speed ($m s^{-1}$) (using model calculated U_{road} , the wind speed at road level), rh , relative humidity (%) (from forcing data), and T_{mrt} . If canopy level rh observed data is available (as opposed to forcing data possibly recorded above the canopy), post processing can recalculate *UTCI* using these values. VTUF-3D does not currently calculate a canopy level rh . This is a current limitation and a future enhancement for the model.

This *UTCI* formula was designed to provide human thermal comfort assessments using thermal environment parameters with fixed values (incorporated into the formula) for metabolic rates and clothing levels (Bröde et al. 2012). While future development is needed to provide wider flexibility to vary metabolic rates and clothing levels, existing versions of this formula were developed to embody equivalent human physiological responses to differing thermal parameters (Havenith et al. 2012; Fiala et al. 2012).

4.3 VTUF-3D model integration

4.3.1 TUF-3D shading logic

In order to understand the changes made to create VTUF-3D, an overview of the previous TUF-3D logic is necessary. TUF-3D sets up a modelling domain by using user specified width/height ratios and calculating a domain of buildings and roads from those, leading to a basic starting point of building heights and locations. Two dimensional (x,y) locations of building locations are configured along with their heights (Figure 4.6) and stored in the building height values (bldht) data object.

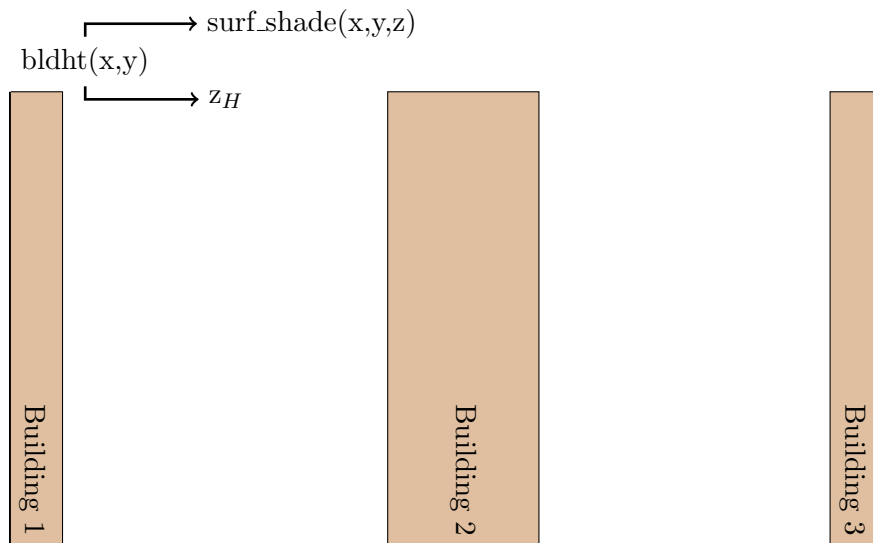


Figure 4.6: Building height arrays, input through the bldht array, used to calculate z_H and create the surf_shade array.

These values are used to calculate z_H , mean building height, as in Equation (4.3.1)

$$z_H = (l_p * \sum_{n=1}^{n_{hts}} H_{blt}) / n_{roofs} \quad (4.3.1)$$

where l_p is length of a patch side (m), H_{blt} is building height (m), n_{hts} is number of building heights, and n_{roofs} is number of roofs.

TUF-3D uses forcing data of temperature, humidity, incoming radiation levels, and wind speed and direction from a location at specified z height (above the canopy) (Appendix A.2 for more details). Wind is used in roughness calculations but not used to resolve movements around the buildings (as a CFD based model would). This simplification is a design decision trade-off to reduce the complexity of the model and the intensity of computations, while still producing accurate enough results (see Section 4.2.2).

The building height values ($bldht$) are then converted into a 3-dimensional (x,y,z) array ($surfShade$). During the model initialisation stage, ray tracing is done (Figure 4.7) between all the elements of the $surfShade$ array to determine which surfaces are visible to each from each surface. This step reduces the number of radiative interactions of surfaces that will need to be considered throughout the simulation run.

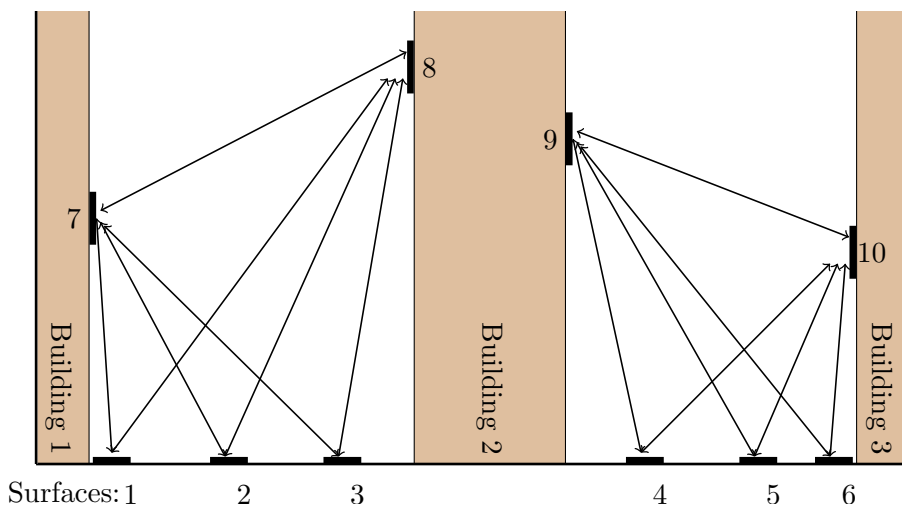


Figure 4.7: Initial view angles ray tracing, run during model initialisation to determine which surfaces are visible to each other.

As the model runs a simulation, at each time step, TUF-3D runs a shading routine (Figure 4.8). In it, the model iterates through each surface in the domain (roads and building walls and roofs) and ray-traces towards the sun. Each of these surfaces (patches) are divided into quarters and each of these are ray-traced from the centre of each quarter (equations fully described in Section 4.2.1.1).

Each surface keeps track of the level of illumination, the shade coefficient for that surface, at each timestep. If the ray passes to the top of the domain without being obstructed (i.e. surface 4) then 0.25 is added to the shade coefficient for that surface. If the ray is obstructed before reaching the top of the domain (i.e. surface 3), then nothing is added. Each surface has potential values of 0, 0.25, 0.5, 0.75 and 1.0. During the later energy balance step, an appropriate amount of incoming radiation is allocated to this surface based on this coefficient.

4.3.2 Integrating vegetation shading and modified ray tracing logic in VTUF-3D

After model improvements to VTUF-3D are made, a similar parallel logic is used to represent the vegetation in the domain. A new user defined data structure (the $veght$ data structure) is

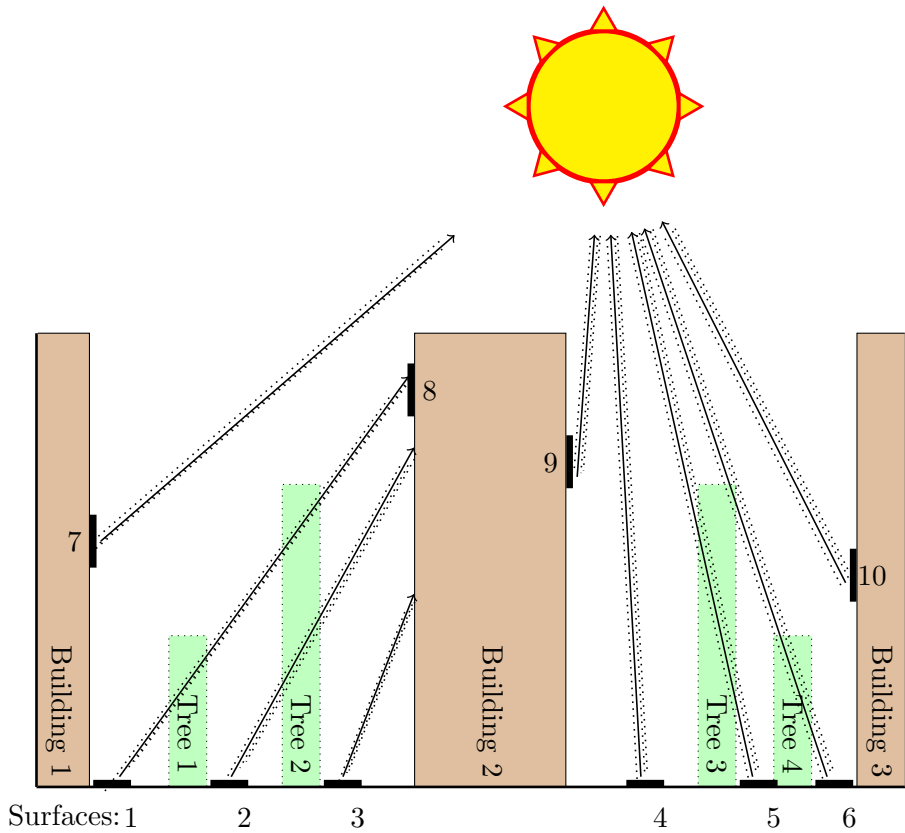


Figure 4.8: TUF-3D unmodified shading logic in which each surface performs four ray traces (from each surface quarter) towards the sun and determines sunlit percentage based on how many rays leave the domain without meeting an obstruction. Trees do not exist in this version (they will be added in Figure 4.10) but are shown to illustrate how their impact is missing from the unmodified logic.

added (Figure 4.9) to the model configuration. In this, the (x,y) locations of vegetation in the domain are specified along with their heights. As with the buildings, this is converted into a 3-dimensional (x,y,z) vegetation shade data structure (*vegshade*).

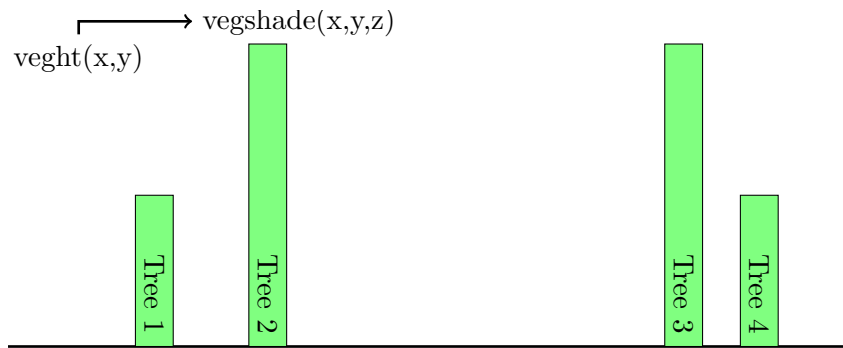


Figure 4.9: Vegetation height arrays, input through the *veght* array, used to create the *vegshade* array.

The domain initiation method has been modified to read in the configuration information. Previously, in TUF-3D, this method calculated and laid out a grid of buildings and roads based

on a width/height ratio. The new modified version now reads in the domain layout directly from configuration files. These configuration files changes will be described in more detail in Appendix B.1.

These vegetation elements are ignored in the initialising ray-tracing (Figure 4.7). As this data is used to determine which surfaces will never be visible to each other, vegetation, depending on its density, may allow some level of transmission and must be considered on a case by case basis during the simulation run.

At each time step during the simulation, VTUF-3D now runs a modified shading routine (Figure 4.10). During the model iteration through each surface in the domain, ray-traces towards the sun are done as described previously. However, each step of the ray trace checks to see if vegetation has been encountered.

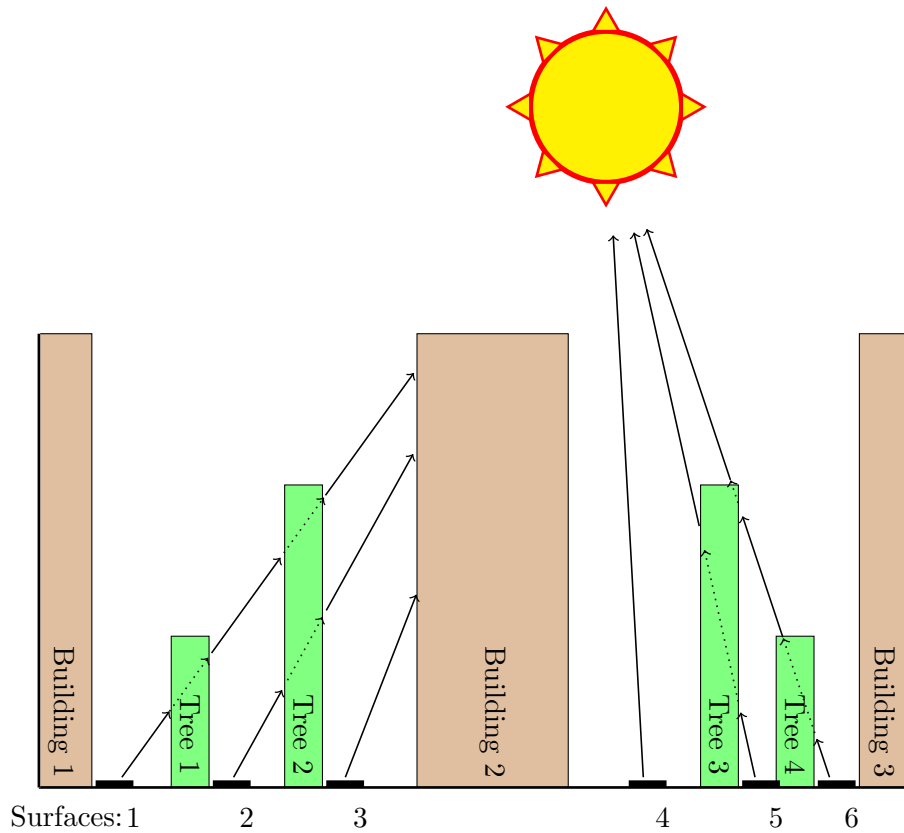


Figure 4.10: VTUF-3D modified shading, timestep ray tracing, using the same process as the unmodified logic but setting a flag for any ray that encounters vegetation.

If vegetation is encountered, a vegetation encountered flag is set. Then the ray trace continues and concludes when it either passes out of the domain or is blocked by a building. Table 4.1 summarises the results for ray tracing the six surfaces in Figure 4.10.

As with the unmodified shading functionality, if a building is found to be shading the surface, the shading factor is zero, whether vegetation is encountered or not (surfaces 1, 2, and 3) since no direct sunlight will reach that surface.

If no buildings or vegetation are encountered, the surface receives the full sunlit factor of 1 (surface 4). If vegetation is found but the ray leaves the domain otherwise unobstructed, the sunlit factor is currently unknown (TBD) and requires more processing (surfaces 5 and 6).

Table 4.1: VTUF-3D modified shading, timestep ray tracing results for Figure 4.10.

Surface	Sunlit factor	Vegetation in Ray
1	0	True
2	0	True
3	0	False
4	1	False
5	TBD	True
6	TBD	True

Note, the previous examples are simplified cases. In the actual VTUF-3D logic, ray tracing is performed four times from four quadrants of that surface and each ray is handled separately. The actual overall sunlit factor result for each surface might be 0%, 25%, 50%, 75% or 100%.

To resolve the sunlit factor for surfaces that encountered vegetation during the ray trace, reverse ray tracing is done for those beams (Figure 4.11). For surfaces 5 and 6, ray tracing is done from the top of the domain back along the radiation path. When the ray encounters vegetation (surfaces 5 and 6), VTUF-3D looks up the tree associated with the ground surface below and calculates the amount of radiation reflected, absorbed, and transmitted through the vegetation (further described in Section 4.3.3).

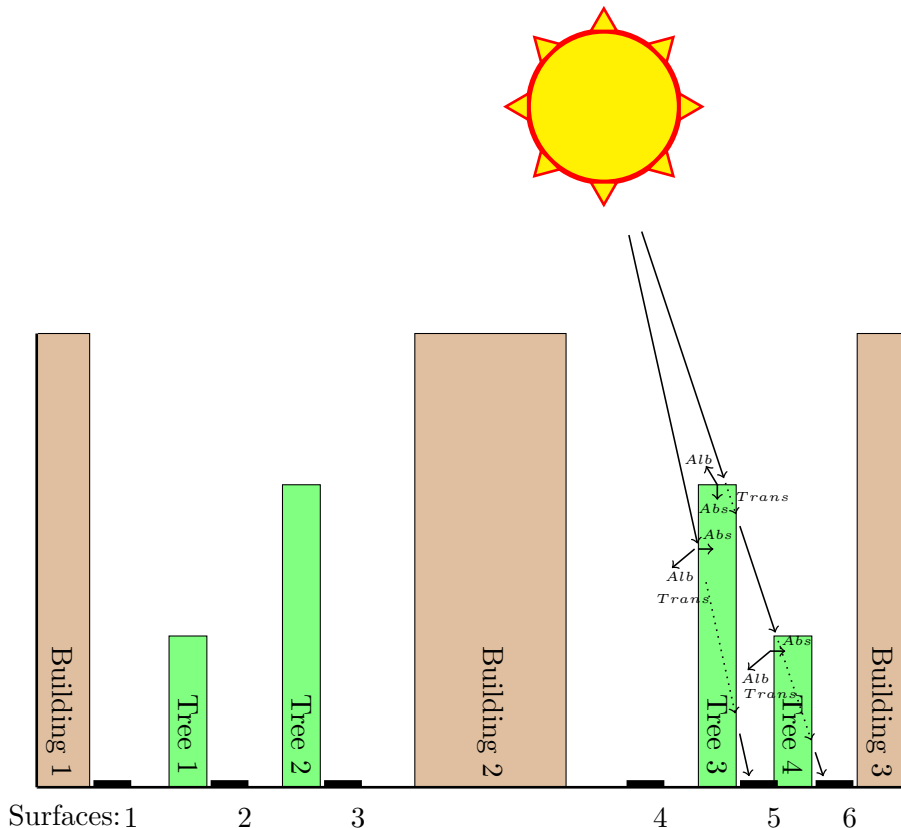


Figure 4.11: VTUF-3D modified shading, reverse ray tracing. For any rays that encounter vegetation in forward ray tracing, reverse ray traces are performed to allocate radiation to intervening encountered surfaces.

The ray tracing continues, allocating the remaining radiation either to further intercepting vegetation or ultimately to the ground surface. Through this reverse ray tracing process, the problem of zero to many surface interceptions is solved by allocating radiation as it is transmitted from the sun and transmits through the zero to many objects it encounters along its path.

4.3.3 MAESPA vegetation transmission and energy balance functionality overview

MAESPA, as originally designed, allows modelling of a stand of trees or of a single grid square containing a single tree. VTUF-3D uses this functionality from MAESPA in two different ways. The first is MAESPA's calculations of radiation movement through the vegetation canopy. Each tree in the VTUF-3D modelling domain is individually modelled by MAESPA before the main modelling run and then these data are extracted by VTUF-3D and used throughout the simulation.

Through these shading modifications, VTUF-3D stores states of and represents vegetation through placeholder simple block structures in VTUF-3D (Figure 4.12), but calculates the underlying processes using their true shapes and types through the MAESPA representation.

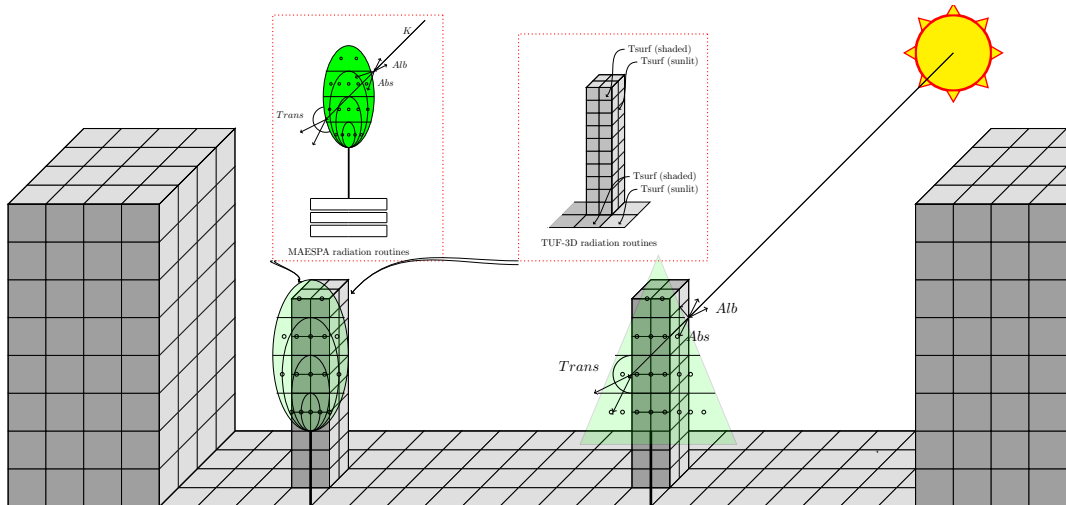


Figure 4.12: TUF-3D/MAESPA vegetation/radiation interactions, using block shaped placeholder vegetation and using MAESPA to determine the radiation interaction values for the vegetation's true shape.

VTUF-3D's configuration system has been expanded to allow mapping of individual trees to a (x,y) location within its domain and to the placeholder vegetation cube and surface structure. These configuration changes (as well as the changes to VTUF-3D configuration) will be further detailed in Appendix B.1.

During the simulation run (described in Section 4.4), calculated transmission values are used to distribute radiation to the appropriate surfaces during the reverse ray tracing process to determine how much radiation is scattered by the vegetation, radiation absorbed by the vegetation, while the remaining amount of radiation is then distributed to subsequent vegetation, and ultimately to the ground surface at the end of the ray.

The second integration of MAESPA is used in the surface energy balances. Flux amounts (pre-calculated offline) for each vegetation element for each time step are loaded at the beginning of the simulation and used to repartition the energy fluxes for those surfaces with vegetation on them, using the appropriate values for either sunlit or shaded vegetation. The logic behind this will be described in Section 4.4.

4.3.4 VTUF-3D use of MAESPA differential shading values

In order to account for inner tree shading or shading by buildings, each tree in the domain is modelled two times, using varied amounts (diffuse only and 100%) of incoming shortwave and the proper data variation is chosen during the model run. The configuration of the individual trees will be described in a following section on modelling configuration (Section 4.3.5).

In order to account for vegetation shaded by buildings and other vegetation, VTUF-3D uses a differential shading scheme to choose the appropriate MAESPA data throughout a simulation. Creation of MAESPA configurations for each tree creates two different MAESPA model runs with differing forcing data. The incoming shortwave is varied in two different ways. The first uses 100% values. The second reduces incoming shortwave to diffuse values only. Proper forcing data will need to be provided by the user to supply these values, such as is used in the validations in the next chapter, Section 5.2.

A data structure, `treeXYMapSunlightPercentageTotal`, is used to keep track of the amount of direct radiation hitting each tree. This is calculated in `shade()`, as described in Section 4.4.5. When the top of a tree (or other vegetation) is encountered by the shading routine, the cumulative percentage of the incoming shortwave radiation beam is allocated to the `treeXYMapSunlightPercentageTotal` for that item of vegetation.

The effect of this is if the vegetation is shadowed, the proper diffuse or 100% shortwave radiation forcing values variation can be used in each timestep for each tree during the energy balance partitioning of each ground surface (Section 4.2.1.7). If the ratio is greater than or equal to 0.50, the 100% shortwave radiation configuration is used. If the ratio is less than 0.50, diffuse configuration is used. As shortwave radiation levels vary in locations in an urban canyon across the diurnal cycle, use of these differential values captures the differing vegetation responses, such as varying levels of photosynthesis due to lower levels of PAR, changes in surface temperatures, and varying vegetation evapotranspiration due to differences in stomatal conductance and vapour pressure deficits.

4.3.5 MAESPA configurations creation

Each tree is modelled individually using MAESPA, so each of these also need to be configured. The same forcing data is used for each of these as the main modelling run. In order to account for shading of trees by buildings and other trees, each tree is modelled twice using modified forcing data.

The first tree variation uses unmodified forcing data, the incoming radiation set to 100%. The second tree variation uses only diffuse radiation. Each of these variations are put into the directory structure shown in Appendix B.2.1. Full details about overall VTUF-3D configuration generation is found in Appendix B.2.

Currently, three vegetations parameterisations (two trees and one grass species) are available, olive tree (*Olea europaea*), brushbox tree (*Lophostemon Confertus*), and tall fescue (*Festuca arundinacea*). Using the templates of parameters described in Section 4.3.6, configurations of

str.dat (tree structure parameters), *phy.dat* (physiological parameters), and *tree.dat* (general tree parameters) are created. Some calculations are done to scale some parameters (crown radius, crown height, trunk height, stem diameter, and total leaf area) based on the grid size and user supplied tree height.

Stem diameter scaling is calculated using the relationships described by Buba (2013) and Sumida et al. (2013). If the trunk height plus canopy height is greater than 7m, then stem diameter is calculated in Equation (4.3.2) as:

$$diam_{stem} = ((H_{trunk} + H_{crown}) - 6.74)/14.4 \quad (4.3.2)$$

where $diam_{stem}$ = stem diameter (m), H_{trunk} = trunk height (m), and H_{crown} = crown height (m).

Tree physical parameter templates (shown below) are based on a 5m tree. Using the modelled height, the parameters will be scaled according to the logic below.

MAESPA uses total leaf area per tree as modelling input, so total leaf area per tree is calculated in Equation (4.3.4) using the scaled tree canopy dimensions in Equation (4.3.3) and leaf area index of the specified species. These specific values for each species will be detailed in the following section (Section 4.3.6).

$$A_{canopy} = (r_{xcrown} * r_{ycrown}) * 3.1415; \quad (4.3.3)$$

where A_{canopy} = canopy area (m^2), r_{xcrown} = crown radius in x direction (m), and r_{ycrown} = crown radius in y direction (m).

$$A_{leaf} = LAI * A_{canopy} \quad (4.3.4)$$

where LAI = leaf area index ($m^2 m^{-2}$) and A_{leaf} = total leaf area (m^2).

4.3.6 MAESPA tree parameterisations

Currently there are parameterisations for two tree species, *Olea europaea* and *Lophostemon Confertus*, as well as turf grass, tall fescue (*Festuca arundinacea*). As all tree parameterisations in VTUF-3D are pluggable, individual trees are added to a domain using a specific set of configuration files with many of the physical properties scaled from a base template. Including additional vegetation types (trees, shrubs, and ground cover) into VTUF-3D can be added by populating the following templates with parameter values based on observations or literature values.

The physiological properties of the two selected trees and grass were integrated into the configuration files. All parameterisations used in this study share some common attributes, summarised in Table 4.2.

MAESPA olive tree (*Olea europaea*) parameterisation

The first complete parameterisation for VTUF-3D is the olive tree (*Olea europaea*). It has been selected because it is a species needed in the Smith St validation (Section 5.4) and observations of parameters are available from Coutts (2014). The physical and meteorological parameters for a 5x5 meter grid square are given in Table 4.3.

Table 4.2: MAESPA tree parameterisations common attributes.

Parameter	Value
Stomatal conductance model	Ball-Berry-Opti model (Medlyn et al. 2011)
Number of layers in the crown assumed when calculating radiation interception	6
Number of points per layer	12
Number of zenith angles for which diffuse transmittances are to be integrated	5
Number of azimuth angles for which diffuse transmittances are to be integrated	11

Table 4.3: MAESPA olive tree (*Olea europaea*) parameterisation, tree dimensions for an example 5x5m grid (to be rescaled for taller/shorter modelled trees).

Parameter	Value	Source
crown radius (m)	2.5	Coutts (2014)
crown height (m)	3.75	Coutts (2014)
trunk height (m)	1.25	Coutts (2014)
leaf area index ($\text{m}^2 \text{ m}^{-2}$)	2.48	Mariscal et al. (2000)
crown shape	round	
z_{Ht} (m)	4.0	Forcing data height
z_{PD} (m)	2.5	2/3 of crown height ‘rule of thumb’ (Grimmond & Oke 1999)
$z_{0,Ht}$ (m)	0.375	1/10 of crown height ‘rule of thumb’ (Grimmond & Oke 1999)

Table 4.4: MAESPA olive tree (*Olea europaea*) parameterisation, with parameter values taken from cited literature sources.

Parameter	Value(s)	Source
Soil reflectance (%PAR, %NIR, and %IR)	0.10, 0.05, 0.05	Levinson et al. (2007); Oke (1987)
Leaf transmittance (%PAR, %NIR, and %IR)	0.01, 0.28, 0.01	Baldini et al. (1997)
Leaf reflectance (%PAR, %NIR, and %IR)	0.08, 0.42, 0.05	Baldini et al. (1997)
Minimum stomatal conductance g_0 ($\text{mol m}^{-2}\text{s}^{-1}$)	0.03	Coutts (2014)
Slope parameter g_1	2.615	Coutts (2014)
# of sides of the leaf with Stomata	1	Fernández et al. (1997)
Width of leaf (m)	0.0102	
CO_2 compensation point ($\mu\text{mol m}^{-2}\text{s}^{-1}$)	55	Coutts (2014)
Max rate electron transport (J_{\max}) ($\mu\text{mol m}^{-2}\text{s}^{-1}$)	112.4	Coutts (2014)
Max rate rubisco activity (VC_{\max}) ($\mu\text{mol m}^{-2}\text{s}^{-1}$)	81.18	Coutts (2014)
Curvature of the light response curve	0.62	Coutts (2014)
Activation energy of J_{\max} (KJ mol $^{-1}$)	35350	Díaz-Espejo et al. (2006)
Deactivation energy of J_{\max} (J mol $^{-1}$)	200000	Medlyn et al. (2005)
Entropy term (KJ mol $^{-1}$)	644.4338	Medlyn et al. (2005)
Quantum yield of electron transport (mol electrons mol $^{-1}$)	0.19	Sierra (2012)
Dark respiration ($\mu\text{mol m}^{-2}\text{s}^{-1}$)	0.94	Coutts (2014)
Specific leaf area ($\text{mm}^2\text{kg}^{-1}$)	5.1	Mariscal et al. (2000)

The configuration scripts will re-scale these parameters for a given modelling domain grid size. The z_{Ht} value, measurement height of wind speed (m), is taken from the measurement height of forcing data. The z_{PD} value, zero-plane displacement height (m), uses a ‘rule of thumb’ and is calculated as 2/3 of the tree crown height. The $z_{0,Ht}$ value, roughness length (m), uses a ‘rule of thumb’ and is calculated as 1/10 of the tree crown height.

The specific physiological parameters for this species are given in Table 4.4 and are used to generate the appropriate *trees.dat*, *str.dat* and *phy.dat* for each olive tree in the domain. Parameter values were taken from the Coutts (2014) observations and supplemented with values from the literature.

MAESPA brushbox tree (*Lophostemon Confertus*) parameterisation

The second complete parameterisation for VTUF-3D is the brushbox tree (*Lophostemon Confertus*). This tree is chosen because it is the most common street tree in Melbourne (Frank et al. 2006), where all of the validation observations data sets are based. This tree has also been the basis of a number of research projects in Melbourne, providing a parameterisation through Coutts et al. (2016) and Coutts et al. (2015b).

The physical and meteorological parameters for a 5x5 meter grid square are given in Table 4.5. The configuration scripts will re-scale these parameters for a given modelling domain grid size. The specific physiological parameters for this species are given in Table 4.6 and are used to generate the appropriate *trees.dat*, *str.dat* and *phy.dat* for each brushbox tree in the domain.

Table 4.5: MAESPA brushbox tree (*Lophostemon Confertus*) parameterisation, tree dimensions for an example 5x5m grid (to be rescaled for taller/shorter modelled trees).

Parameter	Value	Source
crown radius (m)	2.5	Coutts et al. (2016)
crown height (m)	3.75	Coutts et al. (2016)
trunk height (m)	1.25	Coutts et al. (2016)
leaf area index ($\text{m}^2 \text{ m}^{-2}$)	2.0	Wright & Westoby (2000)
crown shape	round	
z_{Ht} (m)	4.0	Forcing data height
z_{PD} (m)	2.5	2/3 of crown height ‘rule of thumb’ (Grimmond & Oke 1999)
$z_{0,Ht}$ (m)	0.375	1/10 of crown height ‘rule of thumb’ (Grimmond & Oke 1999)

Table 4.6: MAESPA brushbox tree (*Lophostemon Confertus*) parameterisation, with parameter values taken from cited literature sources.

Parameter	Value(s)	Source
Leaf reflectance (%PAR, %NIR, and %IR)	0.04, 0.35, 0.05	Fung-yan (1999)
Minimum stomatal conductance g_0 ($\text{mol m}^{-2}\text{s}^{-1}$)	0.01	Coutts et al. (2016)
Slope parameter g_1	3.33	Coutts et al. (2016)
# of sides of the leaf with Stomata	1	Beardsell & Considine (1987)
Width of leaf (m)	0.05	Coutts et al. (2016)
CO_2 compensation point ($\mu\text{mol m}^{-2}\text{s}^{-1}$)	53.06	Coutts et al. (2016)
Max rate electron transport ($\mu\text{mol m}^{-2}\text{s}^{-1}$)	105.76	Coutts et al. (2016)
Max rate rubisco activity ($\mu\text{mol m}^{-2}\text{s}^{-1}$)	81.6	Coutts et al. (2016)
Curvature of the light response curve	0.61	Coutts et al. (2016)
Activation energy of J_{max} (KJ mol $^{-1}$)	35350	Bernacchi et al. (2001)
Deactivation energy of J_{max} (J mol $^{-1}$)	200000	Medlyn et al. (2005)
Entropy term (KJ mol $^{-1}$)	644.4338	Medlyn et al. (2005)
Quantum yield of electron transport (mol electrons mol $^{-1}$)	0.06	Coutts et al. (2016)
Dark respiration ($\mu\text{mol m}^{-2}\text{s}^{-1}$)	1.29	Coutts et al. (2016)
Specific leaf area ($\text{mm}^2\text{kg}^{-1}$)	25.3	Wright & Westoby (2000)

MAESPA grass parameterisation

The third complete parameterisation for VTUF-3D is for grass, tall fescue (*Festuca arundinacea*), a common turf grass. This is an important parameterisation for modelling urban environments as a significant portion of urban surfaces are grass. As will be seen in the validation chapter (Section 5.2), estimates of observed grass cover, for example in the Preston validation scenario, range from 11% to 23%.

This parameterisation is an adaptation of the normal MAESPA tree parameterisations. In it, the vegetation is modelled as a box shaped canopy with a crown height of 0.2 meters. This and the rest of the physical and meteorological parameters for a 5x5 meter grid square are given in Table 4.7, with parameter values taken from the literature.

Table 4.7: MAESPA grass, tall fescue (*Festuca arundinacea*), layer as a box tree on the ground covering the plot area.

Parameter	Value	Source
crown radius (m)	2.5	Radius of 5x5m grid
crown height (m)	0.2	Simmons et al. (2011)
trunk height (m)	0.01	
stem diameter (m)	0.2	
leaf area index ($\text{m}^2 \text{ m}^{-2}$)	7.13	ave. from Bijoor et al. (2014)
crown shape	box	
z_{Ht} (m)	4.0	Forcing data height
z_{PD} (m)	0.066	2/3 of crown height ‘rule of thumb’ (Grimmond & Oke 1999)
$z_{0,Ht}$ (m)	0.02	1/10 of crown height ‘rule of thumb’ (Grimmond & Oke 1999)

Table 4.8: MAESPA grass, tall fescue (*Festuca arundinacea*), layer as a box tree on the ground covering the plot area, with parameter values taken from cited literature sources.

Parameter	Value(s)	Source
Soil reflectance (%PAR, %NIR, and %IR)	0.10 0.05 0.05	Observed, Levinson et al. (2007), Oke (1987)
Leaf transmittance (%PAR, %NIR, and %IR)	0.05 0.45 0.01	C3 grasses, from Katjacnik et al. (2014)
Leaf reflectance (%PAR, %NIR, and %IR)	0.05 0.65 0.08	C3 grasses, from Katjacnik et al. (2014)
Minimum stomatal conductance g_0 ($\text{mol m}^{-2}\text{s}^{-1}$)	0.0	De Kauwe et al. (2015)
Slope parameter g1	5.25	C3 grasses, from De Kauwe et al. (2015)
# of sides of the leaf with Stomata	2	Green et al. (1990)
Width of leaf (m)	0.006	Rademacher & Nelson (2001)
CO_2 compensation point ($\mu\text{mol m}^{-2}\text{s}^{-1}$)	57	Brown & Morgan (1980) at 25 degrees
Max rate electron transport ($\mu\text{mol m}^{-2}\text{s}^{-1}$)	80.95	Tall Fescue from Yu et al. (2012)
Max rate rubisco activity ($\mu\text{mol m}^{-2}\text{s}^{-1}$)	36.14	Tall Fescue from Yu et al. (2012)
Curvature of the light response curve	0.7	Gilmanov et al. (2007)
Activation energy of J_{max} (KJ mol^{-1})	65300	Bernacchi et al. (2001)
Deactivation energy of J_{max} (J mol^{-1})	200000	Medlyn et al. (2005)
Entropy term (KJ mol^{-1})	644.4338	Medlyn et al. (2005)
Quantum yield of electron transport ($\text{mol electrons mol}^{-1}$)	0.05	Monson et al. (1982)
Dark respiration ($\mu\text{mol m}^{-2}\text{s}^{-1}$)	0.6	Estimated for Tall Fescue from Yu et al. (2012)
Specific leaf area ($\text{mm}^2\text{kg}^{-1}$)	23.16	Average from Table 1 in Bijoor et al. (2014) for 3 turfgrasses.

The configuration scripts will re-scale these parameters for a given modelling domain grid size. The specific physiological parameters for this species are given in Table 4.8 and are used to generate the appropriate *trees.dat*, *str.dat* and *phy.dat* for each grass grid square in the domain.

The last configuration file to generate is the MAESPA *points.dat* files. The use of these is described in Section 4.4.4.

The final step in configuration generation is to run each of the MAESPA instances (including the two differential shading variations) over the period being modelled. This data will then be available for use during the VTUF-3D run.

4.4 Running VTUF-3D

4.4.1 Overview of changes in TUF-3D

There are two major integration points within the VTUF-3D model. These are in the radiation distribution logic and in the surface energy balance routines. The first will read vegetation transmission data from MAESPA and use it in the distribution of shortwave radiation and calculation of shading effects. Longwave radiation will be allocated through the differential shading effects (Section 4.3.4).

The second integration will use MAESPA predictions of latent energy fluxes from evapotranspiration and vegetation transpiration and use these values to re-partition energy fluxes on those surfaces that contain vegetation. Also, surface temperatures of the vegetation surfaces will be loaded from MAESPA values. These vegetation surface temperatures and energy fluxes feed back into the domain each timestep through the energy balance partitioning and its impact on air temperature (Section 4.2.1.7).

4.4.2 MAESPA energy flux conversions

Each item of vegetation is modelled in its own MAESPA instance, so each tree must be loaded and processed separately. MAESPA outputs hourly transpiration in units of mm, so they must be converted to W m⁻² of latent energy to be used in the VTUF-3D flux re-partitioning. There is a conversion step required to calculate $Q_{E,et}$, the latent heat flux calculated from et (W m⁻²), using the 2-dimensional area of the tree and the time duration of each timestep in Equation (4.4.1)

$$Q_{E,et} = et \times A_{mm} \times m_{mol,w} \times \Delta H_{vap} \times c_{w,kj} \times Time \quad (4.4.1)$$

where et is evapotranspiration (mm), A_{mm} is the 2-dimensional tree area (mm²), $Time$ is the time (seconds), ΔH_{vap} , the enthalpy of evaporation (=42809 J mol⁻¹), $c_{w,kj}$, the conversion to watts (=1W/1000KJ/sec), and $m_{mol,w}$, the molar mass of water (=18.0152g mol⁻¹).

4.4.3 Loading MAESPA data

As the VTUF-3D model initialises, it loads all of the generated MAESPA data for all the trees and all the different shading configurations. Three main MAESPA output files are accessed for each tree (and their diffuse and 100% incoming radiation variations). MAESPA calculations of radiative transfer are detailed in Section 4.2.1.1.

The first set of data is loaded when `readMaespaTestData()` is called. For each `testflx.dat` output file (output of calculations of PAR transmission to user-defined xyz points) the `TD` variable (relative diffuse transmission) (values from 0-1) is read for each hour of the simulation. During the VTUF-3D simulation, these values will be used to allocate the transmission of shortwave radiation through the tree canopies and determine the amount of radiation reaching the surfaces beyond them.

The second set of data, used for energy flux and energy balance calculations, is loaded from the `watbal.dat` (water balance calculations for each timestep) and `hrflux.dat` (all flux calculations for each target tree for each hourly timestep) files. The specific variables used from these files are shown in Table 4.9.

Table 4.9: MAESPA variables loaded.

Variable	Description	Units
canopystore	storage of intercepted rain	mm
evapstore	evaporation of wet canopy	mm
soilevap	soil evaporation	mm
et	modelled canopy transpiration	mm
Tcan	Average foliage temperature	°C
Tsoil1	Temperature of the first layer of soil	°C

After loading, the amount of Q_E is calculated using Equation (4.4.2)

$$Q_E = Q_{E,et} + Q_{E,soil} + Q_{E,canopy} + Q_{E,evap} \quad (4.4.2)$$

where $Q_{E,et}$, the latent heat flux calculated from `et` (W m^{-2}), $Q_{E,soil}$, the latent heat flux calculated from `soilstore` (W m^{-2}), $Q_{E,canopy}$, the latent heat flux calculated from `canopystore` (W m^{-2}), and $Q_{E,evap}$, the latent heat flux calculated from `evapstore` (W m^{-2}), are all calculated using the conversion in Equation (4.4.1).

4.4.4 Radiation transmission in Maespa

Calculations of radiation transmission use the test points functionality from MAESPA. This allows modelling of PAR transmissions to user-defined xyz points within the tree canopy. The xyz point used to calculate transmission through the tree is half of the grid size (i.e. 2.5 for a 5m grid) and 0.1m to be at the bottom of the tree. This is configured in the `points.dat` configuration file by setting `XYZCOORDS` to '2.5 2.5 0.1' and setting `NOPOINTS` and `INPUTTYPE` to '1'.

The method `getDataForTimeAndDayAndPoint()` in the VTUF-3D `reverseRayTrace()` method reads the hourly output of the test points, the `testflx.dat` data file using the TD, diffuse transmittance to grid point (fraction), value.

4.4.5 VTUF-3D use of MAESPA shading values

For each surface, VTUF-3D ray traces four rays (each surface is split into quarters) to the sun. As described in Section 4.3.2, if vegetation is found in a ray trace from the surface towards the

sun, then a flag is set to also perform a reverse ray trace from the sun back to the surface. The return value from this function is the transmission percentage (0 to 100%) for that ray.

Overall then, the sunlit factor for each surface will then be the addition of those four rays, ranging from 0.0 to 4.0, corresponding to a range of 0 to 100% illumination. The value then is later divided by 4 when it is used to allocate energy transmissions.

The logic to allocate radiation to vegetation surfaces and surfaces shaded by vegetation uses a reverse ray trace from the top of the domain (coming from the sun) to the ground surface. As vegetation is encountered, `getDataForTimeAndDayAndPoint()` is called to read the transmission value for that tree (calculated using the `points.dat` functionality of MAESPA) and reduce the ray strength by that percentage. Tracing continues through any additional vegetation, eventually reaching the ground and allocating the remaining amount of direct shortwave to the ground surface.

4.4.6 Implementation and batch utility

Development of VTUF-3D was conducted in FORTRAN 2003 (GNU 2016a) in Netbeans 8.0.2 (Netbeans 2016) and compiled with gfortran 4.8.4 (GNU 2016b) on Ubuntu 14.04, however, the code should compile on any platform with FORTRAN 2003 support. The original source code for TUF-3D was obtained from the author (Krayenhoff & Voogt 2007) while source code for MAESPA was taken from the MAESPA repository (Duursma 2016). The development process merged these code bases and added the additional functionality described in this chapter.

Model configuration process was developed in Java using the JRE 1.7.0 (Oracle 2016) in Eclipse 4.5.2 (Eclipse Foundation 2016). Data analysis and graphing scripts were generated in R (R Core Team 2013) and Python (Python Software Foundation 2016) using the Matplotlib library (Hunter 2007). Details of post-processing scripts are described in Appendix C.4.

4.5 Design conclusions

These modifications to TUF-3D have created a new model, VTUF-3D, which is now able to model vegetation and account for latent energy fluxes and is suitable to model WSUD features and their HTC impacts (pending a successful validation process). The completion of the model has fulfilled the first research objective of this project.

Two major modifications were made to create VTUF-3D. The first added physical representations of vegetation and allow the shading effects of these features to be modelled. The second adds physiological processes (and associated water cycles) to also be modelled. This modification allows surface energy balances to be repartitioned, accounting for latent energy fluxes, as well as the effects that vegetation shading will have on these energy balances.

A templated scalable configuration system, used to represent arbitrary types of vegetation (or other WSUD features), allows any variety and mix of vegetation to be added to a modelled domain. Also, differential shading functionality allows impacts of urban geometry and inner tree shading on vegetation anywhere in an urban canyon to be properly modelled. Finally, the addition of mean radiant temperature and UTCI output for all surfaces allows detailed analysis of the vegetation's impact on these important parameters on HTC in these areas.

The next step in this project is to validate this new model. This validation process will be performed in the following chapter and will validate many different aspects of VTUF-3D and

ensure that the model is working properly and accurately and is suitable for HTC assessments of urban vegetation.

Chapter 5

Validation and assessment of improved performance of the VTUF-3D model to model urban areas

5.1 Overview of VTUF-3D validation process

Validations of VTUF-3D (Vegetated Temperatures Of Urban Facets) need to be performed to ensure that this new model is making accurate predictions. As an energy balance model, modelled output comparisons to observations of energy fluxes and temperatures are considered fundamental validations (Masson 2002). With the addition of vegetation modelling, it is important that those aspects are also properly validated.

A variety of observation data sets allows validations of a number of different aspects of the model to fulfil these requirements. A validation matrix (Table 5.1) details the specific aspect tested for each data set (and the source of the observations). These include validations against observations of mean radiant temperatures (T_{mrt}), $UTCI$ human thermal index observations, evapotranspiration (ET) and tree physiological observations, and flux energy balance observations. Also, the accuracy of the model will be placed within the results of other urban models from the International Urban Energy Balance Models Comparison Project (Best & Grimmond 2012).

This validation is extensive and considers multiple elements of the model. Several urban models are validated against flux observations, but the combination of validations around fluxes, micro-scale T_{mrt} and $UTCI$, and tree transpiration make this a very comprehensive approach.

5.1.1 Validation objectives

Within the validation process, three sub-objectives will be completed:

- Sub-Objective 1: to evaluate the model in terms of the surface energy balances,
- Sub-Objective 2: to evaluate the model performance for T_{mrt} and $UTCI$,
- Sub-Objective 3: to evaluate the capacity of the model to capture tree transpiration and varying urban influences on vegetation.

Table 5.1: VTUF-3D validation matrix.

Scenarios	Tmrt	UTCI	Transpiration	Flux energy balances
Preston, Melbourne (Coutts et al. 2007)				
Gipps/George St, Melbourne (Coutts et al. 2015a)				
Smith St, Melbourne (Gebert et al. 2012; Coutts 2014)				
Comparison to intercomparison (Best & Grimmond 2012)				

5.2 Model validation using Preston flux observations

5.2.1 Preston validation overview

Preston is a homogeneous, medium density suburb in the northern part of Melbourne, Australia. A 40 meter flux tower recorded observations during 2003 and 2004 (Coutts et al. 2007), providing observed values of Q^* , Q_H , Q_E , air temperature, humidity, wind speed and direction. Q_G was calculated as a residual value. Estimates of Q_F made using an inventory approach, though Q_F is included implicitly in the observations and contributes to the observed sensible heat fluxes.

The use of this data set allows validation of surface energy balances against modelled predictions. This data set was also used as the forcing and comparison data set for Phase 2 and 4 of the International Urban Energy Balance Models Comparison Project (Grimmond et al. 2011; Best & Grimmond 2012). Phase 2 of this comparison project evaluated the performance of 32 urban land surface modelling schemes, forced by and comparing to these observations, using a consistent methodology. Phase 4 re-evaluated many of these modelling schemes for their performance across a variety of seasonal cycles.

A modelled domain (500x500m with a 5m grid resolution, red boxed area of Figure 5.1) was chosen to be representative of the overall area observed by flux tower. The measurement height for the observations ensured that the measured fluxes well represented the local scale (10 to 1000 meters) of the area (Coutts et al. 2007). Additionally, the site selection ensured a homogeneous nature of the overall flux coverage area (Schmid 1994). Because of this, the micro-scale modelled domain will be representative of the observed fluxes observed at a local scale.

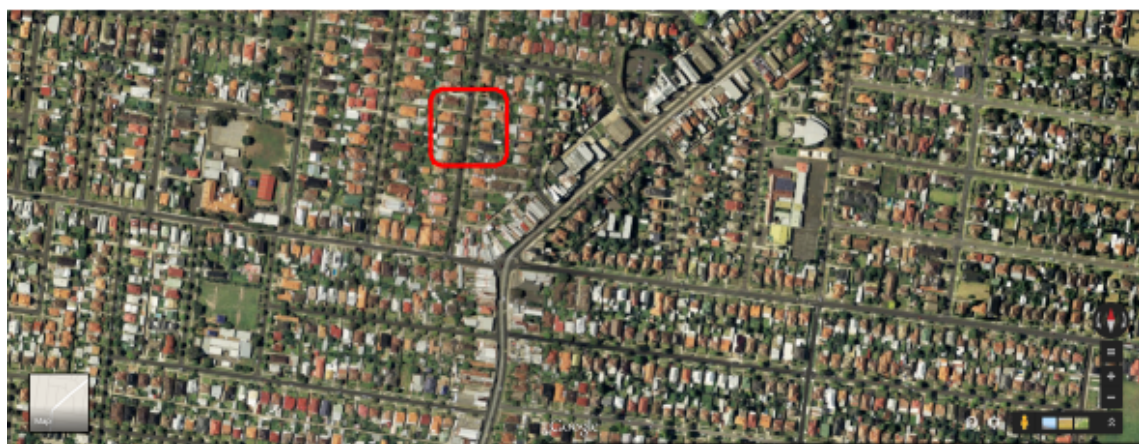


Figure 5.1: Preston suburb and modelled area. Adapted from Google Maps (2015).

Coutts et al. (2007) provides expert and manual classifications (done at the time of the observations, 2003-2004) from aerial imagery (from 2002) within a 500m radius of the observation tower. The selected modelling area is in good agreement with the 500m classification of Coutts et al. (2007) with respect to the pervious/impervious fractions. An analysis by Nury (2015) of the Darebin Council area (55.6 km^2) (which includes Preston) using LIDAR data from 2008 is also included because it provides a more recent set of land surface data for the 500m radius area. Breakdowns of both classifications are shown in Table 5.2.

Table 5.2: Preston land cover breakdowns: using expert and manual classification methods and average of both methods in 500m radius from observation tower (Coutts et al. 2007), Darebin Council land cover fractions (Nury 2015), modelled Preston 5m resolution validation domain land cover fractions (all in percentages).

Source	Buildings	Road	Concrete	Trees	Grass	Water	Total Impervious	Total Vegetation
Expert	44.0	13.0	3.0	29.0	11.0	0.0	60.0	40.0
			16.0					
Manual	45.0	13.0	6.0	16.0	19.0	1.0	64.0	36.0
			19.0					
Average	44.5	13.0	4.5	22.5	15.0	0.5	62.0	38.0
			17.5					
Nury (2015)	32.0	20.6	13.9	10.1	23.4	0	66.5	33.5
			34.5					
Modelled	45.2		19.3	16.0	19.5	0	64.5	35.5

Figure 5.2 (aerial imagery from 2015) was used as an initial basis for the modelling domain (Figures 5.4 and 5.3 showing building and vegetation placement). Some reduction in vegetation cover is seen between the 2004 observation site classification and the 2008 Darebin Council area classification. The modelled vegetation layout (Figure 5.4) was modified slightly (Table 5.2 showing modelled land cover breakdowns) in the validation scenario to account for these changes, and bring the modelled domain into closer agreement to the make-up of the site at the time of the observations.

This introduces a small amount of uncertainty in the exact make-up of the modelling domain and could explain some of the low predictions of Q_E seen later in this validation. While this dataset is at a different scale and from a later time period, it does show good agreement with the total impervious/pervious fraction of the 500m classification. Overall, the modelled domain selection is very similar to the broader area, is representative of the local scale and will allow an appropriate comparison between the observed and modelled results.

The urban form of this area, the Local Climate Zone (LCZ) (Stewart & Oke 2012), would be characterised as LCZ 6 (open low-rise). Other properties of the observation site are listed in Table 5.3.

The modelled land cover fractions of vegetation consist of 19.5% grass and 16.0% trees, matching closely to published land cover classification values for data set. Modelled building densities (Figure 5.3), consisting of 45.2% buildings and 19.3% impervious surfaces, also match closely to published land cover classification data set values. All values are summarised in Table 5.2.

Model parameters were set to the values given in Table 5.4. Most of these values are TUF-3D default values, from Krayenhoff & Voogt (2007). Vegetation settings for the two tree types (a 25%/75% mix of olive (*Olea europaea*) and brushbox (*Lophostemon Confertus*) trees) as



Figure 5.2: Digitisation of Preston suburban street, Oakhill Ave. (1=building heights, 2=vegetation heights (in 5m units)). Adapted from Nearmap (2015).

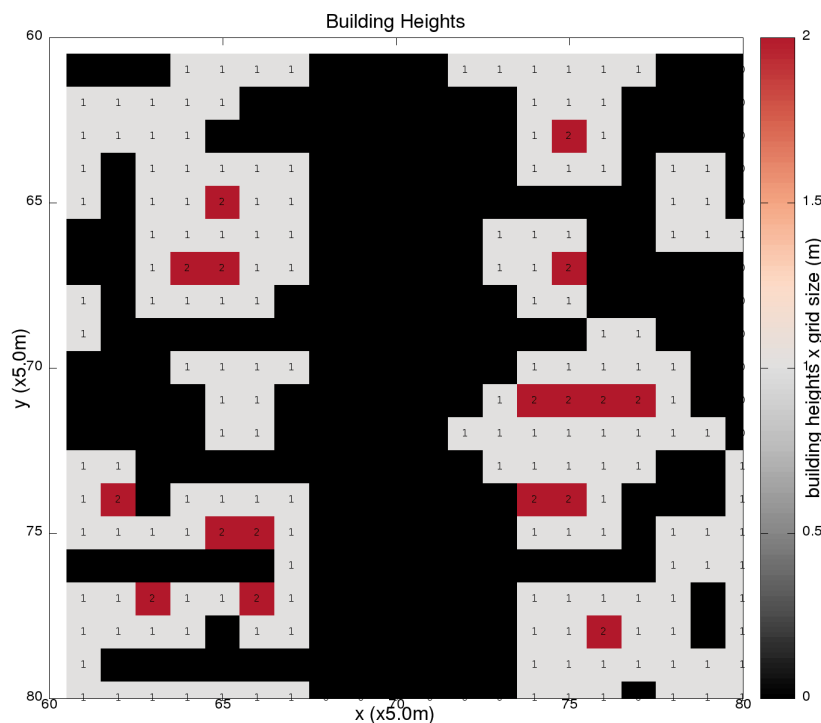


Figure 5.3: Preston validation domain configured building heights (0, 5, 10m) and locations.

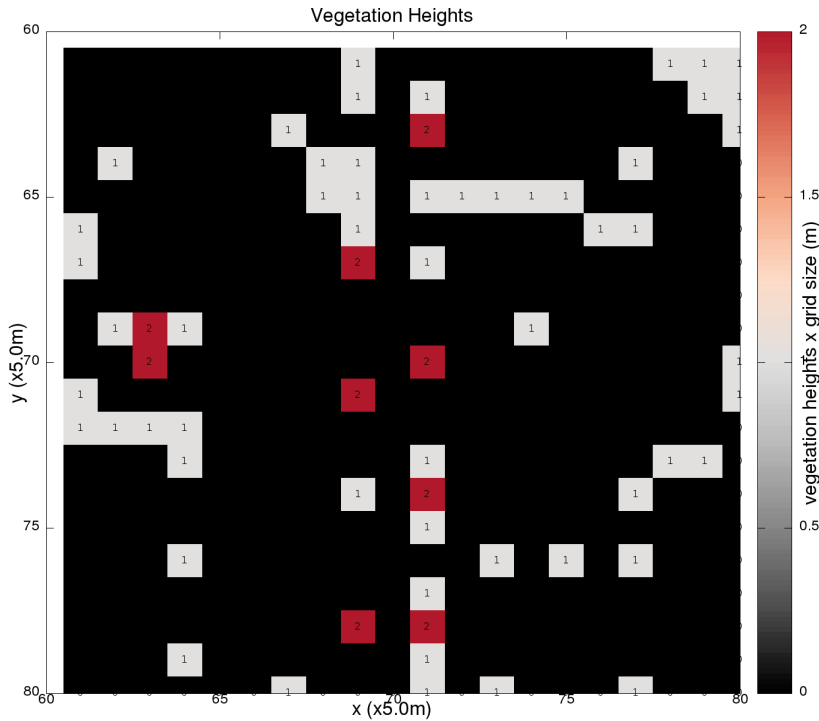


Figure 5.4: Preston validation domain configured vegetation heights (0, 5, 10m) and locations.

Table 5.3: Preston validation site properties (Coutts et al. 2007).

Property	Value(s)
α , albedo	0.15
z_m , instrument height (m)	40
z_0 , roughness length (m)	0.4
z_h , maximum height of roughness elements (m)	12
z_b , mean building height (m)	6.4
$H : W$, mean height to width ratio	0.42
$W : P$, mean wall-to-plan ratio	0.4

well as grass were set to the values given in the model design vegetation parametrisation section (Section 4.3.6). A current limitation of the model is that the available vegetation parametrisations are limited to these three vegetation types. The species mix was chosen to best account for density of canopy cover in the aerial imagery but given this limitation, will not completely reflect the observed species mix and might create some modelling errors from the observed fluxes. However, the two available species are representative of commonly planted trees in Melbourne. A street tree inventory by Frank et al. (2006) finds that brushbox, a native evergreen, is the most common street tree, representing 6.9% of street trees in Melbourne. Olive trees considered suitable for Melbourne's climate conditions (drought tolerant evergreen) and a recommended species for council street tree planting (City of Port Phillip 2010).

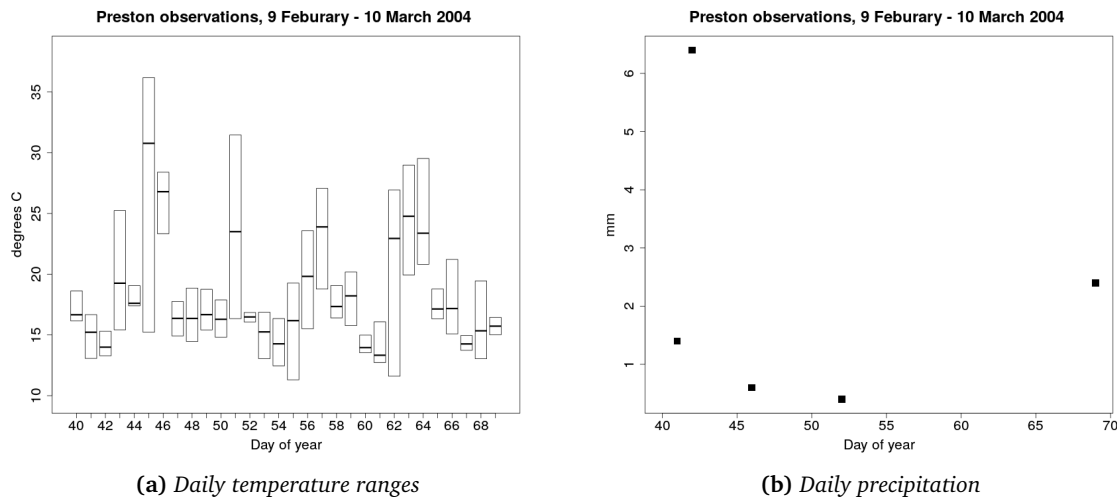
The validation simulation (which is named Pr04Val) was run for 30 days between the dates 10 February 2004 and 10 March 2004, forced by the observations, from Coutts et al. (2007) for those days. Values used from the observations include $K \downarrow$, $L \downarrow$, air temperature, wind speed, wind direction, and air pressure. Forcing data for the vegetation components use shortwave values of mean global and mean diffuse observations taken from one minute solar observations (station 086282, Melbourne Airport) (Bureau of Meteorology 2016b). For full radiation

Table 5.4: Preston validation scenario model parameters.

Parameter	Value(s)	Source
Albedo (roof, street, wall)	0.15, 0.10, 0.30	Krayenhoff & Voogt (2007)
Emissivity (roof, street, wall)	0.92, 0.92, 0.88	Krayenhoff & Voogt (2007)
Forcing data height (m)	40	Coutts et al. (2007)
Mean height of buildings (m)	5.61	Calculated from domain
Mean height of trees (m)	5.7	Calculated from domain
Initial T_{sfc} (roof, street, wall) ($^{\circ}\text{C}$)	18.0, 23.0, 22.0	Krayenhoff & Voogt (2007)
Constant building internal air temperature (base of roofs and walls) ($^{\circ}\text{C}$)	22.0, 20.0	Krayenhoff & Voogt (2007)
Constant deep-ground temperature ($^{\circ}\text{C}$)	19.0	Krayenhoff & Voogt (2007)
Constant building internal floor temperature ($^{\circ}\text{C}$)	15.0	Krayenhoff & Voogt (2007)

vegetation runs, the Mean_global_irradiance_over_1_minute variable from the observations is used. For diffuse runs, the Mean_diffuse_irradiance_over_1_minute variable is used. In addition, the FBEAM variable (fraction of incident PAR which is direct-beam) is set to 0.0 in the forcing data for diffuse runs.

The validation period contained a range of conditions, as shown in Figure 5.5. The period especially features a number of hot days (over 30°C). As one of the major applications of VTUF-3D will be examining high temperature moderation, validation over a period containing these hot days is important.

**Figure 5.5:** Preston observations during the validation period of 9 February - 10 March 2004.

The observation period also contains a number of days with precipitation. With the current VTUF-3D design, precipitation will only be received in grid squares which contain vegetation and pervious surfaces. The expected impact of this is that predictions of Q_E will be understated for days which contain precipitation. Accounting for rainfall on impervious surfaces is a current limitation of VTUF-3D (to be addressed in later versions of VTUF-3D) and caution should be used in modelling periods which contain significant rainfall. For this project, which focuses on temperature moderation in the hottest periods of the year (which contain little rainfall), this should be less of an issue. Also, in most urban areas, precipitation on impervious surfaces will be rapidly removed as stormwater.

5.2.2 Preston validation results and discussion

Observation validation scenario

During this validation, a number of different scenarios (described in Table 5.5) are considered and compared. The validation scenario (named Pr04Val) represents the closest approximation of a domain (at a micro-scale) which could be constructed to match the local scaled flux observations. Note, in all the following comparisons using the Preston observations dataset, gap-filled observations, and the corresponding modelled result for that time period, were removed from both datasets.

Table 5.5: Preston simulations and Intercomparison project compared.

Scenario name	Description
Pr04NoVeg	Baseline no-vegetation simulation with unimproved TUF-3D
Pr04Val	Preston 2004 validation scenario
IntercomparisonNoVeg	Best & Grimmond (2012) intercomparison performance mean of urban models that do not model vegetation, using Coutts et al. (2007) Preston dataset
IntercomparisonTiled	Best & Grimmond (2012) intercomparison performance mean of urban models that tile vegetation, using Coutts et al. (2007) Preston dataset
IntercomparisonIntegrated	Best & Grimmond (2012) intercomparison performance mean of urban models that integrate vegetation, using Coutts et al. (2007) Preston dataset

The first result is given in Figure 5.6. Modelled results for the 30 day run were compared to the observed fluxes (Q^* , Q_H , Q_G , and Q_E). Error analysis of d index of agreement for the Pr04Val validation (Figure 5.6) shows d values of 0.964, 0.652, 0.998, and 0.957 for Q_H , Q_E , Q^* , and Q_G respectively. Error analysis of RMSE (W m^{-2}) shows values of 40.2, 33.1, 19.0, and 52.5.

Individual fluxes (Q^* , Q_H , Q_G , and Q_E) were aggregated into hourly averages over the 30 days and compared to the observations (Figures 5.7 and 5.8). VTUF-3D is able to reproduce the important dynamics of this area, driven by the fluxes. In the observations, the Q_H and Q_G fluxes dominate the urban area, with modest amounts of Q_E fluxes, peaking under 100W m^{-2} during the daytime and falling to roughly zero at night-time.

VTUF-3D captures closely both the magnitude and diurnal cycle of Q_H , with a slight under-prediction during the morning and a slight over-prediction during the late mornings. VTUF-3D also captures closely the cycles of Q^* . The very small divergence between the predicted and observed values can be explained through the dual sources of values of $K \downarrow$ in the forcing data, a distance of approximately 20 km between Preston and the Melbourne Airport observation site, providing varying values as a component of the calculated Q^* which are then compared to only the Preston observations. Q_G shows close agreement except for a slight over-prediction during the mornings, an over-prediction at mid-day, a slight over-prediction during the afternoon cooling period, and a very slight over-prediction during the evening.

In terms of absolute values, in 30 day monthly hourly averages, peaking daily values of Q_H at 1300 are 314 W m^{-2} in observed values compared to modelled values of 294. For the other fluxes, Q_E , Q^* , and Q_G , these values are 93 vs. 40, 621 vs. 612, and 213 vs. 266 W m^{-2} .

(Improved) micro-climate modelling assessment of the influence of WSUD on HTC

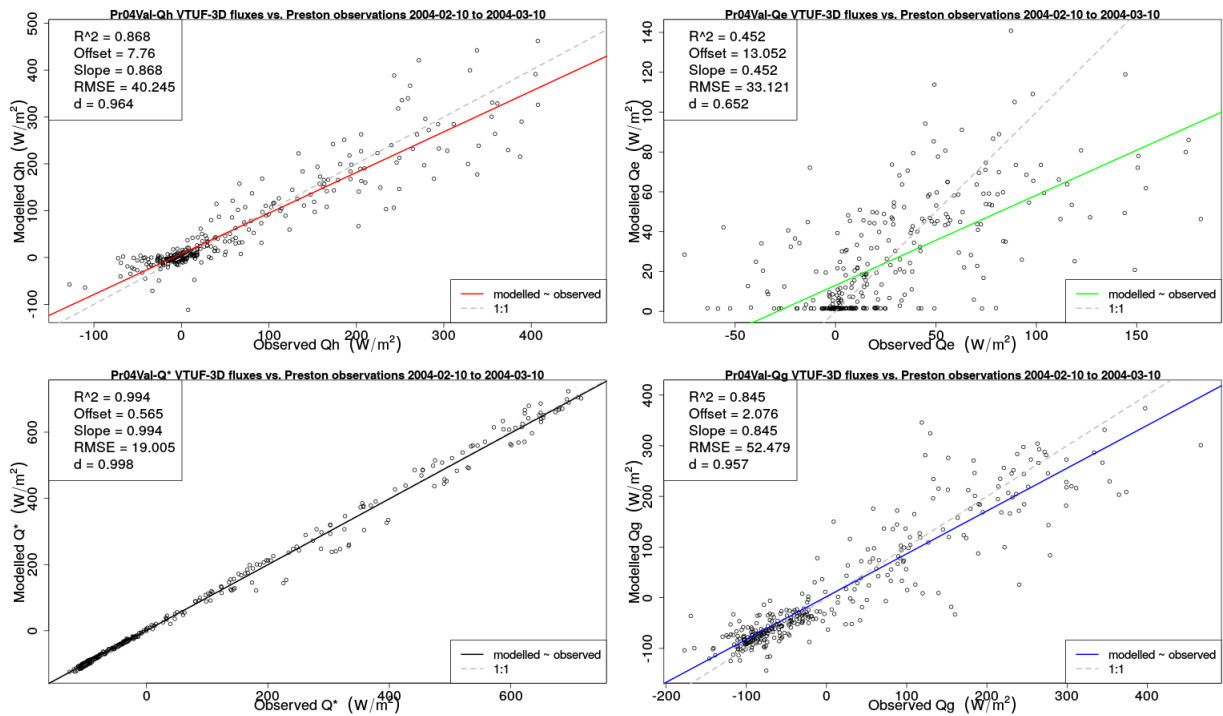


Figure 5.6: Pr04Val scenario modelled vs. observations for Q_H , Q_E , Q^* , and Q_G fluxes for the period 10 February-10 March 2004.

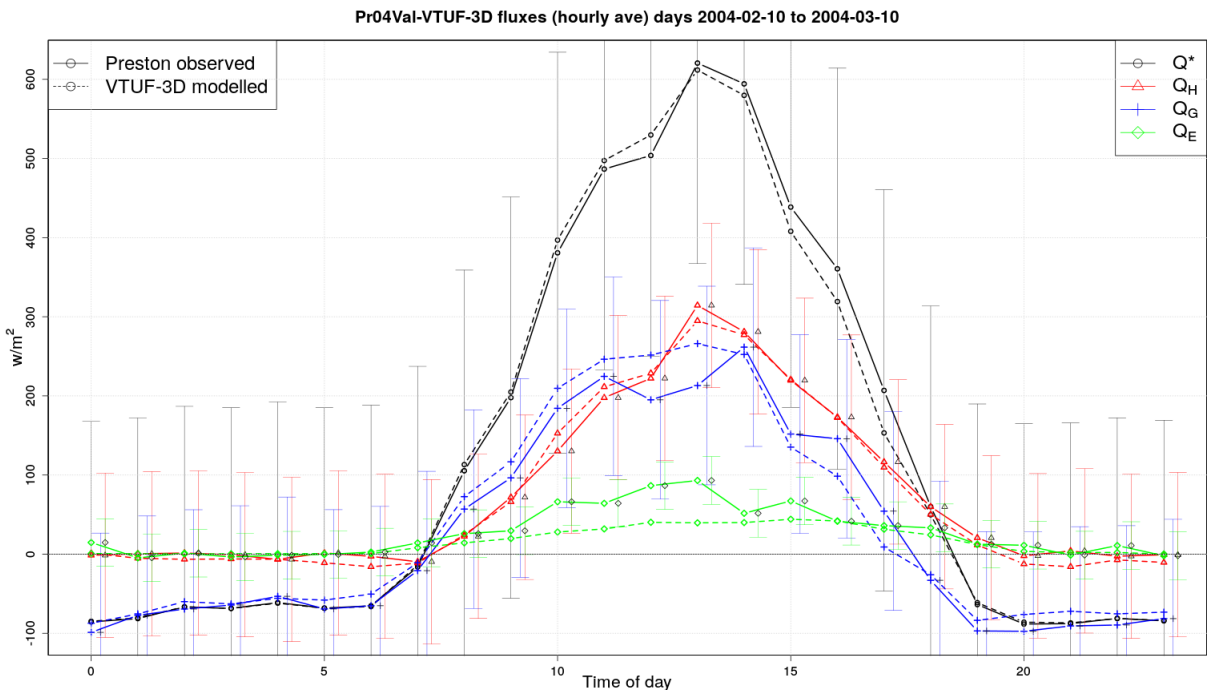


Figure 5.7: Pr04Val run 30 day hourly average VTUF-3D flux comparisons to Preston flux observations for the period 10 February-10 March 2004, with error bars at observations standard deviations.

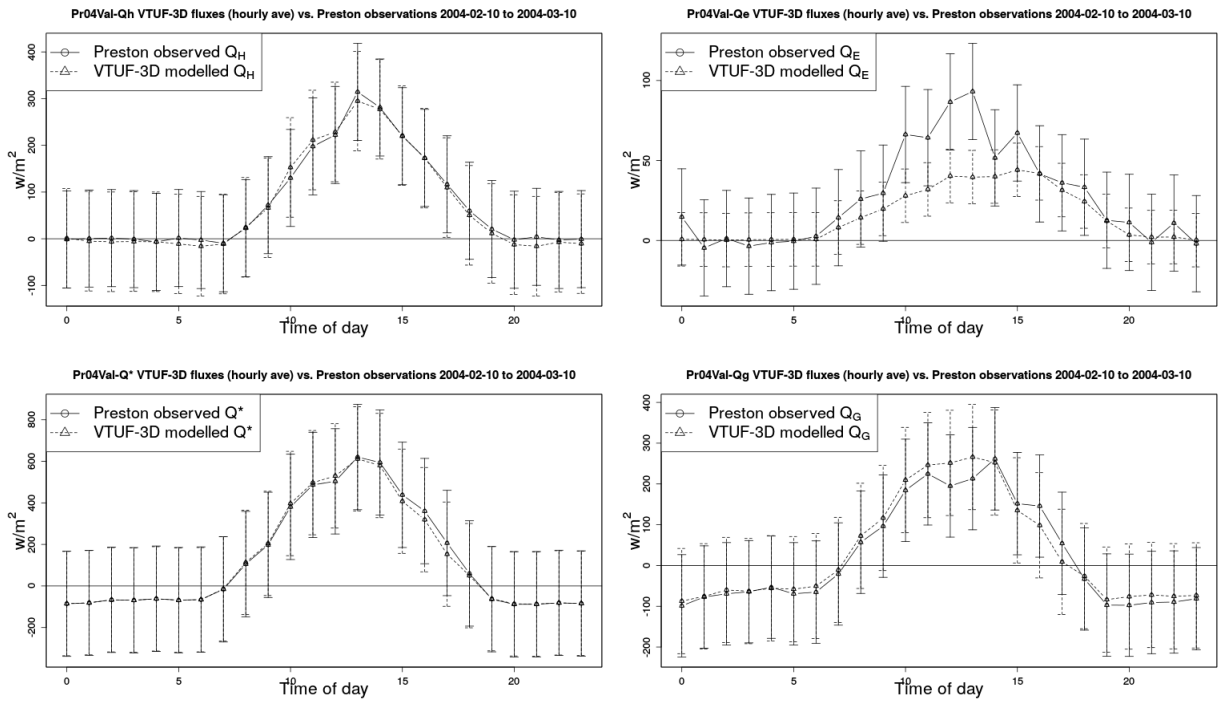


Figure 5.8: Pr04Val run 30 day hourly average VTUF-3D flux comparisons to Preston flux observations for the period 10 February-10 March 2004, with error bars at standard deviations.

As an extension to the TUF-3D model, the addition of vegetation and associated Q_E fluxes to VTUF-3D have created a large improvement to the model. As will be seen in the Intercomparison results (Section 5.2.3), as well as in the results of this intercomparison project (Grimmond et al. 2011; Best & Grimmond 2012), land surface modelling schemes that include vegetation perform better than those that do not.

In addition, schemes that integrate vegetation perform better than those who use a tiling method to include the vegetation. Another important result from this intercomparison project is that Q_E is the least well modelled flux across a range of urban land surface modelling schemes (Grimmond et al. 2010). Even the SUEWS model, which includes vegetation, as well as a very complete urban hydrology, tends to under-estimate Q_E fluxes during day-time (Järvi et al. 2011).

It is anticipated that the innovative method taken in this project, the first time vegetation has been tiled and incorporated into a micro-scaled surface energy balance model, will bring performance improvements over the previous model which did not consider vegetation. This will be seen to be the case, shown in the the results of the Pr04NoVeg no vegetation validation scenario later in this section.

In addition to the improved modelling performance, the addition of vegetation modelling has dramatically improved the applicability of VTUF-3D to a wide range of modelling problems. Indeed, without this addition, the objectives of this project, to determine the thermal comfort improvements due to WSUD features would not be possible.

Despite these improvements to the modelling tool, the fluxes of Q_E show some divergences from the observations. This was anticipated as there are three current limitations of VTUF-3D that can account for low Q_E levels, and need addressing in future versions of the model.

The first is not accounting for precipitation on impervious surfaces. Many spikes of Q_E fluxes are seen in the observations (Figure 5.9) shortly after rainfall. Demuzere et al. (2014) found evaporation from impervious surfaces in urban areas after rainfall can contribute to an approximately 10% increase of Q_E over a two month period, while Wouters et al. (2013) found increases of 45 W m^{-2} in Q_E for up to 12 hours of daylight following rainfall. Until this portion of precipitation received is accounted for in the model, care should be taken when modelling periods which contain precipitation.

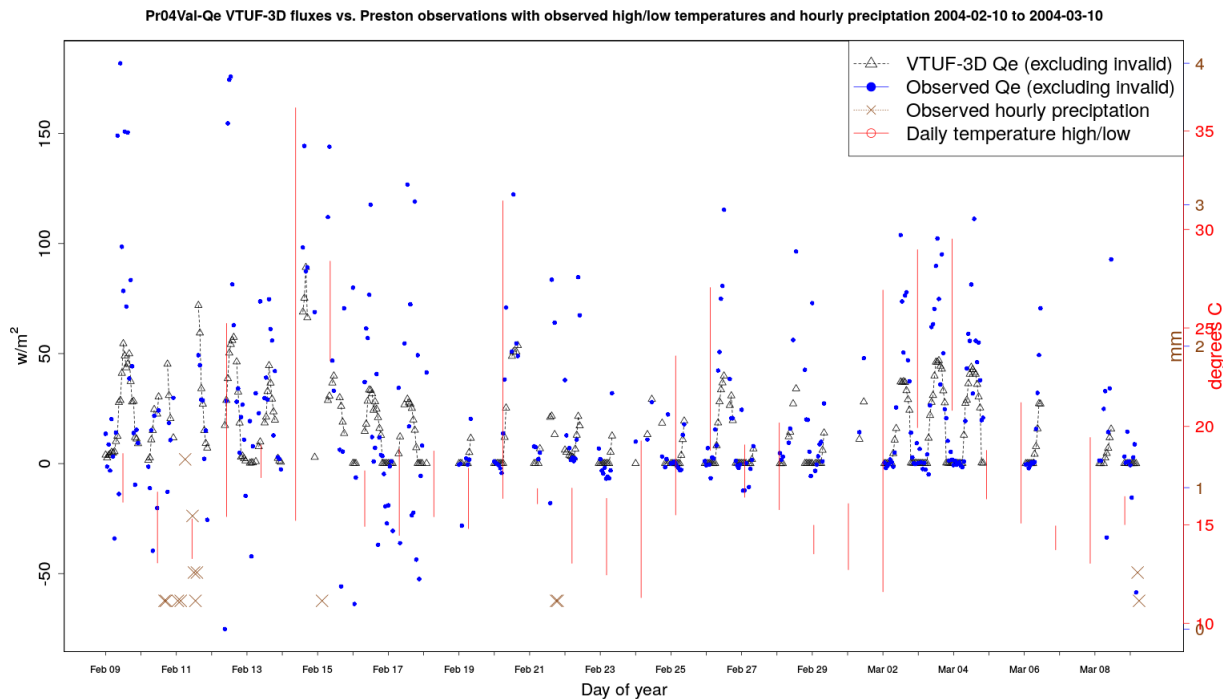


Figure 5.9: Pr04Val modelled Q_E vs. Preston Q_E observations including observation of daily high/low temperatures and hourly rain totals for the period 10 February-10 March 2004.

The second limitation is not accounting for irrigation. While Melbourne was under Stage 2 water restrictions during the observation/modelling period (Melbourne Water 2016a), there would have been some amount of irrigation occurring to contribute to greater observed Q_E fluxes than modelled. Estimates of household irrigation during February 2004 are of frequencies of 2.8 times a week (3.1 for only the homes which irrigate) with average irrigation flows of 16.3 LpM and average durations of 46 minutes per irrigation event (Roberts 2005). This is an important limitation which needs addressing as quantifying the benefits of irrigation as part of WSUD is an intended use of this model.

The third limitation is the full diversity of vegetation and trees of the modelled area are not represented in the modelled domain. Current parametrisations only include grass, brushbox, and olive trees. However, this is not a limitation in the model itself, as any type of vegetation can be plugged into the model. To overcome this deficit, more work needs to be done. Completion of each parametrisation is a time consuming process requiring numerous observations of tree physiology specifications. A standard limitation of many empirical models requiring a choice of either deciduous or evergreen vegetation does not exist in the model itself as these new vegetation types can include either, as long as the proper observations and parametrisations are completed on each type.

Finally, values of Q_F , anthropogenic heat (W m^{-2}), are not accounted for in the VTUF-3D model, but which do contribute to the total Q_H fluxes in the observations. Flux values for this modelling and observation period (summertime) are anticipated to contribute peaks of over 15 W m^{-2} for low density cities and peaks of 30-60 W m^{-2} for medium density areas (Sailor & Lu 2004). In both the observations and modelling results, these unaccounted fluxes will be present in the errors for the four observed and modelled fluxes.

There will remain an amount of uncertainty in comparing the modelled results to the observations because of the nature of both. The observations were collected via a flux tower at 40m height, above the height of the urban roughness sublayer. The modelled results are the average of the fluxes from all of the urban surfaces, within the urban canyon and well within the urban roughness sublayer. While these comparisons can be done (i.e. Grimmond et al. (2011)), there remains an amount of uncertainty as they are comparing two slightly different things.

A final consideration is that the under-prediction of Q_E is likely contributing to the over-estimating of Q_G (calculated as a residual in MAESPA vegetation tiles). An improvement in modelling of the Q_E fluxes will likely lead to an improvement in the modelled Q_G fluxes.

No vegetation baseline scenario

To demonstrate the significant improvement of the model, the VTUF-3D model was run with a no vegetation scenario. This scenario (named Pr04NoVeg), will represent an unimproved TUF-3D without vegetation modelling capability, as the lack of vegetation will not trigger any of the new logic and improvements added to the model. This will allow an analysis of level of improvement of VTUF-3D modelling over the previous TUF-3D model. As discussed early in this section, the Intercomparison project found that models without vegetation were among the poorest performers.

These values show an improvement over the unimproved VTUF-3D model (Pr04NoVeg, shown in Figures 5.10 and 5.11). The unimproved model yields results of d of 0.906, 0.0, 0.989, and 0.877 and RMSE (W m^{-2}) of 87.0, 47.1, 51.6, 75.9 for Q_H , Q_E , Q^* , and Q_G respectively.

To complete the comparison with the unimproved TUF-3D model, fluxes for this same period for scenario Pr04NoVeg are shown (Figure 5.11). As an unimproved model, Q_H is significantly over-predicted during the afternoon and under-predicted in the evenings. Flux Q_G is under-predicted during the afternoons. Finally, Q_E is not implemented in the model, so cannot be predicted at all.

5.2.3 Preston validation intercomparison results and discussion

During this validation, a number of different scenarios are considered and compared. The Pr04Val scenario (a scenario to best represent the area observed by the Preston flux tower observations) is compared to a baseline Pr04NoVeg scenario (an unimproved TUF-3D without vegetation modelling capability). As the observations used in this validation are the same as in Phase 4 of the Intercomparison project (Best & Grimmond 2012), using the Coutts et al. (2007) Preston dataset, the performance of the VTUF-3D model can be placed within this evaluation of urban land surface modelling schemes.

Phase 4 error analysis provides RMSE values for fluxes Q^* , Q_H , Q_G , and Q_E for three classifications of urban models. The three categories of models are those that do not consider vegetation, those who model vegetation using tiles, and models that integrate vegetation into the urban area (referred to as classifications IntercomparisonNoVeg, IntercomparisonTiled, and IntercomparisonIntegrated, described in Table 5.5). These values are taken from Figure 5.12,

(Improved) micro-climate modelling assessment of the influence of WSUD on HTC

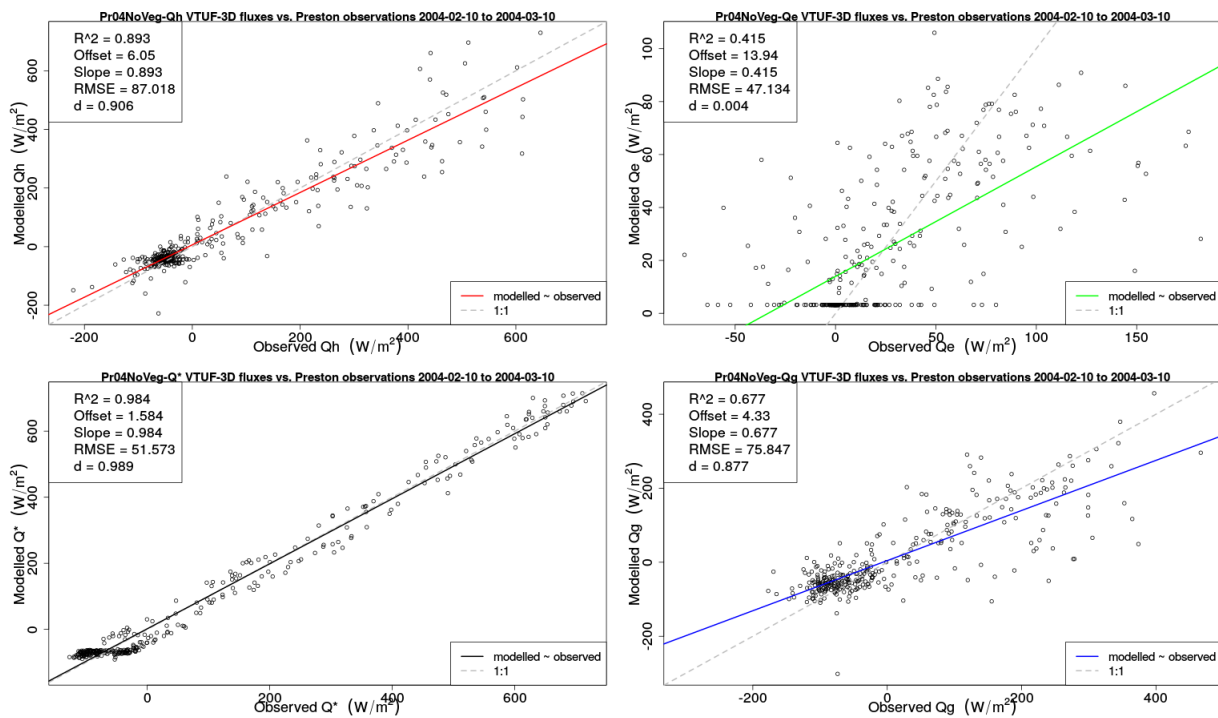


Figure 5.10: Pr04NoVeg scenario modelled vs. observations for Q_H , Q_E , Q^* , and Q_G fluxes for the period 10 February-10 March 2004.

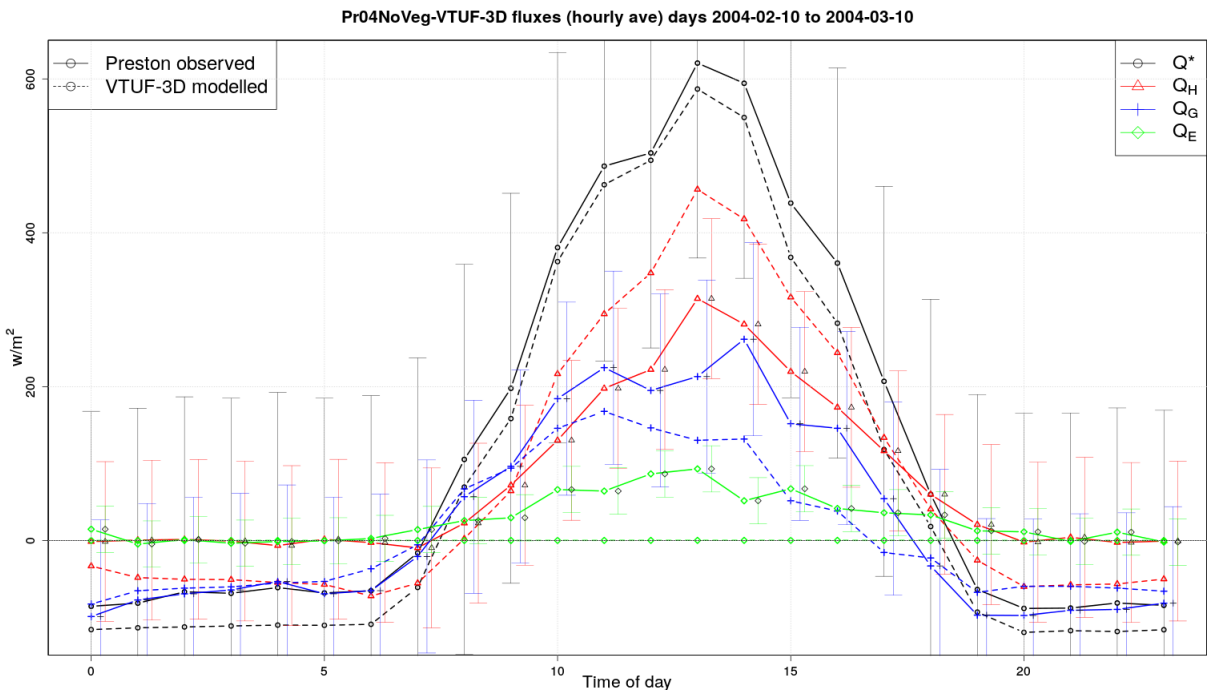


Figure 5.11: Pr04NoVeg run 30 day hourly average VTUF-3D flux comparisons to Preston flux observations for the period 10 February-10 March 2004, with error bars at observations standard deviations.

for the Feb/Mar period, corresponding to the period for which the validation scenarios were run.

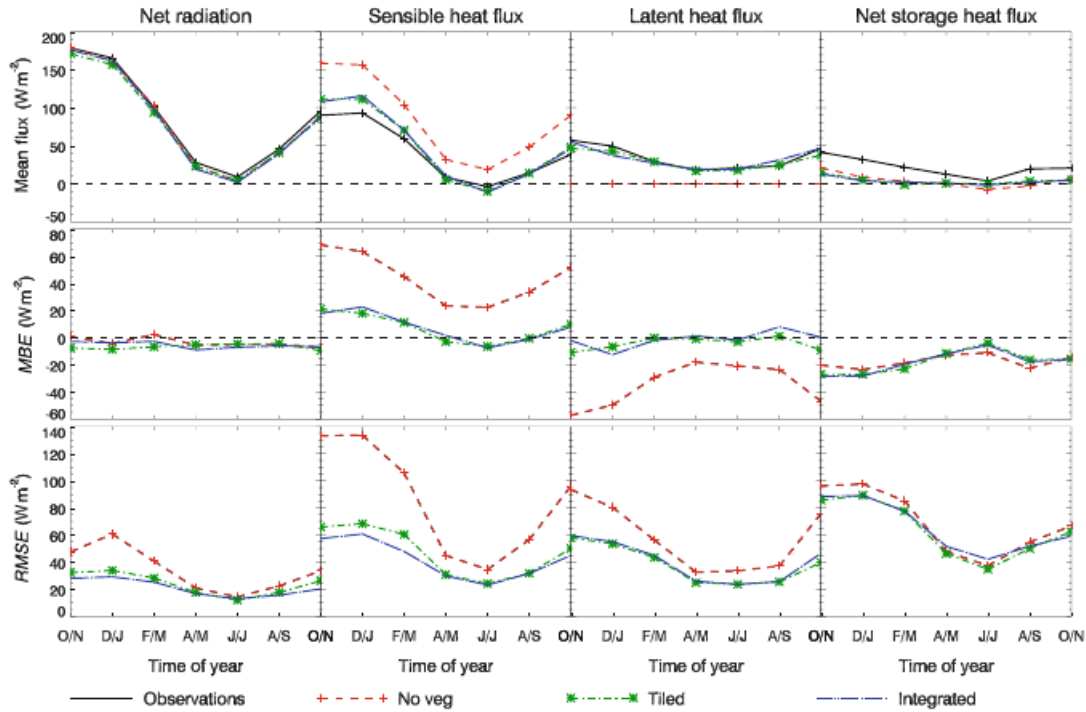


Figure 5.12: Median of the mean modelled flux, MBE, and RMSE for the surface fluxes determined for two month periods, for the models classified by their representation of vegetation. Note the scales are different for each flux (Best & Grimmond 2012).

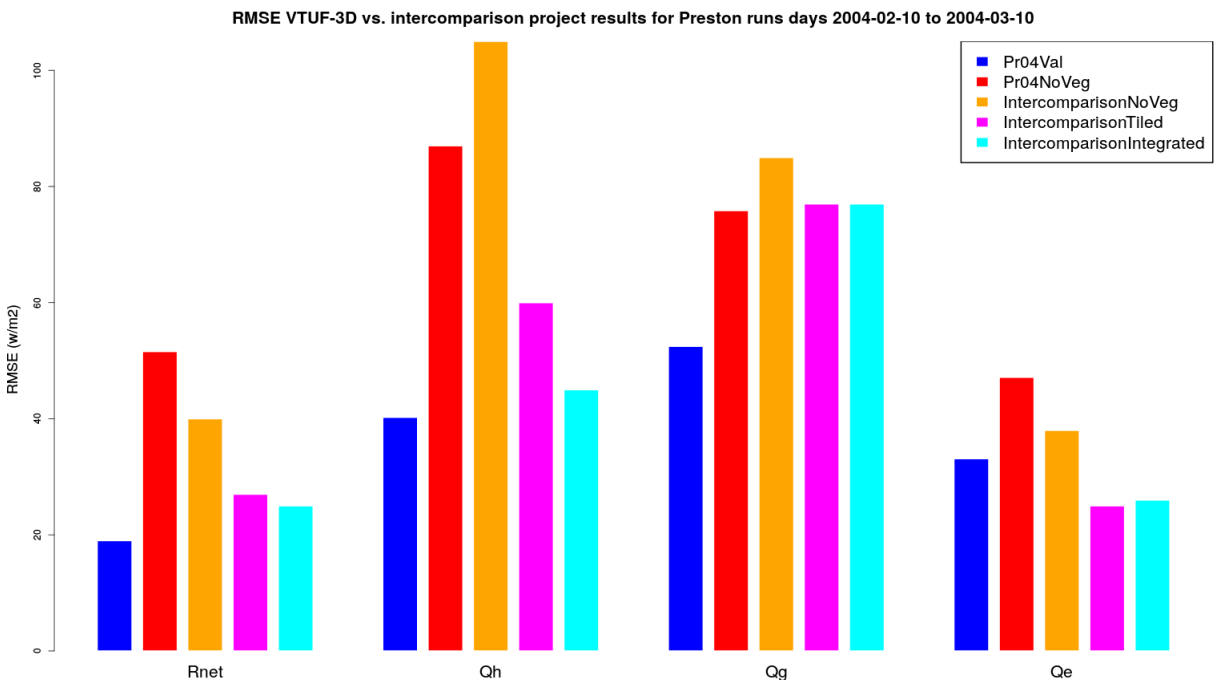


Figure 5.13: RMSE VTUF-3D vs. Intercomparison results comparison for Preston validations scenarios for 10 February-10 March 2004.

In Phase 4 comparisons, for all fluxes, models with integrated vegetation had the lowest RMSE values. These were followed by tiled vegetation models while models without vegetation had the highest values.

In comparison, the VTUF-3D Pr04Val scenario had lower RMSE values for all fluxes except Q_E than each of the Phase 4 three model categories. For Q_E , the VTUF-3D scenario Pr04Val performed better than the no vegetation category, but with slightly higher errors than the tiled and integrated categories.

In terms of absolute differences between RMSE values for the best performing Intercomparison model category, Pr04Val scenario RMSE values differed by -6, -5, -25, and 7 Wm^{-2} for Q^* , Q_H , Q_G , and Q_E respectively.

5.2.4 Preston validation conclusions

This analysis of VTUF-3D performance when comparing predicted results to flux tower observations and in comparison to error rates of other urban models has shown significant improvement over the unimproved (non-vegetated) TUF-3D model. Furthermore, these comparisons to observations show the model is able to capture well the temporal and amplitude variations of fluxes observed by flux towers.

In a comparison of VTUF-3D modelled results to other urban models, VTUF-3D performs well within the range of those other models, even though most of those models are local scaled and not being run at a micro-climate scale. Error analysis puts VTUF-3D's performance in all fluxes except Q^* slightly better than the all categories of these models. With the Q^* flux, VTUF-3D performs with lower errors than the models in the no vegetation category but with slightly higher errors than in the tiled and integrated categories. This validation successfully fulfils sub-objective 1, the evaluation of the model in terms of surface energy balances.

5.3 Model testing and validation using City of Melbourne, George and Gipps St. dataset

While validation against the Preston flux observations indicates that VTUF-3D performs well in partitioning the basic energy fluxes, there are a number of other aspects that need to be validated to allow confidence in the model's accuracy, especially given the intended application of the model to assess the impacts of WSUD and urban greening on micro-climates and HTC. The flux validation ensures that the model models the fundamental drivers of urban climates (Section 2.2.2) and their temporal variations across the diurnal cycle.

Further validation is needed to ensure that the model correctly captures the spatial variations of T_{mrt} driven by these fluxes. These values are also driven by varied shading effects across the urban canyon. Both then are highly influential on thermal comfort, as measured by $UTCi$. The validation will be performed by comparing spatial values of T_{mrt} and $UTCi$ to observed values. Validations of spatial air temperature (T_a) will not be possible as air temperature is only predicted as a single canyon-wide value and not spatially.

5.3.1 George St. and Gipps St. overview

This set of validations was undertaken using observations from George St. and Gipps St. in the City of Melbourne (Coutts et al. 2015a). These observations were taken at a number of observation stations, recording air temperature, wind speed, humidity, and incoming short

wave radiation, located along the two streets. The purpose of this study was to observe and quantify the effects of street trees on HTC and recorded observations in streets with varied canopy cover. Figure 5.14 shows the two streets used in this validation.



Figure 5.14: Location and photos of each street: Gipps St. (OPN), and George St. (TRD). Aerial view of the streets highlighting individual station locations and tree canopy coverage in Gipps St. (OPN), and George St. (TRD) (Coutts et al. 2015a, p.58).

These two streets both have a shallow urban canyon and both orientated are E-W. Gipps St. contains a very limited canopy cover and is designated open (OPN) in the observation study.

George St. contains a dense canopy cover and is designated as treed (TRD). Some of the sensors were placed directly under tree canopies and others out in the open. A main purpose of the VTUF-3D model will be to evaluate the impacts of different arrangements of WSUD features on HTC in urban canyons. Differing amounts of canopy cover are a major factor of these different arrangements. Because of this, a validation using observations from two very similar streetscapes which mainly differ in the amount of canopy cover will be an ideal evaluation of VTUF-3D's spatial accuracy in resolving the impacts of different arrangements of WSUD features on HTC.

Tree cover of Gipps St consists of *Ulmus parvifolia* (Chinese Elm) with median heights of 9.5m and crown diameters of 9.6m. The limited tree cover of George St. also consists of *U. parvifolia*. The entire street canyon floor of both streets were impervious, consisting of concrete and asphalt, with the exception of a small pervious area of 1.2m² surrounding each tree in the road areas. General characteristics of the two sites are summarised in Table 5.6.

Table 5.6: Gipps/George St. validation site characteristics (Coutts et al. 2015a).

Property	Gipps St. (OPN)	George St. (TRD)
Observation stations	5	7
Minimum building height (m)	4	4
Maximum building height (m)	14	11
Average building height (m)	7	8
Street width (m)	25	25
Mean H:W	0.27	0.32
Plan area canopy cover (%)	12	45

Observations were taken at heights of 3.5 to 4.0m on existing light poles at locations indicated in Figure 5.14. The observation period was for 21 months, from October 2011 to June 2013. Each observation station recorded air temperature, wind speed, humidity, incoming shortwave, and black globe temperature. For each, mean radiant temperature was calculated using a formula of Kántor & Unger (2011) (a slight variation of the equation used in this project in Section 4.2.4). *UTCI* was calculated using RayMan Pro 2.1 (Matzarakis et al. 2010) for a 35 year old male, clothing factor of 0.9, and activity rate of 80 W. This temperature was then compared to Bröde et al. (2012) assessment scale of thermal stress.

Station locations (noted on Figure 5.15 as yellow pins and red dots on Figure 5.14) are shown in the modelled domains for both streets. Stations for George St. are referred to as TRD_2, TRD_3, TRD_4, and TRD_5 (also known as EM12, EM9, EM3, and EM2 on Figure 5.15). Stations for Gipps St. are referred to as OPN_3, OPN_4, OPN_5 (also known as EM5, EM11, and EM8). Table 5.7 shows sky view factor (SVF) resulting from buildings and trees at each observation site.

These domains were configured accordingly using a 100x100m subset of the two streets (Figure 5.15). Simulations were run for both streets for the period 1 February 2014 to 1 March 2014 with a domain resolution of 5m grids. Building heights and locations and vegetation location and heights for both streets are shown in Figure 5.16.

Model parameters were set to the values given in Table 5.8. Most of these values are TUF-3D default values, from Krayenhoff & Voogt (2007). Vegetation settings for the mix of two tree

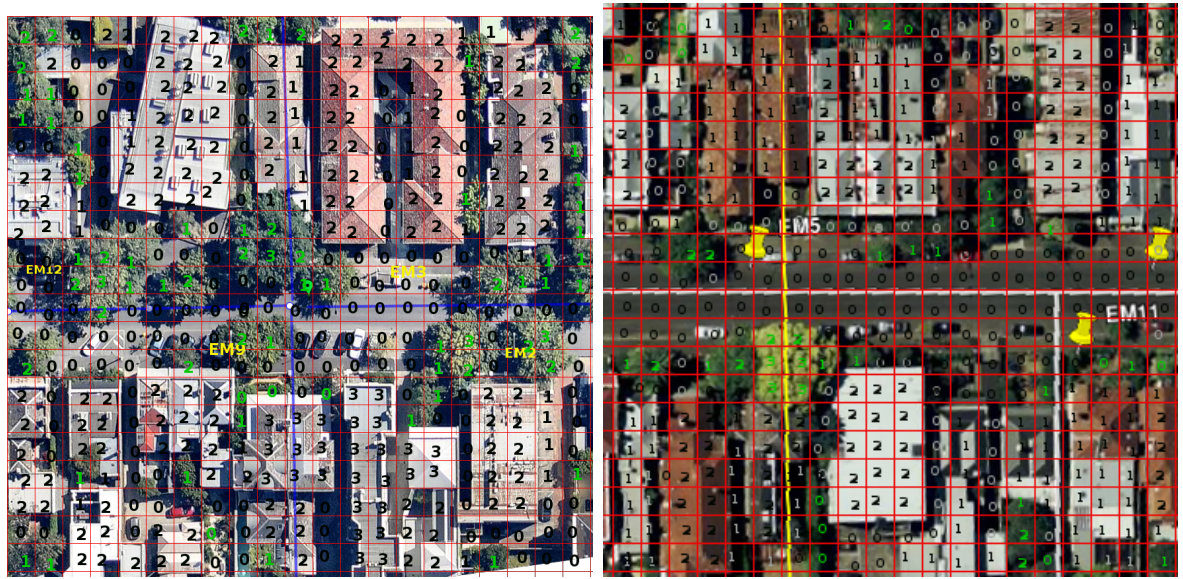


Figure 5.15: George St./Gipps St. - Modelled domains with 4 and 3 observation stations located on street.

Table 5.7: George St./Gipps St. observation station sky view factors (Coutts et al. 2015a).

Observation point	Total SVF	Build. SVF	Trees SVF
OPN_3	0.63	0.81	0.18
OPN_4	0.86	0.94	0.08
OPN_5	0.77	0.78	0.01
TRD_2	0.22	0.85	0.63
TRD_3	0.17	0.70	0.53
TRD_4	0.66	0.81	0.15
TRD_5	0.18	0.71	0.53

types (olive and brushbox) as well as grass are set to the values given in the model design vegetation parametrisation section (Section 4.3.6).

Table 5.8: George/Gipps St. validation scenario model parameters.

Parameter	Value(s)	Source
Albedo (roof, street, wall)	0.15, 0.10, 0.30	Krayenhoff & Voogt (2007)
Emissivity (roof, street, wall)	0.92, 0.92, 0.88	Krayenhoff & Voogt (2007)
Forcing data height (m)	4.0	Coutts et al. (2015a)
Mean height of buildings, George St./Gipps St. (m)	9.4, 6.8	Calculated from domain
Mean height of trees, George St./Gipps St. (m)	7.45, 8.14	Calculated from domain
Initial T_{sfc} (roof, street, wall) ($^{\circ}\text{C}$)	18.0, 23.0, 22.0	Krayenhoff & Voogt (2007)
Constant building internal air temperature (base of roofs and walls) ($^{\circ}\text{C}$)	22.0, 20.0	Krayenhoff & Voogt (2007)
Constant deep-ground temperature ($^{\circ}\text{C}$)	19.0	Krayenhoff & Voogt (2007)
Constant building internal floor temperature ($^{\circ}\text{C}$)	15.0	Krayenhoff & Voogt (2007)

The two validation simulations (which are named GeorgeValidation and GippsValidation) were run for 30 days between the dates 31 January 2012 and 1 March 2012, forced by the observations (of observation station OPN_1), from Coutts et al. (2015a) for those days. Values used from

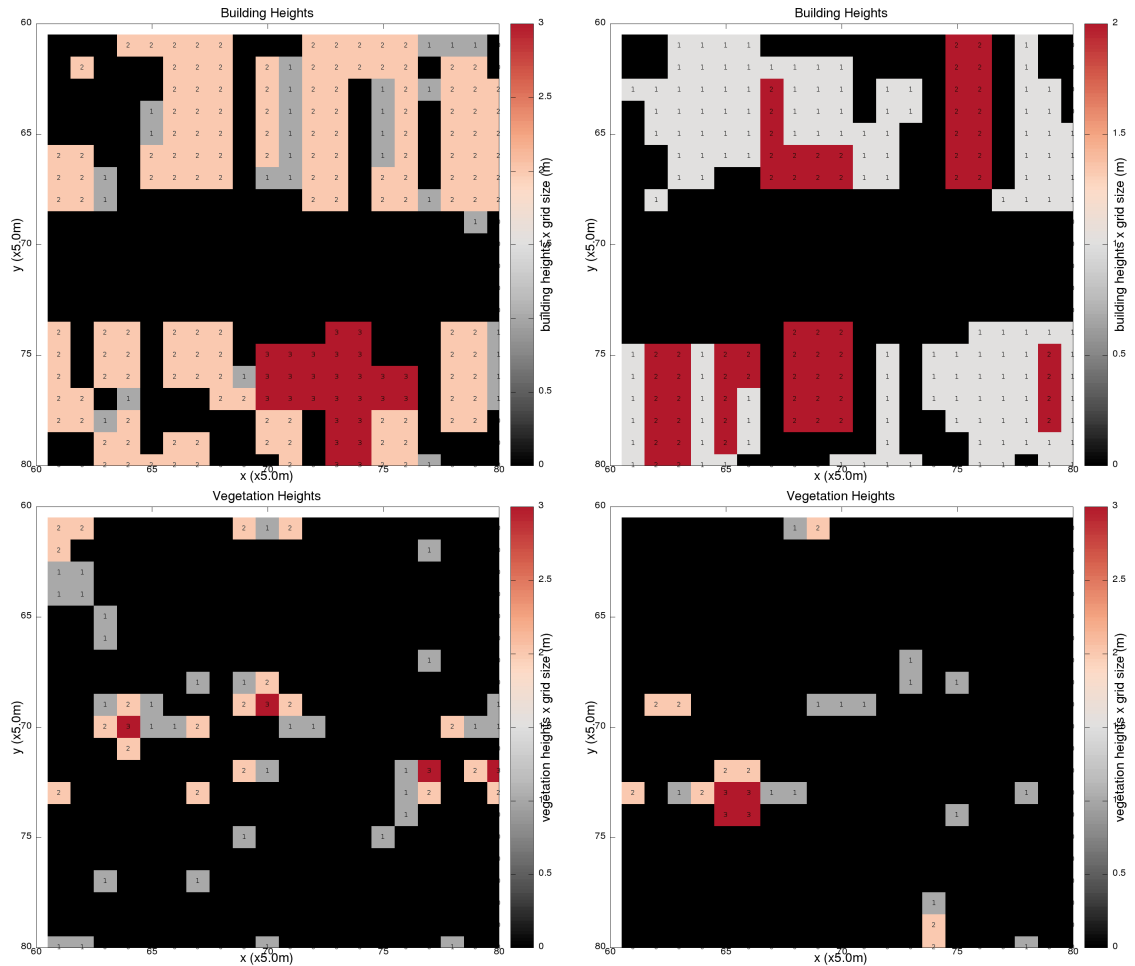


Figure 5.16: Building heights (top) / Vegetation cover (bottom) - George St (left), Gipps St. (right).

the observations include air temperature, wind speed, wind direction, and air pressure. Values for $L \downarrow$ are taken from Melbourne Airport observations (station 086282, Melbourne Airport) (Bureau of Meteorology 2016a). Values for $K \downarrow$ are taken from one minute solar observations (station 086282, Melbourne Airport) (Bureau of Meteorology 2016b) (as described in Section 4.3.4). Forcing data for the vegetation components uses shortwave values of mean global and mean diffuse observations, also from the one minute solar data. Values of CO_2 for vegetation forcing files were set to a constant of 450 ppm throughout the modelling period.

The period covered contains a range of conditions, as shown in Figure 5.17. The period especially features a number of hot days (over 30°C). As one of the major applications of VTUF-3D will be examining high temperature moderation, validation over a period containing these hot days is important. This observation period contains no days with precipitation.

5.3.2 George/Gipps St. validation results

The two scenarios GeorgeValidation and GippsValidation were completed for the February 2012 modelling period. Modelled predictions for the George St. observation locations (TRD_2, TRD_3, TRD_4, and TRD_5) and Gipps St. observation locations (OPN_3, OPN_4, and OPN_5) were extracted from the results and compared to the observations for those locations. Error analysis for these four and three locations for T_{mrt} and $UTCI$ are presented in Figures 5.18

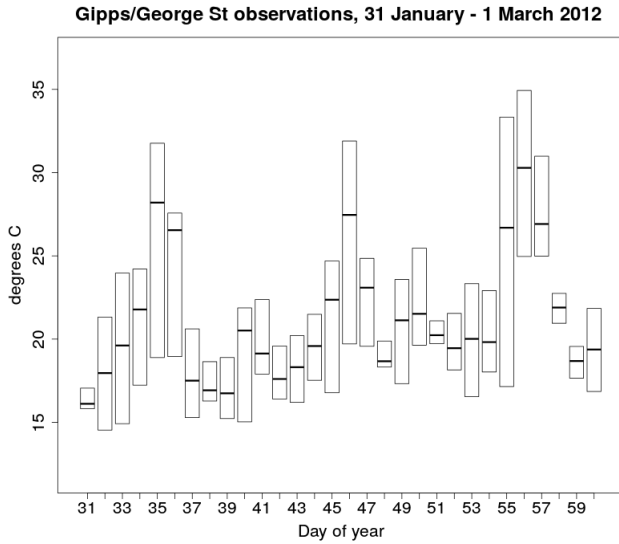


Figure 5.17: Daily maximum, minimum, and mean temperatures of Gipps/George St. observations during the validation period of 31 January - 1 March 2012.

and 5.19 for George St. and Figures 5.20 and 5.21 for Gipps St. A summary of the statistical analysis of RMSE errors and d index of agreement values for T_{mrt} and $UTCI$ are shown in Table 5.9.

Table 5.9: George St. GeorgeValidation and Gipps St. GippsValidation scenarios T_{mrt} and $UTCI$ predicted vs. observations statistical performance.

Observation point	T_{mrt} RMSE ($^{\circ}\text{C}$)	T_{mrt} d	$UTCI$ RMSE ($^{\circ}\text{C}$)	$UTCI$ d
TRD_2	5.48	0.938	3.02	0.931
TRD_3	6.46	0.925	2.74	0.947
TRD_4	7.94	0.913	3.64	0.914
TRD_5	6.74	0.939	2.75	0.953
OPN_3	6.01	0.959	2.33	0.971
OPN_4	6.11	0.959	2.44	0.967
OPN_5	5.82	0.961	2.45	0.965

The model shows reasonably good performance in this spatial point by point comparison. T_{mrt} RMSE values from George St. range from 5.48 to 7.94°C with d index of agreement values ranging from 0.913 to 0.939. $UTCI$ RMSE values range from 2.74 to 3.02°C with d index of agreement values ranging from 0.914 to 0.953. Gipps St. shows similar results, with T_{mrt} RMSE values ranging from 5.82 to 6.11°C with d index of agreement values ranging from 0.959 to 0.961. $UTCI$ RMSE values range from 2.33 to 2.45°C with d index of agreement values ranging from 0.965 to 0.971.

To examine the variations between the different observation points, the four locations for George St. (TRD_2, TRD_3, TRD_4, and TRD_5) observations of T_{mrt} were aggregated into hourly averages over 30 days and compared to the same aggregation of the modelled results (Figure 5.22). This same analysis was also performed for the Gipps St. points (OPN_3, OPN_4,

(Improved) micro-climate modelling assessment of the influence of WSUD on HTC

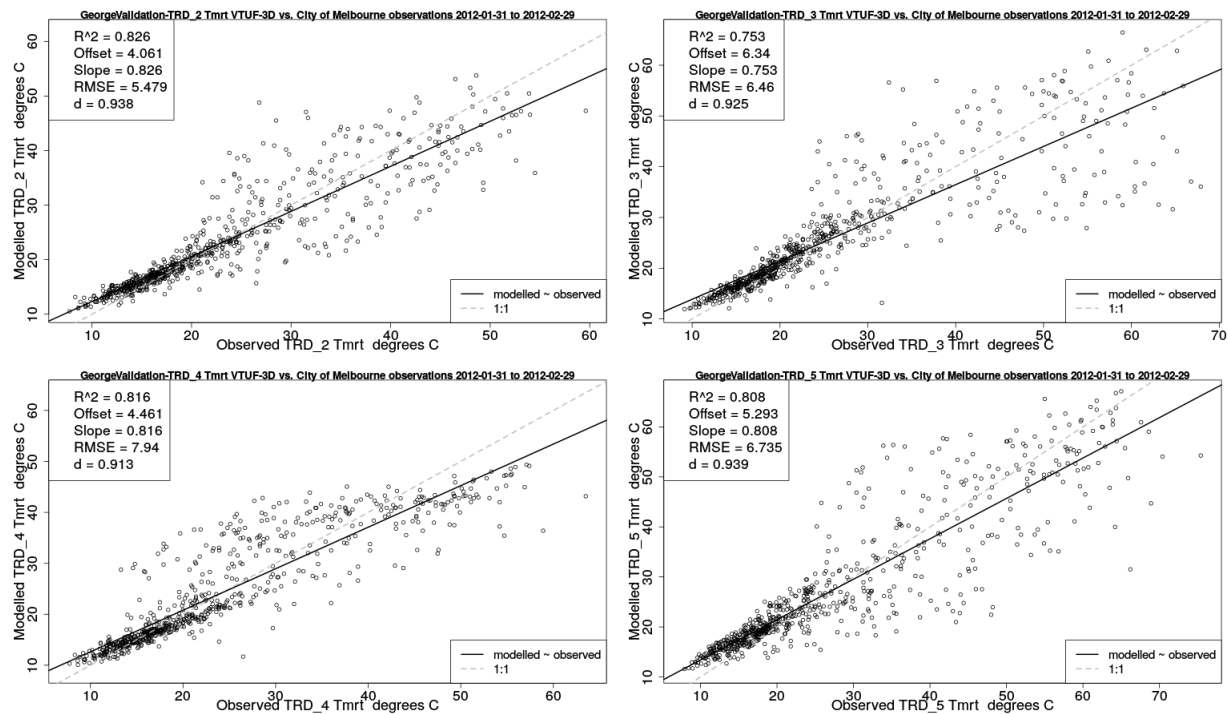


Figure 5.18: George St. GeorgeValidation scenario point comparison of T_{mrt} of 4 observation stations to modelled points.

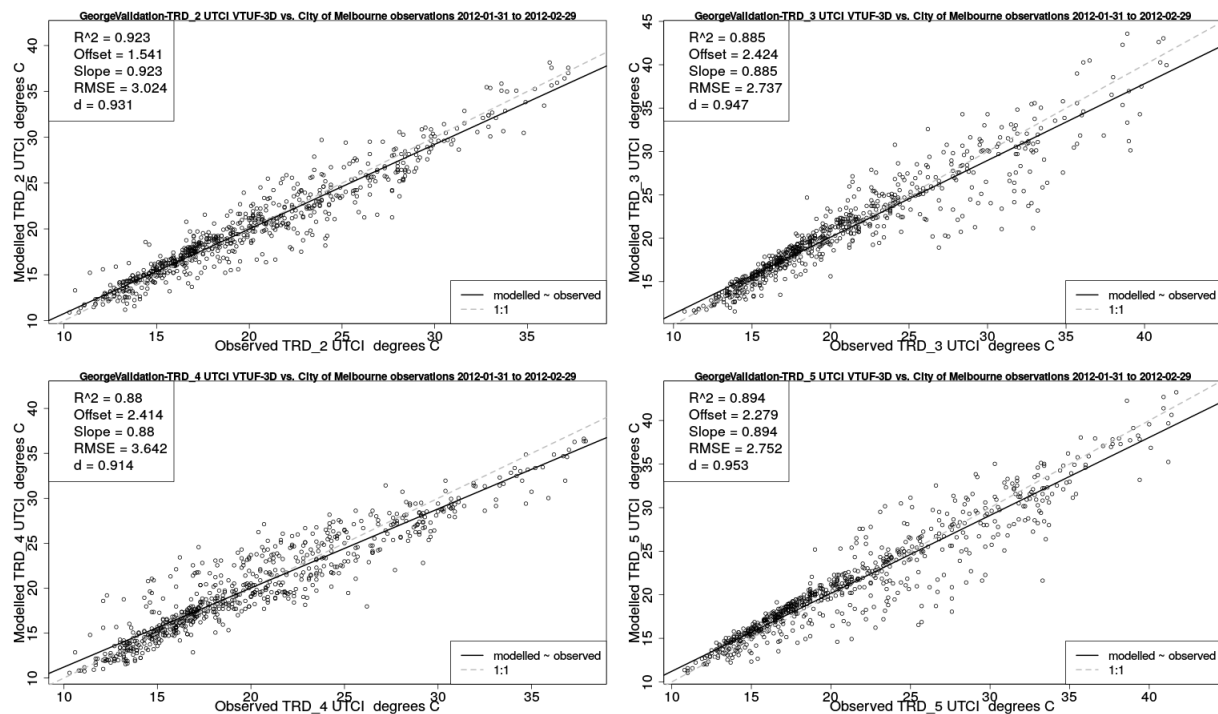


Figure 5.19: George St. GeorgeValidation scenario point comparison of UTCI of 4 observation stations to modelled points.

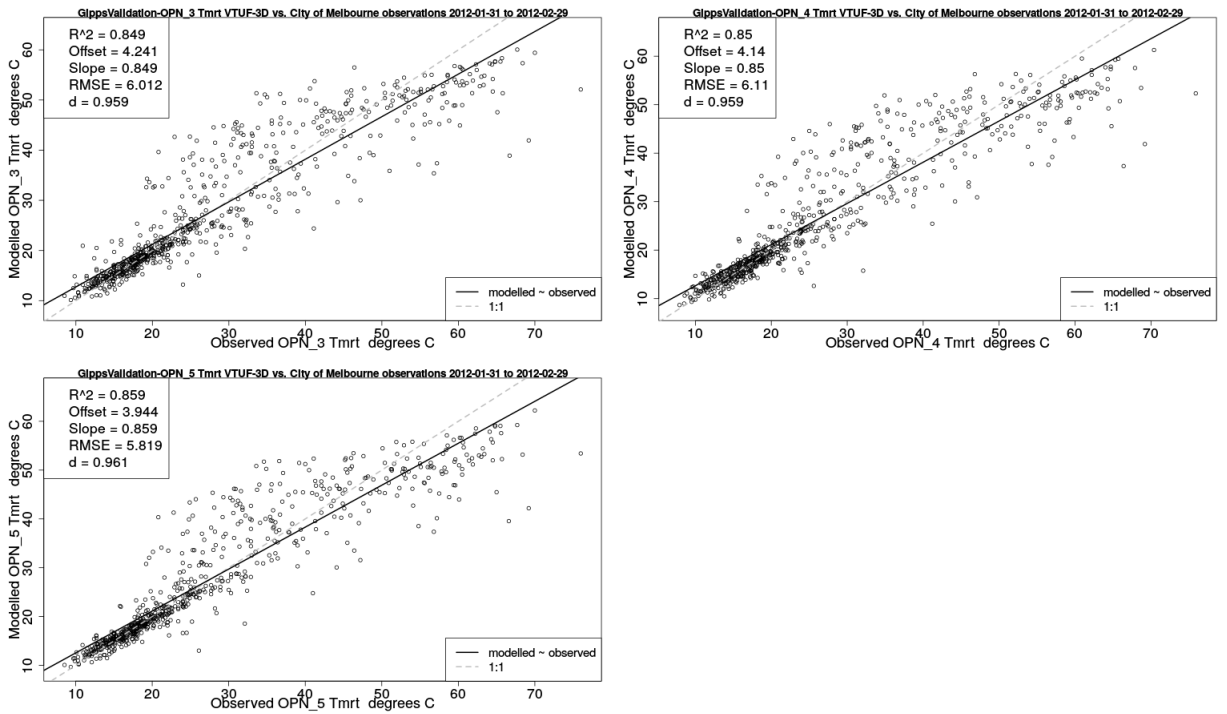


Figure 5.20: Gipps St. GippValidation scenario point comparison of T_{mrt} of 3 observation stations to modelled points.

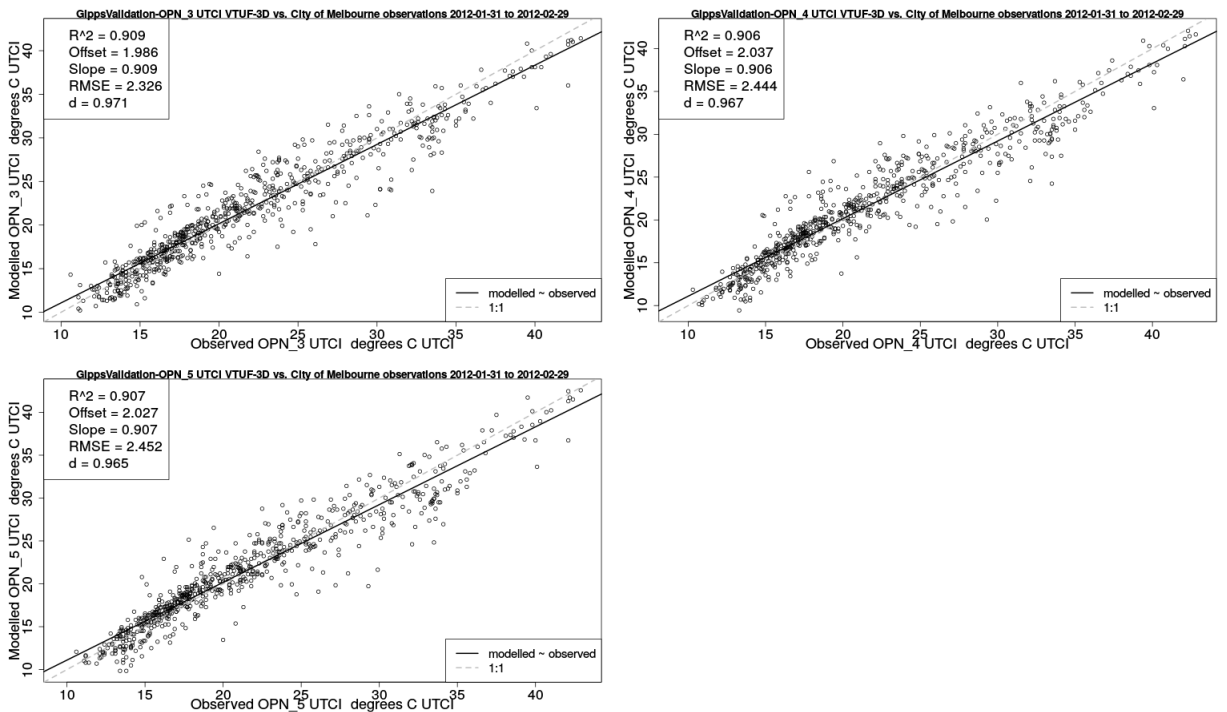


Figure 5.21: Gipps St. GippValidation scenario point comparison of UTCI of 3 observation stations to modelled points.

and OPN_5) in Figure 5.23. For *UTCI*, a similar analysis for the Gipps St. points (OPN_3, OPN_4, and OPN_5) is presented in Figure 5.24.

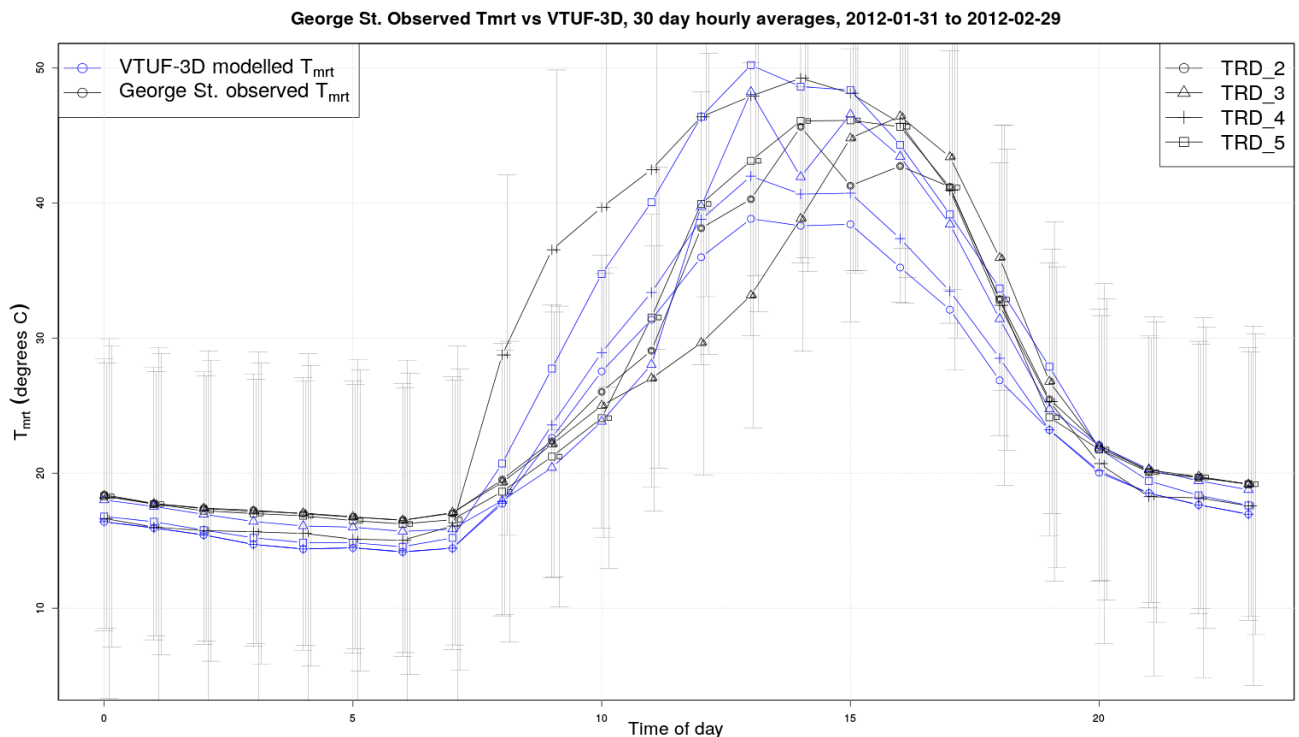


Figure 5.22: George St. GeorgeValidation scenario four observation stations (TRD_2, TRD_3, TRD_4, and TRD_5) values of T_{mrt} aggregated into hourly averages over 30 days compared to modelled points, with error bars at observation standard deviations.

In the observations, the open canyon of Gipps St. shows very little variation in T_{mrt} across the locations while the treed canyon of George St. shows wide variations, especially between stations TRD_2 and TRD_3. TRD_4, a highly exposed location, shows the highest T_{mrt} values in the late mornings, warming quicker than all the other locations, as well as reaching the highest afternoon peak. TRD_3 warms the slowest in the mornings, with early morning building shade with continued early afternoon canopy shading. TRD_2 and TRD_5 also warm slowly in the mornings due to building shading and vegetation shading respectively and both reach a reduced afternoon peak (compared to TRD_4). All observation stations come back into closer agreement in the late afternoons.

The modelled results reproduce the close agreement between the three locations in the open canyon of Gipps St. Variations from the diurnal trends in the observations are seen in slightly slower warming during the mornings but then coming into good agreement at the afternoon peak and throughout the rest of the day and night into the next morning. Very similar patterns are seen in the diurnal trends of *UTCI*, of which T_{mrt} is the main driver, showing slower warming during the mornings. However, lower modelled *UTCI* values during the night-time would suggest there is some room for improvement in modelling wind speed or relative humidity, as modelled values of air temperature and T_{mrt} tend to be slightly high and could not be the source of these lower calculated values.

In the treed canyon, George St., the model shows some of the same variation in T_{mrt} between modelled locations seen in the observations. Modelled values of TRD_4 do reproduce the slower warming trends in the mornings seen in the observations (but diverge in the late mornings).

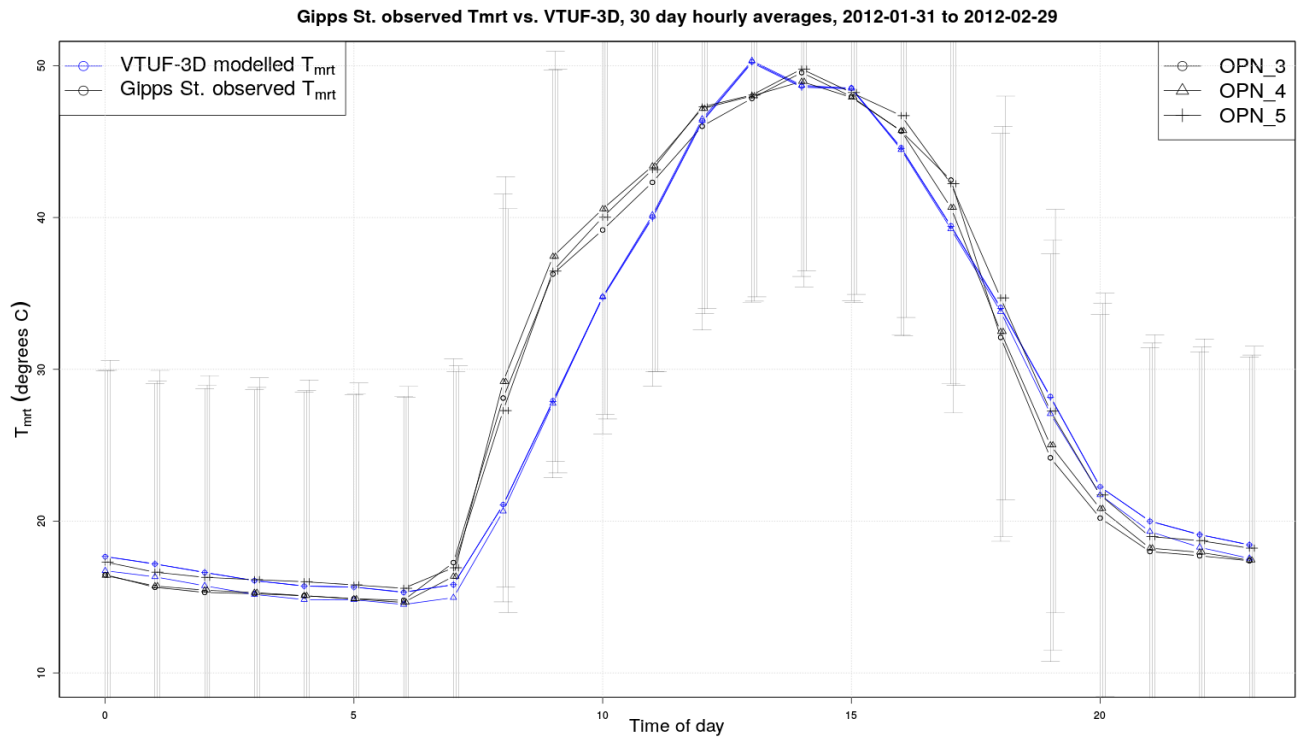


Figure 5.23: Gipps St. GippValidation scenario three observation stations (OPN_3 , OPN_4 , and OPN_5) values of T_{mrt} aggregated into hourly averages over 30 days compared to modelled points, with error bars at observation standard deviations.

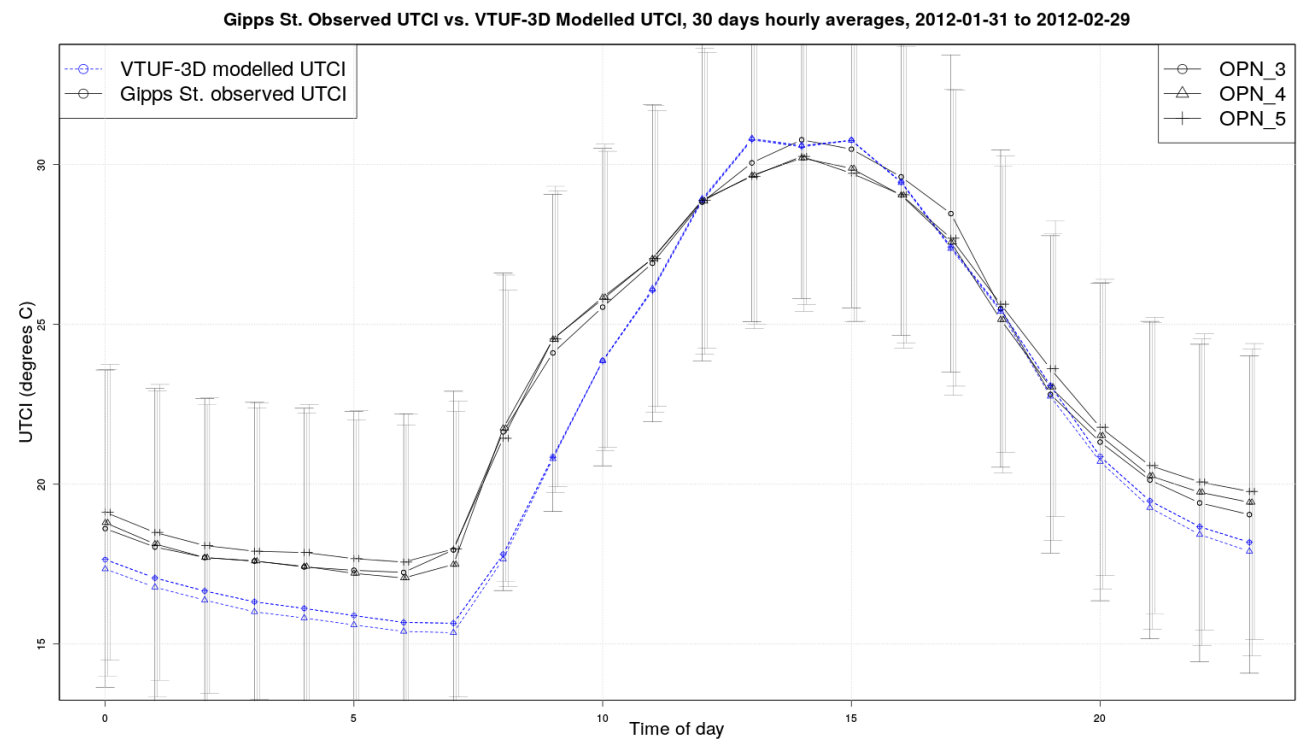


Figure 5.24: Gipps St. GippValidation scenario three observation stations (OPN_3 , OPN_4 , and OPN_5) values of UTCI aggregated into hourly averages over 30 days compared to modelled points, with error bars at observation standard deviations.

However, the stronger warming of TRD_4 seen in the observations is not completely captured by the model. In variations from the observed diurnal trends, the modelling results reproduce well the trends from late afternoon, over night, and into early mornings. The main variability during the warming mornings do not show the wide ranges seen in the observations but follow a more average range between those wider ranges.

There are a number of differences in the way T_g (and its use in calculating T_{mrt}) (see Section 4.2.4) is calculated compared to the observed values, which could explain some of the divergences. First, the modelled results are calculated for each surface in the domain (and only for surfaces in the domain). As there are no surfaces at the locations at which the observations were taken (3.5 to 4m above the ground), the comparisons of T_{mrt} needed to be performed on the modelled results at a 0m height underneath the observation locations. This would lead to lower amounts of $K \downarrow$ (using $K \downarrow_{dir,i}$ from Section 4.2.1.1) reaching the ground due to reduced sky view factors deeper into the urban canyon, especially in the mornings when much of the canyon floor will be in shadow due to lower sun angles.

A second important difference is due to the limitation of domains created using flat cubic surfaces. The globe thermometer in the observation would have been exposed to radiation from all side angles in addition to up and down. As flat surfaces, the modelled points will see a reduction in received shortwave, especially in the mornings. In addition, the lower locations of the points in the canyon will also contribute to lower received shortwave in the same way.

A comparison of modelled T_{can} from scenarios GeorgeValidation and GippValidation to observed T_a of George St. 4 treed canopy stations and Gipps St. 3 open canopy stations is shown in Figure 5.25. Values from both data sets are aggregated into hourly averages over the modelled period.

A direct comparison of these two data sets is difficult as the modelled T_{can} values are averages of the entire canopy air space while the seven observation stations record the air temperatures at 3.5 to 4m height for each specific location. However, the modelled T_{can} of the open canopy street (Gipps St.) shows peak values approximately 1°C warmer (as well as being overall warmer throughout daylight hours) than the treed street (George St.). This result is comparable to the Coutts et al. (2015a) observations and shows the model is able to capture the cooling effects of increased canopy cover in air temperature predictions.

5.3.3 George St. and Gipps St. validation conclusion

This validation was performed in order to complete sub-objective 2, evaluation of model performance for T_{mrt} and $UTCI$. Two contrasting street canyons with varying amounts of canopy cover were used to evaluate the model's performance and test VTUF-3D's ability to predict values of T_{mrt} and $UTCI$, both spatially and temporally.

RMSE and d index of agreement values when comparing the modelled results of both variables to point observations show reasonably good performance of the model. In reproducing diurnal trends of T_{mrt} , VTUF-3D is able to reproduce the overall trends well except is slightly slow to warm during the mornings. In the treed canyon of George St., where wide variations between the observation stations are seen in the observations, VTUF-3D is able to reproduce much of those variations but not the entire range. This indicates that there is still room for improvement in the specific modelling of vegetation in urban canyons and resolving the T_{mrt} values.

The completion of this validation shows that VTUF-3D is able to successfully predict values of T_{mrt} and $UTCI$ across a variety of urban canyons. This validation is an important step in

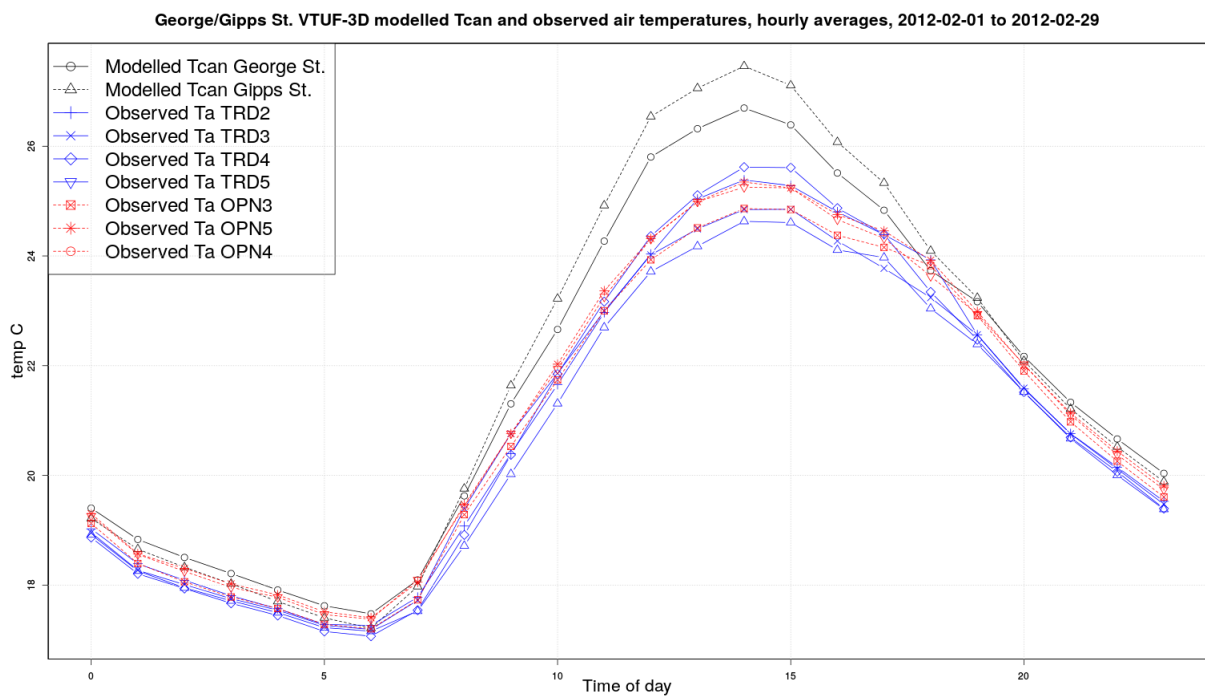


Figure 5.25: George/Gipps St. modelled T_{can} from scenarios *GeorgeValidation* and *GippValidation* compared to observed T_a of George St. 4 treed canopy stations and Gipps St. 3 open canopy stations, aggregated into hourly averages over February 2012 modelled period.

determining the suitability of the model's use in evaluating HTC impacts of WSUD in urban areas.

5.4 Model testing and validation using Smith St dataset

5.4.1 Smith St validation overview

Trees and other vegetation in urban areas face unique challenges. Street trees experience a number of stresses including water shortages, low humidity, high heat, and pollutant loading (Oke 1989). Further, trees are subjected to varied illumination and shading from urban geometry and make up of an urban canyon, however are often isolated, without shading from other nearby trees (Coutts et al. 2016; Coutts & Gebert 2012; Gebert et al. 2012) (Figure 5.26). They are also subjected to heat gain through reflections of shortwave from urban surfaces and increased longwave through warm urban surfaces, as well as reduced night-time cooling due to reduced sky view factors (Oke 1989).

As the VTUF-3D model depends heavily on accurate modelling of effects of vegetation in urban areas and needs to properly account for the urban environment's influence on the vegetation, this aspect of VTUF-3D also needs to be validated. Not all of these aspects can be validated with this data set (i.e. the validation of accurate modelling of vegetation due to high heat loads can be a future validation), but as light availability drives plant water usage (Moriana et al. 2002; Coutts & Gebert 2012), validation of proper modelling of tree transpiration and the physiological response in different positions within the urban canyon can serve to ensure

that VTUF-3D's differential shading functionality (Section 4.3.4) can resolve these effects and provide accurate predictions for different tree locations.

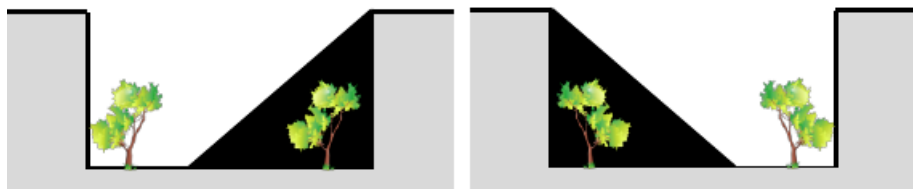


Figure 5.26: Effects of urban canyon shadowing on east and west sides of the street on vegetation physiological response (Gebert et al. 2012).

Smith St. (Figure 5.27) is a north-south street in Melbourne's inner-north, 2 km from the CBD. The urban form of this area, the Local Climate Zone (LCZ) (Stewart & Oke 2012), would be characterised as LCZ 8 (large low-rise). This street is a medium to high density retail area, with a shallow geometry with height to width ratios of 0.5:0.25 and 0.55:0.25 on the east and west sides of the street respectively. The streetscape consists entirely of impervious surfaces (asphalt, concrete, and building materials) with the exception of a very limited number of trees planted in tree pits. Other properties of the observation site are listed in Table 5.10.



Figure 5.27: View of Smith St., Melbourne site and locations on street of observed eucalyptus and olive trees. Red outline showing modelled area. Adapted from Gebert et al. (2012).

The Smith St. study (Gebert et al. 2012) was undertaken to observe tree responses to urban street canyon micro-climates. Eight street trees (planted in tree pits) were the focus of this study. The micro-climate at each tree was monitored. These observations were collected by a number of weather stations over the period 9 February to 13 June 2012, co-located with each street tree (referenced by the blue dots, *Olea europaea*, and green dots, *Eucalyptus olivacea*

Table 5.10: *Smith St. validation site properties (Gebert et al. 2012).*

Property	Value(s)
aspect ratio (east/west side)	0.50-0.25, 0.55-0.25
impervious surfaces (%)	> 85
z_m , instrument height (m)	1

on Figure 5.27). Measurements of air temperature and humidity were taken at a 1m height. Volumetric water content of the soil for the eight trees were also recorded by two 30cm probes for each tree.

In addition to recording weather parameters, readings were taken of each tree's physiological response (transpiration and photosynthesis). These leaf-gas exchange measurements were performed using a Li-6400 (LI-COR 2004) over four cloudless days during the overall observation period.

Model parameters were set to the values given in Table 5.11. Most of these values are TUF-3D default values, from Krayenhoff & Voogt (2007). Vegetation settings for the two tree types (olive and brushbox) as well as grass were set to the values given in the model design vegetation parametrisation section (Section 4.3.6). Olive parametrisations were used for olive trees in the observations while brushbox was used in place of the Eucalyptus species.

Table 5.11: *Smith St. SmithStVal validation scenario model parameters.*

Parameter	Value(s)	Source
Albedo (roof, street, wall)	0.15, 0.10, 0.30	Krayenhoff & Voogt (2007)
Emissivity (roof, street, wall)	0.92, 0.92, 0.88	Krayenhoff & Voogt (2007)
Forcing data height (m)	2	Bureau of Meteorology (2012a)
Mean height of buildings (m)	5.61	Calculated from domain
Mean height of trees (m)	2.5	Calculated from domain
Initial T_{sfc} (roof, street, wall) ($^{\circ}\text{C}$)	18.0, 23.0, 22.0	Krayenhoff & Voogt (2007)
Constant building internal air temperature (base of roofs and walls) ($^{\circ}\text{C}$)	22.0, 20.0	Krayenhoff & Voogt (2007)
Constant deep-ground temperature ($^{\circ}\text{C}$)	19.0	Krayenhoff & Voogt (2007)
Constant building internal floor temperature ($^{\circ}\text{C}$)	15.0	Krayenhoff & Voogt (2007)
Domain composition (Trees/Buildings/Streets) (%)	0.8, 68.0, 31.1	Calculated from domain
Modelled grid size (m)	2.5	Calculated from domain

The validation simulation (which is named SmithStVal) was run for 18 days between February 11, 2012 and February 28, 2012, forced by the observations from Bureau of Meteorology (2012a) (station 086338, Melbourne Olympic Park) for those days. Values used from the observations include $K \downarrow$, $L \downarrow$, air temperature, wind speed, wind direction, and air pressure. Forcing data for the vegetation components use shortwave values of mean global and mean diffuse observations taken from one minute solar observations (station 086282, Melbourne Airport) (Bureau of Meteorology 2016b) (as described in Section 4.3.4). Values of CO_2 for vegetation forcing files were set to a constant of 450 ppm throughout the modelling period.

5.4.2 Smith St validation results

Modelled flux output is extracted from a tree grid square (each containing an olive tree) on both the east and west sides of the street (highlighted with yellow boxes on Figure 5.28). It is not possible to only extract transpiration values from modelled results, so these results will also contain soil evaporation in these grid squares. The Q_E flux values are converted to amounts of tr , transpiration ($\text{mmol H}_2\text{O m}^{-2}\text{s}^{-1}$), using Equation (5.4.1)

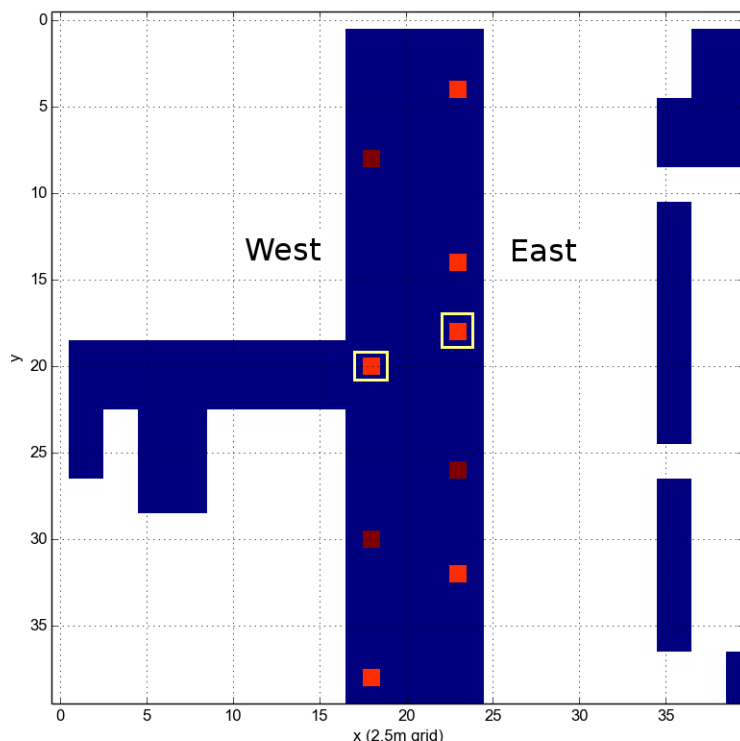


Figure 5.28: Extraction of modelled Q_E values for olive trees (highlighted with yellow boxes) on the east and west sides of Smith St. from validation simulation SmithStVal.

$$tr = \frac{Q_E}{m_{mol,w} * A * E_E * Time} \quad (5.4.1)$$

where Q_E is the latent heat flux (W m^{-2}), $m_{mol,w}$ is the molar mass of water ($=18.0152\text{g mol}^{-1}$), E_E is equivalent evaporation ($=2.45 \times 10^6 \text{ J m}^{-2}\text{h}^{-1}$), A is the leaf area of the tree ($=12.17\text{m}^2$, calculated from leaf area index (LAI) \times tree area, or $2.48\text{m}^2\text{m}^{-2} \times \pi \times 1.25\text{m} \times 1.25\text{m}$), and $Time$ is the time (hours).

The observed transpiration rates (one each for east and west sides of Smith St.) from the VTUF-3D validation scenario SmithStVal were compared to the observed transpiration values from Gebert et al. (2012) and Coutts (2014). The results for 23 February 2012 are shown in Figure 5.29. Also, all fluxes were extracted from the tree locations of both sides of the street and their hourly averages over the 18 day modelling period are presented in Figure 5.30.

Direct comparisons are difficult as the observation data set only consists of 6 data points compared to 24 hourly values for the modelled results. As seen in the levels of incoming shortwave radiation used to force the scenario (Figure 5.29), two dips in radiation levels at 1pm and 4pm can also be seen reflected in modelled transpiration levels. It is uncertain if these would also be reflected in the observations as data points do not exist for these times.

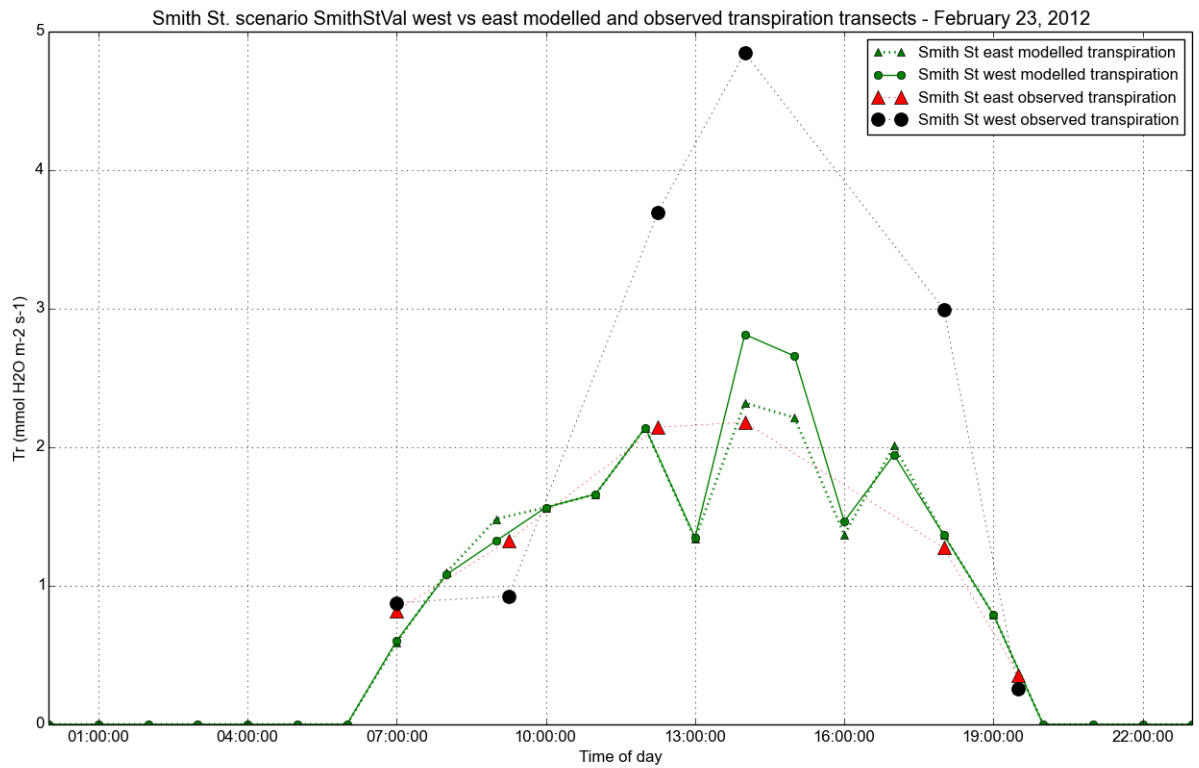


Figure 5.29: VTUF-3D SmithStVal validation showing modelled transpiration along each west and east tree location (of Figure 5.28) for 23 February 2012. Also shown, observed transpiration values for the same tree location.

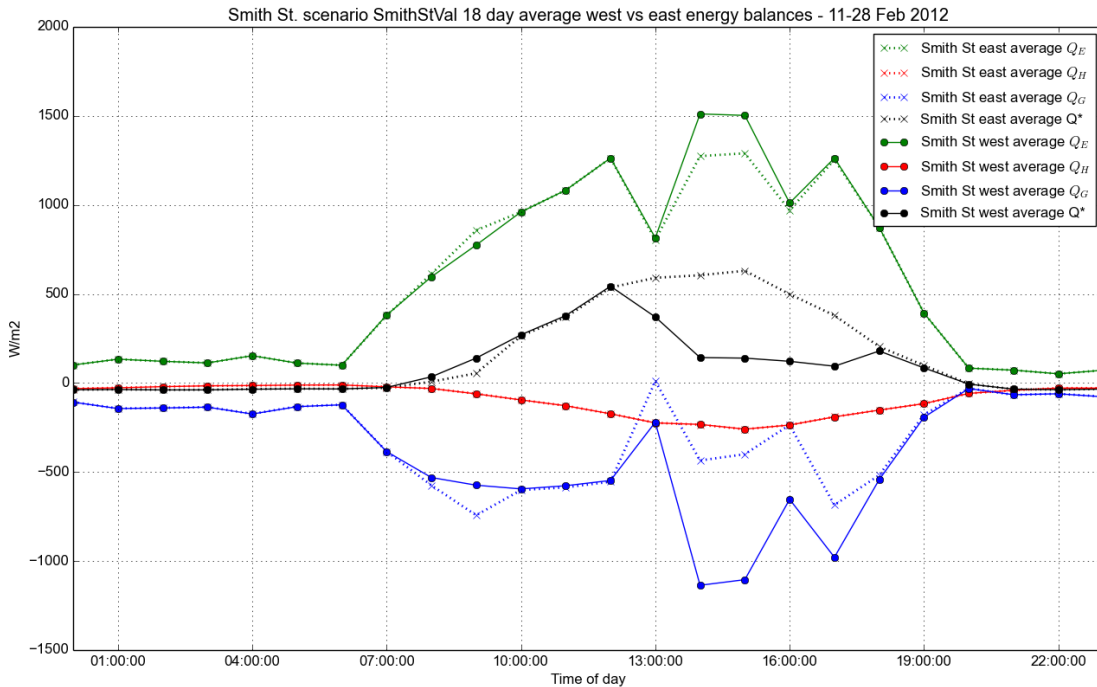


Figure 5.30: VTUF-3D SmithStVal validation showing 18 day hourly average of fluxes along each east and west tree location.

In addition, there is some uncertainty to the magnitude of uncertainties of the leaf scale observations, especially given the relatively small number of data points available. Finally, some differences might exist between the incoming solar radiation used for the forcing (taken from the Melbourne Airport observations) compared to the on-site observations.

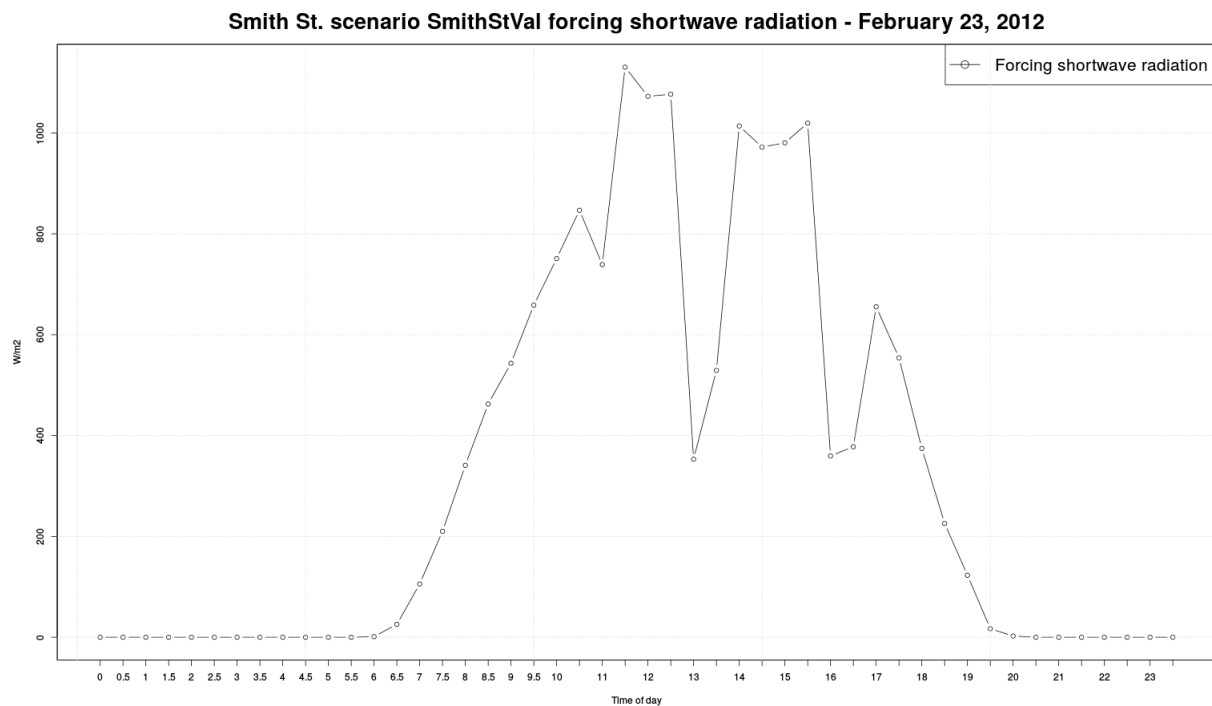


Figure 5.31: Smith St. scenario SmithStVal forcing shortwave radiation for February 23, 2012.

However, the modelled results do broadly reproduce the variations seen in the observations. Overall, higher transpiration rates are seen on the east side of the street in both the modelled results and in the observations. Also, a short reduction in transpiration rates is reproduced by the model on the east side of the street during the morning shading period (8-10am).

On the west side of the street, modelled transpiration closely matches the observations with peaks of $2.3 \text{ mmol H}^2\text{O m}^{-2}\text{s}^{-1}$ compared to observed peaks of $2.2 \text{ mmol H}^2\text{O m}^{-2}\text{s}^{-1}$. For the observed data points which are available, the modelled results also closely match the observed diurnal trends of transpiration.

Modelled peaks of east side transpiration of $2.8 \text{ mmol H}^2\text{O m}^{-2}\text{s}^{-1}$ are seen compared to $4.8 \text{ mmol H}^2\text{O m}^{-2}\text{s}^{-1}$ in the observations, a significant understatement compared to the observed values. As previous validations have shown, VTUF-3D tends to under-estimate values of Q_E , which are derived from predicted transpiration values.

Lower modelled transpiration rates on the east side could have a number of other causes. The model only produces a single canyon averaged air temperature for the modelled domain, and can not account for air temperature variations (and resulting changes to vapour pressure deficits) on the east side during the afternoons. However, with such a small comparison dataset, it is difficult to confirm this conclusion. This highlights a need for additional validations using sap flow data and enhancements to the model to allow better generation of canyon level forcing values to individual vegetation elements. Also, the soil composition of the eastern tree pits varied from standard olive parametrisation which was based on the soil composition of the western tree pits (in terms of soil/sand mixture and moisture content). This points to the

need for a wider range of available vegetation parametrisations to more precisely match each modelling question.

Gebert et al. (2012) also speculated that the eastern trees in the canyon might compensate for missing the morning photosynthesis opportunity with higher rates of photosynthesis during the afternoon, leading to the higher rates of transpiration in the observations. This points out the difficulties of modelling trees, in the highly individualised responses trees can have to varying conditions. There is a need for much more research in this area, observations of urban vegetation, with a better understanding allowing vegetation models to be improved accordingly.

Other modelled fluxes show variations for the tree locations on the east and west sides of the street (Figure 5.30, showing hourly averages of each flux during the modelling period). These values are extracted only from the 2.5x2.5m grid square containing the tree, so high values for Q_E and Q_G and low values for Q_H and Q_G will reflect this. Diurnal patterns for Q^* show varying rates on each side of the street depending on the rates of illumination and shading at those locations. These diurnal patterns follow similar patterns to those seen in observations of east/west street canyons (Nunez & Oke 1977; Mayer et al. 2008).

5.4.3 Smith St validation conclusion

The Smith St. validation was performed to complete sub-objective 3, to evaluate the capacity of the model to capture tree transpiration and varying urban influences on vegetation. This validation has demonstrated that VTUF-3D is able to reproduce the variations in vegetation physiological responses (as well as other variations) due to the influences of the geometry of an urban canyon and shading effects. The model can broadly reproduce the temporal patterns of transpiration as indicated by an extraction of modelled transpiration rates from a single tree from each side of an east/west urban canyon. Also, expected responses of other fluxes are also shown to be influenced by the urban geometry and follow expected patterns of heating and cooling based on changing shading effects during the progress of a day.

This validation highlights that there is scope for more research and comparisons with a variety of observational datasets of urban tree water use. Future validations should be conducted using sap flow measurements, which will provide a richer set of data, as well as more completely cover longer periods of time compared to the fewer number of data points provided by the time consuming and labour intensive methods used in this Smith St. dataset. These validations could add another layer of certainty to the proper functioning of VTUF-3D in regards to urban vegetation.

Nevertheless, the results of this validation are highly encouraging. This validation of the proper modelling of two single trees within a modelled domain goes well beyond the typical validation process for a surface energy balance model. This validation, along with the previous two validation components, provide for good confidence in the model's performance and the level of accuracy the model can already produce.

5.5 VTUF-3D validation conclusion

The second objective of this project is completed by the validation process detailed in this chapter. Three sub-objectives were completed using three different observational data sets to test VTUF-3D's ability to model vegetation in urban areas. These sub-objectives ensured that a

number of different aspects of the model are functioning properly and is suitable for the task of assessing WSUD impacts on HTC.

In the first validation, flux tower observations from Preston allowed validation of the fundamental drivers of urban climates, energy fluxes and surface energy balances. Comparisons to 30 day hourly averages showed a good fit for all of the fluxes. Error analysis comparing the flux predictions to the observed values showed good performance for most of the fluxes, with Q_E showing slightly higher error rates and low predictions of this flux. Future model development will add the ability to account for precipitation on impervious surfaces, add irrigation scenarios, and increase the range of vegetation types available to model. These developments are anticipated to add significantly to the accuracy of Q_E predictions.

Next, in a comparison to the baseline unimproved TUF-3D model, VTUF-3D shows an large improvement in performance. Finally, comparing VTUF-3D to other urban models, shows performance above the mean and close to maximum performance of those other models.

The second validation, using observations from a number of different points in two streetscapes (George and Gipps St.), allowed validation of VTUF-3D's ability to accurately model spatial patterns of T_{mrt} and $UTCI$. The model shows good performance in an error analysis of spatial predictions of T_{mrt} and $UTCI$. In temporal performance, predictions show a good fit with the observations but with some under-prediction during the morning warming period. Future model improvements, especially those highlighted by the Smith St. validation process in the lower transpiration rates of sunlit trees, as well as the future validations using sap flow data, are expected to improve the accuracy of the temporal variations in heavily treed canyons.

Finally, in the third validation using Smith St. data, VTUF-3D's ability to model the effects of the urban environment on vegetation is tested. Using a comparison of east and west sides of the street, comparing observed transpiration to modelled values, VTUF-3D is able to broadly reproduce the temporal patterns of vegetation physiological responses seen in the observations due to urban canyon geometry effects.

With the completion of this validation process and of the second project objective (and its three sub-objectives), VTUF-3D is now considered suitable to model all aspects of WSUD and its impact on human thermal comfort. A demonstration of this will follow in the next chapter and examine the role canopy cover has in moderating temperatures and maintaining human thermal comfort in these streetscapes.

Chapter 6

A demonstration of the VTUF-3D model: an assessment of the impact of urban canopy cover on HTC using canopy cover scenarios

6.1 VTUF-3D canopy cover scenarios

The third and final objective is to demonstrate that the aim of this project has been fulfilled. This demonstration will show that a suitable model has been developed to support the implementation of urban greening and development of thermally comfortable urban environments. It will also show that this model is suitable for assessing human thermal comfort (HTC) impacts of modifying the amounts of vegetation and water in urban areas. This follows from the previous objective, the validation of VTUF-3D (Vegetated Temperatures Of Urban Facets) in Chapter 5. In this, VTUF-3D modelled a variety of scenarios and was able to reproduce the temporal and spatial variations observed in these streetscapes.

This demonstration will use this new model to examine some of the impacts of WSUD on HTC in urban areas at a micro-scale. The introduction of WSUD infrastructure into urban areas raises the question of how to quantify the impacts of these and how this infrastructure can be used most effectively to maximise positive impacts to HTC. Studies indicate that canopy cover (the shading effect) can have the greatest impact on HTC (Ali-Toudert & Mayer 2006a; Shashua-Bar et al. 2010; Sanusi & Adibah 2015), making this the best starting point in this analysis of WSUD impacts. A set of scenarios will concentrate on varying levels of canopy cover and this canopy cover's impact on HTC in the streetscape. These demonstrations will set the stage for the use of VTUF-3D to conduct future detailed studies of a wide variety of factors to maximise the benefits of WSUD infrastructure and urban greening on HTC in urban areas.

This demonstration will use a number of scenarios (each built on the base domains from the validations in Chapter 5), using varying amounts of canopy cover to determine the extent of the cooling effect that can be expected from increasing the canopy cover in urban streetscapes. For each domain, the baseline scenario uses the existing tree cover. Then, additional domains are set up, modifying the tree cover to zero trees, half the number of trees, and double the number of trees (as well as quadrupled for some scenarios). VTUF-3D is run for each variation, generating two days of simulation data.

The analysis process compares predicted differences in $UTCI$ and canyon temperature values between the scenarios. $UTCI$ is used as an overall indicator of HTC, in that it has been shown to represent very well the variability at micro-climate scales and the impacts on human bodies of meteorological conditions, especially that of radiation loading and shading effects (Blazejczyk et al. 2012). This will be ideal to quantify the impacts of vegetation at this scale.

6.2 VTUF-3D Preston canopy cover scenarios

6.2.1 Preston scenarios methods

The Preston scenarios are built on the Preston validation (scenario Pr04Val) domain (Section 5.2 and Figure 5.1). Model parameters are set to the values in Table 5.4. All scenarios contain 45.7% building and 19.5% grass land cover.

The baseline scenario (referred to as PrestonScenarios3-Trees) is identical to the Pr04Val validation scenario in building, street, and vegetation amounts and placement. Three variations were prepared from this baseline. They vary from the baseline only in the amounts of tree cover, and a conversion of streets (asphalt) to trees in some scenarios. These scenarios were designed of zero (PrestonScenarios1-NoTree), halved (PrestonScenarios2-HalfTree), and doubled tree cover (PrestonScenarios4-DoubleTrees) (configurations of tree cover shown in Figure 6.1). These scenarios and other land cover variations are detailed in Table 6.1.

Table 6.1: Preston canopy cover scenarios.

Scenario name	Description	Trees (%)	Streets (asphalt) (%)
PrestonScenarios1-NoTree	Preston with 0 trees	0	34.5
PrestonScenarios2-HalfTree	Preston with 50% less trees	4.0	30.7
PrestonScenarios3-Trees	Current Preston tree cover	7.2	30.7
PrestonScenarios4-DoubleTrees	Preston doubled tree cover	11.0	23.8

The model was run for each scenario for 13-14 February 2004 using a February 13th and 14th subset of the forcing data used in the validation. This corresponds to days 44 and 45 of Figure 5.5. The first day is mild, with a daytime high of 21°C , while the second day is extremely hot, with a high of 38°C .

6.2.2 Preston scenario results

Values of T_{mrt} and $UTCI$ for each surface were used to generate z-slice figures of surfaces at 0m height (Figure 6.2, showing 14 February 2004 at 2pm for each scenario). Next, all surfaces at 0m height for 13-14 February 2004 were averaged for each timestep and this time series charted for that period, as well as the differences between the baseline scenario PrestonScenarios3-Trees and the other three scenarios (Figure 6.3).

Finally, a time series of canyon temperatures (the average air temperature of the entire canyon) over the modelling period is shown (Figure 6.4). This also includes the differences between the baseline PrestonScenarios3-Trees scenario and the other three scenarios. Note, the canyon temperatures of Figure 6.4 are averaged across the air volume of the entire domain, while the $UTCI$ temperatures of Figure 6.3 are only averaged across the surfaces at 0m height (which excludes grid squares which do not have a surface at 0m, i.e. those with buildings).

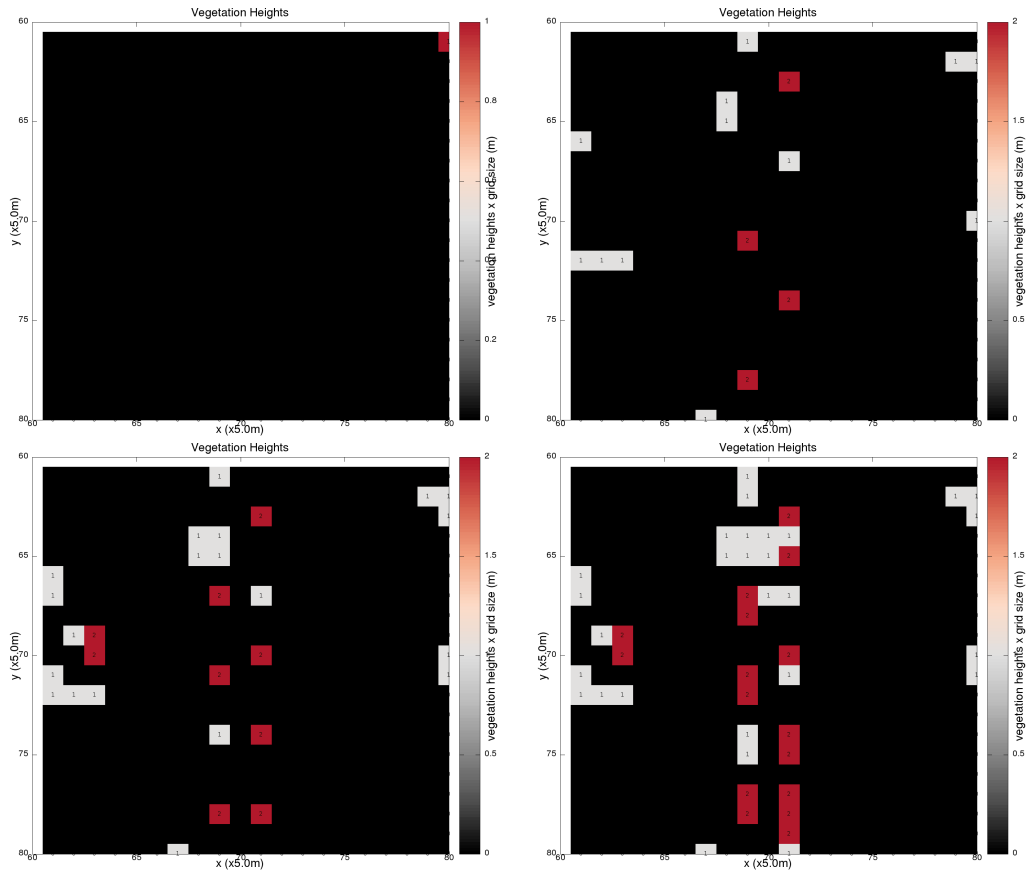


Figure 6.1: Preston tree canopy configuration for four scenarios, PrestonScenarios1- NoTree, PrestonScenarios2-HalfTree, PrestonScenarios3-Trees, and PrestonScenarios4- DoubleTrees, representing zero trees, 50% reduction of trees, existing Preston canopy cover, and doubled canopy cover.

At the hottest point of the day (2pm for 14 February 2004), differences can be seen between the scenarios. Eliminating tree cover, the PrestonScenarios1-NoTree scenario, on Oakhill Ave in Preston will increase the UTCI ($^{\circ}\text{C}$), averaged at 0m height, by over 2.1°C . A reduction of 50% canopy cover, scenario PrestonScenarios2-HalfTree, shows an increase of nearly 1.0°C UTCI. By contrast, doubling the canopy cover, scenario PrestonScenarios4-DoubleTrees, decreases the UTCI by 1.1°C . Overall, the differences between the scenarios with no tree cover and doubling the canopy are 3.2°C .

Localised cooling effects can be even greater. Figure 6.5 shows differences in UTCI between the baseline Tree scenario and the DoubleTree scenario. Cooling directly under trees compared to areas just a few metres away can see differences in selected values of UTCI of approximately -2, -16, and -17°C .

With air temperature, T_{can} , the differences are more modest. The doubled canopy shows a cooling of 0.35 to 0.4°C over the no canopy scenario. Note, these temperatures are the average of the entire urban canyon space while the UTCI temperatures are an average of the surfaces at 0m height.

At night-time, UTCI temperatures also tend to the same patterns, only highly reduced. Overnight differences are seen between no canopy cover and doubled canopy cover of approximately 0.5°C . By contrast, at night time during these hot days, there can be seen some reversals in T_{can} differences. Longwave radiative trapping by vegetation can slow night time cooling

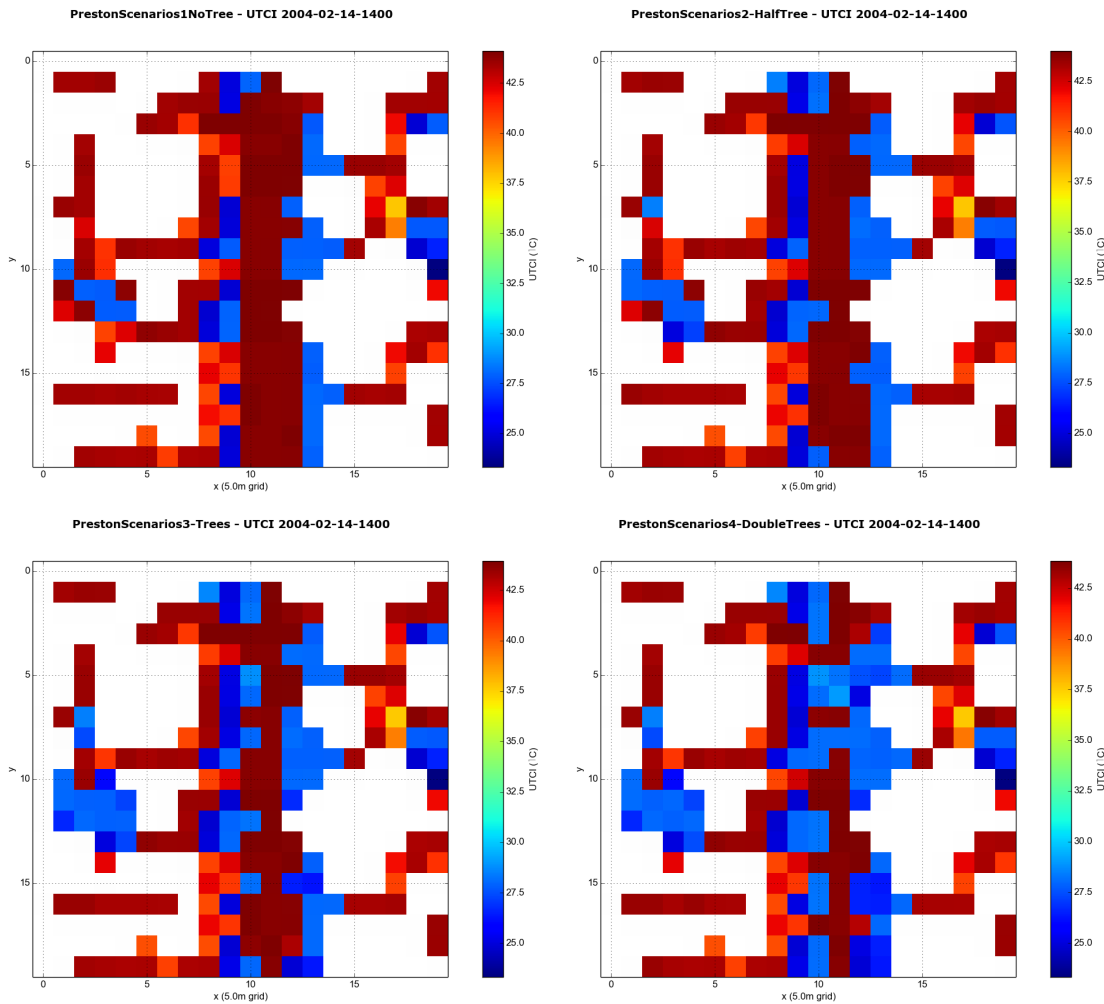


Figure 6.2: $UTCI\ (^{\circ}C)$ of surfaces at 0m height for four scenarios, *PrestonScenarios1-NoTree*, *PrestonScenarios2-HalfTree*, *PrestonScenarios3-Trees*, and *PrestonScenarios4-DoubleTrees*, for modelled timestep 14 February 2004 at 2pm.

(Oke 1987; Arnfield 2003). The doubled canopy scenario cools less quickly than the baseline, showing a positive T_{can} difference of up to $0.1^{\circ}C$. The reduced canopy cover scenarios (0% trees) cool more quickly, showing a negative difference between the baseline of a little over $0.1^{\circ}C$.

6.3 City of Melbourne, Gipps St. scenarios

6.3.1 Gipps St. scenarios methods

A second set of scenarios will look at the impacts of larger increases of the canopy cover in a streetscape. The City of Melbourne, Gipps St. scenarios are built on the Gipps St. validation domain (GippValidation) (Section 5.3 and Figure 5.15). Model parameters are set to the values in Table 5.8. All scenarios contain 49.5% building and 2.2% grass land cover.

The baseline scenario (referred to as CoMGippScenarios3-Trees) is identical to the GippValidation validation scenario in building, street (asphalt), and vegetation amounts and placement. Four variations were prepared from this baseline. They vary from the baseline only in the

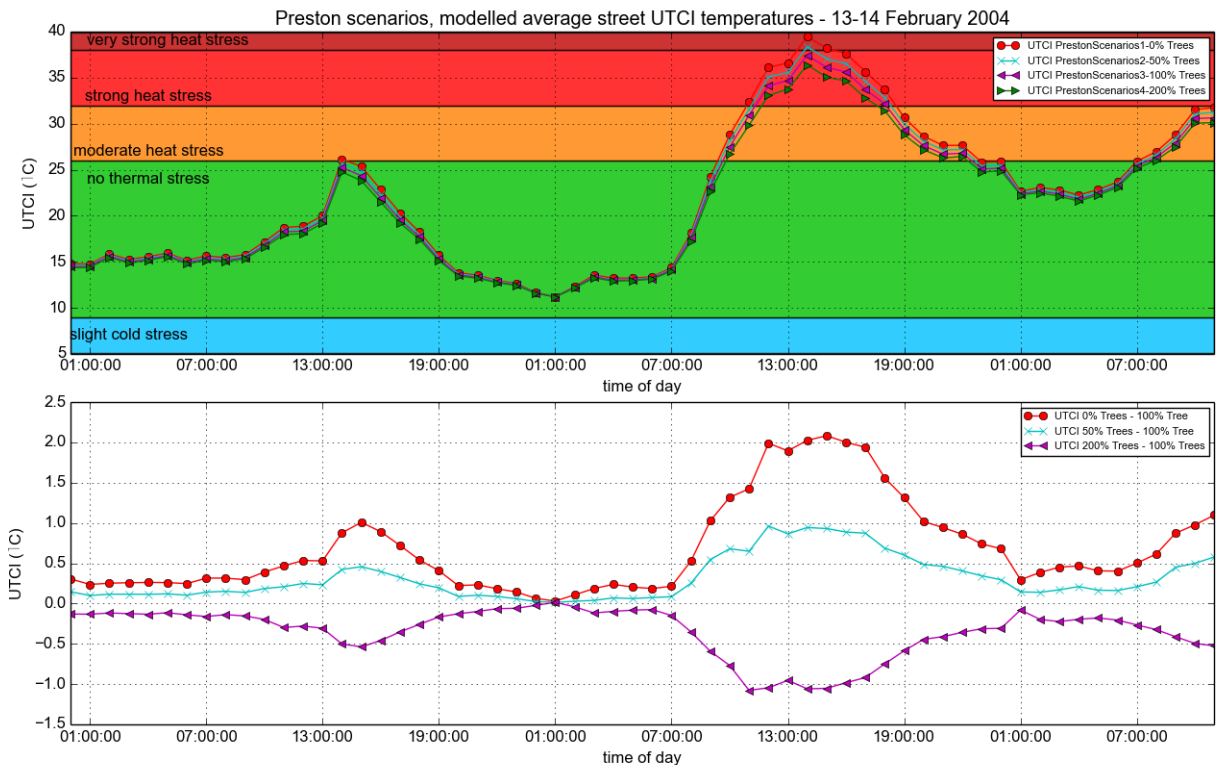


Figure 6.3: Modelled UTCI ($^{\circ}\text{C}$) average of all surfaces at 0m height for four scenarios, PrestonScenarios1- NoTree, PrestonScenarios2-HalfTree, PrestonScenarios3-Trees, and PrestonScenarios4-DoubleTrees over 13-14 February 2004 / Differences in UTCI ($^{\circ}\text{C}$) average of all surfaces at 0m height between baseline PrestonScenarios3-Trees scenario and other three scenarios over 13-14 February 2004.

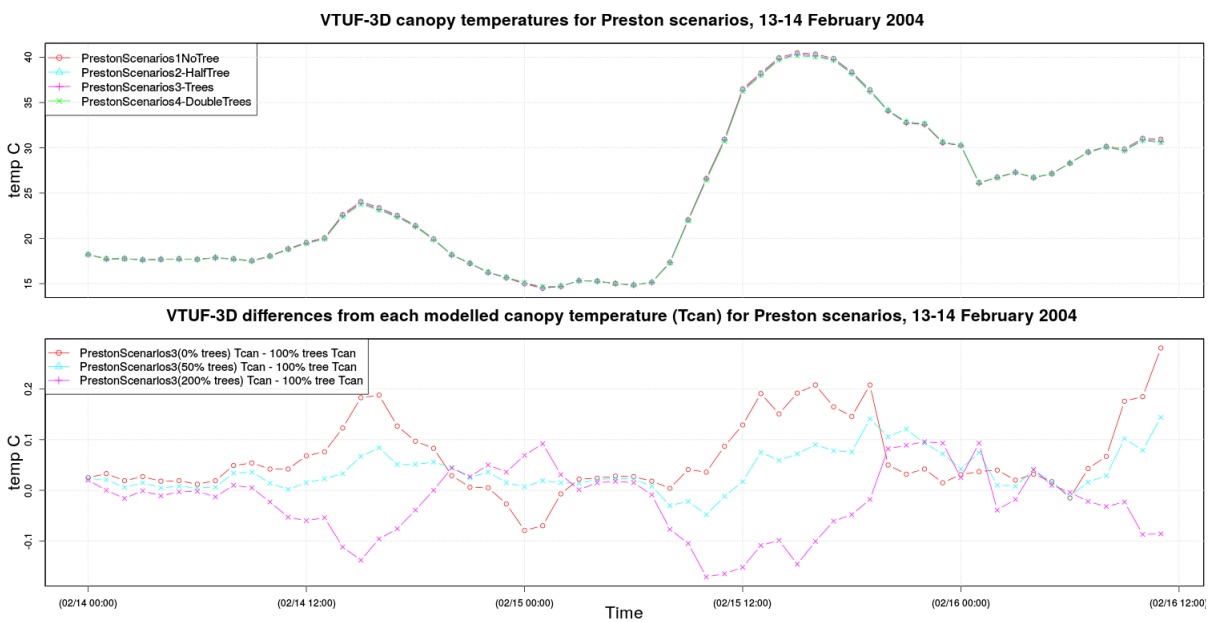


Figure 6.4: Modelled canyon air temperature (T_{can}) of four scenarios, PrestonScenarios1- NoTree, PrestonScenarios2-HalfTree, PrestonScenarios3-Trees, and PrestonScenarios4-DoubleTrees over 13-14 February 2004 / Differences of T_{can} between baseline PrestonScenarios3-Trees scenario and other three scenarios over 13-14 February 2004.

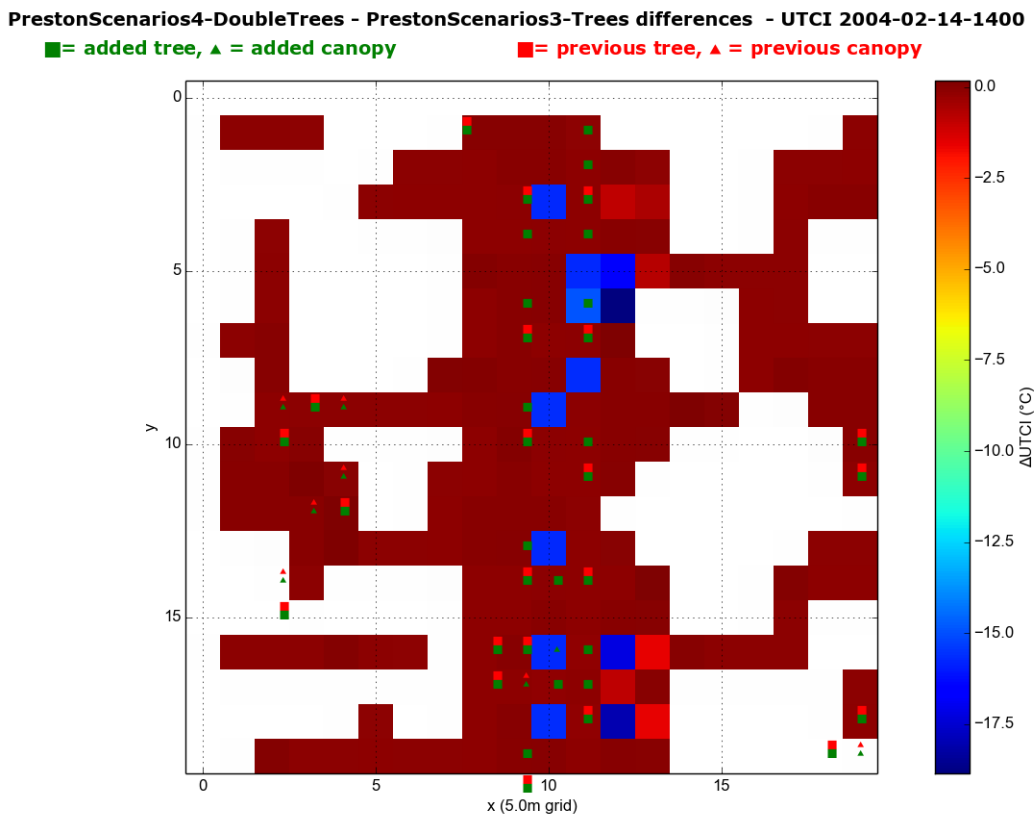


Figure 6.5: Differences in UTCI ($^{\circ}\text{C}$) of all surfaces at 0m height between baseline PrestonScenarios4-DoubleTrees scenario and PrestonScenarios3-Trees at modelled timestep 14 February 2004 2pm. Locations of trees (and extending canopy) shown of baseline PrestonScenarios3-Trees scenario (in red) and added trees (and canopy) in PrestonScenarios4-DoubleTrees scenario (in green).

amounts of tree cover and a reduction of streets (asphalt) cover. These scenarios were designed of zero (CoMGippScenarios1-NoTree), halved (CoMGippScenarios2-HalfTree), doubled tree cover (CoMGippScenarios4-DoubleTrees), and quadrupled tree cover (CoMGippScenarios5-4xTrees) (configurations of tree cover shown in Figure 6.6). These scenarios and other land cover variations are detailed in Table 6.2.

Table 6.2: Gipps St. canopy cover scenarios.

Scenario name	Description	Tree (%)	Streets (asphalt) (%)
CoMGippScenarios1-NoTree	Gipps St. with 0 trees	0	48.1
CoMGippScenarios2-HalfTree	Gipps St. 50% less trees	3.2	45.0
CoMGippScenarios3-Trees	Current Gipps St. canopy	6.7	41.6
CoMGippScenarios4-DoubleTrees	Gipps St. doubled trees	13.0	35.3
CoMGippScenarios5-4xTrees	Gipps St. quadruple trees	21.7	26.6

The model was run for each scenario for 23-24 February 2014 using a February 23rd and 24th subset of the forcing data used in the validation. This corresponds to days 54 and 55 of Figure 5.17. The first day is warm, with a daytime high of 25°C , while the second day is extremely hot, with a high of 37°C .

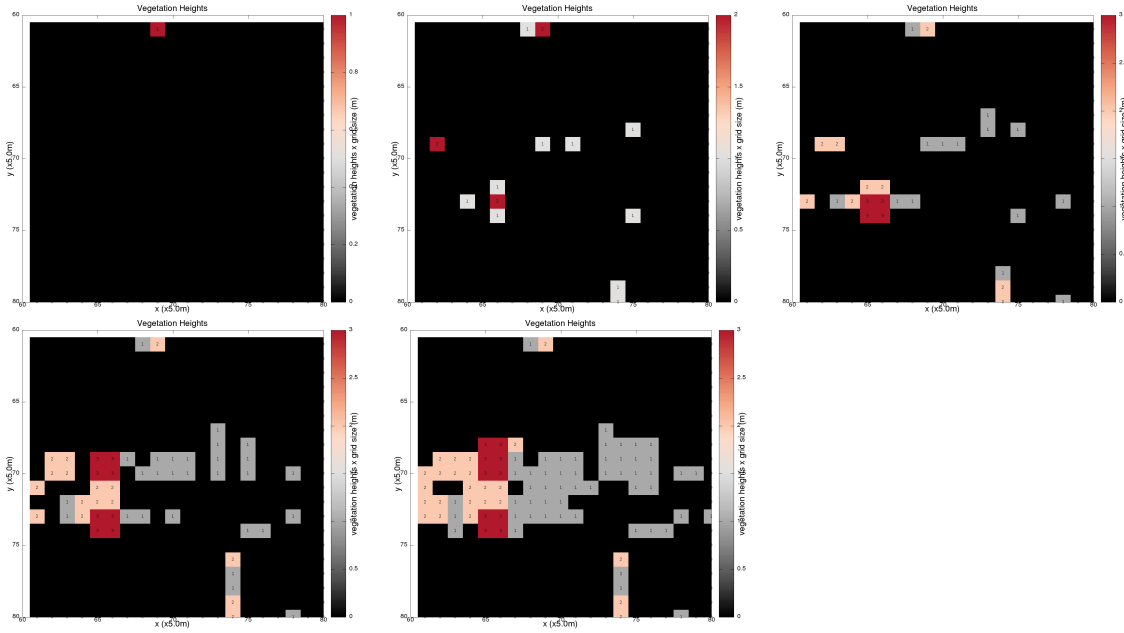


Figure 6.6: Gipps St. tree canopy configuration for five scenarios, CoMGippScenarios1-NoTree, CoMGippScenarios2-HalfTree, CoMGippScenarios3-Trees, CoMGippScenarios4- DoubleTrees, CoMGippScenarios5-4xTrees, representing 0 trees, 50% reduction in trees, existing canopy cover, doubled canopy cover, and quadruple canopy cover.

6.3.2 Gipps St. scenarios results

Values of T_{mrt} and $UTCI$ for each surface were used to generate z-slice figures of surfaces at 0m height (Figure 6.7, showing 24 February 2014 at 3pm for each scenario). Next, all surfaces at 0m height for 23-24 February 2014 were averaged for each timestep and this time series charted for that period, as well as the differences between the baseline scenario CoMGippScenarios3-Trees and the other three scenarios (Figure 6.9). A snapshot difference of $UTCI$ of each surface at 0m in the urban canyon between the baseline CoMGippScenarios3-Trees scenario and the CoMGippScenarios5-4xTrees scenario is presented in Figure 6.8. The location of trees (and extending canopy from those trees) of each scenario are indicated by green and red markers in this figure.

Finally, a time series of canyon temperatures (the average air temperature of the entire canyon) over the modelling period are shown (Figure 6.10). This also includes the differences between the baseline CoMGippScenarios3-Trees scenario and the other four scenarios. Note, the canyon temperatures of Figure 6.10 are averaged across the air volume of the entire domain, while the $UTCI$ temperatures of Figure 6.9 are only averaged across the surfaces at 0m height.

At the hottest point of the day (1pm for 24 February 2012), differences can be seen between the scenarios. Eliminating tree cover, the CoMGippScenarios1-NoTree scenario, on Gipps St. in the City of Melbourne will increase the $UTCI$ ($^{\circ}\text{C}$), averaged at 0m height, by 0.4°C . A reduction of canopy cover by 50%, scenario CoMGippScenarios2-HalfTree, shows an extremely small increased $UTCI$. By contrast, doubling the canopy cover, scenario CoMGippScenarios4-DoubleTrees, decreases the $UTCI$ by nearly 0.9°C , while quadrupling the canopy in CoMGippScenarios5-4xTrees shows a decrease of $UTCI$ of over 2.0°C . Overall, the difference between the street scenario with no tree cover and quadrupling the canopy is nearly 2.5°C $UTCI$.

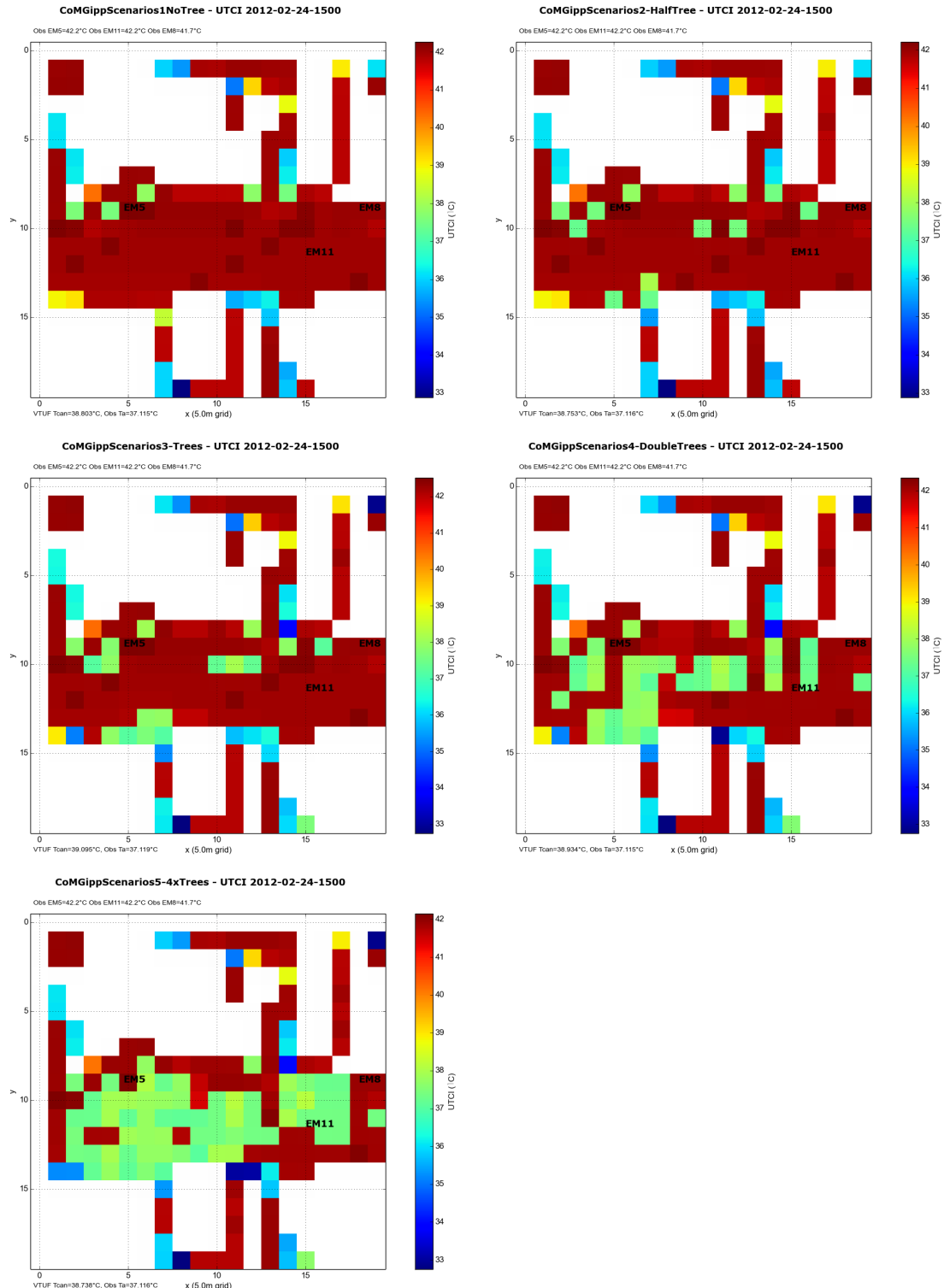


Figure 6.7: UTCI ($^{\circ}\text{C}$) of surfaces at 0m height for five scenarios, CoMGippScenarios1-NoTree, CoMGippScenarios2-HalfTree, CoMGippScenarios3-Trees, CoMGippScenarios4-DoubleTrees, CoMGippScenarios5-4xTrees, for modelled timestep 24 February 2012 3pm.

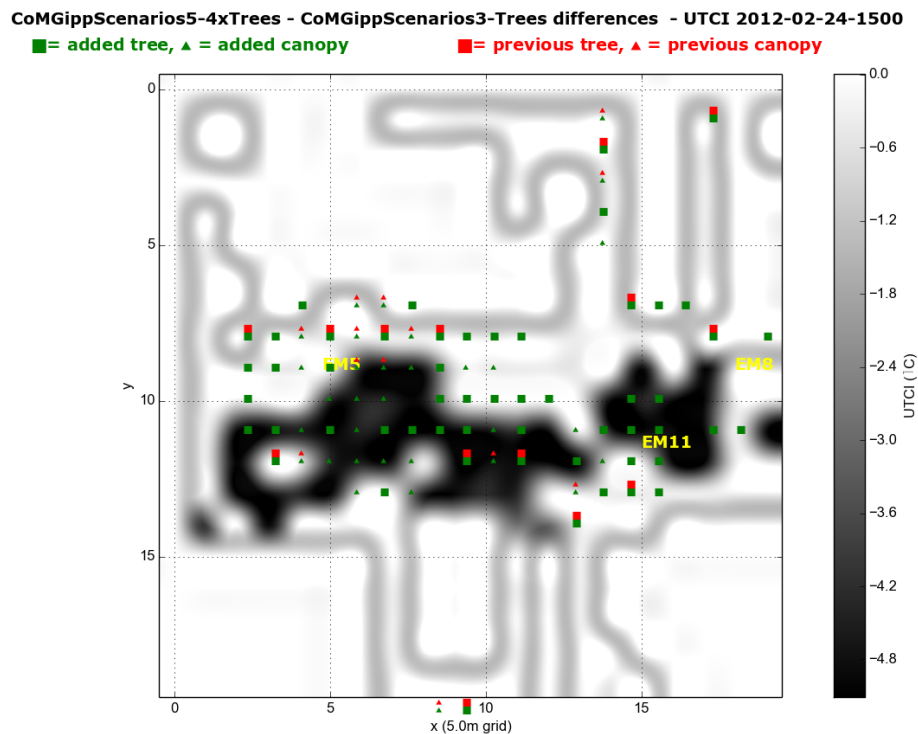


Figure 6.8: Differences in $UTCI$ ($^{\circ}C$) of all surfaces at 0m height between baseline *CoMGippScenarios3-Trees* scenario and *CoMGippScenarios5-4xTrees* at modelled timestep 24 February 2012 3pm. Locations of trees (and extending canopy) shown of baseline *CoMGippScenarios3-Trees* scenario (in red) and added trees (and canopy) in *CoMGippScenarios5-4xTrees* scenario (in green).

The values in the previous analysis are values of $UTCI$ averaged across all the 0m surfaces in the canyon. Localised differences in $UTCI$ are much more substantial. The areas under canopy cover in Figure 6.8 (a snapshot at 24 February 2012 3pm) can see a cooling effect of over 4 to nearly $5^{\circ}C$ compared to areas a few metres away between the existing canopy cover scenario, *CoMGippScenarios3-Trees*, and four times the canopy cover in *CoMGippScenarios5-4xTrees*. At night time during these hot days, these differences narrow rapidly and in some cases reverse. The quadrupled canopy scenario can show differences in $UTCI$ ranging from 0.2 and $-0.2^{\circ}C$.

These same daytime/night time patterns are also seen in the canopy air temperature differences between the scenarios, however the values are more modest. During the hottest point of the day, air temperature differences between scenarios with the baseline scenario and quadrupling the canopy range from 0.4 to nearly $0.6^{\circ}C$. During the night time, the differences are seen of approximately $0.1^{\circ}C$.

6.4 VTUF-3D urban canopy cover scenarios conclusions

One of the important points gleaned from the Preston scenarios is the importance of having some amount of canopy cover in urban streetscapes. While improvements in HTC (as indicated by $UTCI$ temperature reductions) can be gained in doubling the canopy, quite substantial decreases in HTC are seen if the canopy is eliminated from the streetscapes.

The results of the Preston scenarios also point to the shading effect having a large impact on HTC, given the more modest reductions in air temperature compared to the reductions

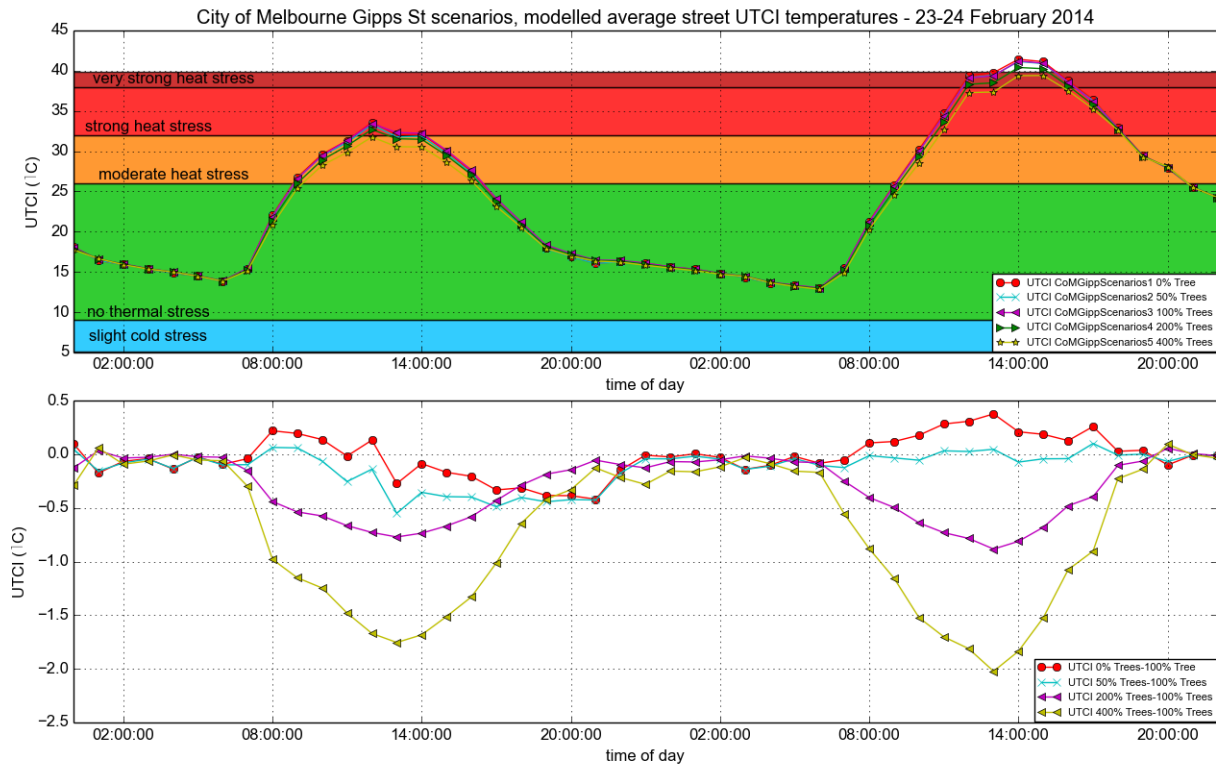


Figure 6.9: Modelled UTCI ($^{\circ}\text{C}$) average of all surfaces at 0m height for five scenarios, CoMGippScenarios1-NoTree, CoMGippScenarios2-HalfTree, CoMGippScenarios3-Trees, CoMGippScenarios4-DoubleTrees, CoMGippScenarios5-4xTrees over 23-24 February 2012 / Differences in UTCI ($^{\circ}\text{C}$) average of all surfaces at 0m height between baseline CoMGippScenarios3-Trees scenario and other four scenarios over 23-24 February 2012.

in UTCI. Finally, while the daytime reductions in temperatures can be significant, increased canopy cover can reverse these trends and contribute to slightly hotter temperatures during the night time due to longwave trapping.

The Gipps St. scenarios show many of the same impacts of modifying canopy cover as in the Preston scenarios. They show the importance of not losing trees in urban streetscapes, as even minimal canopy cover can have a positive impacts on HTC. In these scenarios, an even larger increase in canopy cover (going from doubled to quadrupled) can have the effect of doubling the cooling effect. The scenarios also show that localised impacts (within a few metres of the canopy) can show even more substantial impacts from the increased tree canopy.

Slower cooling at night of higher canopy covered streetscapes are seen in these scenarios. However, they are much smaller than the daytime rates, reduced cooling of 0.2°C UTCI compared to increased cooling during the day of 2.0°C UTCI. Some reversals also occur at night time when the UTCI temperatures are under 15°C , well into a range which should cause no thermal stress, and these very small warming occasions due to increased canopies are much less significant than the daytime cooling effects they bring.

These scenario results show the importance of tree canopies in urban streetscapes in providing improved HTC on hot days. This is seen not only in the amount of cooling produced by increasing the canopy cover of existing streetscapes (as measured by the UTCI HTC index), but perhaps more importantly, the worsening HTC conditions caused by removing or completely eliminating canopy cover.

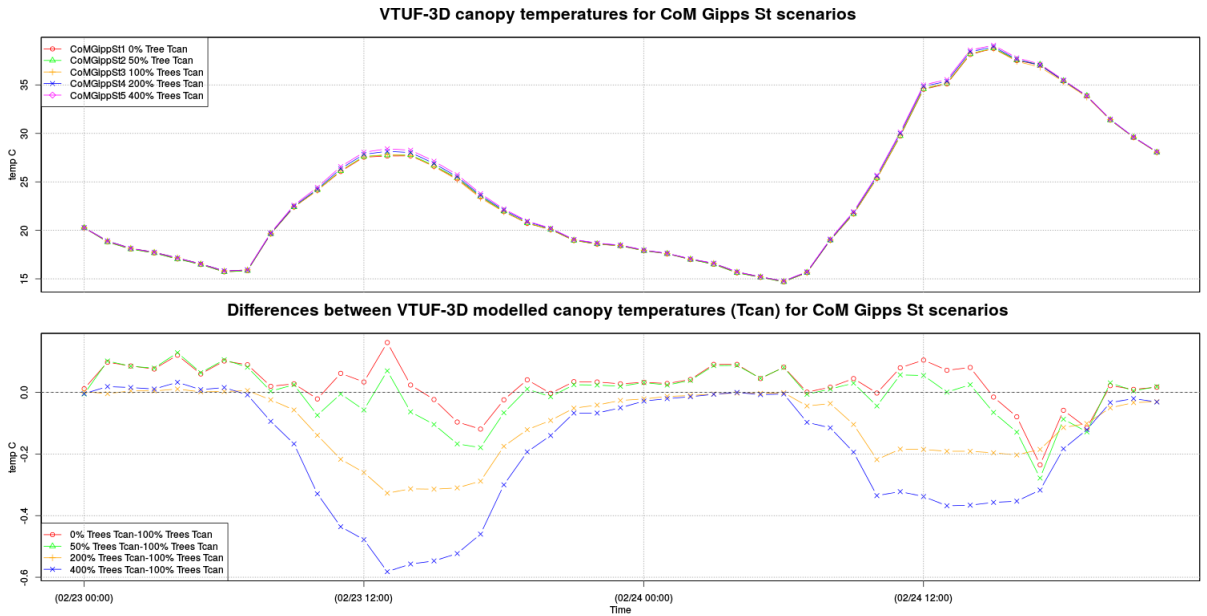


Figure 6.10: Modelled canopy air temperature (T_{can}) of five scenarios, CoMGippScenarios1-NoTree, CoMGippScenarios2-HalfTree, CoMGippScenarios3-Trees, CoMGippScenarios4 -DoubleTrees and, CoMGippScenarios5-4xTrees over 23-24 February 2012 / Differences of T_{can} between baseline CoMGippScenarios3-Trees scenario and other four scenarios over 23-24 February 2012.

The effects can largely be attributed to the shading effects of the vegetation, causing lower surface temperatures and mean radiant temperatures, reducing the radiation loading on the human body. However, an upper limit to these cooling effects, or rate of diminishing return, was not found in this set of scenarios. Further work is needed to find the rate of cooling due to each additional tree and to find the optimal number of and arrangements of these trees to maximise the benefits.

Chapter 7

Conclusion

7.1 Key/Major findings

The successful completion of the research aim of this project has seen the development, evaluation, and demonstration of VTUF-3D (Vegetated Temperatures Of Urban Facets), a new modelling tool needed to assess the impacts of water sensitive urban design (WSUD) features on human thermal comfort (HTC) in urban areas. This new model uses an innovative approach to bring urban greenery into urban micro-climate modelling. It was created through merging two models together, tiling multiple instances of a process-based vegetation model (MAESPA) into a micro-scale surface energy balance radiation model (TUF-3D).

An extensive evaluation of this new modelling tool has demonstrated the model is capable of very good performance. A first set of validations were performed using flux tower observations. Substantial improvements are seen over an unimproved TUF-3D model. More importantly, performance of the VTUF-3D is shown to perform within the range of the best performing urban model land surface schemes in flux partitioning, except for the Q_E flux, in which VTUF-3D performed with only slightly higher errors than the models which include vegetation through tiling or integration. Error rates for VTUF-3D in these fluxes show d index of agreement values of 0.964, 0.652, 0.998, and 0.957 for the Q_H , Q_E , Q^* , and Q_G fluxes respectively, and RMSE values of 40.2, 33.1, 19.0, and 52.5 Wm^{-2} .

A second set of validations shows low error rates in validations against observations in different locations in the canyon of T_{mrt} and $UTCI$ in urban streetscapes with both an open canopy cover and those with a more extensive canopy. In the treed canyon, error analysis values for T_{mrt} RMSE values range from 5.48 to 7.94°C with good d index of agreement values ranging from 0.913 to 0.939. $UTCI$ returns strong results with RMSE values ranging from 2.74 to 3.02°C with d index of agreement values ranging from 0.914 to 0.953. In the open canyon, error analysis values for T_{mrt} RMSE values range from 5.82 to 6.11°C with very good d index of agreement values ranging from 0.959 to 0.961. $UTCI$ returns error results of RMSE ranging from 2.33 to 2.45°C with d index of agreement values ranging from 0.965 to 0.971.

A final set of validations was performed to ensure VTUF-3D can correctly account for the impact the geometry of an urban area can have on urban vegetation. These influences, especially varying amounts of incoming radiation due to shading from the urban geometry, should cause variations in the physiological responses of the vegetation on different sides of the street. In an analysis of the modelled results, comparisons of modelled tree transpiration to observed values broadly reproduce the variations seen in the observations of transpiration for both sides

of the street. These results give confidence that this aspect of urban vegetation modelling is functioning well.

A variety of approaches were considered in creating this model. As the literature review detailed, schemes to model the influences of vegetation range from very simple to extremely complex. This model aimed to balance simplicity and usability with accuracy. The results of the validations demonstrate that the simplifications taken in model design, configuration, and operation have not compromised the accuracy of the model, and is quite suitable for its intended usage of assessing HTC impacts of urban greenery.

There is some research in the literature about urban greening benefits to HTC, but not enough to fully quantify these benefits and how to maximise the effects. The introduction of WSUD into cities in order to augment water supplies and promote urban waterways health can also have positive climate benefits. The increased urban greening and increased water availability in cities, as part of water sensitive urban design, can help reverse some of the contributors to urban heat.

Modelling with VTUF-3D confirms the importance of urban vegetation in delivering HTC benefits. Modelling results show that air temperatures can differ by 1°C between open streetscapes and those with a moderate canopy cover. Even greater benefits can be seen in looking at the HTC impacts. Modelling shows substantial increases in thermal comfort due to canopy shading effects in values of T_{mrt} , mean radiant temperature, and the impact this has in reducing UTCI values.

Modelling scenarios of increasing canopy cover show a difference in $UTCi$ between a streetscape with all trees removed and one with quadrupled canopy cover of 2.5°C . The elimination of the existing canopy of a typical street shows an increase in UTCI by 0.4°C , showing the importance of maintaining existing urban canopy cover and the health of these trees. Localised differences in $UTCi$ are much more substantial, showing a cooling effect of over 4 to nearly 5°C compared to areas a few metres away.

7.2 Research implications

Urban areas face increasingly difficult challenges, as outlined in Chapter 1. Cities are growing larger, becoming more crowded, and filled with increasingly ageing and vulnerable populations. At the same time, climate change (along with changing rain patterns) and urban design are making cities hotter places to be. In order to adapt to these changing conditions, strategies are needed to promote thermal comfort.

In this context, this project set out to answer three research questions. The first question, can a model be devised for HTC assessments of WSUD, was answered in the model design chapter (Chapter 4) as well as the model validation chapter (Chapter 5). Through the validations, the design (and model implementation) was shown to function well, making VTUF-3D a suitable model for WSUD assessments of HTC. The validation process also answered the second research question, can this new model be shown to be accurate and suitable for these assessments, by showing that VTUF-3D is accurate and suitable. Finally, the third research question, can this new model be demonstrated as able to start answering questions and inform planning decisions with urban climate knowledge about how to best utilise urban greening to maximise the thermal comfort impacts, was answered in the canopy cover scenarios chapter (Chapter 6). This demonstration of VTUF-3D showed the value in urban canopy cover and did so with quantifiable improvements to HTC due to increased canopy cover of streetscapes.

Now with a suitable tool to model and study in detail the impacts of urban greening on HTC, recommendations and guidelines on how to best use urban greenery can be developed. Questions can be answered as to the optimal arrangement of canopy cover to give the maximum benefits. Performance of future scenarios can also help inform responses to future challenges, both in terms of urban redesign and planning for emergency responses.

With the VTUF-3D's micro-climate resolution, urban areas can be studied metre by metre and proper mitigation strategies designed for every section of the urban canyon, allowing effort to be focused on areas with the greatest need. It is sufficiently scaled to resolve human level interactions with their surroundings and provide variables to calculate HTC (such as T_{mrt}). The built in output of T_{mrt} and $UTCI$ allows examination of these values without requiring addition steps. Finally, with the ability to insert any type of vegetation (or WSUD feature) using physiological and physical vegetation templates, the model is applicable to a unlimited number of scenarios and modelling questions.

7.3 Contribution to the research field

The development of VTUF-3D, a new micro-scaled model, has created a model suitable for 3D urban environments. It captures the driving processes of urban climates and the interactions with buildings and urban surfaces. The development process has added physical representations of vegetation into the new VTUF-3D model. With this addition, and using the vegetation absorption, transmission, and reflection functionality of MAESPA, the shading effects of vegetation can be resolved in the model. A second modification adds the physiological processes of vegetation (along with soil and associated water) from MAESPA and re-partitions the energy balances appropriately for the areas of a modelled domain containing vegetation. These two modifications have now completed the interactions of soil, plants, and atmosphere and their interactions with urban surfaces and captures the processes of all driving energy and water budgets.

More specifically, in making these changes, VTUF-3D has created new logic which resolve shading effects. New logic was also added to modify surface energy balances for those surfaces which contain vegetation. This change along with the other modification now contributes to the accurate predictions of surface temperatures for each surface in the domain.

In order to fulfil the requirement in the objective to model a wide variety of WSUD features, a pluggable system of MAESPA vegetation parameterisations has been created. For this project, parameterisations for brushbox and olive trees along with a common turf grass have been implemented. As these parameterisations use scalable templates for physical properties and allow a wide variety of physiological parameters to be set for each type of vegetation, any arbitrary WSUD feature can be created and inserted into a modelled domain.

This new integrated approach to include vegetation into a surface energy balance model now makes it possible to model any urban environment. This new model will allow research into a wide variety of urban morphologies, quantifying the benefits of a wide variety of urban arrangements and allow planning for future changes and challenges in climate and urban design.

7.4 Future research

The three objectives of this project, model creation, validation and demonstration, have been fulfilled by the completion of this project, but more work needs to be done in understanding the full impacts of WSUD on HTC in urban areas.

The first of these is a more advanced treatment of wind. Currently, the VTUF-3D model only uses wind in roughness layer calculations. Advection of fluxes by wind is not currently accounted for in the model. A first step towards this could be to add an initiation step to run the domain through a CFD type analysis and create lookup tables of vector directions and lengths for eight wind directions for each surface.

A second issue to investigate is the night time transpiration of vegetation. Studies show that there is some transpiration at night (Lindén et al. 2015) or negative values, but MAESPA currently gives results of 0 Wm^{-2} for non-daylight hours. Accounting for these fluxes in MAESPA will help to make VTUF-3D's predictions of latent energy more accurate and more realistic.

Another improvement would be to add a more complete urban hydrology. This would allow the effects of irrigation on HTC to be examined. Also, issues with low Q_E predictions were highlighted in the validations (Section 5.2.2). The addition of irrigation as well as evaporation off of impervious surfaces is anticipated to increase the accuracy of these predictions.

Additional MAESPA vegetation parameterisations need to be added to account for additional WSUD features. Currently, only two types of street trees and a turf grass parameterisation are available to be modelled by VTUF-3D. Additional work is needed to parameterise many of the commonly used street trees. Also, common WSUD features, including such items as swales, tree pits, and infiltration pits, remain to be parameterised. This issue was also identified as contributing to low Q_E predictions. Adding the ability to model exactly the vegetation needed in the scenario can help minimise this issue.

Validation of the model using other locations and climates would ensure that VTUF-3D is suitable for other locations outside of Melbourne during the summer. These could include winter validations or validations using observations from semi-tropical regions such as Singapore.

Additional validations using sap flow/tree water usage are also desirable and will add additional confidence in the proper functioning of the vegetated components of the model.

Finally, usability issues in the model need to be addressed. The configuration process and analysis process is complex and requires many hand coded files. This process can be replaced by a more friendly graphic interface allowing use of the model by less expert users and enable the model to be adopted potentially even in the urban planning community.

Appendices

Appendix A

TUF-3D configuration files

A.1 parameters.dat

note: H/W of an individual canyon can be calculated by: $H/W = \sqrt{lpin} * bh_o_bl / (1 - \sqrt{lpin})$ (ALTHOUGH, the model will increase the resolution if it is too low for any given facet, and this may result in the lambdap, bh_o_bl, or H/W ratios that you want not being met exactly)

Parameters in the order that they are read in:

```
vfcalc
yd,outpt_tm,start_time,end_time
matlab_out

radiative forcing and surface temperature
lwv,swv
frcKdn,frcLdn,frcTsfc
press

radiative parameters
dalb
albr,albs,albw
emisr,emiss,emisw
emiss_var
emissInter,emissNS,emissEW
cloudtype

domain geometry
numres
do k=1,numres
    resin(k)
enddo

facet surface temperatures
Tsfcr,Tsfcs,Tsfew

loop parameters
stror_in,strorint,strormax
xlat_in,xlatint,xlatmax
numlp
do k=1,numlp
```

```

    lpin(k)
enddo
numbhbl
do l=1,numbhbl
    bh_o_bh(l)
enddo

```

Explanation of the parameters:

note: 'roads' and 'streets' are used interchangeably

model/integration parameters

VFCALC: if vfcalc=0 (means no vf calcs) the file "vfinfo.dat" with the correct view factor info must be in the run directory;

vfcalc=1 means exact plane parallel view factor calcs;

vfcalc=2 means contour integration view factor calcs;

note: vfcalc must be 1 or 2 if looping through lambdap is turned on (i.e. numlp > 1)

YD: julian day (affects diurnal evolution of solar angle)

OUTPT_TM: (hours) the timestep between radiation calculations (and writing of model outputs)

MATLAB_OUT: 'T' = write out files containing patch vertices and patch faces, as well as patch surface temperature (Tsfc), patch brightness temperature (Tbright), and patch net shortwave (Kstar); these three quantities can then be easily visualized in Matlab with the 'patch' command; 'F' - do not write these files

radiative parameters

DALB: (W/m²) accuracy to which the effective albedo/emissivity of the canyon/cavity portion of the domain will be calculated; that is, reflections will continue until the change in albedo between timesteps is less than "dalb"

ALBR,ALBS,ALBW: albedo of roof, street, and wall patches, respectively

EMISR,EMISS,EMISW: emissivity of roof, street, and wall patches, respectively

EMISS_VAR: if true, the emissivity of the street varies (see next 3 parameters)

EMISSINTER,EMISSNS,EMISSEW: if emiss_var is true, these are the emissivity of the intersection, of the N-S streets, and of the E-W streets, respectively

CLOUDTYPE: For shortwave and longwave radiation; 0=clear, and higher values (to a maximum of 7) are progressively thicker clouds; 1=cirrus, 2=cirrostratus, 3=altocumulus, 4=altostratus, 5=cumulonimbus, 6=stratocumulus, 7=thick stratus (Ns?) - all assumed to be 100% cloud cover

radiative forcing and surface temperature

LWV: if true longwave radiation exchange is modelled

SWV: if true shortwave radiation exchange is modelled

FRCKDN: if true, incoming shortwave is read in from the forcing file and interpolates temporally as needed, otherwise the model calculates incoming solar (and requires forcing air temperature and humidity); either way, the model calculates the relative fractions of direct and diffuse

FRCLDN: if true, incoming longwave is read in from the forcing file and interpolates temporally as needed, otherwise the model calculates incoming longwave (and requires forcing air temperature and humidity)

FRCTSFC: if true, roof, road and wall average kinetic surface temperatures are read in from the forcing file and interpolated as needed; if false, these temperatures are assumed constant and read in from the parameter file

domain geometry

NUMRES: number of minimum resolutions (i.e. values of 'minres') to loop through
RESIN(k): the values of 'minres' to loop through (from k=1 to k=numres) ['minres' is the minimum resolution of any given facet (i.e. roof, road, or wall) - recommended value is 4 or greater (6 or higher is ideal); resolution of all other facets will be adjusted to maintain all geometric ratios while ensuring that all facets have a minimum of 'minres' patches across them in both dimensions (NOTE: THIS IS THE KEY PARAMETER THAT CONTROLS THE ACCURACY OF THE RADIATION SCHEME VS. THE COMPUTATIONAL EXPENSE - minres = 2 will give a quick estimate, minres = 4 tends to be a reasonable balance between speed and accuracy, and minres = 6 tends to give very accurate results but can be very computationally expensive and can require a lot of memory, relative to the speed and memory of a typical desktop; it is also useful to remember that the minimum resolution for solar radiation absorption is effectively 2*minres - see the BLM paper for an explanation)]

initial and constant temperatures

TSFCR,TSFCS,TSFCW: (deg C) surface temperatures (roofs, roads and walls, respectively); if frcTsfc is True, then these temperatures are not used, and Tsfc for the three facet types are instead read in from the forcing file

loop parameters (for multiple simulations with the same forcing data, but with different street orientations, latitudes, lambdap ratios, and combinations thereof)

STROR_IN,STRORINT,STRORMAX: (degrees from alignment with cardinal directions) initial, loop interval, and final street orientation orientation

XLAT_IN,XLATINT,XLATMAX: (degrees) initial, loop interval, and final latitude; XLATINT must be positive; XLAT_IN and XLATMAX can be negative (to indicate the southern hemisphere)

NUMLP: number of lambdap ratios to loop through

LPIN(k): the lambdap ratios (from k=1 to k=numlp)

NUMBHBL: number of bh (building height) to bl (building width) ratios to simulate for each lambdap

BH_O_BL(k): the bh/bl ratios (from l=1 to l=numbhbl)

A.2 forcing.dat

```
numfrc,starttime,deltatfrc
do k=1,numfrc+1
    Kdnfrc(k),Ldnfrc(k),Tafrc(k),eafrcc(k),Troffrc(k),
    Troadfrc(k),Twallfrc(k)
    timefrc(k)=starttime+real(k-1)*deltatfrc
enddo
```

NUMFRC: The number of forcing timesteps over which the model will run,"i.e. total model integration time divided by the timestep of the input "forcing data (note: there must be numfrc+1 rows of forcing data,"because data from the start time and end time both must be present)

STARTTIME: The time at the start of the simulation (in hours from "midnight) in local mean solar time (i.e., in a time zone such that" the smallest solar zenith angle occurs exactly at noon)

DELTATFRC: (hours) the timestep of the forcing data

KDNFRC(k): (W/m²) downwelling shortwave radiation flux density

LDNFRC(k): (W/m²) downwelling longwave radiation flux density

TAFRC(k): (deg C) near-surface air temperature

EAFRC(k): (mb) near-surface water vapour pressure

TROOFFRC(k): (deg C) near-surface air temperature

TROADFRC(k): (deg C) near-surface air temperature

TWALLFRC(k): (deg C) near-surface air temperature

Appendix B

New VTUF-3D configuration process

B.1 VTUF-3D and MAESPA configuration changes

In its unmodified form, TUF-3D is configured by two main user defined files, *parameters.dat* and *forcing.dat*. These files are fully documented in Appendix A. *Forcing.dat* supplies meteorological forcing data, including incoming shortwave and longwave, air temperature, and vapour pressure, for the duration of the simulation. *Parameters.dat* sets the main properties of the domain being simulated, such as location, orientation, width/height ratios, albedos and emissivities, and other modelling options. These files remain unmodified in their use in VTUF-3D.

The normal configuration and usage of the default MAESPA configurations are described in Medlyn & Duursma (2014). In order to add new functionality and modelling options, new files have been added to the VTUF-3D configuration process. To link TUF-3D and MAESPA within VTUF-3D, a new mapping file is introduced, *treemap.dat*. A sample configuration is shown in Appendix B.3 and explained in detail in the configuration process (Section 4.3.5). All other TUF-3D and MAESPA configuration files remain unchanged from the original models.

B.2 Configuration generation

B.2.1 Overview

In order to simplify the use of the VTUF-3D model, a number of utilities have been created to generate the configuration files needed to run a given simulation. The model will expect to find a number of configuration files and a specific directory structure to organise these files. The general pattern of these directories is:

```
<Run name>
  1
    1 <directory containing MAESPA tree 1, diffuse only>
    2 <directory containing MAESPA tree 1, 100% radiation>
  2
    1 <directory containing MAESPA tree 2, diffuse only>
    2 <directory containing MAESPA tree 2, 100% radiation>
  3 <tree directories continue sequentially>
    1
```

└ 2

The overall model configuration, used by CreateMaespaRun, is given in the *messagesConfig.properties* file, setting values for run directory, Julian day start and end, year of run, grid size in meters, and forcing data source (to be loaded from the appropriate Sqlite database), all referenced by the model run (i.e. "PrestonScenarioX", a user defined scenario name, in the listing below).

```
#PrestonScenarioX
CreateMaespaRunAndProcess.runDirectory.PrestonScenarioX=/home/kerryt/Documents/
VTUF-Runs/PrestonScenarioX
CreateMaespaRunAndProcess.start.PrestonScenarioX=40
CreateMaespaRunAndProcess.end.PrestonScenarioX=70
CreateMaespaRunAndProcess.gridSize.PrestonScenarioX=5
CreateMaespaRunAndProcess.forcing.PrestonScenarioX=Preston
CreateMaespaRunAndProcess.year.PrestonScenarioX=2004
```

B.2.2 Create streets and buildings

As a first step, four comma separated value (CSV) files are read, containing x,y locations and values for building heights, vegetation heights, vegetation types, and a tree map. The heights are multiples of the grid size (i.e. with a 5m grid size, a 10m building's value is 2). Currently, supported vegetation types are:

```
OLIVE_CONFIG_TYPE = 1;
BRUSHBOX_CONFIG_TYPE = 3;
NEW_GRASS_PARAMETERIZATION = 4;
```

The three types of vegetation currently implemented in VTUF-3D, two tree species, *Olea europaea* and *Lophostemon Confertus*, and turf grass, tall fescue (*Festuca arundinacea*) are further detailed in Section 4.3.6.

All trees in a domain are given individual sequential numbers (i.e. 1, 2, 3, etc.), so they can be modelled separately. If a tree canopy is larger than the grid size and extends into neighbouring grid squares (user defined while inputting a scenario domain), the grid square of the trunk is given a positive value while the other grid squares containing the canopy are given negative values (i.e. tree 3 might have neighbouring grid square values of 3, -3, and -3). This allows non-vegetative surfaces to be overshadowed by a canopy.

B.3 treemap.dat

```
&count
numberTreePlots=539
/
&runSwitches
partitioningMethod=17
/

&location
xLocation=0 0 0 0 0 0 0 etc.
yLocation=2 3 4 7 8 9 12 13 etc.
phyfileNumber=1 2 2 1 2 2 1 2 etc.
strfileNumber=1 2 2 1 2 2 1 2 etc.
```

```
treesfileNumber=1 2 2 1 2 2 1 2 etc.  
treesHeight=0 1 1 0 1 1 0 1 etc.  
trees=1 17 -18 1 17 -18 1 17 etc.  
/  
&buildingcount  
numberBuildingPlots=441  
/  
&buildinglocation  
xBuildingLocation=0 0 0 0 0 0 0 etc.  
yBuildingLocation=0 1 5 6 10 11 15 16 etc.  
buildingsHeight=2 2 2 2 2 2 2 etc.  
/  
&domain  
width=35  
length=35  
configTreeMapCentralArrayLength=25  
configTreeMapCentralWidth=5  
configTreeMapCentralLength=5  
configTreeMapX=35  
configTreeMapY=35  
configTreeMapX1=15  
configTreeMapX2=19  
configTreeMapY1=15  
configTreeMapY2=19  
configTreeMapGridSize=5.0  
configTreeMapNumsfcab=41  
configTreeMapHighestBuildingHeight=3  
/
```

Appendix C

VTUF-3D configuration creation

C.1 Domain creation

Using the CSV files loaded in Appendix B.2.2, the *treemap.dat* file is created (and example given in Appendix B.3). In this file, the number of grid spaces with trees is configured in *numberTreePlots*. For each of those tree plots, the *xLocation*, *yLocation*, *phyfileNumber*, *strfileNumber*, *treesfileNumber*, and *treesHeight* are specified. The (X,Y) location specifies its place in the domain.

MAESPA in its original form stores tree properties in the files *phy.dat* (physiology information), *str.dat* (canopy structure), and *trees.dat* (tree characteristics). Using the *treemap.dat* file, VTUF-3D maps each individual tree to its individual configuration and tree information will be loaded from files indexed by *phyX.dat*, *strX.dat*, and *treesX.dat* for each X value mapped in the *treemap.dat* configuration.

A similar structure in *treemap.dat* configures the buildings in the domain. Number of buildings are given in *numberBuildingPlots*. For each of those buildings, the *xBuildingLocation*, *yBuildingLocation*, and *buildingsHeight* are specified. The last domain properties values specified in *treemap.dat* are the domain size, *width* and *height*, in number of grids in each direction.

The overall configuration for VTUF-3D, *parameter.dat*, is created. An example is shown in Appendix A.1. Forcing data is loaded from a Sqlite database. The query for this database brings back the proper set of data for the time period as well as the given location. An example is shown in Appendix A.2

C.2 Create post-processing scripts

A number of scripts are created to be used in the post-processing analysis. In this step, a number of Python and R scripts are created. They will be described in more detail in the post processing step (Appendix C.3).

C.3 VTUF-3D Post-processing

In order to complete analysis of a simulation, and to provide additional output not built into the VTUF-3D model, a number of additional scripts are available. These scripts are generated

during the configuration generation with characteristics specific to each scenario. These are detailed in Appendix C.2.

C.4 Scripts

- TUF_ave_graphs.R, used to generates figures for 30 day hourly averages of the Q^* , Q_H , Q_E , ΔQ_S fluxes. If applicable, (the run uses Preston forcing data), these fluxes will be compared to observation fluxes.
- TUF_Graphs.R is used to generate numerous figures of every item in the output.
- GenerateUTCIFiles.py is used to read the VTUF-3D output (and forcing data input) and generate $UTCI$ and T_{mrt} data for each surface in each time step.
- MatlabPatchesPlot3.py is used to create 3D figures of T_{sfc} predictions. If applicable, (the run uses City of Melbourne Gipps and George St. or Lincoln Square data), points will be annotated on these figures with observation data.
- MatlabPatchesPlot4.py is the same as MatlabPatchesPlot3.py but plots $UTCI$ predictions.
- MatlabPatchesPlot6.py is used to generate 30 day hourly aggregates of predicted VTUF-3D points vs. observations.
- MatlabPatchesPlot8.py is used to create ground level z-slices for each time step of $UTCI$, T_{mrt} , and T_{sfc} predictions.
- UTCI.py is the utility script used by the other scripts to calculate T_{mrt} and $UTCI$ values.
- TUF_EnergyClosure_graph.R is used to look at the 30 day $Q^* - Q_H - Q_E - \Delta Q_S = 0$ values to ensure that the model is conserving energy and achieving energy closure.

Bibliography

- ABS (2013), 3222.0 - Population Projections, Australia, 2012 (base) to 2101. Australian Bureau of Statistics. <http://www.abs.gov.au/Ausstats/abs@.nsf/mf/3222.0>, (accessed 8 July 2016).
- Acero, J.A. & Herranz-Pascual, K. (2015), A comparison of thermal comfort conditions in four urban spaces by means of measurements and modelling techniques. *Building and Environment*, 93:pp. 245–257.
- Ahrens, C. (2004), *Essentials of Meteorology: An Invitation to the Atmosphere*. Brooks Cole.
- Alexander, L. & Arblaster, J. (2009), Assessing trends in observed and modelled climate extremes over Australia in relation to future projections. *International Journal of Climatology*, 435(July 2008):pp. 417–435.
- Ali, M.H. (2010), *Fundamentals of Irrigation and On-farm Water Management*. Springer, New York.
- Ali-Toudert, F. & Mayer, H. (2006a), Thermal comfort in an east-west oriented street canyon in Freiburg (Germany) under hot summer conditions. *Theoretical and Applied Climatology*, 87(1-4):pp. 223–237.
- Ali-Toudert, F. & Mayer, H. (2006b), Numerical study on the effects of aspect ratio and orientation of an urban street canyon on outdoor thermal comfort in hot and dry climate. *Building and Environment*, 41(2):pp. 94–108.
- Allen, D.M., Heaviside, C., Vardoulakis, S., Huntingford, C., Masato, G., Guillod, B.P., Frumhoff, P., Bowery, A., Wallom, D. & Myles (2016), Attributing human mortality during extreme heat waves to anthropogenic climate change. *Environmental Research Letters*, 11(7):pp. 1–8.
- Arnfield, A. (1990), Canyon geometry, the urban fabric and nocturnal cooling: a simulation approach. *Physical Geography*, 11(3):pp. 220–239.
- Arnfield, A. (2003), Two decades of urban climate research: a review of turbulence, exchanges of energy and water, and the urban heat island. *International Journal of Climatology*, 23(1):pp. 1–26.
- ASHRAE (2008), AHSRAE Technical Committee 2.1 - Physiology and Human Environment. Frequently Asked Questions. American Society of Heating Refrigeration and Air-Conditioning Engineers. <http://tc21.ashraetc.org/faq.html>, (accessed 24 September 2012).
- ASHRAE (2009), Thermal Comfort. In: *ASHRAE Fundamentals Handbook*, chapter 9, ASHRAE, pp. 9.1–9.30.
- Bailey, B.N., Overby, M., Willemsen, P., Pardyjak, E.R., Mahaffee, W.F. & Stoll, R. (2014), A scalable plant-resolving radiative transfer model based on optimized GPU ray tracing. *Agricultural and Forest Meteorology*, 198-199:pp. 192–208.

- Bailey, B.N., Stoll, R., Pardyjak, E.R. & Miller, N.E. (2016), A new three-dimensional energy balance model for complex plant canopy geometries: Model development and improved validation strategies. *Agricultural and Forest Meteorology*, 218-219(February):pp. 146–160.
- Bailey, W. & Davies, J. (1981), Bulk stomatal resistance control on evaporation. *Boundary-Layer Meteorology*, 20(1):pp. 401–415.
- Baldini, E., Facini, O., Nerozzi, F. & Arboree, C. (1997), Leaf characteristics and optical properties of different woody species. *Trees*, 12:pp. 73–81.
- Ball, J.T., Woodrow, I.E. & Berry, J.A. (1987), A model predicting stomatal conductance and its contribution to the control of photosynthesis under different environmental conditions. In: *Progress in Photosynthesis Research* (ed. J. Biggins), 953, Martinus-Nijhoff Publishers, Dordrecht, the Netherlands, pp. 221–224.
- Beardsell, D.V. & Considine, J.A. (1987), Lineages, Lineage Stability and Pattern Formation in Leaves of Variegated Chimeras of *Lophostemon confertus* (R. Br.) Wilson & Waterhouse and *Tristaniopsis laurina* (Smith) Wilson & Waterhouse (Myrtaceae). *Aust. J. Bot.*, 35(6):pp. 701–714.
- Bernacchi, C.J., Singsaas, E.L., Pimentel, C., Portis, A.R. & Long, S.P. (2001), Improved temperature response functions for models of Rubisco-limited photosynthesis. *Plant, Cell and Environment*, 24(2):pp. 253–259.
- Best, M.J. & Grimmond, C.S.B. (2012), Analysis of the Seasonal Cycle Within the First International Urban Land-Surface Model Comparison. *Boundary-Layer Meteorology*, 146(3):pp. 421–446.
- Beven, K. (1979), A sensitivity analysis of the Penman-Monteith actual evapotranspiration estimates. *Journal of Hydrology*, 44(3-4):pp. 169–190.
- Bi, P., Williams, S., Loughnan, M., Lloyd, G., Hansen, A., Kjellstrom, T., Dear, K. & Saniotis, A. (2011), The effects of extreme heat on human mortality and morbidity in Australia: implications for public health. *Asia-Pacific Journal of Public Health*, 23(2 Suppl):pp. 27S–36.
- Bijoor, N.S., Pataki, D.E., Haver, D. & Famiglietti, J.S. (2014), A comparative study of the water budgets of lawns under three management scenarios. *Urban Ecosystems*, 17(4):pp. 1095–1117.
- Blazejczyk, K., Epstein, Y., Jendritzky, G., Staiger, H. & Tinz, B. (2012), Comparison of UTCI to selected thermal indices. *International Journal of Biometeorology*, 56(3):pp. 515–535.
- Bohenstengel, S., Schlünzen, K.H. & Grawe, D. (2004), Influence of thermal effects on street canyon circulations. *Meteorologische Zeitschrift*, 13(5):pp. 381–386.
- Bonan, G. (2002), Hydrological Cycle. In: *Ecological Climatology*, chapter 5, Cambridge University Press, pp. 1–33.
- Bowler, D.E., Buyung-Ali, L., Knight, T.M. & Pullin, A.S. (2010), Urban greening to cool towns and cities: A systematic review of the empirical evidence. *Landscape and Urban Planning*, 97(3):pp. 147–155.
- Briggs, L.J. & Shantz, H. (1912), The Wilting Coefficient and Its Indirect Determination. *Botanical Gazette*, 53(1):pp. 20–37.

- Bröde, P. (2009), Program for calculating UTCI Temperature (UTCI) released for public use after termination of COST Action 730, UTCI, Version a 0.002, October 2009. http://www.utci.org/public/UTCI%20Program%20Code/ReadMe_UTCI_a002.txt.
- Bröde, P., Błazejczyk, K., Fiala, D., Havenith, G., Holmér, I., Jendritzky, G., Kuklane, K. & Kampmann, B. (2013), The Universal Thermal Climate Index UTCI compared to ergonomics standards for assessing the thermal environment. *Industrial Health*, 51:pp. 16–24.
- Bröde, P., Fiala, D., Blazejczyk, K., Holmér, I., Jendritzky, G., Kampmann, B., Tinz, B. & Havenith, G. (2012), Deriving the operational procedure for the Universal Thermal Climate Index (UTCI). *International Journal of Biometeorology*, 56(3):pp. 481–494.
- Brown, R.H. & Morgan, J.A. (1980), Photosynthesis of Grass Species Differing in Carbon Dioxide Fixation Pathways 1. *Plant Physiology*, 66(4):pp. 541–544.
- Bruse, M. (1999), *The influences of local environmental design on microclimate- development of a prognostic numerical Model ENVI-met for the simulation of Wind, temperature and humidity distribution in urban structures*. Ph.D. thesis, University of Bochum, Germany (in German).
- Bruse, M. (2004), ENVI-met 3.0: Updated model overview. *University of Bochum*. Retrieved from: www.envi-met.com.
- Bruse, M. & Fleer, H. (1998), Simulating surface-plant-air interactions inside urban environments with a three dimensional numerical model. *Environmental Modelling and Software*, 13(3-4):pp. 373–384.
- Buba, T. (2013), Relationships between stem diameter at breast height (DBH), tree height, crown length, and crown ratio of Vitellaria paradoxa C. F. Gaertn in the Nigerian Guinea Savanna. *African Journal of Biotechnology*, 12(22):pp. 3441–3446.
- Buck, A.L. (1981), New Equations for Computing Vapor Pressure and Enhancement Factor. *Journal of Applied Meteorology*, 20(12):pp. 1527–1532.
- Bureau of Meteorology (2012a), Melbourne (Olympic Park), Victoria, Daily Weather Observations. <http://www.bom.gov.au/climate/dwo/IDCJDW3033.latest.shtml>, Commonwealth of Australia, (Accessed 1 August 2016).
- Bureau of Meteorology (2012b), Record-breaking La Niña events. <http://www.bom.gov.au/climate/enso/history/ln-2010-12/>, Commonwealth of Australia, (Accessed 1 August 2016).
- Bureau of Meteorology (2016a), Latest Weather Observations for Melbourne Airport. <http://www.bom.gov.au/products/IDV60901/IDV60901.94866.shtml>, Commonwealth of Australia, (Accessed 1 August 2016).
- Bureau of Meteorology (2016b), One Minute Solar Data. <http://www.bom.gov.au/climate/data/oneminsolar/about-IDCJAC0022.shtml>, Commonwealth of Australia, (Accessed 1 August 2016).
- Bush, S.E., Pataki, D.E., Hultine, K.R., West, A.G., Sperry, J.S. & Ehleringer, J.R. (2008), Wood anatomy constrains stomatal responses to atmospheric vapor pressure deficit in irrigated, urban trees. *Oecologia*, 156(1):pp. 13–20.
- Cadenasso, M.L., Pickett, S.T.A. & Schwarz, K. (2007), Spatial heterogeneity in urban ecosystems: reconceptualizing land cover and a framework for classification. *Frontiers in Ecology and the Environment*, 5(2):pp. 80–88.

- Cambell, G.S. & Norman, J.M. (1998), *An Introduction to Environmental Biophysics*. Springer-Verlag, New York, 2nd edition.
- Campbell, G.S. (1974), A simple method for determining unsaturated conductivity from moisture retention data. *Soil Sci.*, 117:pp. 311–314.
- CD-adapco (2011), CD-adapco website. <http://www.cd-adapco.com/>, (accessed 2 November 2011).
- Chen, D., Wang, X., Thatcher, M., Barnett, G., Kachenko, A. & Prince, R. (2014a), Urban vegetation for reducing heat related mortality. *Environmental Pollution*, 192:pp. 275–284.
- Chen, F., Kusaka, H., Bornstein, R., Ching, J., Grimmond, C.S.B., Grossman-Clarke, S., Loridan, T., Manning, K.W., Martilli, A., Miao, S., Sailor, D., Salamanca, F.P., Taha, H., Tewari, M., Wang, X., Wyszogrodzki, A.A. & Zhang, C. (2011), The integrated WRF/urban modelling system: development, evaluation, and applications to urban environmental problems. *International Journal of Climatology*, 31(2):pp. 273–288.
- Chen, Y.C., Lin, T.P. & Matzarakis, A. (2014b), Comparison of mean radiant temperature from field experiment and modelling: a case study in Freiburg, Germany. *Theoretical and Applied Climatology*, 118(3):pp. 535–551.
- Choudhury, B.J. & Monteith, J.L. (1988), A four-layer model for the heat budget of homogeneous land surfaces. *Q. J. Roy. Meteorol. Soc.*, 114:pp. 373–398.
- Chow, W.T.L., Brennan, D. & Brazel, A.J. (2012), Urban Heat Island Research in Phoenix, Arizona: Theoretical Contributions and Policy Applications. *Bulletin of the American Meteorological Society*, 93(4):pp. 517–530.
- City of Melbourne (2011), Urban Forest Strategy : Making a great city greener 2012-2032. <http://www.melbourne.vic.gov.au/Environment /UrbanForest/Pages/About.aspx>, (accessed 16 January 2012).
- City of Port Phillip (2010), Greening Port Phillip: Street Tree Planting Guide 2010-2015. <http://www.portphillip.vic.gov.au/street-tree-planting-guide-2010-2015.pdf>, (accessed 22 August 2017).
- Cleugh, H. & Grimmond, S. (2012), Urban Climates and Global Climate Change. In: *The Future of the World's Climate* (eds. A. Henderson-Sellers & K. McGuffie), Elsevier B.V, 2nd edition, pp. 47–76.
- ClimateWorks (2010), Low Carbon Growth Plan. <http://www.climateworksaustralia.org/>, (accessed 25 May 2011).
- Collins, M., Knutti, R., Arblaster, J., Dufresne, J.L., Fichefet, T., Friedlingstein, P., Gao, X., Gutowski, W., Johns, T., Krinner, G., Shongwe, M., Tebaldi, C., Weaver, A. & Wehner, M. (2013), Long-term Climate Change: Projections, Commitments and Irreversibility. In: *Climate Change 2013: The Physical Science Basis. Contribution of Working Group I to the Fifth Assessment Report of the Intergovernmental Panel on Climate Change* (eds. V.B. Stocker, T.F. D. Qin, G.-K. Plattner, M. Tignor, S.K. Allen, J. Boschung, A. Nauels, Y. Xia & P. Midgley), chapter 12, Cambridge University Press, Cambridge, United Kingdom and New York, NY, USA., pp. 1029–1136.
- Coutts, A.M., Beringer, J. & Tapper, N. (2010), Changing Urban Climate and CO₂ Emissions: Implications for the Development of Policies for Sustainable Cities. *Urban Policy and Research*, 28(1):pp. 27–47.

- Coutts, A.M., Beringer, J. & Tapper, N.J. (2007), Impact of Increasing Urban Density on Local Climate: Spatial and Temporal Variations in the Surface Energy Balance in Melbourne, Australia. *Journal of Applied Meteorology and Climatology*, 46(4):pp. 477–493.
- Coutts, A.M., Daly, E., Beringer, J. & Tapper, N.J. (2013), Assessing practical measures to reduce urban heat: Green and cool roofs. *Building and Environment*, 70:pp. 266–276.
- Coutts, A.M., Tapper, N.J., Beringer, J., Loughnan, M. & Demuzere, M. (2012), Watering our Cities: The capacity for Water Sensitive Urban Design to support urban cooling and improve human thermal comfort in the Australian context. *Progress in Physical Geography*, 37(1):pp. 2–28.
- Coutts, A.M., White, E.C., Tapper, N.J., Beringer, J. & Livesley, S.J. (2015a), Temperature and human thermal comfort effects of street trees across three contrasting street canyon environments. *Theoretical and Applied Climatology*, 124(1):pp. 55–68.
- Coutts, A.M. (2014), Trees in the street canyon environment: Exposure and response under changing micro-climates and water availability. In: *11th Symposium on the Urban Environment, 94th AMS Annual Meeting, 2-6 February 2014, Atlanta, GA.*, pp. 1–20.
- Coutts, A. & Gebert, L. (2012), Tree response to urban environmental conditions and water availability. In: *ICUC8-8th International Conference on Urban Climates, 6th-10th August 2012, Dublin, Ireland*.
- Coutts, A., Moore, C., Tapper, N.J. & White, E.C. (2016), Microclimate of isolated trees in the urban environment. In: *2nd Urban Tree Diversity Conference, Melbourne, Australia, 22-24 February 2016*.
- Coutts, A., Szota, C. & Thom, J. (2015b), Passive irrigation of street trees to improve tree health and support urban cooling. In: *9th International Conference on Urban Climate, 20-24 July 2015, Toulouse, France*.
- Cowan, I. & Farquhar, G. (1977), Stomatal function in relation to leaf metabolism and environment. *Symp Soc Exp Biol.*, 31(February 1977):pp. 471–505.
- CSIRO (2008), Regional temperature projections in Australia to 2100 for three climate cases, data prepared for the Garnaut Climate Change Review. Technical report, CSIRO, Aspendale, Victoria.
- Dai, Y., Dickinson, R. & Wang, Y. (2004), A two-big-leaf model for canopy temperature, photosynthesis, and stomatal conductance. *Journal of Climate*:pp. 2281–2299.
- de Dear, R. (2004), Thermal comfort in practice. *Indoor Air*, 14(Suppl 7):pp. 32–39.
- de Dear, R., Brager, G. & Cooper, D. (1997), Developing an Adaptive Model of Thermal Comfort and Preference. Technical report, Macquarie Research Ltd., Macquarie University/Center for Environmental Design Research, University of California.
- De Kauwe, M.G., Kala, J., Lin, Y.S., Pitman, A.J., Medlyn, B.E., Duursma, R.A., Abramowitz, G., Wang, Y.P. & Miralles, D.G. (2015), A test of an optimal stomatal conductance scheme within the CABLE land surface model. *Geoscientific Model Development*, 8(2):pp. 431–452.
- Deardorff, J.W. (1978), Efficient Prediction of Ground Surface Temperature and Moisture, With Inclusion of a Layer of Vegetation. *Journal of Geophysical Research*, 83(C4):pp. 1889–1903.

- Declet-Barreto, J., Brazel, A.J., Martin, C.A., Chow, W.T.L. & Harlan, S.L. (2012), Creating the park cool island in an inner-city neighborhood: heat mitigation strategy for Phoenix, AZ. *Urban Ecosystems*.
- Demuzere, M., Coutts, A., Göhler, M., Broadbent, A., Wouters, H., van Lipzig, N. & Gebert, L. (2014), The implementation of biofiltration systems, rainwater tanks and urban irrigation in a single-layer urban canopy model. *Urban Climate*, 10:pp. 148–170.
- Derkley, K. (2014), Reform locks up our suburbs. <http://www.theage.com.au/victoria/reform-locks-up-our-suburbs-20140614-3a4l4.html>, (accessed 9 July 2014).
- Díaz-Espejo, A., Walcroft, A.S., Fernández, J.E., Hafridi, B., Palomo, M.J. & Girón, I.F. (2006), Modeling photosynthesis in olive leaves under drought conditions. *Tree Physiology*, 26(11):pp. 1445–1456.
- DSE (2002), Melbourne 2030, Planning for sustainable growth. <http://www.nre.vic.gov.au/melbourne2030online/>, (accessed 25 May 2011).
- Dupont, S., Calmet, I. & Mestayer, P.G. (2002), Urban Canopy Modeling Influence on Urban Boundary Layer Simulation. In: *AMS 4th Symposium on Urban Environment, Norfolk, Virginia, 20-24 May 2002*, pp. 151–152.
- Dupont, S., Otte, T. & Ching, J. (2004), Simulation of meteorological fields within and above urban and rural canopies with a mesoscale model. *Boundary-Layer Meteorology*, 113:pp. 111–158.
- Duursma, R.A. & Medlyn, B.E. (2012), MAESPA: a model to study interactions between water limitation, environmental drivers and vegetation function at tree and stand levels, with an example application to [CO₂] x drought interactions. *Geoscientific Model Development*, 5(4):pp. 919–940.
- Duursma, R. (2008), MAESPA: Development of a soil-plant-atmosphere model. <https://maespa.github.io/docs/MAESPAseminar.pdf>.
- Duursma, R. (2016), A soil-plant-atmosphere model based on MAESTRA and SPA. <https://bitbucket.org/remkoduursma/maespa>, (accessed 27 June 2016).
- Eclipse Foundation (2016), Eclipse IDE for Java Developers, Version: Mars.2 Release (4.5.2). <http://www.eclipse.org/>.
- Ehrhard, J., Khatib, I., Winkler, C., Kunz, R., Moussiopoulos, N. & Ernst, G. (2000), The microscale model MIMO: development and assessment. *Journal of Wind Engineering and Industrial Aerodynamics*, 85(2):pp. 163–176.
- ESS (2006), STATUS OF AIR CONDITIONERS IN AUSTRALIA - Updated with 2005 data. Energy Efficient Strategies. [http://www.energystorage.gov.au/wp-content/uploads/Energy_Rating_Documents/Library/Cooling/Air_Conditioners/200509-ac-aust.pdf](http://www.energyrating.gov.au/wp-content/uploads/Energy_Rating_Documents/Library/Cooling/Air_Conditioners/200509-ac-aust.pdf), (accessed 24 September 2012).
- Fanger, P. (1972), *Thermal Comfort*. McGraw-Hill, New York.
- Farmer, J.T. & Howell, J.R. (1998), Comparison of Monte Carlo Strategies for Radiative Transfer in Participating Media. *Advances in Heat Transfer*, 31(C):pp. 333–429.
- Farquhar, G., Caemmerer, S.V. & Berry, J.A. (1980), A Biochemical Model of Photosynthetic CO₂ Assimilation in Leaves of C3 Species. *Planta*, 90:pp. 78–90.

- Fawcett, A.A., Iyer, G.C., Clarke, L.E., Edmonds, J.A., Hultman, N.E., McJeon, H.C., Rogelj, J., Schuler, R., Alsalam, J., Asrar, G.R., Creason, J., Jeong, M., McFarland, J., Mundra, A. & Shi, W. (2015), Can Paris pledges avert severe climate change? *Science (New York, N.Y.)*, 350(6265):pp. 1168–1169.
- Federer, C., Vorosmarty, C. & Fekete, B. (2003), Sensitivity of annual evaporation to soil and root properties in two models of contrasting complexity. *Journal of Hydrometeorology*, 4:pp. 1276–1290.
- Fernández, J.E., Moreno, F., Girón, I.F. & Blázquez, O.M. (1997), Stomatal control of water use in olive tree leaves. *Plant and Soil*, 190(2):pp. 179–192.
- Fiala, D., Havenith, G., Bröde, P., Kampmann, B. & Jendritzky, G. (2012), UTCI-Fiala multi-node model of human heat transfer and temperature regulation. *International Journal of Biometeorology*, 56(3):pp. 429–441.
- Frank, S., Waters, G., Beer, R. & May, P. (2006), An Analysis of the Street Tree Population of Greater Melbourne at the Beginning of the 21st Century. *Arboriculture & Urban Forestry*, 32(July):pp. 155–163.
- Frich, P., Alexander, L.V., Della-Marta, P., Gleason, B., Haylock, M., Tank Klein, A.M.G. & Peterson, T. (2002), Observed coherent changes in climatic extremes during the second half of the twentieth century. *Climate Research*, 19(3):pp. 193–212.
- Fung-yan, M. (1999), *Hyperspectral Data Analysis of Typical Surface Covers in Hong Kong*. Masters thesis, The Chinese University of Hong Kong.
- Gagge, A., Stolwijk, J. & Nishi, Y. (1971), An effective temperature scale based on a simple model of human physiological regulatory response. *ASHRAE Trans.*, 77(1):pp. 21–36.
- Gardner, W.R. (1960), Dynamic aspects of water availability to plants. *Soil Sci.*, 89:pp. 63–73.
- Garnaut, R. (2008), Projecting Australian Climate Change. In: *Garnaut Climate Change Review*, chapter 5, Cambridge University Press, Melbourne., pp. 105–120.
- Gebert, L., Coutts, A. & Beringer, J. (2012), *Response of trees to the urban environment*. Honors thesis, Monash University.
- Gilmanov, T.G., Soussana, J.F., Aires, L., Allard, V., Ammann, C., Balzarolo, M., Barcza, Z., Bernhofer, C., Campbell, C.L., Cernusca, A., Cescatti, A., Clifton-Brown, J., Dirks, B.O.M., Dore, S., Eugster, W., Fuhrer, J., Gimeno, C., Gruenwald, T., Haszpra, L., Hensen, A., Ibrom, A., Jacobs, A.F.G., Jones, M.B., Lanigan, G., Laurila, T., Lohila, A., G.Manca, Marcolla, B., Nagy, Z., Pilegaard, K., Pinter, K., Pio, C., Raschi, A., Rogiers, N., Sanz, M.J., Stefani, P., Sutton, M., Tuba, Z., Valentini, R., Williams, M.L. & Wohlfahrt, G. (2007), Partitioning European grassland net ecosystem CO₂ exchange into gross primary productivity and ecosystem respiration using light response function analysis. *Agriculture, Ecosystems and Environment*, 121(1-2):pp. 93–120.
- GNU (2016a), FORTRAN 2002 - GCC Wiki. <https://gcc.gnu.org/wiki/Fortran2003>.
- GNU (2016b), gfortran - the GNU Fortran compiler, part of GCC. <https://gcc.gnu.org/wiki/GFortran>.
- Google Maps (2015), Preston, Victoria 3072. <http://maps.google.com.au/maps>.

- Green, R., Beard, J. & Casnoff, D. (1990), Leaf blade stomatal characterizations and evapotranspiration rates of 12 cool-season perennial grasses. *HortScience*, 25(7):pp. 760–761.
- Green, W.H. & Ampt, G.A. (1911), Studies on Soil Physics. 1. The flow of air and water through soils. *Journal of Agricultural Science*, IV(1):pp. 1–24.
- Grimmond, C.S.B., Blackett, M., Best, M.J., Baik, J.J., Belcher, S.E., Beringer, J., Bohnenstengel, S.I., Calmet, I., Chen, F., Coutts, A., Dandou, A., Fortuniak, K., Gouvea, M.L., Hamdi, R., Hendry, M., Kanda, M., Kawai, T., Kawamoto, Y., Kondo, H., Krayenhoff, E.S., Lee, S.H., Loridan, T., Martilli, A., Masson, V., Miao, S., Oleson, K., Ooka, R., Pigeon, G., Porson, A., Ryu, Y.H., Salamanca, F., Steeneveld, G., Tombrou, M., Voogt, J.A., Young, D.T. & Zhang, N. (2011), Initial results from Phase 2 of the international urban energy balance model comparison. *International Journal of Climatology*, 31(2):pp. 244–272.
- Grimmond, C.S.B., Blackett, M., Best, M.J., Barlow, J., Baik, J.J., Belcher, S.E., Bohnenstengel, S.I., Calmet, I., Chen, F., Dandou, a., Fortuniak, K., Gouvea, M.L., Hamdi, R., Hendry, M., Kawai, T., Kawamoto, Y., Kondo, H., Krayenhoff, E.S., Lee, S.H., Loridan, T., Martilli, a., Masson, V., Miao, S., Oleson, K., Pigeon, G., Porson, a., Ryu, Y.H., Salamanca, F., Shashua-Bar, L., Steeneveld, G.J., Tombrou, M., Voogt, J., Young, D. & Zhang, N. (2010), The International Urban Energy Balance Models Comparison Project: First Results from Phase 1. *Journal of Applied Meteorology and Climatology*, 49(6):pp. 1268–1292.
- Grimmond, C.S.B. & Oke, T.R. (1991), An Evapotranspiration-Interception Model for Urban Areas. *Water Resources Research*, 27(7):pp. 1739–1755.
- Grimmond, C.S.B. & Oke, T. (2002), Turbulent Heat Fluxes in Urban Areas: Observations and a Local-Scale Urban Meteorological Parameterization Scheme (LUMPS). *Journal of Applied Meteorology*, 41:pp. 792–810.
- Grimmond, C. & Oke, T. (1999), Aerodynamic properties of urban areas derived from analysis of surface form. *Journal of Applied Meteorology*, 38:pp. 1262–1292.
- Grimmond, C., Oke, T. & Steyn, D. (1986), Urban Water Balance 1. A Model for Daily Totals. *Water Resources Research*, 22(10):pp. 1397–1403.
- Gromke, C., Blocken, B., Janssen, W., Merema, B., van Hooff, T. & Timmermans, H. (2015), CFD analysis of transpirational cooling by vegetation: Case study for specific meteorological conditions during a heat wave in Arnhem, Netherlands. *Building and Environment*, 83:pp. 11–26.
- Haddad, S., Osmond, P. & King, S. (2013), Metabolic Rate Estimation in the Calculation of the PMV For Children. In: *47th International Conference of the Architectural Science Association*, pp. 241–250.
- Hamdi, M., Lachiver, G. & Michaud, F. (1999), A new predictive thermal sensation index of human response. *Energy and Buildings*, 29(2):pp. 167–178.
- Harman, I.N. & Belcher, S.E. (2006), The surface energy balance and boundary layer over urban street canyons. *Quarterly Journal of the Royal Meteorological Society*, 132(621):pp. 2749–2768.
- Harman, I.N., Barlow, J.F. & Belcher, S.E. (2004), Scalar Fluxes from Urban Street Canyons Part II: Model. *Boundary-Layer Meteorology*, 113(3):pp. 387–410.

- Havenith, G., Fiala, D., Blazejczyk, K., Richards, M., Bröde, P., Holmér, I., Rintamaki, H., Benshabat, Y. & Jendritzky, G. (2012), The UTCI-clothing model. *International Journal of Biometeorology*, 56(3):pp. 461–470.
- Heudorf, U. & Meyer, C. (2005), Health effects of extreme heat—an example of the heat wave and mortality in Frankfurt am Main in August 2003. *Gesundheitswesen*, 67(5):pp. 369–74.
- Holtslag, A. & Van Ulden, A. (1983), A simple scheme for daytime estimates of the surface fluxes from routine weather data. *Journal of Climate and Applied Meteorology*, 22:pp. 517–529.
- Hottel, H.C. & Cohen, E.S. (1958), Radiant Heat Exchange in a Gas-filled Enclosure: Allowance for Nonuniformity of Gas Temperature. *A.I.Ch.E. Journal*, 4:pp. 3–14.
- Hottel, H. & Sarofim, A. (1967), *Radiation heat transfer*. McGraw-Hill, New York.
- Hunter, J.D. (2007), Matplotlib: A 2D graphics environment. *Computing In Science & Engineering*, 9(3):pp. 90–95.
- IPCC (2007), IPCC Fourth Assessment Report - Climate Change 2007: Synthesis Report. <http://www.ipcc.ch/ipccreports/ar4-wg1.htm>, (accessed 25 May 2011).
- IPCC (2013a), Climate Change 2013: The Physical Science Basis. Contribution of Working Group I to the Fifth Assessment Report of the Intergovernmental Panel on Climate Change. Technical report, Intergovernmental Panel on Climate Change, Cambridge, United Kingdom and New York, NY, USA.
- IPCC (2013b), Summary for Policymakers. In: *Climate Change 2013: The Physical Science Basis. Contribution of Working Group I to the Fifth Assessment Report of the Intergovernmental Panel on Climate Change* (eds. V.B. Stocker, T.F. D. Qin, G.-K. Plattner, M. Tignor, S.K. Allen, J. Boschung, A. Nauels, Y. Xia & P. Midgley), Cambridge University Press, Cambridge, United Kingdom and New York, NY, USA., pp. 3–29.
- Jackson, R.B., Canadell, J., Ehleringer, J.R., Mooney, H.A., Sala, O.E. & Schulze, E.D. (1996), A global analysis of root distributions for terrestrial biomes. *Oecologia*, 108(3):pp. 389–411.
- Janhall, S. (2015), Review on urban vegetation and particle air pollution - Deposition and dispersion. *Atmospheric Environment*, 105:pp. 130–137.
- Järvi, L., Grimmond, C.S.B., Taka, M., Nordbo, A., Setälä, H. & Strachan, I.B. (2014), Development of the Surface Urban Energy and Water Balance Scheme (SUEWS) for cold climate cities. *Geoscientific Model Development*, 7(4):pp. 1691–1711.
- Järvi, L., Grimmond, C. & Christen, A. (2011), The Surface Urban Energy and Water Balance Scheme (SUEWS): Evaluation in Los Angeles and Vancouver. *Journal of Hydrology*, 411(3-4):pp. 219–237.
- Jarvis, P.G. & McNaughton, K.G. (1986), Stomatal Control of Transpiration: Scaling Up from Leaf to Region. *Advances in Ecological Research*, 15(C):pp. 1–49.
- Jeans, J.H. (1917), The Equations of Radiative Transfer of Energy. *Monthly Notices of the Royal Astronomical Society*, 78(1):pp. 28–36.
- Jones, H. (1992), *Plants and Microclimate*. Cambridge University Press, Cambridge.
- Jones, R.N., Chiew, F.H., Boughton, W.C. & Zhang, L. (2006), Estimating the sensitivity of mean annual runoff to climate change using selected hydrological models. *Advances in Water Resources*, 29(10):pp. 1419–1429.

- Jones, W. (2001), *Air Conditioning Engineering*. Elsevier Butterworth-Heinemann, Oxford, 5th edition.
- Kalkstein, L.S. & Smoyer, K.E. (1993), The impact of climate change on human health: Some international implications. *Experientia*, 49(11):pp. 969–979.
- Kanda, M., Kawai, T., Kanega, M., Moriwaki, R., Narita, K. & Hagishima, a. (2005), A Simple Energy Balance Model for Regular Building Arrays. *Boundary-Layer Meteorology*, 116(3):pp. 423–443.
- Kántor, N. & Unger, J. (2011), The most problematic variable in the course of human-biometeorological comfort assessment - the mean radiant temperature. *Open Geosciences*, 3(1):pp. 90–100.
- Katjacnik, K., Vogel-Mikus, K. & Gaberscik, A. (2014), Silicified structures affect leaf optical properties in grasses and sedge. *Journal of Photochemistry and Photobiology B: Biology*, 130:pp. 1–10.
- Katsouyanni, K., Pantazopoulou, A., Touloumi, G., Selepидаки, I., Moustris, K., Asimakopoulos, D., Poulopoulou, G. & Trichopoulos, D. (1993), Evidence for interaction between air pollution and high temperature in the causation of excess mortality. *Archives of Environmental Health*, 75(6):pp. 235–242.
- Kirkham, M.B. (2014), *Principles of Soil and Plant Water Relations*. Academic Press, Oxford, 2nd edition.
- Konarska, J., Lindberg, F., Larsson, A., Thorsson, S. & Holmer, B. (2014), Transmissivity of solar radiation through crowns of single urban trees-application for outdoor thermal comfort modelling. *Theoretical and Applied Climatology*, 117(3-4):pp. 363–376.
- Kondo, H., Genchi, Y., Kikegawa, Y., Ohashi, Y., Yoshikado, H. & Komiyama, H. (2005), Development of a Multi-Layer Urban Canopy Model for the Analysis of Energy Consumption in a Big City: Structure of the Urban Canopy Model and its Basic Performance. *Boundary-Layer Meteorology*, 116(3):pp. 395–421.
- Kowalczyk, E., Garratt, J. & Krummel, P. (1991), A soil-canopy scheme for use in a numerical model of the atmosphere: 1D stand-alone model. *CSIRO Division of Atmospheric Research technical paper, no. 23*.
- Krayenhoff, E.S., Christen, A., Martilli, A. & Oke, T.R. (2014), A Multi-layer Radiation Model for Urban Neighbourhoods with Trees. *Boundary-Layer Meteorology*, 151(1):pp. 139–178.
- Krayenhoff, E.S., Santiago, J.L., Martilli, A., Christen, A. & Oke, T.R. (2015), Parametrization of Drag and Turbulence for Urban Neighbourhoods with Trees. *Boundary-Layer Meteorology*, 156(2):pp. 157–189.
- Krayenhoff, E.S. & Voogt, J.A. (2007), A microscale three-dimensional urban energy balance model for studying surface temperatures. *Boundary-Layer Meteorology*, 123(3):pp. 433–461.
- Krayenhoff, E. (2005), *A Microscale 3-D Urban Energy Balance Model for Studying Surface Temperatures*. Master's thesis, Department of Geography, Western University, London, ON, Canada.
- Krüger, E., Minella, F. & Rasia, F. (2011), Impact of urban geometry on outdoor thermal comfort and air quality from field measurements in Curitiba, Brazil. *Building and Environment*, 46(3):pp. 621–634.

- Kunz, R., Khatib, I. & Moussiopoulos, N. (2000), Coupling of mesoscale and microscale models - an approach to simulate scale interaction. *Environmental Modelling & Software*, 15(6-7):pp. 597–602.
- Kusaka, H., Kondo, H., Kikegawa, Y. & Kimura, F. (2001), A simple single-layer urban canopy model for atmospheric models: Comparison with multi-layer and slab models. *Boundary-Layer Meteorology*, 101(ii):pp. 329–358.
- Lacser, A. & Otte, T.L. (2002), Implementation of an Urban Canopy Parameterization in MM5. In: *Fourth Symposium on Urban Environment, American Meteorological Society, Norfolk, VA*, pp. 153–154.
- Lalic, B. & Mihailovic, D.T. (2004), An Empirical Relation Describing Leaf-Area Density inside the Forest for Environmental Modeling. *Journal of Applied Meteorology*, 43(4):pp. 641–645.
- Laschewski, G. & Jendritzky, G. (2002), Effects of the thermal environment on human health: an investigation of 30 years of daily mortality data from SW Germany. *Climate Research*, 21:pp. 91–103.
- Lee, S.H. (2011), Further Development of the Vegetated Urban Canopy Model Including a Grass-Covered Surface Parametrization and Photosynthesis Effects. *Boundary-Layer Meteorology*, 140(2):pp. 315–342.
- Lee, S.H. & Park, S.U. (2008), A Vegetated Urban Canopy Model for Meteorological and Environmental Modelling. *Boundary-Layer Meteorology*, 126(1):pp. 73–102.
- Lehmann, I., Mathey, J., Rößler, S., Bräuer, A. & Goldberg, V. (2014), Urban vegetation structure types as a methodological approach for identifying ecosystem services - Application to the analysis of micro-climatic effects. *Ecological Indicators*, 42:pp. 58–72.
- Lemonsu, A., Masson, V., Shashua-Bar, L., Erell, E. & Pearlmuter, D. (2012), Inclusion of vegetation in the Town Energy Balance model for modelling urban green areas. *Geoscientific Model Development*, 5(6):pp. 1377–1393.
- Leuning, R. (1995), A critical appraisal of a combined stomatal-photosynthesis model for C3 plants. *Plant, Cell & Environment*, 18(4):pp. 339–355.
- Levinson, R., Berdahl, P., Akbari, H., Miller, W., Joedicke, I., Reilly, J., Suzuki, Y. & Vondran, M. (2007), Methods of creating solar-reflective nonwhite surfaces and their application to residential roofing materials. *Solar Energy Materials and Solar Cells*, 91(4):pp. 304–314.
- LI-COR, B. (2004), Using the LI-6400. *LI-6400XT*, 6:pp. 1181–1229.
- Liljegren, J.C., Carhart, R.A., Lawday, P., Tschopp, S. & Sharp, R. (2008), Modeling the wet bulb globe temperature using standard meteorological measurements. *Journal of Occupational and Environmental Hygiene*, 5(10):pp. 645–655.
- Lindberg, F. & Grimmond, C.S.B. (2011), The influence of vegetation and building morphology on shadow patterns and mean radiant temperatures in urban areas: model development and evaluation. *Theoretical and Applied Climatology*, 105(3-4):pp. 311–323.
- Lindberg, F., Holmer, B. & Thorsson, S. (2008), SOLWEIG 1.0-modelling spatial variations of 3D radiant fluxes and mean radiant temperature in complex urban settings. *International Journal of Biometeorology*, 52(7):pp. 697–713.

- Lindén, J., Simon, H., Fonti, P., Esper, J. & Bruse, M. (2015), Observed and modeled transpiration cooling from urban trees in Mainz, Germany. In: *9th International Conference on Urban Climate, 20-24 July 2015, Toulouse, France*, pp. 1–13.
- Litvak, E., McCarthy, H.R. & Pataki, D.E. (2012), Transpiration sensitivity of urban trees in a semi-arid climate is constrained by xylem vulnerability to cavitation. *Tree Physiology*, 32(4):pp. 373–388.
- Loridan, T., Grimmond, C., Offerle, B.D., Young, D.T., Smith, T.E.L., Järvi, L. & Lindberg, F. (2011), Local-scale Urban Meteorological Parameterization Scheme (LUMPS): Longwave radiation parameterization and seasonality-related developments. *Journal of Applied Meteorology and Climatology*, 50:pp. 185–202.
- Loughnan, M., Nicholls, N. & Tapper, N. (2010a), Mortality-temperature thresholds for ten major population centres in rural Victoria, Australia. *Health & Place*, 16(6):pp. 1287–90.
- Loughnan, M., Nicholls, N. & Tapper, N. (2012), Hot Spots Project: A spatial vulnerability analysis of urban populations to extreme heat events. http://www.health.vic.gov.au/environment/heatwave/agencies/research_pubs.htm, (accessed 16 October 2012).
- Loughnan, M.E., Nicholls, N. & Tapper, N.J. (2010b), When the heat is on: Threshold temperatures for AMI admissions to hospital in Melbourne Australia. *Applied Geography*, 30(1):pp. 63–69.
- Mariscal, M.J., Orgaz, F. & Villalobos, F.J. (2000), Modelling and measurement of radiation interception by olive canopies. *Agricultural and Forest Meteorology*, 100(2-3):pp. 183–197.
- Martilli, A., Clappier, A. & Rotach, M. (2002), An urban surface exchange parameterisation for mesoscale models. *Boundary-Layer Meteorology*, 104:pp. 261–304.
- Masanauskas, J. (2013), City residents to face higher-density living under plan to fix Melbourne's urban boundary. <http://www.heraldsun.com.au/news/city-residents-to-face-higher-density-living-under-plan-to-fix-melbournes-urban-boundary/>, (accessed 9 July 2014).
- Mascart, P., Noilhan, J. & Giordani, H. (1995), A modified parameterization of flux-profile relationships in the surface layer using different roughness length values for heat and momentum. *Boundary-Layer Meteorology*, 72:pp. 331–344.
- Masson, V. (2002), Evaluation of the Town Energy Balance (TEB) scheme with direct measurements from dry districts in two cities. *Journal of Applied Meteorology*, 41(2000):pp. 1011–1026.
- Masson, V., Le Moigne, P., Martin, E., Faroux, S., Alias, A., Alkama, R., Belamari, S., Barbu, A., Boone, A., Bouyssel, F., Brousseau, P., Brun, E., Calvet, J.C., Carrer, D., Decharme, B., Delire, C., Donier, S., Essaouini, K., Gibelin, A.L., Giordani, H., Habets, F., Jidane, M., Kerdraon, G., Kourzeneva, E., Lafaysse, M., Lafont, S., Lebeaupin Brossier, C., Lemonsu, A., Mahfouf, J.F., Marguinaud, P., Mokhtari, M., Morin, S., Pigeon, G., Salgado, R., Seity, Y., Taillefer, F., Tanguy, G., Tulet, P., Vincendon, B., Vionnet, V. & Volodire, A. (2013), The SURFEXv7.2 land and ocean surface platform for coupled or offline simulation of earth surface variables and fluxes. *Geoscientific Model Development*, 6(4):pp. 929–960.
- Masson, V. (2000), A physically-based scheme for the urban energy budget in atmospheric models. *Boundary-Layer Meteorology*, 94(3):pp. 357–397.

- Matzarakis, A., Rutz, F. & Mayer, H. (2007), Modelling radiation fluxes in simple and complex environments—application of the RayMan model. *International Journal of Biometeorology*, 51(4):pp. 323–34.
- Matzarakis, A., Rutz, F. & Mayer, H. (2010), Modelling radiation fluxes in simple and complex environments: basics of the RayMan model. *International Journal of Biometeorology*, 54(2):pp. 131–9.
- Mayer, H., Holst, J., Dostal, P., Imbery, F. & Schindler, D. (2008), Human thermal comfort in summer within an urban street canyon in Central Europe. *Meteorologische Zeitschrift*, 17(3):pp. 241–250.
- Medlyn, B. (2004), A MAESTRO retrospective. In: *Forests at the Land-Atmosphere Interface* (eds. M. Mencuccini, J. Grace, J.B. Moncrieff & K. McNaughton), March 1971, chapter 8, CAB International, pp. 105–121.
- Medlyn, B.E. & Duursma, R.A. (2014), MAESTRA Manual. <http://bio.mq.edu.au/research/projects/maestra/manual.htm>, (accessed 3 July 2014).
- Medlyn, B.E., Duursma, R.A., Eamus, D., Ellsworth, D.S., Prentice, I.C., Barton, C.V.M., Crous, K.Y., De Angelis, P., Freeman, M. & Wingate, L. (2011), Reconciling the optimal and empirical approaches to modelling stomatal conductance. *Global Change Biology*, 17(6):pp. 2134–2144.
- Medlyn, B.E., Robinson, A.P., Clement, R. & McMurtrie, R.E. (2005), On the validation of models of forest CO₂ exchange using eddy covariance data: some perils and pitfalls. *Tree Physiology*, 25(7):pp. 839–857.
- Melbourne Water (2016a), History of our water supply system. <http://www.melbournewater.com.au/aboutus/historyandheritage/history-of-our-watersupply-system/pages/history-of-our-water-supply-system.aspx>, (accessed 29 June 2016).
- Melbourne Water (2016b), Water flowing into Melbourne’s main water supply reservoirs (annual totals). <http://www.melbournewater.com.au/waterdata/waterstorages/Pages/Inflow-over-the-years.aspx>, (accessed 20 April 2016).
- Mitchell, V.G., McMahon, T.A. & Mein, R.G. (2003), Components of the Total Water Balance of an Urban Catchment. *Environmental Management*, 32(6):pp. 735–746.
- Mitchell, V., Cleugh, H., Grimmond, C. & Xu, J. (2008), Linking urban water balance and energy balance models to analyse urban design options. *Hydrological Processes*, 22(16):pp. 2891–2900.
- Mitchell, V., Mein, R. & McMahon, T. (2001), Modelling the urban water cycle. *Environmental Modelling and Software*, 16(7):pp. 615–629.
- Mochida, A., Iizuka, S., Tominaga, Y. & Lun, I.Y.F. (2011), Up-scaling CWE models to include mesoscale meteorological influences. *Journal of Wind Engineering and Industrial Aerodynamics*, 99:pp. 187–198.
- Monson, R.K., Littlejohn, Jr., R.O. & Williams, III, G.J. (1982), The quantum yield for CO₂ uptake in C3 and C4 grasses. *Photosynthesis Research*, 3(2):pp. 153–159.
- Monteith, J.L. (1965), Evaporation and environment. *Symposia of the Society for Experimental Biology*, 19:pp. 205–234.

- Moriana, A., Villalobos, F.J. & Fereres, E. (2002), Stomatal and photosynthetic responses of olive (*Olea europaea* L.) leaves to water deficits. *Plant, Cell & Environment*, 25(3):pp. 395–405.
- Murakami, S., Ooka, R., Mochida, A., Yoshida, S. & Kim, S. (1999), CFD analysis of wind climate from human scale to urban scale. *Journal of Wind Engineering and Industrial Aerodynamics*, 81(1):pp. 57–81.
- Nearmap (2015), Preston, Victoria 2072. <http://nearmap.com>.
- Neitsch, S., Arnold, J., Kiniry, J. & Williams, J. (2011), Soil & Water Assessment Tool Theoretical Documentation Version 2009. Technical report, Texas A&M University.
- Netbeans (2016), Netbeans Integrated Development Environment 8.0.2. <https://netbeans.org>.
- Nice, K.A. (2011), *The micro-climate of a mixed urban parkland environment*. Masters thesis, Monash University.
- Nicholls, N. & Alexander, L. (2007), Has the climate become more variable or extreme? Progress 1992-2006. *Progress in Physical Geography*, 31(1):pp. 77–87.
- Nicholls, N., Skinner, C., Loughnan, M. & Tapper, N. (2008), A simple heat alert system for Melbourne, Australia. *International Journal of Biometeorology*, 52(5):pp. 375–84.
- Noilhan, J. & Planton, S. (1989), A simple parameterization of land surface processes for meteorological models. *Monthly Weather Review*, 117:pp. 536–549.
- Norman, J.M. (1979), Modelling the complete crop canopy. In: *Modification of the Aerial Environment of Crops* (eds. B. Barfield & J. Gerber), Am. Soc. Agric. Eng. Monogr. No. 2, ASAE, St Joseph, MI, pp. 249–277.
- Norman, J.M. (1993), Scaling Processes between Leaf and Canopy Levels. In: *Scaling Physiological Processes: Leaf to Globe* (eds. J.R. Ehleringer & C.B. Field), chapter 4, Academic Press, San Diego, pp. 41–76.
- Nunez, M. & Oke, T.R. (1977), The Energy Balance of an Urban Canyon. *Journal of Applied Meteorology*, 16:pp. 11–19.
- Nury, S.N. (2015), *Informed implementation of greening as a heat mitigation measure in Melbourne, Australia: a remote sensing study*. Ph.D. thesis, Monash University.
- Oke, T. (1982), The energetic basis of the urban heat island. *Quarterly Journal of the Royal Meteorological Society*, 108:pp. 1–24.
- Oke, T. (1987), *Boundary Layer Climates*. Routledge, London and New York, 2nd edition.
- Oke, T. (1988a), Street design and urban canopy layer climate. *Energy and Buildings*, 11(1-3):pp. 103–113.
- Oke, T. (1988b), The urban energy balance. *Progress in Physical Geography*, 12(4):pp. 471–508.
- Oke, T. (1989), The micrometeorology of the urban forest. *Philosophical Transactions of the Royal Society of London. Series B, Biological Sciences*, 324(1223):pp. 335–349.
- Oke, T. (2009), The need to establish protocols in urban heat island work. In: *Eighth Symposium on the Urban Environment, 12-15 January 2009, Phoenix, Arizona*, p. 1.
- Olesen, B. (1982), Thermal Comfort. *Technical Review*, 2:pp. 3–41.

- Oleson, K.W., Bonan, G.B., Feddema, J., Vertenstein, M. & Grimmond, C.S.B. (2008), An Urban Parameterization for a Global Climate Model. Part I: Formulation and Evaluation for Two Cities. *Journal of Applied Meteorology and Climatology*, 47(4):pp. 1038–1060.
- OpenFOAM (2011), OpenFOAM website. <http://www.openfoam.com/>, (accessed 2 November 2011).
- Oracle (2016), Java Platform Standard Edition 7 Documentation. <http://docs.oracle.com/javase/7/docs/index.html>.
- Otte, T. & Lacser, A. (2004), Implementation of an urban canopy parameterization in a mesoscale meteorological model. *Journal of Applied Meteorology*, 43(2002):pp. 1648–1665.
- Overgaard, J. (2005), *Energy-Based Land Surface Modelling: New Opportunities in Integrating Hydrological Modelling*. Ph.D. thesis, DTU Technical University of Denmark.
- Penman, H.L. (1948), Natural evaporation from open water, bare soil and grass. *Proc. Roy. Soc. London*, A193:pp. 120–146.
- Peter McNabb & Associates Pty Ltd & University of Melbourne Research Team (2001), 4.3 Urban Dynamics in the Melbourne Metropolitan Area Affecting The Network of Centres in ACTIVITY CENTRES REVIEW: A study of policy and centres of activity in metropolitan Melbourne and Geelong. http://www.dpcd.vic.gov.au/_data/assets/pdf_file/0015/42810/Technical_Report_8_activity_centres_c.pdf, (accessed 3 October 2012).
- Philip, J. (1966), Plant water relations: some physical aspects. *Annual Review of Plant Physiology*, 17:pp. 245–268.
- Pielke, R.A. (1984), *Mesoscale Meteorological Modeling*. Academic Press, New York.
- Population Division of the Department of Economic and Social Affairs of the United Nations Secretariat (PDDESA) (2007), World Population Prospects: The 2006 Revision and World Urbanization Prospects: The 2007 Revision. <http://www.un.org/esa/population/publications/wup2007/>, (accessed 16 January 2012).
- Poumadère, M., Mays, C., Le Mer, S. & Blong, R. (2005), The 2003 heat wave in France: dangerous climate change here and now. *Risk Analysis*, 25(6):pp. 1483–94.
- Press, W.H., Teukolsky, S.L.A., Flannery, B.N.P. & Vetterling, W.M.T. (1990), *Numerical Recipes: FORTRAN*. Cambridge University Press.
- PWC (2011), Protecting human health and safety during severe and extreme heat events: A national framework. PricewaterhouseCoopers Australia. <http://www.pwc.com.au/industry/government/assets/extreme-heat-events-nov11.pdf>, (accessed 15 September 2012).
- Python Software Foundation (2016), Python Language Reference, version 2.7. <https://www.python.org/>.
- R Core Team (2013), R: A Language and Environment for Statistical Computing. R Foundation for Statistical Computing, Vienna, Austria. ISBN 3-900051-07-0, URL <http://www.R-project.org/>.
- Rademacher, I.F. & Nelson, C. (2001), Nitrogen Effects on Leaf Anatomy within the Intercalary Meristems of Tall Fescue Leaf Blades. *Annals of Botany*, 88(5):pp. 893–903.

- Ranger, N., Gohar, L.K., Lowe, J.A., Raper, S.C.B., Bowen, A. & Ward, R.E. (2012), Is it possible to limit global warming to no more than 1.5C? *Climatic Change*, 111(3-4):pp. 973–981.
- Raupach, M.R. (1992), Drag and drag partition on rough surfaces. *Boundary-Layer Meteorology*, 60(4):pp. 375–395.
- Roberts, P. (2005), Yarra Valley Water: 2004 Residential End Use Measurement Study. <https://www.yvw.com.au/yvw/groups/public/documents/document/yvw1001680.pdf>, (accessed 29 June 2016).
- Rosenfeld, A., Akbari, H., Romm, J. & Pomerantz, M. (1998), Cool communities: strategies for heat island mitigation and smog reduction. *Energy and Buildings*, 28:pp. 51–62.
- Rosenzweig, C., Solecki, W.D., Cox, J., Hodges, S., Parshall, L., Lynn, B., Goldberg, R., Gaffin, S., Slosberg, R.B., Savio, P., Watson, M. & Dunstan, F. (2009), Mitigating New York City's Heat Island: Integrating Stakeholder Perspectives and Scientific Evaluation. *Bulletin of the American Meteorological Society*, 90(9):pp. 1297–1312.
- Rotach, M. (1995), Profiles of turbulence statistics in and above an urban street canyon. *Atmospheric Environment*, 29(13):pp. 1473–1486.
- Rutter, A.A.J., Morton, A.J. & Robins, P.C. (1975), A PREDICTIVE MODEL OF RAINFALL INTERCEPTION IN FORESTS II . GENERALIZATION OF THE MODEL AND COMPARISON WITH OBSERVATIONS IN SOME CONIFEROUS AND HARDWOOD STANDS. *Journal of Applied Ecology*, 12(1):pp. 367–380.
- Sailor, D.J. & Lu, L. (2004), A top-down methodology for developing diurnal and seasonal anthropogenic heating profiles for urban areas. *Atmospheric Environment*, 38(17):pp. 2737–2748.
- Sanderson, B.M., O'Neill, B.C., Kiehl, J.T., Meehl, G.A., Knutti, R. & Washington, W.M. (2011), The response of the climate system to very high greenhouse gas emission scenarios. *Environmental Research Letters*, 6(3):pp. 1–11.
- Sanusi, M. & Adibah, R. (2015), *The importance of street trees for human thermal comfort in a warming climate*. Ph.D. thesis, University of Melbourne.
- Schlünzen, K.H., Grawe, D., Bohnenstengel, S.I., Schlüter, I. & Koppmann, R. (2011), Joint modelling of obstacle induced and mesoscale changes - Current limits and challenges. *Journal of Wind Engineering and Industrial Aerodynamics*, 99(4):pp. 217–225.
- Schlünzen, K.H., Hinneburg, D., Knoth, O., Lambrecht, M., Leitl, B., Lopez, S., Panskus, H., Renner, E., Schatzmann, M., Schoenemeyer, T., Trepte, S. & Wolke, R. (2003), Flow and Transport in the Obstacle Layer : First Results of the Micro-Scale Model MITRAS. *Journal of Atmospheric Chemistry*, 44:pp. 113–130.
- Schmid, H.P. (1994), Source areas for scalars and scalar fluxes. *Boundary-Layer Meteorology*, 67(3):pp. 293–318.
- Shahidan, M.F., Jones, P.J., Gwilliam, J. & Salleh, E. (2012), An evaluation of outdoor and building environment cooling achieved through combination modification of trees with ground materials. *Building and Environment*, 58:pp. 245–257.
- Shashua-Bar, L. & Hoffman, M. (2000), Vegetation as a climatic component in the design of an urban street: An empirical model for predicting the cooling effect of urban green areas with trees. *Energy and Buildings*, 31:pp. 221–235.

- Shashua-Bar, L., Potchter, O., Bitan, A., Boltansky, D. & Yaakov, Y. (2010), Microclimate modelling of street tree species effects within the varied urban morphology in the Mediterranean city of Tel Aviv, Israel. *International Journal of Climatology*, 57(March 2009):pp. 44–57.
- Siegel, R. & Howell, J. (2001), *Thermal radiation heat transfer*. Taylor and Francis-Hemisphere, Washington, 4th edition.
- Sierra, A.M. (2012), *Measuring and modeling canopy photosynthesis of olive orchards*. Msc thesis plant production systems, Instituto de Agricultura Sostenible (IAS - CSIC).
- Sillmann, J., Kharin, V.V., Zwiers, F.W., Zhang, X. & Bronaugh, D. (2013), Climate extremes indices in the CMIP5 multimodel ensemble: Part 2. Future climate projections. *Journal of Geophysical Research D: Atmospheres*, 118(November 2012):pp. 2473–2493.
- Simmons, M., Bertelsen, M., Windhager, S. & Zafian, H. (2011), The performance of native and non-native turfgrass monocultures and native turfgrass polycultures: An ecological approach to sustainable lawns. *Ecological Engineering*, 37(8):pp. 1095–1103.
- SOLWEIG (2011), SOLWEIG website. <http://www.gvc.gu.se/Forskning/klimat/stadsklimat/gucg/software/solweig/>, (accessed 2 November 2011).
- Soux, A., Voogt, J.A. & Oke, T.R. (2004), A model to calculate what a remote sensor 'sees' of an urban surface. *Boundary-Layer Meteorology*, 111(1):pp. 109–132.
- Spagnolo, J. & de Dear, R. (2003), A field study of thermal comfort in outdoor and semi-outdoor environments in subtropical Sydney Australia. *Building and Environment*, 38(5):pp. 721–738.
- Spangenberg, J. & Shinzato, P. (2008), Simulation of the influence of vegetation on microclimate and thermal comfort in the city of São Paulo. *Revista SBAU*, 4:pp. 1–19.
- State of Victoria (2014), Plan Melbourne: Metropolitan Planning Strategy. <http://www.planmelbourne.vic.gov.au/Plan-Melbourne>, (accessed 9 July 2014).
- Stewart, I.D. & Oke, T.R. (2012), Local Climate Zones for Urban Temperature Studies. *Bulletin of the American Meteorological Society*, 93(12):pp. 1879–1900.
- Strengers, Y. (2008), Comfort expectations: the impact of demand-management strategies in Australia. *Building Research & Information*, 36(4):pp. 381–391.
- Sturman, A., McGowan, A. & Spronken-Smith, R. (1999), Mesoscale and local climates in New Zealand. *Progress in Physical Geography*, 23(4):pp. 611–635.
- Sumida, A., Miyaura, T. & Torii, H. (2013), Relationships of tree height and diameter at breast height revisited: analyses of stem growth using 20-year data of an even-aged Chamaecyparis obtusa stand. *Tree Physiology*, 33(1):pp. 106–118.
- Sumner, D.M. & Jacobs, J.M. (2005), Utility of Penman-Monteith, Priestley-Taylor, reference evapotranspiration, and pan evaporation methods to estimate pasture evapotranspiration. *Journal of Hydrology*, 308(1-4):pp. 81–104.
- Tan, C.L., Wong, N.H., Jusuf, S.K. & Chiam, Z.Q. (2015), Impact of plant evapotranspiration rate and shrub albedo on temperature reduction in the tropical outdoor environment. *Building and Environment*, 94(P1):pp. 206–217.
- Taylor, B. & Guthrie, P. (2008), The first line of defence: Passive design at an urban scale. In: *Air Conditioning and the Low Carbon Cooling Challenge conference proceedings, 27-29 July 2008, Network for Comfort and Energy Use in Buildings, London*, pp. 1–25.

- Taylor, H.M. & Keppler, B. (1975), Water uptake by cotton root systems: an examination of assumptions in the single root model. *Soil Sci.*, 120:pp. 57–67.
- Tominaga, Y., Sato, Y. & Sadohara, S. (2015), CFD simulations of the effect of evaporative cooling from water bodies in a micro-scale urban environment: Validation and application studies. *Sustainable Cities and Society*, 19:pp. 259–270.
- Tsiros, I.X. (2010), Assessment and energy implications of street air temperature cooling by shade trees in Athens (Greece) under extremely hot weather conditions. *Renewable Energy*, 35(8):pp. 1866–1869.
- Tuzet, A., Perrier, A. & Leuning, R. (2003), A coupled model of stomatal conductance, photosynthesis and transpiration. *Plant, Cell and Environment*, 26:pp. 1097–1116.
- UNDESA (2015), World Urbanization Prospects: The 2014 Revision. <https://esa.un.org/unpd/wup/>, (accessed 22 August 2016).
- UNEP (2011), The Emissions Gap Report: Are the Copenhagen Accord Pledges Sufficient to Limit Global Warming to 2C or 1.5C. United Nations Environment Programme. <http://www.unep.org/publications/ebooks/emissionsgapreport/>, (accessed 21 December 2011).
- Victoria Department of Health (2010), Heatwave Plan for Victoria 2009-2010: Protecting health and reducing harm from heatwaves. http://www.health.vic.gov.au/environment/downloads/heatwave_plan_vic.pdf, (accessed 24 September 2012).
- Vu, T.C., Ashie, Y., Asaeda, T., Ca, V.T., Ashie, Y. & Asaeda, T. (2002), A k-e turbulence closure model for the atmospheric boundary layer including urban canopy. *Boundary-Layer Meteorology*, 102(3):pp. 459–490.
- Wang, Y. & Leuning, R. (1998), A two-leaf model for canopy conductance, photosynthesis and partitioning of available energy I: Model description and comparison with a multi-layered model. *Agricultural and Forest Meteorology*, 91:pp. 89–111.
- Wang, Y.P. & Jarvis, P.G. (1990), Description and validation of an array model - MAESTRO. *Agricultural and Forest Meteorology*, 51:pp. 257–280.
- Wang, Y.P., Jarvis, P. & Benson, M.L. (1990), Two-Dimensional Needle-Area Density Distribution within the Crowns of Pinus radiata. *Forest Ecology and Management*, 32:pp. 217–237.
- Wang, Y., Bakker, F., de Groot, R., Wortche, H. & Leemans, R. (2015), Effects of urban trees on local outdoor microclimate: synthesizing field measurements by numerical modelling. *Urban Ecosystems*, 18(4):pp. 1305–1331.
- Wang, Z.H. (2014), Monte Carlo simulations of radiative heat exchange in a street canyon with trees. *Solar Energy*, 110:pp. 704–713.
- Wang, Z.H., Bou-Zeid, E., Au, S.K. & Smith, J.A. (2011), Analyzing the sensitivity of WRF's single-layer urban canopy model to parameter uncertainty using advanced Monte Carlo simulation. *Journal of Applied Meteorology and Climatology*, 50(9):pp. 1795–1814.
- Wang, Z.H., Bou-Zeid, E. & Smith, J.A. (2013), A coupled energy transport and hydrological model for urban canopies evaluated using a wireless sensor network. *Quarterly Journal of the Royal Meteorological Society*, 139:pp. 1643–57.

- Wang, Z.H., Zhao, X., Yang, J. & Song, J. (2016), Cooling and energy saving potentials of shade trees and urban lawns in a desert city. *Applied Energy*, 161:pp. 437–444.
- Watt, M., Oliphant, M., Outhred, H. & Collins, R. (2003), Using PV to Meet Peak Summer Electricity Loads. ANZSES Destination Renewables, Australia. <http://www.ceem.unsw.edu.au/sites/default/files/uploads/publications/Watt - PV Peak Load - Solar 2003.pdf>.
- Weiss, A. & Norman, J.M. (1985), Partitioning solar radiation into direct and diffuse, visible and near-infrared components. *Agricultural and Forest Meteorology*, 34(2-3):pp. 205–213.
- White, E., Coutts, A., Tapper, N. & Beringer, J. (2012), Urban microclimate & street trees: Understanding the effects of street trees on human thermal comfort. Technical report, CRC for Water Sensitive Cities, Monash University.
- WHO (2016), World Health Organization | Urban Population Growth. http://www.who.int/gho/urban_health/situation_trends/urban_population_growth_text/en/, (accessed 29 April 2016).
- Williams, M., Bond, B.J. & Ryan, M.G. (2001a), Evaluating different soil and plant hydraulic constraints on tree function using a model and sap flow data from ponderosa pine. *Plant, Cell and Environment*, 24(7):pp. 679–690.
- Williams, M., Law, B.E., Anthoni, P.M. & Michael, H. (2001b), Use of a simulation model and ecosystem flux data to examine carbon - water interactions in ponderosa pine. *Tree Physiology*, 21:pp. 287–298.
- Winslow, C.E.A., Herrington, L.P. & Gagge, A.P. (1936), A NEW METHOD OF PARTITIONAL CALORIMETRY. *American Journal of Physiology*, 116(3):pp. 641–655.
- Wong, T.H.F. & Brown, R.R. (2009), The water sensitive city: principles for practice. *Water Science and Technology*, 60(3):pp. 673–82.
- Wouters, H., Demuzere, M., Ridder, K.D. & Nicole, P.M. (2013), The impact of impervious water-storage parameterization on urban climate modelling. *Urban Climate*, 11:pp. 24–50.
- Wright, I.J. & Westoby, M. (2000), Cross-species relationships between seedling relative growth rate, nitrogen productivity and root vs leaf function in 28 Australian woody species. *Functional Ecology*, 14(1):pp. 97–107.
- Yaghoobian, N., Kleissl, J. & Krayenhoff, E.S. (2010), Modeling the Thermal Effects of Artificial Turf on the Urban Environment. *Journal of Applied Meteorology and Climatology*, 49(3):pp. 332–345.
- Yamada, T. (1982), A numerical study of turbulent airflow in and above a forest canopy. *J. Meteorol Soc Japan*, 60:pp. 439–454.
- Yamada, T. & Koike, K. (2011), Downscaling mesoscale meteorological models for computational wind engineering applications. *Journal of Wind Engineering and Industrial Aerodynamics*, 99(4):pp. 199–216.
- Yamaoka, N., Yoshida, H., Tanabe, M., Yamashita, M. & Koga, T. (2008), Simulation study of the influence of different urban canyons element on the canyon thermal environment. *Building Simulation*, 1(2):pp. 118–128.

Yu, J., Chen, L., Xu, M. & Huang, B. (2012), Effects of Elevated CO₂ on Physiological Responses of Tall Fescue to Elevated Temperature, Drought Stress, and the Combined Stresses. *Crop Science*, 52(4):p. 1848.